

**ON DEPRESSION STORAGE, ITS MODELING AND SCALE**

**A Thesis**

**Presented to**

**The Faculty of Graduate Studies**

**of**

**The University of Guelph**

**by**

**MOHAMMAD JAVAD ABEDINI**

**In partial fulfillment of requirements**

**for the degree of**

**Doctor of Philosophy**

**June, 1998**

**©Mohammad Javad Abedini, 1998**



National Library  
of Canada

Acquisitions and  
Bibliographic Services

395 Wellington Street  
Ottawa ON K1A 0N4  
Canada

Bibliothèque nationale  
du Canada

Acquisitions et  
services bibliographiques

395, rue Wellington  
Ottawa ON K1A 0N4  
Canada

*Your file Votre référence*

*Our file Notre référence*

The author has granted a non-exclusive licence allowing the National Library of Canada to reproduce, loan, distribute or sell copies of this thesis in microform, paper or electronic formats.

The author retains ownership of the copyright in this thesis. Neither the thesis nor substantial extracts from it may be printed or otherwise reproduced without the author's permission.

L'auteur a accordé une licence non exclusive permettant à la Bibliothèque nationale du Canada de reproduire, prêter, distribuer ou vendre des copies de cette thèse sous la forme de microfiche/film, de reproduction sur papier ou sur format électronique.

L'auteur conserve la propriété du droit d'auteur qui protège cette thèse. Ni la thèse ni des extraits substantiels de celle-ci ne doivent être imprimés ou autrement reproduits sans son autorisation.

0-612-33293-4

## ABSTRACT

### ON DEPRESSION STORAGE, ITS MODELING AND SCALE

Mohammad Javad Abedini  
University of Guelph, 1998

Advisors:  
Dr. W. T. Dickinson  
Dr. R. P. Rudra

Depression storage can be a significant storage element on a watershed surface, accounting for the retention of much water. This research was undertaken to investigate effects of surface storage elements on catchment response at a range of spatial scales and experimental settings. The spatial scales included small-scale laboratory experiments, small-scale field experiments and large-scale field experiments. Interactions of surface treatments, slope orientations, rainfall patterns, initial soil-water conditions and surface storage elements, and resulting effects on runoff response including the timing of outflow hydrographs, were considered at these spatial scales.

Surface topography was measured with the aid of a laser scanner down to a 3-mm grid spacing. After the spatial location of depressional storages was delineated using digital elevation data, the results were linked to the GRID module of ARC/INFO via an indicator variable to derive polygon coverage of depressional areas versus non-depressional areas in a spatial context. From the pond analysis and associated spatial mapping, it became clear that most estimates and/or geometric characteristics relating to size and spatial location of depression storage, including area, volume and depth, are scale dependent. These geometric objects may best be described by resorting to fractal geometry, a popular tool for quantifying variability across scales.

Indirect characterization of surface storage elements was achieved via observation of rainfall and the corresponding surface runoff at different spatial scales. From the analysis of runoff response data, it was found that when there is no infiltration,

depression effects can be detected in response, i.e. effects due to size of depressions and spatial location of different sizes. In the presence of infiltration, separation of depression storage effects from infiltration effects on catchment response was found to be extremely difficult if not impossible.

A simple holistic type approach was suggested to model depression storage. Application of the modeling approach showed that for simple depressional cases with no infiltration, differences in response due to various spatial patterns of depressions could be delineated well as measured by a coefficient of determination statistic, with  $R^2$  values above 0.90 for the majority of cases. In such situations, the parameters took on values which appeared to have physical meaning in terms of physical characteristics such as mean time of travel and mean depth of depressional storage. For simple and more complex situations involving infiltration at a range of scales (from small plots to small watersheds), modeling applications showed that response could still be estimated well with a simple holistic model. However, the parameters can take on values which may or may not have any physical meaning at all. In all such modeling exercises, the mean time of travel was found to be the most stable; the mean depth of storage was quite stable and the recession constant was the least stable parameter.

# ACKNOWLEDGMENTS

**In the name of God, the Compassionate, the Merciful**

*Ali (AS):* A good scientist is he who admits that what he knows is insignificant to what he does not know.

I am indebted to many people for advice and constant encouragement: Acknowledgment to Dr. W. T. Dickinson must be first and foremost for invoking the project, for freely sharing his wisdom and knowledge during the course of the work and above all his friendship. I am struck by the large element of chance involved in being in the right place at the right time with the right person. I wish to express my admiration and deepest respect for him. He is an outstanding teacher and researcher and I continue to be inspired by his courage and strength of spirit. I have been privileged in this regard and will never ever forget this great fortune.

There are many other people who have helped bring this dissertation to fruition. My advisors Dr. W. T. Dickinson and Dr. R. P. Rudra have allowed me the freedom to study the various aspects of this undertaking according to what interested me most. At the same time they have offered very helpful insight that has gradually narrowed this study to a manageable task and brought it to its conclusion on a realistic schedule. I am very indebted to them. Without their guidance I would likely still be exploring several other research objectives associated with this study. My gratitude also goes to other members of my advisory committee members (H. R. Whiteley and D. A. Swayne) for their helpful discussions, comments and careful review of the contents of

this thesis and for many interesting and helpful suggestions they have provided me to improve its quality.

The direct and indirect contributions of the faculty and staff of the School of Engineering, University of Guelph are also greatly appreciated. Chief among those were the people who provided me with levels of technical expertise which can only be described as world class. Not only were the school's facilities made available to me, but also individuals gave me support and suggestions on several occasions. Dave Tiechrobe, deserves special credit for keeping me and the equipment running during the many crises, real and imagined that occurred with all the equipments. I would also like to thank Ms. Dianne Duncan in particular for assisting in preparing some of the diagrams. To this end, I was also admirably assisted by Paul Found and Bill Verspagen. I am grateful for the opportunity I was given for my career development in the school.

The project was supported financially through scholarship provided by the Iranian Ministry of Culture and Higher Education which enabled me to pursue the doctoral degree program at the University of Guelph, Canada. Their moral and financial support is gratefully appreciated. The support of the Natural Science and Engineering Research Council of Canada (NSERC), in the form of research grants to Dr. Dickinson is also gratefully acknowledged.

Thanks are also due to my fellow graduate students and colleagues here and world-wide with whom I have had many philosophical discussions concerning various aspects of this study.

Special thanks must be extended to Dr. B. Nickling at Department of Geography, University of Guelph, Dr. Chi-hua Huang at NSERL, Purdue University and Dr. Soroosh Sorooshian at University of Arizona for their generous sharing of knowledge and providing the necessary software which allowed me to complete this project on a realistic schedule.

Finally, I wish to express gratitude to my family: My wife, Homayra for her

constant encouragement, without which this effort would have remained a dream; My children Zahra, Reza and Amin for their patience and sacrifice; My father, a hard-working and honest man, who has helped me throughout my life and studies, and my mother who fostered my ambition and love toward my engineering profession.

My sincere thanks to all those who paved the way for me to reach this point.

My last words are praise be to Almighty God, the Lord of the Worlds who gave me the gift of life to keep searching for what it is all about.

# Contents

<b>1</b>	<b>INTRODUCTION</b>	<b>1</b>
<b>2</b>	<b>LITERATURE REVIEW</b>	<b>7</b>
2.1	Introduction . . . . .	7
2.2	Storage Routing Models . . . . .	9
2.3	Distributed Watershed Models . . . . .	12
2.4	Probability-based Watershed models . . . . .	18
2.5	Literature Review on Surface Profilers . . . . .	20
2.6	Estimation of Micro-relief Surface Storage . . . . .	22
2.7	Partial-Contributing-Area Concept . . . . .	25
2.8	Types of Runoff Mechanisms . . . . .	26
2.8.1	Infiltration–excess Overland Flow (Horton Mechanism) . . . . .	26
2.8.2	Saturated and Unsaturated Soil-water Movement . . . . .	27
2.8.3	Saturation–excess Overland Flow (Dunne Mechanism) . . . . .	28
2.9	Major Shortcomings of Past Efforts . . . . .	29
2.9.1	Consistency Between Model Structure and Available Data . . . . .	30
2.9.2	Internal Validation vs. External Validation . . . . .	32
2.9.3	Hypothesis Testing . . . . .	33
2.9.4	Scale Problem . . . . .	34
2.9.5	Known Problem vs. Known Solution . . . . .	36
2.9.6	Conceptual Understanding of Runoff Processes . . . . .	37

2.10	Lessons to be Learned From Past Efforts . . . . .	38
<b>3</b>	<b>PROPOSED RESEARCH</b>	<b>41</b>
3.1	Major Hypothesis . . . . .	41
3.2	Objectives of the Study . . . . .	41
3.3	Suggested Approach . . . . .	42
3.3.1	Preliminary Studies . . . . .	42
3.3.2	Field Studies . . . . .	42
3.3.3	Model Studies . . . . .	43
<b>4</b>	<b>EXPERIMENTAL METHODS</b>	<b>44</b>
4.1	Introduction . . . . .	44
4.2	Small-scale Laboratory Experiments . . . . .	45
4.2.1	Experimental Flume . . . . .	45
4.2.2	Rainfall Simulator . . . . .	47
4.2.3	Rainfall Simulator Calibration . . . . .	47
4.2.4	Qualitative Discussion of Simulated Rainfall Characteristics . .	52
4.2.5	Rainfall Treatment . . . . .	54
4.2.6	Runoff Measurement Facility . . . . .	56
4.2.7	Preliminary Runs . . . . .	57
4.2.8	Surface Preparation . . . . .	62
4.2.9	Surface Treatment . . . . .	64
4.2.10	Slope Treatment . . . . .	68
4.2.11	Procedural Design of Lab Experimentation . . . . .	68
4.2.12	Experimental Procedure . . . . .	70
4.3	Small-scale Field Experiments . . . . .	72
4.3.1	The Study Area . . . . .	72
4.3.2	Sample Micro-catchments . . . . .	74
4.3.3	Micro-topography Characterization . . . . .	78

4.3.4	Surface Treatment . . . . .	85
4.3.5	Rainfall Treatment . . . . .	86
4.3.6	Runoff Measurement System . . . . .	89
4.4	Large Scale Catchment Experiment . . . . .	90
4.4.1	The Study Area . . . . .	90
<b>5</b>	<b>CHARACTERISTICS OF SURFACE DEPRESSIONS</b>	<b>94</b>
5.1	Introduction . . . . .	94
5.2	Analysis of Laser-Scanned Digital Elevation Data . . . . .	95
5.2.1	Manipulation of Upper and Lower 1% Elevation Data . . . . .	95
5.2.2	Manipulation of Ground Control Points . . . . .	96
5.2.3	Merging of the Two Pieces . . . . .	97
5.2.4	Frequency Analysis of Elevation Data . . . . .	99
5.2.5	Spatial Analysis of Elevation Data . . . . .	102
5.3	Manipulation of Missing Values . . . . .	116
5.4	Surface-shaded Relief Display . . . . .	118
5.5	Characterization of Surface Depressions . . . . .	123
5.6	Results and Discussion . . . . .	127
5.6.1	Effects of Grid Spacing on Pondered Area . . . . .	132
5.6.2	Effects of Grid Spacing on Total Volume of Depressions . . . . .	133
5.6.3	Effects of Grid Spacing on Number of Depressions . . . . .	134
5.6.4	Contributing Area vs. Pond Area . . . . .	136
5.7	Spatial Mapping of Depressions . . . . .	138
5.7.1	Effect of Re-sampling on Spatial Mapping . . . . .	146
5.8	Implications of Pond Results . . . . .	152
5.8.1	Scale-invariance property . . . . .	152
5.8.2	Power Law Relationship Among Various Geometric Attributes	155

<b>6</b>	<b>Rainfall:Runoff Experimental Results and Discussion</b>	<b>157</b>
6.1	Introduction . . . . .	157
6.2	Small-scale Laboratory Experiments . . . . .	158
6.2.1	Sample Results of Laboratory Experiments . . . . .	158
6.2.2	Discussion of Experimental Results . . . . .	168
6.3	Small-scale Field Experiments . . . . .	172
6.3.1	Sample Results of Field Experiments . . . . .	172
6.3.2	Discussion of Experimental Results . . . . .	184
6.4	Large-scale Field Experiments . . . . .	187
6.4.1	Sample Results of Field Experiments and their Discussion . . . . .	188
6.4.2	Discussion of Comparative Results . . . . .	193
<b>7</b>	<b>MODELING STUDIES</b>	<b>198</b>
7.1	Introduction . . . . .	198
7.2	Identification of Stores . . . . .	199
7.3	Mathematical Formulation–Electrical Analogy . . . . .	201
7.4	Analogy Between Electrical and Hydrological System . . . . .	209
7.5	A Hypothetical Example . . . . .	213
7.6	Simulation Run . . . . .	215
7.6.1	Scale Issue in the Proposed Methodology . . . . .	216
7.6.2	Effects of Storage Capacity of Each Depression . . . . .	217
7.6.3	Effects of Channel Resistance . . . . .	218
7.6.4	Effects of Initial Condition . . . . .	218
7.6.5	Capability of the Model . . . . .	219
7.6.6	Discussion of Model . . . . .	221
7.7	Decision on Model Structure . . . . .	226
7.8	Two Main Processes in Rainfall-Runoff Modeling . . . . .	228
7.8.1	Storage Processes . . . . .	228
7.8.2	Translation processes . . . . .	229

7.8.3	Power-law Distributions of Discharge . . . . .	231
7.9	Mathematical Formulation–Hydrological Analogy . . . . .	233
7.10	Theory of Non-interacting Storage Elements . . . . .	237
7.10.1	Calculation of basin soil-water deficit . . . . .	242
7.10.2	Relation of Actual to Potential Evaporation . . . . .	243
7.10.3	Incorporation of Drainage into Model Structure . . . . .	244
7.11	Theory of Interacting Storage Elements . . . . .	248
7.11.1	Calculation of Basin Water Storage . . . . .	249
7.11.2	Relation of Actual to Potential Evaporation . . . . .	250
7.11.3	Incorporation of Drainage into Model Structure . . . . .	252
7.11.4	Transmission of Runoff . . . . .	253
7.12	Selection of Probability Density Function for Depression Storage . . . . .	254
7.12.1	The Exponential Distribution . . . . .	255
7.12.2	The Weibull Distribution . . . . .	256
7.13	Selection of Probability Density Function for Time of Travel . . . . .	256
7.13.1	The Convection-Diffusion Equation . . . . .	257
7.14	A Bivariate Exponential Storage-Translation Model . . . . .	261
7.15	Probability Distributed Model of Infiltration-excess Overland Flow . . . . .	262
7.16	Development of Probability-distributed Approach for Particular Dis- tribution . . . . .	266
7.17	Model Application . . . . .	270
7.18	Model Structure Identification and Verification . . . . .	271
7.19	Model Sensitivity Analysis . . . . .	273
7.20	Model Application for Small-Scale Lab Experiment . . . . .	274
7.20.1	Smooth Surface Treatment . . . . .	274
7.20.2	Other Surface Treatments . . . . .	284
7.21	Modeling Application for Small-Scale Field Experiments . . . . .	295
7.22	Modeling Application for Large-Scale Field Experiment . . . . .	302

7.23 Discussion of Results . . . . .	306
<b>8 CONCLUSIONS AND RECOMMENDATIONS</b>	<b>309</b>
8.1 Introduction . . . . .	309
8.2 Conclusions . . . . .	310
8.3 Recommendations for Further Research . . . . .	312
<b>BIBLIOGRAPHY</b>	<b>314</b>
<b>APPENDICES</b>	<b>331</b>
<b>A Laboratory Experimental Results</b>	<b>331</b>
<b>B Results of Analysis of Variance</b>	<b>340</b>

# List of Tables

4.1	Summary of nozzles and conditions explored in calibration runs. . . . .	49
4.2	Summary of typical results from two calibration methods . . . . .	51
4.3	Temporal patterns of possible rainfall treatments . . . . .	54
4.4	Temporal patterns of rainfall chosen for laboratory experiments . . . . .	55
4.5	Summary of simulation run selected for construction . . . . .	63
4.6	Total potential volume of depression storage at different slope. . . . .	64
4.7	Pattern to pattern and day to day variability in rainfall intensity . . . . .	69
4.8	Slope to slope variability in rainfall intensity within a single day. . . . .	70
4.9	Summary of scanning results for the three plots. . . . .	85
4.10	Selected Sub-watershed Characteristics within the Lake Erie Watershed.	92
5.1	Elevation statistics for the three field micro-catchments. . . . .	99
5.2	Fractal (fBm) and basic models parameters for various micro-catchments.	114
5.3	Summary results of pond analysis. . . . .	126
5.4	Summary results for analysis of nested design. . . . .	128
5.5	One-way analysis of Variance of data for key variables. . . . .	130
5.6	Results of multiple range analysis for key variables w.r.t. grid spacing.	142
6.1	Summary of experimental runs (water balance components) for surface treatment II. . . . .	160
6.2	Summary of experimental runs (water balance components) for various surface treatments ( $S = 10\%$ ). . . . .	161

6.3	Summary of infiltration capacity (mm/hr) calculations for surface treatment IV. . . . .	170
6.4	Summary of infiltration rate (mm/hr) calculations for surface treatment IV. . . . .	171
6.5	Summary of experimental runs (water balance components) for small-scale field experiment. . . . .	175
6.6	Typical rainfall-runoff events on the selected small watersheds. . . . .	189
7.1	Comparison of analogous quantities in electrical and hydrological system	212
7.2	Possible combinations of pdf for storage and time of travel. . . . .	262
7.3	Model output for combination of slope and rainfall treatments—One parameter model, flat surface (without data smoothing). . . . .	276
7.4	Model output for combination of slope and rainfall treatments—One parameter model, flat surface (With data smoothing). . . . .	279
7.5	Model output for combination of slope and rainfall treatments—One parameter Model, flat surface (After zero correction). . . . .	280
7.6	Model output for combination of slope and rainfall treatments—One and two-parameter models, flat surface (after correction for zero-runoff period). . . . .	283
7.7	Model output for combination of slope and rainfall treatments—Two parameter model, surface treatment II. . . . .	286
7.8	Model output for combination of slope and rainfall treatments—Two parameter model, surface treatment III. . . . .	289
7.9	Model output for combination of slope and rainfall treatments—Two and three parameter model, surface treatment IV. . . . .	290
7.10	Model output for combination of slope and rainfall treatments—Two and three-parameter models, surface treatment V. . . . .	293
7.11	Summary of simulation runs for small-scale field experiment. . . . .	297
7.12	Model output for two Exponential Distribution Function Models. . . . .	304

7.13 Results of simulation runs with various fixed values of $k_b$ , Essex test sub-watershed. . . . .	305
B.1 One-way analysis of Variance of data for key variables. . . . .	341
B.2 One-way analysis of Variance of data for key variables. . . . .	342
B.3 One-way analysis of Variance of data for key variables. . . . .	343
B.4 One-way analysis of Variance of data for key variables. . . . .	344

# List of Figures

2.1	The optical arrangement of the laser profiler system. . . . .	21
4.1	Raingauge distribution . . . . .	48
4.2	Typical runoff curve used for rainfall simulator calibration. . . . .	51
4.3	Various rainfall treatments. . . . .	56
4.4	Typical data-logger calibration curve . . . . .	58
4.5	Observation of runoff at various temporal scales. . . . .	60
4.6	Runoff measurement via rotating turntable and datalogger and their comparison. . . . .	61
4.7	Definition sketch for depression storage. . . . .	62
4.8	Constructed positive and negative mold . . . . .	65
4.9	Surface treatment II within the flume. . . . .	66
4.10	Various surface treatments. . . . .	67
4.11	Runoff plots, University of Guelph, Ontario, Canada. . . . .	73
4.12	One of micro-catchment after removing vegetative cover . . . . .	76
4.13	One of the micro-catchments after sealing of the surface. . . . .	77
4.14	The control logic of the laser scanner electronics. . . . .	81
4.15	The relationship between laser scanner bit number and relative elevation. . . . .	83
4.16	One of the micro-catchments during the course of scanning. . . . .	86
4.17	Rate of water depletion for different plots. . . . .	88
4.18	Location of pilot watersheds in Southern Ontario. . . . .	93

5.1	Frequency histogram and some relevant statistics for DEMs for three micro-catchments. . . . .	101
5.2	Experimental variogram along three different directions, Plot I. . . . .	104
5.3	Experimental variogram along three different directions, Plot II. . . . .	105
5.4	Experimental variogram along three different directions, Plot III. . . . .	106
5.5	Variogram modeling-Single structure. . . . .	110
5.6	Variogram modeling-Double structure. . . . .	111
5.7	Variogram modeling-Triple structure. . . . .	112
5.8	Histogram and selected statistics of DEM for plot I. . . . .	119
5.9	Adjusted histogram and surface-shaded relief display for plot I. . . . .	120
5.10	Adjusted histogram and surface-shaded relief display for plot II. . . . .	121
5.11	Adjusted histogram and surface-shaded relief display for plot III. . . . .	122
5.12	Total ponded area as a function of grid spacing for various plots. . . . .	133
5.13	Total depressions volume as a function of grid spacing for various plots. . . . .	134
5.14	Total number of depressions as a function of grid spacing for various plots. . . . .	136
5.15	Contributing area as a function of pond area in $cm^2$ for various plots . . . . .	137
5.16	Contributing area as a function of pond area in pixel units for various plots. . . . .	139
5.17	Spatial mapping of depression for various grid spacing, plot I. . . . .	143
5.18	Spatial mapping of depression for various grid spacing, plot II. . . . .	144
5.19	Spatial mapping of depression for various grid spacing, plot III. . . . .	145
5.20	Spatial mapping of depression for various grid spacing, plot I (Elimination of first column). . . . .	149
5.21	Spatial mapping of depression for various grid spacing, plot I (Elimination of first row). . . . .	150
5.22	Spatial mapping of depression for various grid spacing, plot I (Elimination of second row). . . . .	151

6.1	Catchment response of various surface treatments for different rainfall patterns and slopes. . . . .	164
6.2	Cumulative storage of various surface treatments for different rainfall patterns with different slopes. . . . .	165
6.3	Catchment response of various surface treatments for different rainfall patterns, $S = 10\%$ . . . . .	166
6.4	Cumulative storage curves for various surface treatments for various rainfall patterns and $S = 10\%$ (potential storage= $911 \text{ cm}^3$ ). . . . .	167
6.5	Catchment response comparison for various plots for MLH rainfall pattern-plastic cover. . . . .	179
6.6	Catchment response comparison for various plots for different rainfall patterns-wet condition. . . . .	180
6.7	Cumulative storage + infiltration curves of various plots for different rainfall patterns-wet condition. . . . .	181
6.8	Catchment response comparison for various plots for different rainfall patterns-dry condition. . . . .	182
6.9	Cumulative storage + infiltration curves of various plots for different rainfall patterns-dry condition. . . . .	183
6.10	Sample observed runoff hydrographs-PWS Watershed in Southern Ontario. 190	
6.11	Sample observed storage graphs-PWS Watershed in Southern Ontario.	191
6.12	Comparison of cumulative storage curves for laboratory and field experiment, MLH rainfall pattern . . . . .	196
7.1	Schematic arrangement of stores in a typical hill-slope . . . . .	201
7.2	Typical network of reservoirs and conduits. . . . .	202
7.3	A typical node (a). Non-leaky capacitor (b). Leaky capacitor. . . . .	202
7.4	System configuration. . . . .	213
7.5	Micro-catchment outflow hydrograph for nodes (1,3), (2,3), (3,3). . . . .	215

7.6	Total outflow from the micro-catchment. . . . .	217
7.7	Effects of surface storage components on outflow hydrograph. . . . .	218
7.8	Outflow hydrograph for changed position of one large depressions. . .	219
7.9	Effects of channel resistance on outflow hydrograph. . . . .	220
7.10	Outflow hydrograph for different position of resistive elements. . . . .	221
7.11	Effects of rainfall intensity on outflow hydrograph. . . . .	222
7.12	Effects of initial condition on outflow hydrograph. . . . .	222
7.13	Variation of voltage level at node (2, 3) with time. . . . .	223
7.14	Point representation of runoff production . . . . .	233
7.15	Basin representation by storage elements of different depths and their associated density function. . . . .	235
7.16	Direct runoff production from a population of stores . . . . .	238
7.17	Evolution of the water profile across non-interacting stores of different depth in response to net rainfall, $\pi_i = (-2, -2, 2, -1, 5)$ , falling in successive time intervals with storage full at $t = 0$ . . . . .	240
7.18	Calculation of basin soil-water deficit and actual evaporation at time $t$ .	243
7.19	Water level across stores of different depth according to the equal stor- age mode of water distribution. . . . .	250
7.20	Graphical representation of storage capacity distribution and its rela- tionship to $S(t)$ and other variables. . . . .	251
7.21	Basin direct runoff production for probability-based infiltration capa- city model. . . . .	265
7.22	Graphical representation of observed vs. simulated runoff for various rainfall patterns before data smoothing, flat surface at $S = 10\%$ . . . .	278
7.23	Graphical representation of observed vs. simulated runoff for various rainfall patterns after zero correction, flat surface at $S = 10\%$ . . . . .	281
7.24	Graphical presentation of observed vs. simulated runoff for various rainfall, plot treatments and antecedent moisture conditions . . . . .	301

7.25 Graphical presentation of observed vs. simulated runoff for two typical events . . . . .	305
A.1 Catchment response of surface treatment I for different rainfall patterns and slopes. . . . .	332
A.2 Catchment response of surface treatment II for different rainfall patterns and slopes. . . . .	333
A.3 Catchment response of surface treatment III for different rainfall patterns and slopes. . . . .	334
A.4 Catchment response of surface treatment IV for different rainfall patterns and slopes. . . . .	335
A.5 Catchment response of surface treatment V for different rainfall patterns and slopes. . . . .	336
A.6 Catchment response of various surface treatments for different slopes, LMH rainfall pattern. . . . .	337
A.7 Catchment response of various surface treatments for different slopes, HML rainfall pattern. . . . .	338
A.8 Catchment response of various surface treatments for different slopes, MLH rainfall pattern. . . . .	339

# Chapter 1

## INTRODUCTION

It has been acknowledged that surface depressions/micro-relief play a significant regulatory role in the generation of surface runoff and the yield of sediment (Dunne et al., 1991; Hairsine et al., 1992; Huang and Bradford, 1992). Linsley (1967) emphasized the importance of catchment-surface features in the following way:

The model (Stanford Watershed Model) suggests certain long-term data problems which should be seriously considered now. Experience with the model has been that the most important part of the total runoff process is the land surface phase. If the storage and retention on the surface and the infiltration losses are not correctly modeled, it is impossible to reproduce the hydrograph. On the other hand, if the land surface model is effective and produces an accurate time distribution of runoff increments, *a relatively simple storage routing procedure* is sufficient to reproduce the hydrograph with considerable accuracy. It is probable that the nonlinearity indicated by many analyses of stream hydrographs is as much a result of incorrect assessment of the runoff increments and improper treatment of the division between surface runoff and inter-flow as any other possible causes.

Many hydrologic phenomena and transport processes occurring on or across the land surface are associated with rainfall-runoff transfer. Erosion, sedimentation and transport of plant nutrients, pesticides and pollutants are examples of phenomena closely associated with the rainfall-runoff process. Consequently, due to the “piggy-back” nature of non-point-source-pollution models, any improvement in the performance of rainfall-runoff models will have a major impact on subsequent results. For accurate modeling of such phenomena throughout a catchment, one needs to know not only the temporal variation in discharge at the catchment outlet, but also the temporal variation in the storage and transmission of water everywhere throughout the catchment. Most hydrologic and water quality models represent the three-dimensional nature of surface topography very crudely, and therefore do not represent the spatial distribution of hydrologic processes very well.

Agricultural lands or other watershed surfaces have varying degrees of micro-relief surface storage. In some specific situations, these surface depressions and/or micro-relief have been utilized in ways which are useful for dealing with/managing land resources. This storage is highly dependent on the recent history of the soil surface, as it is modified by the action of rain, wind, tillage and cultivation practices, and will manifest itself at a range of spatial scales. Micro-relief storage at various spatial scales can be used to enhance soil and water conservation. This is accomplished mainly by adapting tillage methods that produce rough surfaces with high relatively surface storage, thereby increasing infiltration, reducing surface runoff and water erosion.

However, the manner in which surface micro-relief affects surface hydrology is quite complex. Dunne et al. (1991), while investigating the effects of micro-topography on

infiltration argued that since micro-topography appeared to be so important in affecting infiltration as well as local flow, it is surprising that the hillslope characteristic has received scant attention in hydrologic studies. Furthermore, in reviewing the literature on the impact of micro-relief surface storage on catchment response, Hairsine et al. (1992) realized that models of overland flow are sensitive to soil micro-topography and surface pore structure. The former affects depressional storage and consequently the routing of overland flow, while the latter affects soil hydraulic properties, notably the infiltrability.

The complex nature of the watershed surface features along with other attributes such as soil hydraulic properties, climate, soil-water content, vegetative cover, geology and their interaction with each other restricts the extrapolation of information obtained at small scales to larger scales. Hence, there is a need for such tools as a proper model structure to safely transfer information between various spatial scales. In the case of mathematical models, surface properties of catchments have been among the factors which have not received proper attention in an objective way, resulting in varying degrees of discrepancy between simulated and observed responses (Beven, 1989; Grayson et al., 1992b).

Attempts have been made to deal with some of these complexities. Indeed, the literature is replete with various types and forms of transport process techniques for modeling water and solute movement on and/or across the land surface. However, a common feature in all such modeling approaches is that the investigator was somehow concerned with macroscopic aspects of surface topography such as diverging, converging or plane elements of a complex watershed, whereas the scale of soil erosion

and overland flow processes is more or less comparable to microscopic aspects of surface topography (Goodrich et al., 1991; Kibler and Woolhiser, 1970; Moore and Grayson, 1991; Singh and Woolhiser, 1976). Application of such methods is justified as long as the ground surface is relatively smooth. For surfaces where the scale of roughness is similar to flow depth, neither the macroscopic viewpoint nor the St. Venant equations and simplification such as the kinematic wave approximation is appropriate (Goodrich et al., 1991).

To date, our ability to characterize surface relief is quite inadequate for modeling hydrologic and associated processes in situations where management of the surface plays a significant role. In light of this shortcoming, another situation requiring attention for hydrologic modeling is the case when the slope of the land is mild and the surface is characterized by numerous depressions (Dunne, 1995). For such a surface, when the rainfall intensity exceeds the infiltrability, micro-relief surface depressions begin to fill. Since the depressions vary in size, some will begin to overflow before others are being filled, thus initiating runoff. Meanwhile, infiltration continues and the rainfall may increase or decrease in intensity, or cease. Linsley et al. (1949) noted that micro-relief depressions of various sizes can be superimposed and interconnected, and that each depression has a unique contributing area of its own. This chain of events continues with successively larger portions of overland flow contributing water to streams, until such time as all depression storages within the basin are filled. Water held in depressions at the end of a rainfall event will stay there for a period of time and will be depleted either by evaporation or infiltration. Thus, the process of micro-relief and its interaction with surface runoff is quite complex.

For a realistic simulation of catchment response, a conceptual hydrologic model must account for the rate of accretion to and depletion from depressional storages. A pertinent question is: How should a rainfall-runoff model be structured to accommodate spatial variations in depressional storages? Since the pioneering work conducted by Ullah (1974), not much research has utilized his findings regarding the frequency distributions of various features of depression storages. Quantification of various features of depressional storages (Ullah and Dickinson, 1979a; Ullah and Dickinson, 1979b), and their spatial scaling (Huang and Bradford, 1990a), has been successfully undertaken in the past. What remains to be accomplished is to investigate on a quantitative basis the effects of the spatial pattern of depressional storages on catchment response.

The general objective of this study has been to model the movement of water from surfaces characterized by numerous depressions, building upon previous work done in this regard. Acknowledging the two main processes of lagging and routing in rainfall-runoff modeling, a mixed probability distribution approach for both storage and time of travel has been adopted, whereby measurable inputs are transformed into outputs via a convolution integral. The form of the probability distribution being proposed for both surface storage and time of travel has been drawn from independent research done in this regard (Pilgrim, 1977; Ullah, 1974).

The theoretical background to the cited problem as it exists in current literature is reviewed in Chapter 2, while the specific objectives of this study are listed in Chapter 3. The study area along with details of experimental methods is covered in Chapter 4. Chapter 5 reports on pond characterization and quantification, while

Chapter 6 reports on the presentation and discussion of rainfall-runoff experimental results. Chapter 7 is totally devoted to modeling studies, starting with structuring of the model to accommodate spatial patterns of depressions: first, in an electrical analog sense; and then using a probabilistic model to accommodate spatial patterns of depression in a hydrological sense. In Chapter 8, results of the study are summarized and discussed, some conclusions drawn and recommendations for further study made.

## Chapter 2

# LITERATURE REVIEW

### 2.1 Introduction

In the hydrologic cycle, water either moves through the cycle or is stored in some parts of the cycle some of the time. These two mechanisms of transmission and storage are responsible for the timing of various processes of the hydrologic cycle in space, and are dealt with by such means as routing and lagging, using convection and diffusion equations or direct solution of the momentum equation and the continuity equation. To convert rainfall to runoff, the cited transmission and storage mechanisms have been included in various ways in various models. This review of literature focuses primarily on storage elements over the ground surface and the manner in which these elements have been dealt with in various hydrologic models at various spatial scales.

As there has not been universal agreement on fundamental spatial units (i.e. plot, field, ...) for watershed work, the classification suggested by Ponce (1989) has been adopted to deal with storage and translation. This classification was based mainly on the spatial and temporal variability of rainfall and the lack or availability of a channel

storage effect. According to this classification, a small catchment lacks both spatial and temporal variability of rainfall and the channel storage effect is not dominant. For a midsize catchment, temporal variability in rainfall is allowed, but neither spatial variability in rainfall nor a channel storage effect is present. For a large catchment, both spatial and temporal variability in rainfall as well as a channel storage effect are present.

For the sake of convenience, literature regarding the inclusion of surface storage and transmission mechanisms in various models at different spatial scales is reviewed according to the evolution of scientific hydrology. For example, at early stages of hydrologic research, these two major mechanisms were included by means of a conceptual store and the convolution of either a unit hydrograph or an area per time vs. time concentration curve. After the 1960's, with the tremendous advance in digital computer technology, attention was switched to a continuum-mechanics approach, so that the continuity equation combined with the momentum equation and the resulting partial differential equation is solved by means of numerical methods. Another approach, similar and parallel to conceptual modeling but somewhere in-between the two approaches mentioned above was adopted by a few researchers. They tried to deal with surface storage and transmission in a probabilistic sense. In addition to the modeling research, a few studies which were undertaken to collect elevation data and measure characteristics of surface storage at different spatial scales are reviewed separately.

The review of literature also touches on key concepts such as partial contributing areas and dominant runoff mechanisms to pave the way for a delineation of major

shortcomings in recent rainfall-runoff modeling. The review concludes with some lessons to be learned for the development of a holistic type of rainfall-runoff model.

## 2.2 Storage Routing Models

In almost all modeling exercises in this category, the raw precipitation data have been first converted to rainfall excess either explicitly or implicitly in a decoupled way, by hypothesizing the dominant runoff mechanism (i.e. Hortonian or Dunne mechanisms to be explained later) and then the resulting rainfall excess hyetograph has been used for further analysis. The runoff hydrograph is computed by routing rainfall excess through a model representing storage in the drainage basin. The storage considered is only temporary storage, and not the water retained over a period that is long in comparison to the response time of the hydrograph. Storage in this context is the total volume of water in transit to the basin outlet. This conceptualized storage is located primarily in the channels throughout the drainage basin, comprising the main stream, tributary channels, and the contributing area component of storage in overland flow over the surface of the drainage basin that feeds into the channels.

The volume of storage  $S$  at any time in each element of the drainage basin system has often been related to the corresponding discharge  $Q$  in that element at the same time. The most common form of the assumed relationship is:

$$S = kQ^m \tag{2.1}$$

where  $k$  and  $m$  are dimensional and dimensionless parameters, respectively. If  $m = 1$ ,

the system is linear. The corresponding discharge is the outflow discharge from the storage. It can be seen that the storage described above is highly distributed in a physical or spatial sense.

For small catchments, the Rational Method was one of the earliest attempts to model outflow peak (Dooge, 1973). At first only the translational component of runoff was incorporated into that simple model by forcing the rainfall duration to be equal to the time of concentration of the catchment. Later with the introduction of the runoff coefficient,  $C$ , a damping aspect was also incorporated into the model.

For midsize catchments, the so called "time-area method" was one of the earliest attempts to model surface runoff hydrographs. The time-area method is essentially an extension of the runoff concentration principle in the Rational method, accounting for translation only but not including a storage effect. In this method, the rainfall-excess hyetograph is convoluted with the area per time vs. time concentration curve to produce a time wise variation of runoff at the catchment outlet (Laurenson, 1964). Another approach somewhat parallel to the time-area method, was adopted by Clark (1945) to model the runoff hydrograph. In his method, a unit effective rainfall along with an area per time vs. time concentration curve was used to produce the "unit hydrograph" for the catchment. Since the unit hydrograph calculated in this way lacked runoff diffusion, Clark (1945) suggested that the resulting unit hydrograph be routed through a linear reservoir.

Another noteworthy effort was the cascade of linear reservoirs proposed by Nash (1957). Such a cascade has been a widely used method of hydrologic catchment routing. As its name implies, the method is based on the connection of several linear

reservoirs in series. For  $N$  such reservoirs, the outflow from the first is taken as inflow to the second, the outflow from the second as inflow to the third, and so on, until the outflow from the  $(N - 1)$ th reservoir is taken as inflow to the  $N$ th reservoir. The outflow from the  $N$ th reservoir constitutes the outflow from the cascade of linear reservoirs. Dooge (1959) subsequently developed the background theory for all such conceptual models. He envisioned a catchment as being conceptually equivalent to a series of alternating linear reservoirs and linear channels. This conceptualization has enabled him to realistically introduce catchment shape effects into his formulation in light of which previous efforts such as the Rational Method, the time-area method, Clark's unit hydrograph and a cascade of reservoirs represented special cases. For large catchments, storages have been arranged to represent the stream network of the drainage basin. The distributed nature of storage has been represented by separate series of concentrated storages or other forms of storage for the main stream, major tributaries and their contributing areas, providing a degree of physical realism. Models such as RORB (Laurenson and Mein, 1988) and Watershed Bounded Network Model (WBNM) (Boyd et al., 1972) are examples of this category.

The RORB model is the most widely used storage routing model. This model has superseded the unit hydrograph for estimating outflow hydrographs (Laurenson and Mein, 1988). In this model, the drainage basin is divided into number of subareas based on watershed boundaries. Nodes, which are points of input and output within the model, are located at centroids of subareas for input of rainfall excess, at confluences of streams for hydrograph additions, upstream and downstream of reservoirs, at diversion sites, and at gauging stations and at design sites. Nonlinear concentrated

storage elements, as described by Eq. (2.1), are used for each reach. The RORB model is efficient from a practical point of view, because it embodies much of the physical nature of the drainage basin and has one calibration parameter which corresponds to  $k$  in Eq. (2.1).

The Watershed Bounded Network Model (WBNM) is similar to the RORB model (Boyd et al., 1972; Boyd et al., 1987). The storages apply to subareas rather than to the channels between nodes. The model also incorporates a more detailed consideration of basin geomorphology. Two types of subareas are used in the model. It includes ordered basins where only rainfall excess is transformed to streamflow at the outlet, and inter-basin areas where upstream runoff is transmitted through the subareas in a main channel; and there is the transformation of rainfall excess to streamflow.

## 2.3 Distributed Watershed Models

Detailed system models of catchment behavior represent a different component of the modeling spectrum when compared to storage routing models. In this class of models, mechanisms of reservoir and channel action are introduced in a distributed fashion by combining continuity and momentum equations.

For small-sized catchments (i.e. hillslopes), one of the earliest attempts at modeling overland flow was initiated by Wooding (1965a, b, c). In his approach, a complex watershed was modeled as two symmetrical lateral planes contributing to a channel bisecting the area. Schematically, the model could be likened to a tipped-open book with the channel in the center, so that there is a lateral slope for the planes but also a down channel slope for the channel and planes. In Wooding's approach, the kinematic

version of the Saint Venant equation was solved analytically using the method of characteristics.

Kibler and Woolhiser (1970) considered the kinematic cascade model, involving a number of discretized planes. In their approach, each plane was allowed to have its own characteristics, resulting in a distributed model. Parlange et al. (1981) also examined flow over a plane, presenting a general analytical solution with excess rainfall being a function of time. Singh and Woolhiser (1976) investigated kinematic flow on an inverted cone (i.e. with converging elements); and examination of flow on a regular cone (i.e. with diverging elements) was initiated by Singh and Agiralioğlu (1981a; b). Such surfaces may represent parts of a watershed, or be used as basic building blocks for a complete watershed.

A comprehensive physical science approach to partial-area quantification within a hillslope was pioneered by Freeze (1972a, 1972b) . By coupling subsurface flow and channel flow, the variable source area concept was given a coherent structure by the mathematical model describing the generation of runoff from a hillslope and small upland catchments. The model yielded numerical solutions to equations describing saturated and unsaturated subsurface flow, return flow, direct precipitation onto saturated areas and flow in small channels. Freeze (1972b) investigated runoff production under a range of rainfall storms, soil conductivity, hillslope shape and soil thickness. In that study, the occurrence of overland flow was deliberately avoided by selecting large values for soil hydraulic conductivity. Subsurface storm-flow occurred (as observed in the field studies) due to the impedance of permeable soils. Most of the infiltrating water was stored within the soil, raising the water table to the land

surface over an expanding area. Return flow occurred over the saturated area, as the lower part of the hillslope became a seepage face. The rise of the water table was fed mainly by vertical percolation rather than by horizontal seepage, and the production of overland flow depended upon development of the subsurface flow system.

Smith and Woolhiser (1971a) coupled an overland flow model (in the form of a kinematic cascade) to a subsurface flow model, in the sense that they determined infiltration from the plane at any point with a one-dimensional, vertical saturated-unsaturated flow calculation. Coupling of all three kinds of flow (i.e. overland flow, subsurface flow and channel flow) in a physically-based fashion was hampered by large spatial and temporal variabilities of soil hydraulic properties, and of relevant physiographical conditions (Van de Griend and Engman, 1985). A fundamental lack of correspondence between the theoretical models and reality was the major limitation of the approach (Freeze, 1978).

Engman and Rogowski (1974), using the partial-contributing-area concept, tried to simulate infiltration-excess overland flow in a physically-based deterministic manner. Their model attempted to account for natural hillslope variability in terms of necessary input, initial and boundary conditions. In this analysis, the initial soil-water content appeared to be the most important controlling parameter.

O'Loughlin (1981) using an analytical approach, concluded that the size of wet areas (contributing areas) in converging zones could be expected to be more stable than in the other two zones (i.e. plane slope or diverging slope). Under dry conditions, plane slope or diverging slope seepage may shrink back to the stream edge while converging wet zones tend to persist.

Among midsize and large scale watershed models for which surface storage has been tackled in a distributed manner, VSA1, VSA2 (Variable Source Area), SHE (Systeme Hydrologique Europeen), TOPOG and CASC2D are considered. In these models, variable source area concepts have been incorporated into the model structure either explicitly or implicitly.

In an attempt to improve the cost effectiveness of programs for targeting Best Management Practices (BMPs) in a Virginia watershed, Loganathan et al. (1989) used VSA2 to simulate watershed response. Based upon applications of the model, it was found that deterministic simulation was not always representative of the critical area growth pattern where large standard deviations in hydraulic conductivity occurred. As a result, hydraulic conductivity was treated as a log-normal, distributed, random variable. A Monte Carlo simulation procedure was adopted to compute water content for varying hydraulic conductivity.

Three European organizations (the British Institute of Hydrology, the Danish Hydraulic Institute, and the French consulting company SOGREAH) jointly developed the Systeme Hydrologique Europeen (SHE) model (Abbott et al., 1986a; Abbott et al., 1986b). In this model, all primary processes of the land phase of the hydrologic cycle are modeled in a separate component. Interception is modeled by the Rutter accounting procedure; evapotranspiration by the Penman-Monteith equation; overland and channel flow by simplifications of the St. Venant equations; unsaturated zone flow by the one-dimensional Richards equation; saturated zone flow by the two-dimensional Boussinesq equation; and snowmelt, by an energy budget method. The spatial distribution of catchment parameters, precipitation input and hydrolo-

gical response is achieved using orthogonal grid squares; and the model uses modular construction for the addition of new components. The model is physically based, and its primary components are modeled either by finite-difference representation of the partial-differential equations involving mass, momentum and energy conservation, or by empirical equations derived from independent experimental research. As overland flow and ground water flow are linked together by a one-dimensional, vertical-unsaturated flow model. The major assumption made in the model is that water can enter the stream channel only through either overland flow or ground water flow paths, but not from interflow.

TOPOG, a physically-based, distributed-parameter catchment framework, was developed at the CSIRO (O'Loughlin, 1990; Vertessy et al., 1993). It has been referred to as a framework because it involves several models which have been designed for a variety of problems. This package is divided into 2 parts: the terrain analysis software and the hydrologic models. The terrain-analysis procedures used in TOPOG are similar to those adopted in the TAPES-C package (Moore and Grayson, 1991), and have been employed recently in the THALES model (Grayson et al., 1992a). There are several hydrologic modules associated with TOPOG, but the one which is suitable for the detection of source areas is topog-dynamic (Vertessy, 1995), a fully distributed, transient model. One has the option of using two different forms of the Richards equation (1 implicit, 1 explicit solution) or a simplified bucket model which is analogous to TOPMODEL (except it is fully distributed). Infiltration/subsurface flow schemes are coupled to a kinematic wave overland flow model (there is also a sediment transport model coupled to it too).

Recently, Moore and Grayson (1991) used the “stream path” or “stream tube” analogy first proposed by Onstad and Brakensiek (1968) to partition a complex watershed into elements bounded by contour lines (equipotential lines) and streamlines. In this case, surface runoff enters an element orthogonal to the upslope contour line and exits orthogonal to the downslope contour line, with the adjacent stream lines being no-flow boundaries. For this form of partitioning a catchment, one-dimensional flow was assumed within each element, allowing water movement in a complex three-dimensional catchment to be represented by a series of coupled one-dimensional equations.

A common feature in all the above modeling exercises is that the investigator was somehow concerned with macroscopic aspects of surface topography such as diverging, converging or plane elements of a complex watershed, whereas the scale of soil erosion and overland flow processes is more or less comparable to microscopic aspects of surface topography. Application of such methods seems justified as long as the ground surface is relatively smooth. However, for surfaces where the scale of roughness is similar to flow depth, neither the macroscopic viewpoint nor the kinematic wave approximation is appropriate.

CASC2D (Julien et al., 1995) is considered to be the most recent development in two-dimensional hydrodynamic modeling of runoff processes. The physically-based CASC2D model simulates spatially-varied surface runoff while fully utilizing raster GIS and radar-rainfall data. The model uses the Green and Ampt method for infiltration, and the diffusive wave formulation for overland and channel flow routing enables over-bank flow storage and routing. This model can also handle infiltration-excess overland flow from moving rain-storms.

## 2.4 Probability-based Watershed models

Due to pertinent spatial and temporal variability in factors affecting rainfall-runoff processes including surface storage, a number of researchers have tried to adopt a compromise between the two school of thoughts regarding conceptual and distributed watershed modeling.

At the hillslope scale, Freeze (1980) used a stochastic-conceptual type approach to simulate the two distinct runoff mechanisms (Horton and Dunne Mechanisms) that can identify source-area generation on hillslopes. No redistribution of runoff was allowed in this approach. The time of travel routing technique was used to translate generated runoff to the catchment outlet. Results of this work have indicated that each of the parameters representing the spatial stochastic properties of the saturated hydraulic conductivity distribution on a hillslope exerts an important influence on the statistical properties of runoff events arising from a hillslope. The results of the study showed that the mean value of hydraulic conductivity is the most important parameter followed by standard deviation and autocorrelation function.

The conceptual advances made by a number of authors (Beven, 1977; Laurenson, 1964; Sugawara, 1961) were translated into procedures for representing the hydrologically important features of landscapes in TOPMODEL, a model proposed by Beven and Kirkby (1979) and further extended by Beven and Wood (1983). Beven (1977), recognizing a number of disadvantages associated with physical approaches to source area detection, developed TOPMODEL in an attempt to retain some of the advantages of the lumped model approach while taking into account benefits of the

distributed nature of the system considered to be important. TOPMODEL was originally developed for detection of the saturation-excess overland flow process (Beven and Kirkby, 1979), and later an infiltration-excess overland flow was also incorporated into the model (Sivapalan et al., 1987). In essence, TOPMODEL calculates the temporal deficit in readily-drained soil-water on a hillslope by a series of steady-state water balance calculations, by incorporating the spatial variation of macro-topography and soil properties. Recently this model has been used for categorizing watershed response in various basins (Larsen et al., 1994).

After recognizing the difficulties associated with using an optimization approach for parameter estimation for Explicit Soil Moisture Accounting (ESMA) models, Moore and Clarke (1981) and Moore (1985) adopted a new approach in which the catchment is considered to consist of a statistical population of soil-water stores. Runoff is generated through a soil-water accounting procedure; and a probabilistic description of soil-water storage and travel times is used for routing runoff. This results in a small number of model parameters. The derivatives of the Simple Least Square (SLS) objective function were continuous in the parameter space, which allowed the use of an efficient gradient procedure for parameter optimization. Although an elegant theoretical formulation was provided, the practical potential of the model remains unproven and independent verification of hypotheses embedded in the model structure has been lacking. Furthermore, it is not clear if the model's simple structure can account for variations in catchment response associated with different climatic regimes without extending the model to the point whereby it was originally developed. Full account of Moore and Clarke's model is provided in chapter seven.

## 2.5 Literature Review on Surface Profilers

The measurement of surface micro-topography has been attempted with various methodologies with varied degrees of success. Over the past few decades, a considerable amount of design work has been done on soil profilers. A chronological summary of their development has been presented by Zobeck and Onstad (1987) and Hirschi et al. (1987). Profilers can be categorized into two types: contact and non-contact. Contact soil profilers touch the soil surface with a rod or pin, measuring the distance from the soil surface to a reference plane. Non-contact profilers measure the distance from the soil surface to a reference plane without touching the surface and have for the most part superseded other methodologies. An obvious advantage of a non-contacting profiler is that it can be used on soft or fragile surfaces. These types of profilers have high scanning rates so that surface elevation can be measured quite rapidly. As well, surfaces with large elevational variations can be measured with a high degree of vertical and horizontal spatial resolution. Optical scanners can typically resolve elevation on the order of  $\geq 0.5$  mm for surfaces with an elevational variation of 350 mm.

Non-contact profilers use two types of sensors, optical and/or ultra-sonic. Design of ultra-sonic profilers has been discussed in Kolstad and Schuler (1980) and Robichaud and Molnau (1990). It would appear that optical profiler systems have become the accepted standard design based on their ability to provide very detailed elevational data for a wide range of surface types.

The most common optical, non-contact profiler design is based on triangulation principles which are illustrated in Figure (2.1). The principle upon which the scanner

operates is that a narrow beam of light from a laser source, projected normal to the surface, intersects the surface and the scattered light is collected by a lens system. An image of the point of intersection of the surface and the beam is focused on a linear photo-diode array mounted behind the lens. The position of the image on the array is a measure of the location of the surface. The resolution and range of the system depends upon the lens magnification as well as the number and spacing of the diodes. This type of design has been reported by Thwaite and Bendelli (1980), Huang et al. (1988) and Huang and Bradford (1990b).

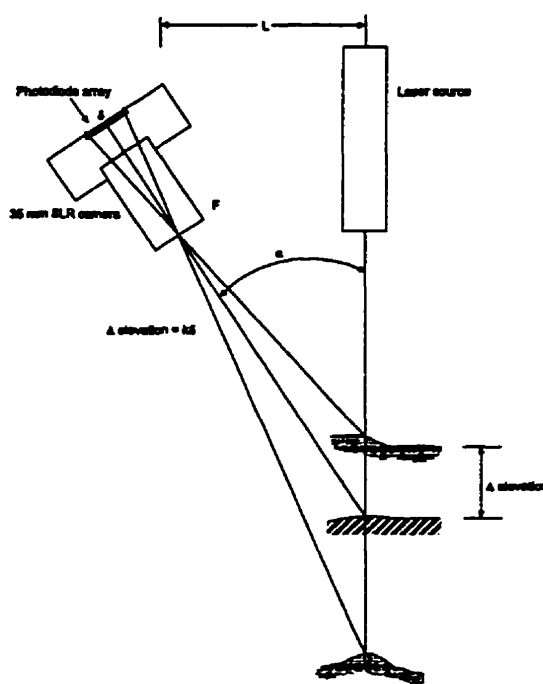


Figure 2.1: The optical arrangement of the laser profiler system.

This methodology has some deficiencies. According to Bertuzzi et al. (1990), a major pitfall of this method is the loss of the image of the spot on the array detector; the image may drop out when the optical axis of the lens is interfered by a soil aggregate. However, researchers utilizing triangulation-based laser scanners typically

find that for surfaces of elevational relief of less than 350 *mm*, the loss of data is less than 10 percent. Loss of data increases as elevation relief increases beyond a prescribed range and data is not allowed to be used if the percentage of bad data exceeds 20 percent loss.

Bertuzzi et al. (1990) have developed an alternative optical laser scanner based on the principle of "defect of focus". In this system, soil elevation is measured by projecting a laser beam normally to the surface and measuring the ratio of the referenced light intensity, which is the output of the central cell of a photo-diode array to the total light intensity measured by the entire array. Caussignac et al. (1990) have shown theoretically that this ratio is related to the variation of height of the laser spot due to the soil roughness.

## 2.6 Estimation of Micro-relief Surface Storage

Various researchers have characterized micro-relief surface storages using various degrees of rigor. At an early stage of surface-storage quantification, attention was focused either directly or indirectly on random roughness and its relationship with surface storage in the form of depression storage (Mitchell and Jones, 1976; Mitchell and Jones, 1978; Mwendera and Feyen, 1992; Ullah, 1974; Zobeck and Onstad, 1987).

Mitchell and Jones (1976) presented a power-law relationship between storage and depth based on the ranking of elevation data while disregarding the spatial position of elevation data. This research has found limited application because surface storage is a spatially-distributed process controlled by local topography. Mwendera and Feyen (1992), acknowledging the dynamic nature of surface storage, tried to capture

fluctuations in the random roughness by proposing the following exponential function:

$$RR = C_1 + C_2 \exp(-C_3P)$$

where  $C_1$ ,  $C_2$  and  $C_3$  are regression coefficients representing the effect of rainfall and soil properties. In this study, depression storage was determined by covering the test plot with a transparent microfilm similar to those used in wrapping cold foods. A polynomial relationship was developed to relate depression storages to random roughness and slope steepness. It was claimed that the developed relationship explains 99% of the variations in the data. Onstad (1984) reported similar observations from his investigations. Zobeck and Onstad (1987) concluded that tillage and rainfall have significant effect on random roughness.

Moore and Larson (1979) developed a computational procedure which incorporated the spatial nature of the surface-depressional pattern to quantify surface micro-relief surface storage. Onstad (1984) used this procedure to analyze digitized surfaces, and developed an empirical relationships between depressional storage, surface roughness and slope steepness. Ullah and Dickinson (1979a, b) used a slightly different procedure and showed that surface storage decreases with an increase in slope. A roughness parameter was not included in their study. The results of their study led to the following conclusions:

1. The spatial distribution of depressions on a surface has both random and direction-oriented components.
2. The available data indicate a significant relationship between land slope and

total volume of depression storage. The reduction in total volume of storage with increasing slope was both due to reduction in the number of depressions and reduced depths and surface areas of depressions.

3. There exist definable relationships among the three geometric properties of depressions (i.e. depth, area and volume) which could be used to compute one with the help of the other. The form of the relationships appears to be applicable to all sizes of depressions.
4. The frequency distribution of any of the three geometric properties can be approximated by the Weibull distribution.

Huang and Bradford (1990a) have examined, via a Monte Carlo type simulation, the geometric features of depressional storages for a Markov-Gaussian (M-G) type surface roughness model. The gist of their paper was to demonstrate the scale dependency of depressional-storage quantification. For a free drainage type boundary condition, they have obtained two scaling relationships: one relates the storage at zero slope to the sample length scale, and the other relates storage to slope. They found that these two relationships fully describe the surface storage characteristics of the M-G surfaces with the particular type of boundary condition.

Hairsine et al. (1992) realized that models of overland flow are sensitive to soil micro-topography and surface pore structure. The former affects depressional storage and consequently the routing of overland flow, while the latter affects soil hydraulic properties, notably the infiltrability.

## 2.7 Partial-Contributing-Area Concept

The concept that surface runoff (i.e. overland flow), does not originate uniformly from the whole area of a watershed was suggested by Betson (Betson, 1964; Betson et al., 1968; Betson and Marius, 1969). So-called partial-area hydrology was based on the division of a watershed into areas that produce surface runoff (contributing areas) and areas that do not produce surface runoff during a storm event. This areal delineation concept, and recognition of the dynamic nature of contributing areas, has provided an important framework for physically-based distributed watershed modeling. There have, however, been two basic problems associated with the identification and quantification of contributing source areas. *First*, partial contributing areas were originally described with respect to invariable surficial hydrological conditions (Betson, 1964). More evidence has revealed that a series of hydrological (Freeze, 1972b; Freeze, 1980), geomorphological, topographical (Beven and Wood, 1983) and pedological (O'Loughlin, 1981; O'Loughlin, 1990) conditions may be responsible for the existence of areas contributing to runoff. Thus a profound integrated knowledge of site-specific hydrological information is required, making generalization of the concept extremely difficult (Van de Griend and Engman, 1985). *Second*, the characterization of contributing areas is made even more difficult by their dynamic nature as opposed to the "fixed source areas" originally suggested by Betson (1964). Partial contributing areas have been found to vary seasonally and even during storms. Therefore, the identification and characterization of these areas has been based mainly on detailed field surveys as summarized by Dunne (Dunne, 1978; Dunne, 1983). In the

case of modeling of contributing areas, independent validation is extremely difficult if not impossible.

Remote sensing is the most promising tool for identification and quantification of such contributing areas. Two principle attributes of remote sensing contribute to its potential for the objective mapping of contributing areas. It provides spatial information, and specific wavelengths may be useful for the identification of vegetation differences, temperature differences and changes in soil-water content, all directly associated with contributing areas. However, the effectiveness of remote sensing has been restricted to date by the lack of sufficiently fine temporal and spatial resolution for delineating source areas.

## **2.8 Types of Runoff Mechanisms**

When rain and/or meltwater reach the surface of the ground, it encounters a filter that is of great importance in determining the pathways by which hillslope runoff will reach a stream channel. The paths taken by the water are determined by many characteristics of the landscape, uses to which the land is put, and strategies employed for soil conservation management. A spectrum of hydrological situations and runoff mechanisms are discussed in the following sections.

### **2.8.1 Infiltration–excess Overland Flow (Horton Mechanism)**

When the rate of rainfall or snowmelt is greater than the capacity of the soil to absorb water, surface saturation and ponding occur, resulting in the classical conceptual mechanism of runoff generation first espoused by Horton (Horton, 1933) and further

investigated by Chorley (1978). This mechanism of runoff generation is called Hortonian mechanism. Hortonian overland flow has been connected predominantly with arid and semi-arid regions, where surface vegetation is absent or sparse and the soils exhibit low infiltrabilities. In humid environments, such overland flow is also common when rainfall intensities are sufficiently high. According to criteria reported by Freeze (1980), the conditions necessary for generation of overland flow by the Horton mechanism are:

- A rainfall rate greater than the saturated hydraulic conductivity of the soil and,
- A rainfall duration longer than the required ponding time for a given initial soil-water profile.

### **2.8.2 Saturated and Unsaturated Soil-water Movement**

When water infiltrates into soil, it may be stored in the soil or may move toward stream channels by a variety of routes. If the soil or rock is deep and of uniform permeability, water in the unsaturated soil that is not held by capillary and other forces moves more or less downward to the zone of saturation. As rates of ground water flow through the zone of saturation are generally relatively slower than surface flow and underground flow paths are relatively long, leading to large storage amounts, most water taking these routes contributes to baseflow between rainstorms. Some ground-water discharge can contribute directly to stormflow hydrographs; and baseflows antecedent to stormflows can be significant in determining the size of flood peaks (O'Loughlin, 1981; O'Loughlin, 1986). In very permeable rock formations such as some fractured limestones and basalts, the rate of movement in the saturated zone

may be so rapid that a considerable amount of stormflow can originate from the ground water. Generally, however, water taking the longer and slower paths below ground dominates the baseflow component of streams rather than their stormflow.

Due to soil layering, percolating water may encounter an impeding horizon at some shallow depth, leading to a portion if not all of the water being diverted horizontally driven by a suction potential that dominates gravity potential, reaching the stream channel often by a relatively short route. Because of factors such as a shorter route, somewhat high permeability of topsoil and porous weathered rocks above unweathered less porous rock, and generally greater potential gradients in upper sloping horizons, subsurface water diverted horizontally often reaches stream channels more quickly than other ground water flow. Some of this water, sometimes classified as unsaturated soil-water movement or subsurface stormflow, can arrive at the channel network quickly enough to contribute to storm hydrographs.

### **2.8.3 Saturation-excess Overland Flow (Dunne Mechanism)**

In some parts of hillslopes, vertical and horizontal percolation may cause soil to become saturated throughout its depth; and surface saturation occurs not because of ponding on the surface, but due to the water table rising to the surface. Ponding and overland flow occur at the time when no further soil-water storage is available in the profile. When full saturation occurs, some of the water moving by the shallow subsurface path exfiltrates from the soil surface at lower surface elevations and reaches the stream channel as overland flow. Such water is often referred to as return flow. Rainfall occurring on the saturated soil areas cannot infiltrate, and therefore runs over

the surface; and this contribution to overland flow is difficult to separate from return flow. Storm runoff from these two sources has been classified as saturation-excess overland flow. Its movement over the surface allows it to attain sufficient velocities to reach stream channels during or shortly after rainstorms, and so such flow usually contributes to storm hydrographs.

Regarding the source and volumes of water available to be stored and transmitted over the ground surface, the Horton and Dunne mechanisms seem most important. The Horton mechanism is generally more common on upslope areas, while the Dunne mechanism is more common on near-channel wetlands. Hortonian overland flow occurs from the partial areas of hillslopes where surface hydraulic conductivities are relatively low, while Dunne overland flow is generated from partial hillslope areas where water table is shallowest. Both mechanisms lead to variable source areas that expand and contract through wet and dry periods, and often occur simultaneously within a given watershed (Freeze, 1980).

## 2.9 Major Shortcomings of Past Efforts

It is clear from past efforts that the development of watershed response models has traditionally followed a set pattern involving the following steps: (a) collecting and analyzing data; (b) developing a conceptual model which embodies important hydrological characteristics of a catchment; (c) translating the conceptual model into a mathematical model; (d) calibrating the mathematical model to fit historical data by adjusting various coefficients; and (e) validating the calibrated model using another historical data set. Some major shortcomings which have become apparent upon nu-

merous applications of this procedure are summarized and discussed in the following subsections.

### **2.9.1 Consistency Between Model Structure and Available Data**

Model building efforts can be usefully examined with reference to a spectrum (Young, 1978). At one end of the spectrum are proponents of the white box school of thought—those employing a deductive reasoning approach (pioneered by Horton, 1933). At the other end are proponents of the black box school of thought—those using an inductive reasoning approach (pioneered by Sherman, 1932). Proponents of each approach take existing theories and develop models for the problem under consideration. The major difference between the two approaches relates to the manner in which the experimental data are considered. In the white box approach, emphasis is placed on cause (i.e. input parameters); while in the black box approach, emphasis is placed on cause and effect, even if only in a crude manner. In the white box approach, emphasis is also placed on process description (without reference to available data); while in the black box approach, emphasis is placed on describing system behavior on the basis of system inputs and outputs.

Using a white box approach, the modeler tries to build a model based on existing theories regardless of the spatial and temporal resolution of data available. As a result, one tends to develop a model involving a large number of parameters without being too concerned about the data which are needed to support the model structure. Upon applying the developed model, the modelers or the users have often discovered that a small number of parameters from a set of many parameters were sensitive to output

response. In light of such results, one may raise the question: Are model results really insensitive to the remaining parameters, or are the available data not capable of capturing the dynamics of processes associated with these parameters? It could be argued that there should be a closer relationship between model building and the availability of data than there often has been in hydrologic modeling efforts.

With a black box approach, there is little hope of a complete system state description; as a result, there is virtually no chance of improving understanding of the internal behavior of the system. This kind of approach, therefore, is of prime importance when hydrology is considered to be fundamentally a machine for driving water resources projects (Klemeš, 1986a).

Moore and Clarke (1981), in reviewing difficulties associated with system identification of rainfall-runoff models, argued that the main problem is somehow concerned with the lack of a sound model structure. Difficulties which they identified included: (1) interdependence among model parameters, causing a large number of combinations of parameter values to yield similar low values of the objective function, further causing optimization methods to make very slow progress in such regions of the parameter space (interdependence may also be an indication of parameter redundancy); (2) indifference of the objective function to parameter values such that an appreciable change in the value of one parameter causes little or no change in the objective function; (3) 'discontinuities' or, more precisely, points in the parameter space at which the objective function while still continuous is non-differentiable, and (4) local minima caused by non-convexity of the objective function, leading to the search by means of an optimizing algorithm to be terminated at a point on the objective function surface

lower than all surrounding points, but with higher values than a point in another region of the surface.

From studies carried out with full-scale field data, there is considerable evidence that both white and black box approaches have yielded only limited success to date. Indeed, there is a debate in science between advocates of the inductive and deductive schools of thought (Phillips and Pugh, 1994). One possible resolution of this debate would be to combine the two schools of thought in order to take advantage of both, leading to grey box approach in which model building and experimental data would interact with each other. With such an approach, models and data would each drive and direct the other; good models would illuminate the type and quantity of data needed to test hypotheses; and data of good quality would permit development and validation of more complete models and new hypotheses (Dozier, 1992; Ward, 1984).

### **2.9.2 Internal Validation vs. External Validation**

Watershed response models of many kinds have been developed primarily to match estimated and measured hydrographs at the outlets of selected watersheds. This task can be argued to be relatively straightforward, given input-output data and a reasonable calibration procedure (Band, 1995). Based on this history, it can be concluded that accurate representation of internal watershed processes in such models is not required for them to be physically accurate, just properly calibrated. Unfortunately, failure to recognize hydrologic modeling as fundamentally involving curve fitting has contributed considerable ambiguity and mystery to this field of endeavor. For example many combinations of input parameters are equally likely to give rise to

plausible results (Andersson, 1992; Grayson et al., 1992a; Vertessy et al., 1993).

### **2.9.3 Hypothesis Testing**

An essential problem in hydrological science is to have or produce the right quantity of water with the right quality in the right place at the right time. This problem has always been present, and remains a real challenge for further investigation. The literature is literally full of attempts to address this problem with little success. Popper (1972) elaborated on such difficulties in this way. He drew a distinction between science and non-science on the basis of whether the hypothesis associated with any attempt to describe nature could be formulated in a manner such that it could be unambiguously falsified. Given currently available field observations regarding the behavior of environmental systems, “comprehensive” hydrologic models—enormously complex assemblies of a great many hypotheses—cannot be effectively falsified. The inability to falsify these models is a function of : uncertainty in the field data, which are heavily corrupted by noise; limitations in current methods of system identification; and, in the event of demonstrating a significant mismatch between the model outputs and observations, inability to distinguish among the multitude of hypotheses which could be false. In terms of the Popperian school of thought, the majority of what we have done in hydrological science should be classified as non-science, as we have been unable to validate our claims (Oreskes et al., 1994).

It has been suggested that hydrologic model structures as well as incorporated parameters should have a sound physical foundation, and that it should be possible to validate each of the structural components separately (Klemeš, 1986b). Further, the

models should be spatially and temporally transferable, and the parameters should be derivable from estimates of real world characteristics at any location. Finally, each model should satisfy the intended objective for a particular watershed for a range of possible conditions. There is much work yet to be done to achieve such goals.

#### **2.9.4 Scale Problem**

The term “scale” means different things to different people both within and among disciplines. In hydrology, we appear to be at the definition stage, with no overall agreement. To start, it would seem to be important to clarify the context in which we are using the word scale, as scale has different meanings in different contexts. Some of the contexts in which the word scale had been used in hydrology are summarized below:

1. With regard to hydrologic modeling, one can think of three different scales (both in time and space): the process scale, the observation scale and the model scale.

It would be interesting and helpful in a modeling exercise to have all of the above scales identical; unfortunately, this is seldom if ever the case. It was repeatedly mentioned in the literature that hydrologic processes should be addressed at their proper scale(s) (both spatial and temporal). What is meant here by scale? Is it indeed possible to find a proper scale for each process under consideration? Perhaps when we talk about scale in this context, we should use the phrase “scale of variability” instead of the word scale itself. Intuitively, one speaks of the spatial scale of a problem as the distance over which one must travel before some quantity of interest changes significantly.

Let us assume that we want to investigate the pattern of soil-water over the landscape. Two adjacent samples of soil, separated by 1 mm, are likely to have very similar soil-water contents (within the limits of sampling error of course). Conversely, soil samples separated by 1 km might be expected to differ greatly in soil-water content. An observer would understand that the relevant spatial scale was greater than 1 mm and less than 1 km. This example raises two points. First, when one speaks of scale, one is usually considering variability. The terms scale and scale of variability might very well be synonymous. Second, the appropriate spatial scale is likely to depend upon the variable of interest. For example, precipitation depths separated by 1 km might very well be identical, while the associated soil-water contents are likely to differ substantially. Therefore the spatial scale suitable for precipitation is likely to be very different from the spatial scale suitable for surface soil-water content. Intuitively, this discussion about spatial scales could be equally applied to time scales and temporal variability. An appropriate definition would then be that period over which one expects to see a significant change in the variable of interest.

2. Another important feature of scale which has a bearing on the present discussion is the lack of recognition of interconnectedness of scales of various processes in both time and space. This topic has received considerable attention in the finite difference branch of numerical modeling.

3. Whether dealing with small or large watersheds in hydrology, there is a need for an approach or theory that will allow prediction of an appropriate partitioning of rainfall for example at any scale of interest. This requirement for such a unified theory might be referred to as a scale problem. There is also a need for a theory that would allow

the use of information gained at one scale to be used appropriately and effectively for making predictions at other scales, be they smaller or larger. This too could be called a scaling problem, but alternatively has been termed an aggregation/disaggregation problem (Beven, 1995). In Geostatistical jargon, this is referred to as “change of support” (Clark, 1979; Isaaks and Srivastava, 1989). It is indeed a real challenge to know when and how to use point measurements to represent a variable over larger areas or when and how to use outputs (or algorithms determined from outputs) obtained at say a laboratory or small plot scale to represent a process at a field or watershed scale. Many geostatisticians suggest that there are tools for doing these things, such as Block Kriging; however, this claim is yet to be confirmed or validated.

4. Another context regarding the issue of scale relates to the design of optimum data-collection networks, with reference to the appropriate selection of: the number of sampling stations; the location of the stations; the sampling frequency, in time and the duration of the sampling program.

#### **2.9.5 Known Problem vs. Known Solution**

It has been stated that it is easier to look for a problem to fit a known solution than to look for a solution to a known problem (Klemeš, 1983). It has indeed become a bit of a habit in hydrology to fix the model and then to redefine the problem appropriate for the existing model. Perhaps needless to say, we ought better to define the problem as clearly and precisely as possible and then to try to develop or search for a model which addresses and pertains to the predefined problem.

## 2.9.6 Conceptual Understanding of Runoff Processes

Our conceptual understanding of surface runoff processes has reached a point where we know that as soon as rainfall intensities at the soil surface exceed the infiltrability, rainfall excess begins to fill surface depressions. We also know that the sequence of events which takes place after the development of rainfall excess requires recognition of the following facts (Linsley et al., 1949):

1. Each surface depression has its own capacity or maximum depth.
2. As each depression is filled to the capacity, further inflow is balanced by outflow plus infiltration and perhaps evaporation.
3. Depressions of various sizes are usually superimposed and interconnected. In other words, most large depressions encompass many interconnected small ones.
4. Each depression, until such time as it is filled, has a definite drainage area of its own.

Shortly after the beginning of rainfall excess, the smallest depressions can become filled and localized overland flow begins. Most of this water likely goes to fill larger depressions, but some of it may follow an unobstructed path to the nearest stream channel. This chain of events continues, with successively larger portions of overland flow contributing water to streams, until such time as all depression storage within the basin is filled. Water held in depressions at the end of a rainfall event will remain there for a period of time and then will be depleted either by evaporation or infiltration through the soil mantle. To date, there have been few if any efforts to model the above sequence of events in surface runoff modeling.

## 2.10 Lessons to be Learned From Past Efforts

From the literature review and discussion of shortcomings of past efforts in rainfall-runoff modeling, the following lessons or points have been identified for serious consideration for incorporation into a new rainfall-runoff model.

*First*, regarding the interaction between model structure and available data: comparing the soil surface environment with the atmosphere and the subsurface environment, it is clear that at least in the latter two, water flow is continuous over a defined field and prediction of flow is therefore amenable to solution by such schemes as finite difference or finite element methods. In the surface environment, the flow is more likely to be crossing through many different kinds of sub-environments and undergoing phase changes, e.g. evaporation; and the nature of the flow environment is very greatly influenced by the nature of environment itself. Numerical methods can be used to represent the surface environment only in continuous water bodies such as lakes and estuaries and to some degree in rivers. The land surface portion of the hydrologic cycle is too complex to be treated in this manner because of the complicated variations in the nature of the flow environment.

It follows from this that if we proceed first to describe the nature of the flow environment using all available data, we should then have identified the range of available options for modeling to a significant extent because as the data needed to support the model having been defined. This might be termed “data-determined modeling” (Maidment, 1995). Then we can use theory that is appropriate to the level of available data. In most cases, this theory will be much simpler than is normally

considered in process representation because the data clearly do not support a greater degree of sophistication. In essence, this approach excludes models which are much more complicated than are justified by the available data.

*Second*, as was noted in Subsection (2.9.1), a grey box approach seems most desirable. Taking that approach to hydrologic model building implies trying to integrate the best from the physically-based and conceptual schools of modeling in a landscape mosaic context (Andersson, 1992). In some respects, the two schools are actually not that different, since both depend on calibration, and both can lead to models which have routines where a simple formulation encompasses a number of different processes. However, joining the two approaches implies solving the governing flow equations, subject to constraints and thresholds provided by a conceptual understanding of the surface flow processes. Details about such a hybrid approach are provided in a subsequent chapter on model development.

*Third*, as far as internal validation is concerned, opinions regarding the success of any model should be linked to the purpose for which it was developed. There are at least three fields of application for runoff models (Andersson, 1992; Grayson et al., 1992b; Blöschl and Sivapalan, 1995): (i) practical interest in management of water resources and estimations of risk, (ii) testing of hypotheses regarding the scientific understanding of selected flow processes, and (iii) forecasting effects of future changes of climate, land use and management.

For (i), the success of a model may be determined from the fit obtained between measured and simulated flows. However, a “good fit” between measured and modeled runoff does not necessarily mean that the model offers a physically-correct description

of the processes involved.

For studies within fields (ii) and (iii), often also involving modeling of chemical or biological variables, it is necessary that the model works right for the right reason (Klemeš, 1986a). One way to address this issue is to use sub-catchment runoff for cross-checking. Ground-water levels and tensiometer readings within and around the watershed may also be useful for the above purpose. It has also been suggested to use spatial patterns of internal variables (i.e. variables internal to the model) to assess the accuracy of models within the catchment.

*Fourth*, efforts should be made to independently test various components of a model structure before the components are aggregated together.

*Fifth*, with regard to scale problems, the same model structure should be applied at a range of spatial scales (e.g. lab, field and watershed scales) under a range of climatic regimes to test its flexibility.

## Chapter 3

# PROPOSED RESEARCH

### 3.1 Major Hypothesis

The major theme of this research has been to investigate the effect of surface storage (i.e. depression storages) on catchment response at a range of spatial scales. The hypothesis can be stated:

The size and spatial distribution of surface storage elements (i.e. depression storages) over a watershed can significantly affect surface runoff response from that watershed, whatever its area.

### 3.2 Objectives of the Study

The specific objectives of the proposed study have been:

1. To measure and quantitatively describe surface depressions at various spatial scales (e.g. in the lab, on a micro-plot); in particular, the quantification should provide the following geometric features for each depression:
  - (a) x, y coordinate of lowest point,

- (b) x, y coordinate(s) of overflow point(s),
  - (c) Maximum depth of each depression above which water will start to overflow,
  - (d) Surface area at overflow depth,
  - (e) Volume or capacity at overflow depth, and
  - (f) Contributing area for each depression.
2. To investigate the stochastic spatial structure of various features of depressional storage including area, volume and maximum depth as obtained from analyses of digital elevation data by variogram modeling of these features;
  3. To measure and analyze runoff response from surfaces with various spatial patterns of depressions (e.g. in the lab, on micro-plots); and
  4. To develop a mathematical model for runoff response which takes into account the size and spatial distribution of surface depressions in a statistical sense.

### **3.3 Suggested Approach**

The research plan of operation proposed for the accomplishment of the above objectives can be summarized as follows:

#### **3.3.1 Preliminary Studies**

These studies included the development of a preliminary model and conduction of laboratory controlled experiments to address the research hypothesis.

#### **3.3.2 Field Studies**

The proposed field studies included quantification and mapping of depression storages in a spatial context for a few micro-catchments. They also involved the exciting of

each micro-catchment with rainfall of various temporal patterns, and the measurement and analysis of the corresponding surface runoff. Rainfall and runoff data were also collected at a plot/small watershed scale to test the possibility of using the same model structure at a range of spatial scales.

### **3.3.3 Model Studies**

Modeling studies include testing the model structure with collected input/output data and also hypothesis testing.

## Chapter 4

# EXPERIMENTAL METHODS

### 4.1 Introduction

The issue of scale both in time and space has received extensive attention in recent years, considered by many to have been a major obstacle in the objective description and evaluation of rainfall-runoff processes. As noted in the Literature Review, it has been argued that components of the hydrologic response (e.g. evapotranspiration, surface runoff and subsurface flow) of a land surface are functions of the extent of the area being considered. Changing the spatial scale of the study area could be expected to lead to a change in the dominant hydrologic processes, possibly changing outflow hydrographs and/or other outputs. Therefore, the experimental methods in this study were designed to collect data at different spatial scales with the hope of adopting a multi-scale modeling approach for the sake of testing hypotheses at a range of spatial scale.

Spatial scales used by various researchers in the past have included micro-plots (i.e. unit areas), plots (i.e. hillslopes), fields (i.e. zero order catchments) and watersheds

(i.e. higher order catchments). At an early stage of this research, the plan was to either collect or use existing data from a wide range of scales, such as that cited above. However, available resources and also time constraints hampered such a plan. Instead, in light of available resources, the experimental design and collection of data were limited to three distinct spatial scales: a small-scale laboratory experiment, a small-scale field experiment and large-scale field experiment, being somewhat analogous to a micro-plot, a field and a watershed respectively. The collected data could be further classified into two distinct types: details about surface depressions (on the laboratory and small plot surfaces), and rainfall:runoff data (for the laboratory, small plot and small watershed scales).

In this chapter, a rationale is offered for the selection of each of the spatial scales, and the experimental apparatus used for each scale briefly explained. Sample experimental runs used to calibrate various facilities associated with each spatial scale are explained in some detail, and the possibility of incorporating various treatments such as surface treatments, slope adjustments and temporal rainfall patterns are explored. In moving from the smallest scale to the larger scales, the degree of control over the system decreased dramatically, so that for the large-scale field experiments no treatment was controlled.

## **4.2 Small-scale Laboratory Experiments**

### **4.2.1 Experimental Flume**

A question that was addressed at a very early stage was: Should a laboratory experiment be conducted? Such an experiment was justified in the following manner:

- Laboratory experimental setups represent about the smallest scale at which hydrologic processes are explored;
- An excellent facility offering considerable versatility, was already conveniently available in the School of Engineering Research and Development Laboratory, University of Guelph;
- The versatility of the facility allowed the introduction of substantial control on most variables of interest; and
- In this particular experimental design, the laboratory facility could also be used to calibrate instruments to be used in the field.

The flume used for the laboratory experiments was designed and built in 1987 for these and research reported by Tossel (1987) and Mackenzie (1995). The dimensions of the flume, 0.69 m wide  $\times$  1.52 m long, were determined largely by the areal coverage and uniformity of available simulated rainfall (Tossel et al., 1990) and the development of a convenient, effective runoff measurement instrument. The available facility could be fitted with a variety of fiberglass surfaces relatively easily and at reasonable cost. The overall slope could be set to any gradient between 0 and 14%. The soil flume was supported on a rigid steel frame on wheels, with a depth of 26 cm acting as a support for the fiberglass surface used in this study.

A detailed description of the flume and associated equipment, including the rainfall simulator, nozzles and runoff collection devices can be found in Chapter Four of Mackenzie (1995). Key apparatus elements used in the present study are discussed below.

### **4.2.2 Rainfall Simulator**

For the sake of expediting micro-scale hydrologic studies in the laboratory and field, the Guelph Rainfall Simulator II (GRSII) was developed by Tossel (1987) and later modified and used by Guy (1990) and Mackenzie (1995). The most recent model employs continuous-spray, wide-angle, low to medium to high flowrate, full-jet nozzles to reproduce storm intensities ranging between 20 and 200 mmh<sup>-1</sup>. Modifications include a capability for switching the nozzles automatically without a need to change nozzle height or cease rainfall application. Three nozzles were selected for use in this study: the Spraying Systems Inc. 1/8GGSS4.3W, 1/4GGSS10W and 3/8GGSS20W wide angle nozzles. The ability to switch between nozzles to create a single rainfall event was achieved via connecting the nozzles to the main water supply line by short high-pressure rubber hoses. Water supply to these three short hoses was controlled by solenoid actuated on:off valves.

Calibration of the rainfall simulator involved the development of relationships between simulated intensity and spatial uniformity, on the one hand, and nozzle size, nozzle water pressure and height of nozzle above the study surface, on the other. The gravimetric and volumetric methods employed to calibrate the rainfall simulator are described in subsequent sections.

### **4.2.3 Rainfall Simulator Calibration**

Two options, a gravimetric method and a volumetric method, were used to calibrate the rainfall simulator. Each option had its advantages and disadvantages, as explained below.

### Gravimetric Method

Small plastic cups, with wall diameter narrower than 1.0 mm, were used as test rain gauges in the laboratory setup. These rain gauges were placed throughout the study flume on a regular  $160 \times 160$  mm grid, as shown in Figure (4.1). The inside diameter of each gauge at the upper lip was 59 mm.

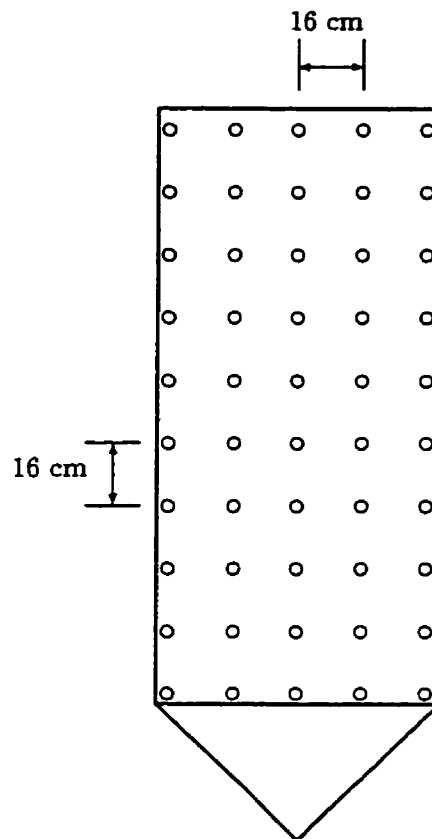


Figure 4.1: Raingauge distribution

A range of nozzles were calibrated for simulated rainfall intensity and spatial uniformity for a range of water pressures and at a number of nozzle heights. The nozzle specification, pressure and height combinations are summarized in Table (4.1). The nozzle height was measured from the nozzle outlet to the top of the measurement

gauge located directly beneath the nozzle; and results of calibration runs for 110 and 130 cm heights were used for field experiments (described in Section 6.3.1), while results of calibration runs for 170 cm were used for the laboratory experiments. Calibration runs were 30 minutes in duration, except when the intensity was high enough to fill the rain gauges before this time elapsed; and the runs were performed with the experimental flume set at a mean slope of 10%. After each calibration run, the volume of rain collected in each gauge was recorded and converted to a depth of simulated rainfall in mm. The average rain intensity over the study area was computed to be the arithmetic mean of the gauge catches; and the spatial uniformity coefficient was found using the Christiansen (1942) method:

$$UC = 100 \times \left( 1 - \frac{\sum_{i=1}^n |x_i - \bar{x}|}{\sum_{i=1}^n x_i} \right) \quad (4.1)$$

where  $UC$  = coefficient of uniformity,  $x_i$  = amount of rain in  $i$ th rain gauge,  $\bar{x}$  = mean depth of rainfall and  $n$  = number of rain gauges.

A summary of results from the calibration runs are provided in Table (4.2).

Table 4.1: Summary of nozzles and conditions explored in calibration runs.

Nozzle Height, cm	Nozzle Identification code	Water Pressure, kpa
170	1/8GGSS4.3W	83
	1/4GGSS10W	62
	3/8GGSS20W	48
110	1/8GGSS4.3W	83
	1/4GGSS10W	69-76
130	3/8GGSS20W	62-69

### **Volumetric Method**

The “effective rainfall intensity”, i.e. the temporal and areal average which would account for the measured runoff volume, was used as an indirect calibration technique. First, the depression storages on the experimental surface (described in Section 4.2.8) were filled with water to eliminate the effect of depressions. Then, a typical rainfall event, consisting of three pulses, each of different intensity lasting for three minutes, with a total duration of nine minutes was applied to the depression-filled surface. Effective rainfall intensities were determined from derivatives of the measured cumulative time-wise variation of runoff corrected for the areas of the collecting device and the experimental flume. Figure (4.2) illustrates a cumulative runoff curve used for volumetric calibration, and Table (4.2) summarizes example results of a few calibration runs.

It is worth noting that the gravimetric method is the more physically realistic of the two methods, also providing information on the spatial pattern of simulated rainfall. The volumetric method provides a very time efficient approach although it is indirect.

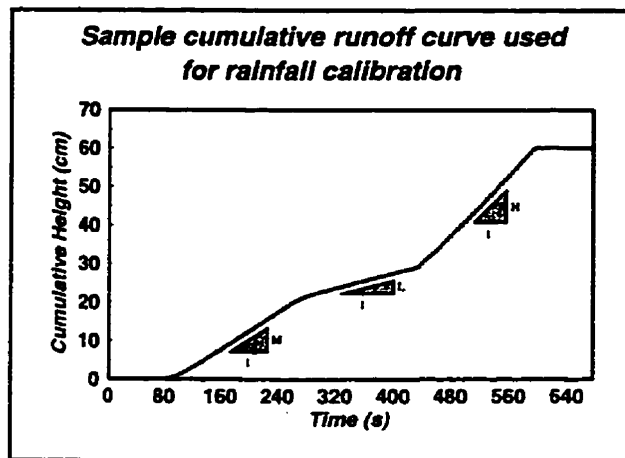


Figure 4.2: Typical runoff curve used for rainfall simulator calibration.

Table 4.2: Summary of typical results from two calibration methods

Nozzle type	Gravimetric method			Volumetric method		
	Intensity mm/hr	UC (%)	Replication	Intensity mm/hr	UC (%)	Replication
Nozzle height = 110 cm						
1/8GGSS4.3W	25.7	74.5	2	27.3	-	9
1/4GGSS10W	46.6	63.8	3	49.1	-	7
3/8GGSS20W	96.7	41.1	2	95.3	-	9
Nozzle height = 130 cm						
1/8GGSS4.3W	22.7	75.4	2	24.4	-	9
1/4GGSS10W	-	-	-	43.6	-	6
3/8GGSS20W	81.7	41.4	2	77.5	-	9
Nozzle height = 170 cm						
1/8GGSS4.3W	19.4	80.5	4	21.0	-	2
1/4GGSS10W	35.2	88.7	2	32.9	-	2
3/8GGSS20W	54.8	44.8	2	52.9	-	2

#### **4.2.4 Qualitative Discussion of Simulated Rainfall Characteristics**

When experimental data are used for modeling studies, it is usually assumed that the rainfall is uniformly distributed over the surface. In reality this is not the case, depending on the nature of the experimental setup. In the laboratory portion of this study, the rain gauge data revealed that the upper end of the experimental flume received about 5% more rain than the lower end for the steepest slope condition, 14%. A further qualitative observation regarding the spatial uniformity of rainfall revealed that a number of the nozzles generated a circle of high intensity rainfall close to the periphery of the area receiving rainfall. The area receiving rainfall could be increased by increasing the supply line water pressure, causing an increase in spray angle near the nozzle. The size of the area receiving rainfall was also affected by the nozzle height, it was found convenient to hold this parameter constant during the course of experimentation. The best spatial uniformities were achieved when the aforementioned circle of high intensity was purposely moved off the study area by increasing the supply line pressure. This practice also spread the amount of applied water over a larger area, thereby reducing the simulated rainfall intensity. The flow rate of water through the nozzles was much more sensitive to the nozzle diameter than to the supply line pressure; and qualitative observations of the spatial distribution of rainfall generated by the selected Spraying Systems Inc. nozzles facilitated the final selection of nozzle and pressure combinations.

The observed drop size distribution varied with the nozzle diameter. These rainfall characteristics studied in detail by Tossel (1987), were observed but not measured in this study. For the same supply line pressure, a nozzle with a large diameter, e.g.,

3/8", produced a larger drop size distribution than a nozzle with a small diameter, e.g., 1/8". Furthermore, the drop size distribution was inversely affected by supply line pressure; and the nature of this relationship did not appear to be linear. For example, changes in supply line pressure between about 8 and 83 kpa for the 1/4" nozzle did not cause any noticeable change in the mean drop diameter. Outside of this range, a small increase in supply line pressure would cause a noticeable decrease in the mean drop size. In addition, it was found that as the drop size increased, the rainfall became less uniform. These qualitative observations agreed with quantitative measurements made by others (Tossel et al., 1990; Tossel et al., 1990) and with unpublished data collected by Dave Teichrobe of the School of Engineering, University of Guelph.

The net result of the study of nozzle characteristics was a tendency toward highly-uniform-low intensity rainfall regardless of the nozzle selected. In order to achieve high rainfall intensities, the high-intensity ring had to be allowed to fall on the study area by decreasing the supply line pressure and hence the nozzle spray angle. This latter practice yielded rather poor spatial uniformity. This trend can be noticed in Table (4.2) under the 3/8GGSS20W nozzle with a supply line pressure of 48 kpa. This nozzle was selected for use only because of its high intensity. Subsequent modeling studies (see Section 7.20.1) showed that experimental results obtained using the 3/8GGSS20W nozzle could not be regarded with much confidence because of the low spatial uniformity.

#### 4.2.5 Rainfall Treatment

The availability of nozzles to produce a range of simulated rainfall intensities (i.e. low intensities from 12.1 to 21.0 mm/hr, medium intensities from 32.1 to 35.2 mm/hr and high intensities from 37.0 to 54.9 mm/hr), and a capability for activating the nozzles sequentially within a single simulated event, provided an opportunity to have many different combinations of rainfall treatments as shown in Table (4.3).

Table 4.3: Temporal patterns of possible rainfall treatments

Rainfall treatment	Description
I	Low → Medium → High
II	Low → High → Medium
III	Medium → Low → High
IV	Medium → High → Low
V	High → Low → Medium
VI	High → Medium → Low

To perform the laboratory experiments in a realistic period of time, the number of rainfall treatments was reduced from six to three, as shown in Table (4.4), still yielding a wide range of temporal patterns of rainfall intensity.

Temporal sequences of different simulated rainfall intensities were used for the laboratory and field experiments for a number of reasons as noted in the following:

- It has been argued that the timing of runoff hydrographs can be directly affected by the timing of rainfall intensity patterns on small areas (such as unit areas) while such timing may be less important at larger scales (DeCoursey, 1996). Since the laboratory setup available allowed switching between different rainfall intensities in a single event, providing a unique opportunity to touch on the above proposition, the way was paved for selection of “combinations of rainfall rates”

rather than constant rates.

- It has been argued that rainfall-runoff models should have a sound structure so that they are applicable under different rainfall regimes (Klemeš, 1986b). Again, the possibility of being able to switch between different rainfall intensities in a single event provided a unique opportunity to check the soundness of model structure under different rainfall regimes.
- In preliminary field experiments, a particular ranking of hydrograph timing was noticed from one micro-catchment to another. In order to confirm whether this ranking was accidental or not, sequences of rainfall intensities were considered appropriate for such purposes.
- The desire to explore possible interactions between rainfall patterns and spatial variability of infiltration and/or micro-topography also prompted the selection of “combinations of rainfall rates” rather than a constant rate.

Table 4.4: Temporal patterns of rainfall chosen for laboratory experiments

Rainfall treatment	Description
I	Medium → Low → High (MLH)
II	High → Medium → Low (HML)
III	Low → Medium → High (LMH)

Figure (4.3) summarizes the different rainfall treatments, each event consisting of three pulses of different intensities, each pulse lasting for two minutes, with a total event duration of six minutes. As for the length of time selected for each pulse and for the total duration of the rainfall event, the main constraint was the maximum capacity of the water collector. A 2 minute interval for each pulse and a total duration of 6

minutes seemed optimum for producing a total rainfall volume which matched the volume of the water collector.

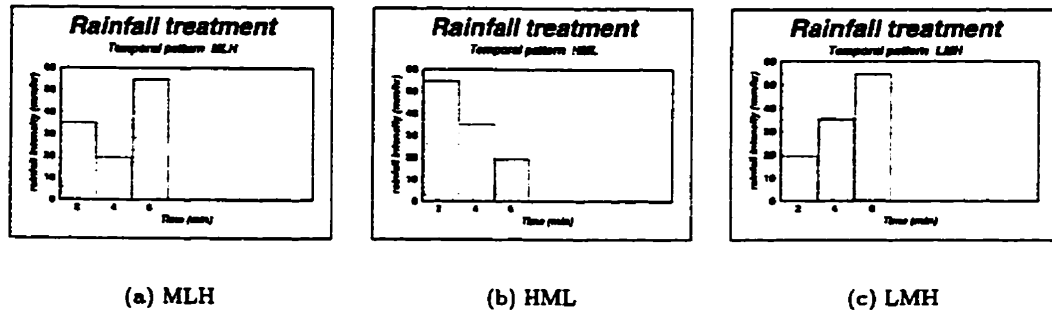


Figure 4.3: Various rainfall treatments.

#### 4.2.6 Runoff Measurement Facility

Measurement of the time-wise variation of runoff could be achieved in the laboratory setup via two methods: a gravimetric and a volumetric method. With the gravimetric method, runoff could be measured using a rotating turntable located under the outflow of the soil flume. The rotating turntable is driven by a variable speed motor and a gear box, and this system allows for a very wide range of rotation speeds. The rotating turntable has two horizontal circular plates that rotate together. The upper of the two plates has ten holes drilled in it around the perimeter at regular spacing. These holes allow for the placement of funnels to capture runoff from the soil flume, delivering it to collection containers mounted on the lower plate. Runoff from the soil flume is initially captured in a stationary funnel on top of the turntable, and this stationary funnel delivers runoff into the rotating funnels below. Sample collection rates and the time for each sample can be calculated by dividing the total time required for several

samples to be collected by the number of samples. Runoff in this study was collected in one liter Nalgene bottles. After collection, the weight of each bottle and its contents was obtained and the known weight of the empty bottle subtracted to determine the amount of runoff collected.

For the volumetric method, the runoff response could be directed to a cylinder ( $D = 4''$ ) equipped with a manometer. A transducer, installed at the bottom of the cylinder, registers cumulative water height; and the transducer itself is connected to an analog card of a CR10 Campbell Scientific datalogger. The electrical signal registered by the transducer in the form of a millivolt signal is logged by the datalogger at a preset specified time interval. The datalogger is connected to an IBM-compatible computer to transmit raw data stored in the datalogger, and the IBM-based PC208 software developed by Campbell Scientific retrieves the data in plain ASCII format. The raw data are then imported into a spreadsheet or data base programs for further processing.

The suitability of these runoff-measurement methods and the selection of a method for the present study are discussed in Section 4.2.7.

#### **4.2.7 Preliminary Runs**

More than 300 experimental runs were conducted to explore and calibrate various aspects of the laboratory system. Some of the items relating to the measurement of runoff are discussed below.

### Datalogger Calibration

The digital data provided by the datalogger in millivolt units was converted to water height in the water collector by means of calibration curves such as the one shown in Figure (4.4); and then through a conversion factor (ratio of the flume surface area to the water collector area) water height was changed to runoff rate. As the coefficients for this calibration curve were very sensitive to a small displacement in the water collector, a calibration curve was created for each day of experimentation.

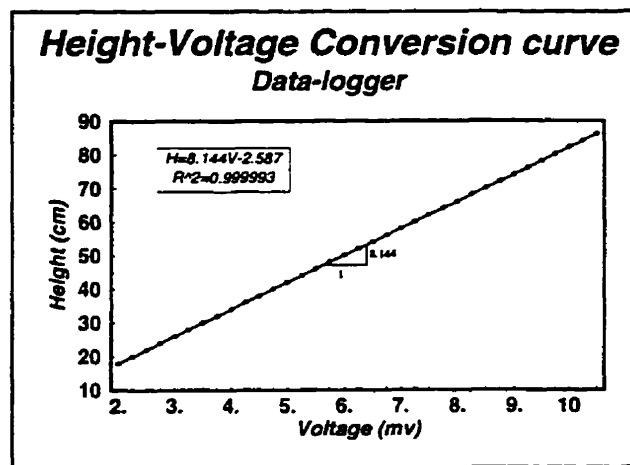


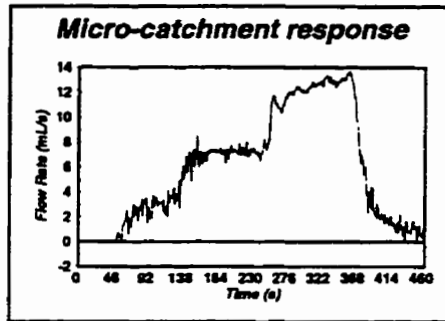
Figure 4.4: Typical data-logger calibration curve

### Optimum Temporal Resolution

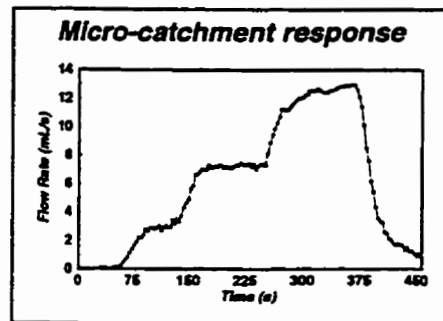
To explore an optimum temporal resolution for the runoff data, the datalogger was preset at different time intervals ( $\Delta t = 1, 3, 5, 8, 10$  s) and runoff was measured with different temporal resolution. At small time steps (e.g.  $\Delta t = 1$  or  $3$  s), the derivative of cumulative runoff fluctuated at times between positive and negative values. At large time steps (e.g.  $\Delta t = 10$  s), some of the time-wise variations of runoff were damped out, diminishing the opportunities to distinguish treatment effects. On the

basis of these observations, a 5 s time step was selected for determining experimental runoff hydrographs (see Figure (4.5)).

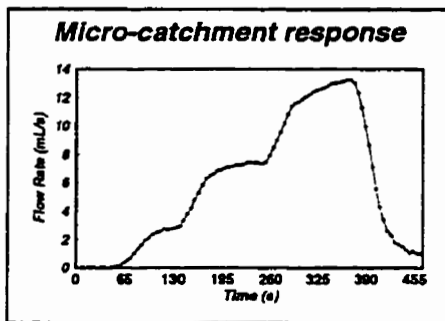
It is important to note that the selection of an optimum temporal resolution is objective dependent. In this study, the main criterion for selecting the time step was to minimize noise in the runoff rate output. Other criteria could very well lead to another optimum resolution. Cushman (1987) considered temporal resolution of observations to be a separate source of randomness in experimental data.



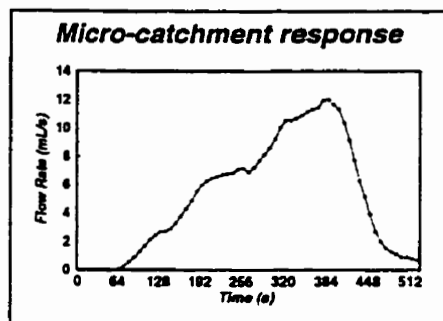
(a)  $\Delta t = 1 \text{ s}$



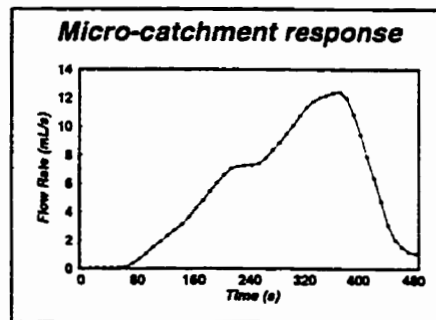
(b)  $\Delta t = 3 \text{ s}$



(c)  $\Delta t = 5 \text{ s}$



(d)  $\Delta t = 8 \text{ s}$



(e)  $\Delta t = 10 \text{ s}$

Figure 4.5: Observation of runoff at various temporal scales.

### **Turntable vs. Datalogger Runoff Measurement**

Runoff from the laboratory facility could be measured by means of either a rotating turntable, suitable for monitoring runoff volumes in time intervals no less than 10 s (Mackenzie, 1995), or a cumulative tank equipped with a datalogger set to record volumes as depths with a resolution of as small as one second. The turntable allowed accurate volume measurements in relatively large time intervals and was time consuming to generate. The tank and datalogger provided a very efficient but indirect method for monitoring runoff rate.

To check the relative accuracy of the two methods available, test runs were performed using both approaches simultaneously. A comparison of results from these tests is presented in Figure (4.6). As it is clear from these results that the two methods could be expected to yield comparable runoff rates, the simpler, less time-consuming datalogger system was used for the laboratory experimental runs.

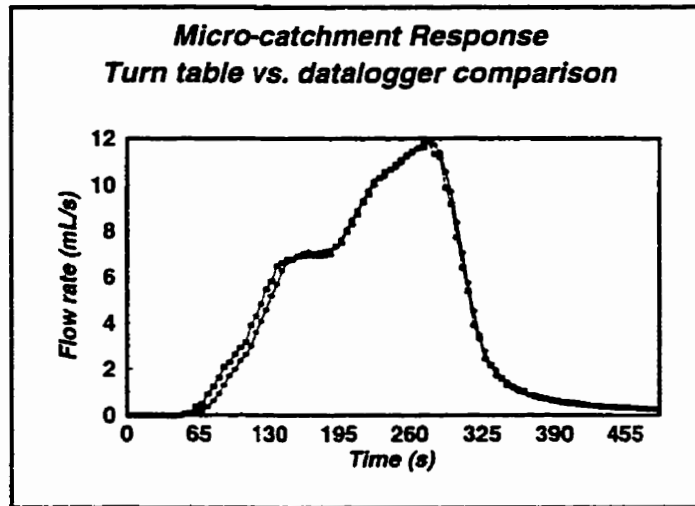


Figure 4.6: Runoff measurement via rotating turntable and datalogger and their comparison.

#### 4.2.8 Surface Preparation

Depression storage over the ground surface results from micro and macro fluctuations in surface topography. To create representative surface depressions in a laboratory setting, one could synthetically create a rough topographic surface and then map the depressions over the surface. This route was not pursued in this research due to constraints associated with surface preparation, and the lack of availability of a laser scanner and associated technicians at the time of performing this experiment. Rather, depressions of a fixed semi-spherical geometrical shape were chosen. Figure (4.7) reveals examples of the shapes used, along with some geometric properties.

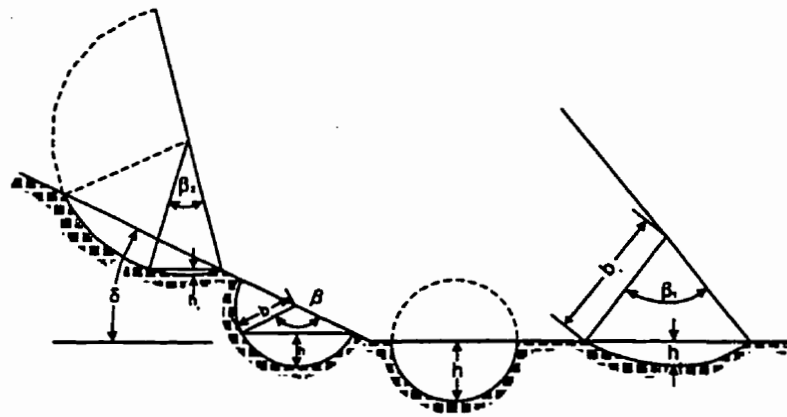


Figure 4.7: Definition sketch for depression storage.

Decisions were then required regarding matters such as the location and distance between depressions both along and across the experimental flume and the frequency distributions of geometric characteristics. Ullah (1974) found that the Weibull distribution best captured the frequency distribution of various geometric features of depressions on a natural hillslope including depth, surface area and volume. For the sake of calculating the number of depressions in the lab experiments, it was therefore

assumed that their surface areas were distributed according to a Weibull distribution. The distances between depressions across the flume were assumed to be normally distributed. To locate the depressions along the flume, it was further assumed that each depression was located at the center of a rectangle, an arrangement first used by Haan and Johnson (1968). This last assumption implicitly implied that the incremental contributing area of each depression was rectangular in shape.

Incorporation of the above assumptions into a FORTRAN algorithm led to the delineation of depressions over the experimental flume surface. Selecting different seed numbers, different patterns of depressions were created, from which one was selected for construction. Table (4.5) summarizes the results of the simulation used for construction. As is clear from the table, increasing the diameters of the depressions decreases their number.

Table 4.5: Summary of simulation run selected for construction

Depression No.	Diameter cm	Frequency of occurrence
1	1.9	29
2	2.03	21
3	2.57	20
4	3.21	12
5	4.05	8
6	5.71	6
7	6.05	6

By reference to Figure (4.7), one could easily calculate the volume of storage up to the depth  $h$  for each depression. After some rigorous mathematical manipulation, the volume of storage at overflow depth as a function of radius of depression and overall slope,  $\delta$  would become:

$$V_s = \frac{1}{3}\pi b^3(1 - \sin \delta)^2(2 + \sin \delta) \quad (4.2)$$

By noting the number of depressions in each class summarized in Table (4.5), total volume of storage for each slope was calculated and summarized in Table (4.6).

Table 4.6: Total potential volume of depression storage at different slope.

Overall Slope, %	$\delta$ Degree	Total Volume, $cm^3$
6	3.43	974.3
8	4.57	942.6
10	5.71	911.1
12	6.84	880.0
14	7.97	849.1

Figure (4.8) shows the positive and negative molds which were constructed with a fiberglass material. Figure (4.9) shows one typical surface placed in the flume. This particular surface design differs from typical natural surfaces in two important ways. In nature, depression storages are rarely if ever row-wise; and natural depressions tend to exhibit a nested structure (e.g. two small depressions might combine to form a larger depression). Nested depressions can result in not all depressions generating runoff at the same time. Rather they are likely to contribute to runoff at different times within the same rainfall event.

#### 4.2.9 Surface Treatment

Five different surface treatments were considered for the laboratory experimentation. The surface was impermeable for three of them and permeable for the other two. Among the three impermeable surface treatments, the first one was selected to be flat

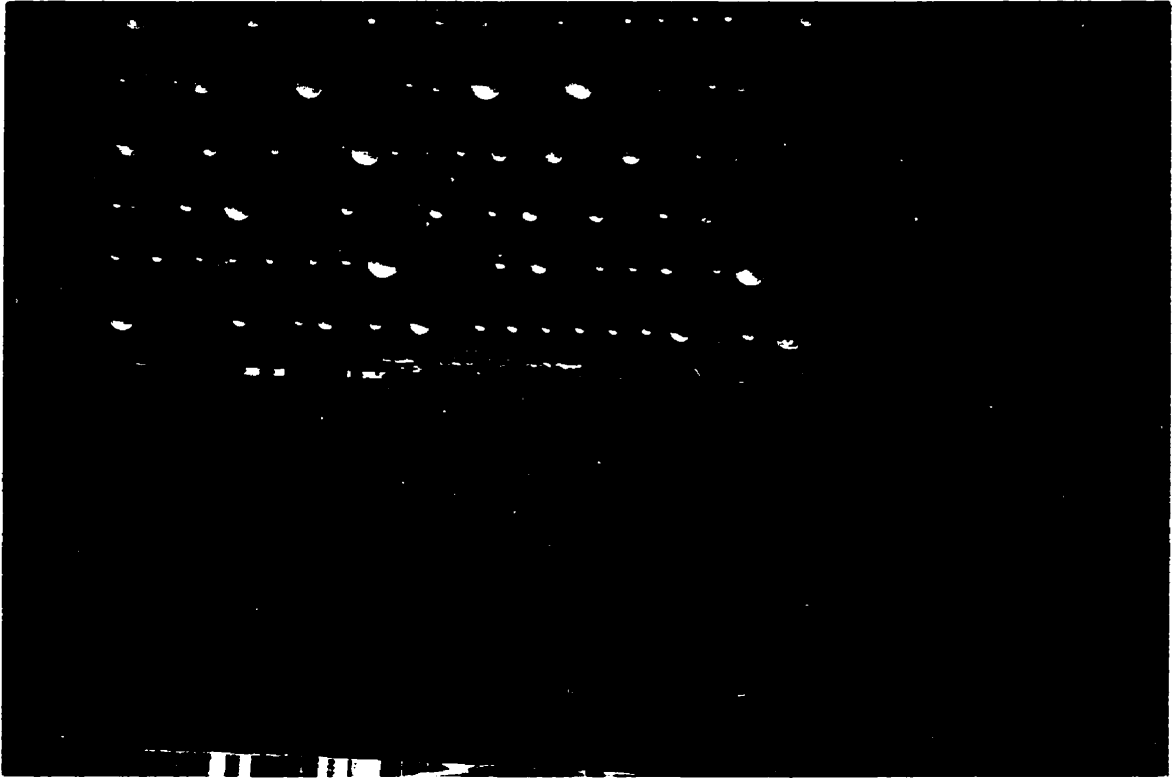


Figure 4.8: Constructed positive and negative mold

(i.e. with no depressions) to serve as a comparative benchmark. The second surface treatment had relatively large depression storages near the outlet (surface treatment II), while the third treatment had relatively small depression storages near the outlet (surface treatment III). The first permeable surface was basically surface treatment II with an infiltrating part near the outlet (surface treatment IV); for the second permeable treatment, the infiltrating part was located relatively far from the outlet (surface treatment V). In both cases, the infiltrating part was created by drilling holes in a few depressions, each hole having a diameter equal to 10% of the depression diameter. No particular infiltration rate was considered for this purpose. To reduce the effect of surface tension and also simulate some surface roughness, a uniform-sized sand (i.e. Ottawa sand) was glued to the surface to a thickness of 1 to 3 grain

diameters. Figure (4.10) illustrates the various surface treatments.



Figure 4.9: Surface treatment II within the flume.

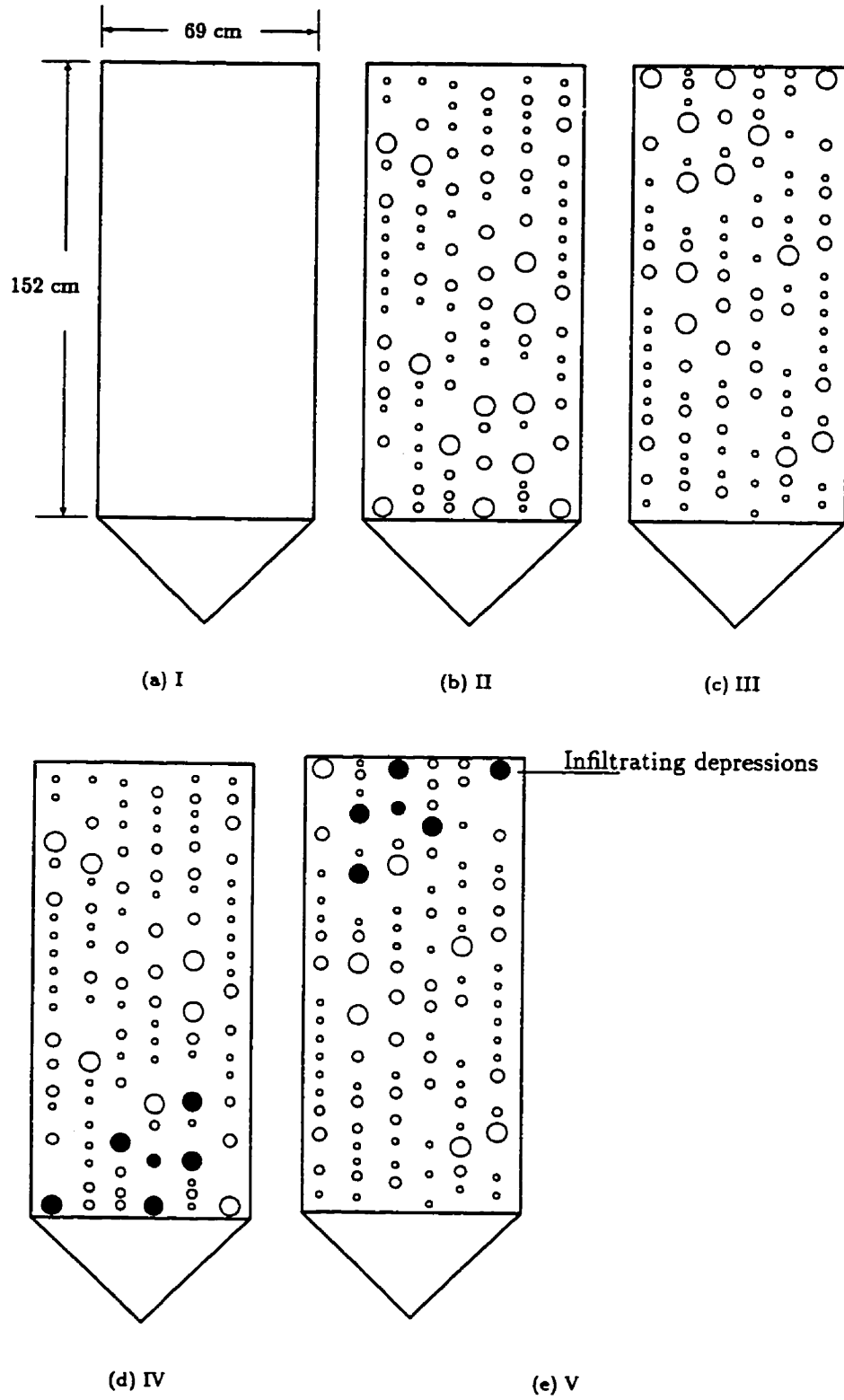


Figure 4.10: Various surface treatments.

#### **4.2.10 Slope Treatment**

To explore possible interactions between depression storage, overall slope and related effects on micro-catchment response, five different slopes between 6 and 14% (in increments of 2%) were used for the experiment.

#### **4.2.11 Procedural Design of Lab Experimentation**

It was necessary to choose an optimum design for the laboratory experiment to address the stated objectives. One possibility was to start by fixing the surface treatment and slope and then change the rainfall pattern; another possibility was to fix the surface treatment and rainfall pattern and then change the slope. Initially the first option was selected. Fixing the surface treatment and slope and then applying the various rainfall patterns gave rise to six experimental events. Selecting three replications for each event, and at least one calibration run for each rainfall pattern, typically led to 24 experimental runs. Conducting such a set of runs took more than a single working day. After the experiments for a single surface treatment had been performed for various slopes (approximately 120 runs), it was noticed that there could be considerable variability in rainfall intensity from one pattern to another and from one day to another day, as shown in Table (4.7); and there was concern that such variability might mask other effects. To eliminate the impacts of pattern to pattern and also day to day variability in rainfall intensity, the second experimental design option was finally chosen, varying slope for a fixed rainfall pattern and surface treatment. When it was observed that the experimental runs could be readily replicated, the number of replications was reduced to two. Further, the six rainfall treatments were reduced to

three (see Table (4.4)), when it was found that the nature of results from the three which were canceled were very similar to those for the selected ones.

Table 4.7: Pattern to pattern and day to day variability in rainfall intensity

Date	Rainfall intensity in mm/hr																	
	LMH			LHM			MLH			MHL			HML			HLM		
	L	M	H	L	M	H	L	M	H	L	M	H	L	M	H	L	M	H
May 29, 1996	15.1	34.3	42.3	13.0	34.0	43.4	.	.	.	.	.	.	.	.	.	.	.	.
May 31, 1996	.	.	.	.	.	.	15.7	32.1	42.0	14.4	31.2	39.1	.	.	.	.	.	.
June 2, 1996	.	.	.	.	.	.	.	.	.	.	.	.	15.4	32.1	37.1	14.9	33.2	38.3
June 3, 1996	14.6	34.6	39.7	13.8	33.4	38.3	.	.	.	.	.	.	.	.	.	.	.	.
June 4, 1996	.	.	.	.	.	.	16.3	33.6	39.9	15.7	33.2	38.6	16.2	33.6	37.0	15.3	34.5	37.0
June 6, 1996	13.0	33.5	48.3	.	.	.	.	.	.	.	.	.	.	.	.	.	.	.
June 8, 1996	.	.	.	.	.	.	.	.	.	14.0	33.9	49.5	14.2	33.1	48.7	14.7	32.8	49.4
June 10, 1996	.	.	.	.	.	.	14.2	33.4	54.9	.	.	.	.	.	.	.	.	.
June 11, 1996	12.3	33.0	46.5	12.1	32.5	43.3	13.7	32.6	44.3	.	.	.	.	.	.	.	.	.
June 13, 1996	.	.	.	.	.	.	.	.	.	.	.	.	13.4	33.8	48.7	12.7	33.4	47.5

Calibration of the rainfall simulator for each rainfall pattern was performed on three slopes, namely 6%, 10% and 14%. As a result, 13 experimental runs were conducted for each rainfall pattern, a task which could be undertaken within a single day. Table (4.8) illustrates the variability in rainfall intensity observed to occur from slope to slope for each rainfall pattern within a single day.

Table 4.8: Slope to slope variability in rainfall intensity within a single day.

Date	Slope	Rainfall intensity in mm/hr								
		LMH			HML			MLH		
		L	M	H	L	M	H	L	M	H
June 15, 1996	6%	12.11	32.9	47.7	-	-	-	-	-	-
	10%	12.7	33.9	48.1	-	-	-	-	-	-
	14%	12.7	35.0	51.4	-	-	-	-	-	-
June 17, 1996	6%	-	-	-	13.5	34.1	47.7	-	-	-
	10%	-	-	-	12.1	33.5	47.3	-	-	-
	14%	-	-	-	14.1	34.8	47.9	-	-	-
June 19, 1996	6%	-	-	-	-	-	-	14.3	35.2	48.9
	10%	-	-	-	-	-	-	13.6	35.0	47.6
	14%	-	-	-	-	-	-	13.8	36.0	48.4

#### 4.2.12 Experimental Procedure

A typical experimental run consisted of applying one of the selected rainfall treatments to surface treatments set at one of the prescribed slopes in the laboratory flume. For each experimental run, the following variables were measured and/or calculated.

**Total runoff volume:** Runoff was collected in a water collector, and the accumulated runoff volume was measured continuously. A graduated manometer was installed besides the water collector and the height of water in the manometer along with its corresponding datalogger reading were recorded for further calibration. The

total volume of runoff for each experimental run was calculated by subtracting the initial datalogger reading from the final datalogger reading, and multiplying the result by a datalogger conversion factor (see Section 4.2.7).

**Total water loss:** The total amount of water trapped in depressional storages at the end of each experimental run was measured gravimetrically by collecting water from all depressions and finding the net weight/volume of water, i.e. after water collection, the weight of the bottle and its contents was obtained and the known weight of the empty bottle subtracted to determine the volume of water trapped in depressions.

**Runoff hydrograph:** The runoff hydrograph for each experimental run was determined from the cumulative runoff volume data by passing the record of cumulative runoff through a derivative filter to provide a time sequence of runoff rates.

**Time synchronization:** A stopwatch was used to synchronize the rainfall treatment pulses with datalogger reading. While the rainfall simulator was off, the time on computer screen corresponding to initial water height in the cylinder was recorded and stopwatch was activated concurrently. Later on, the rainfall simulator was also activated keeping track of time via the stopwatch.

## **4.3 Small-scale Field Experiments**

It was acknowledged earlier that the laboratory experiment involved depressions located in rows and lacking a nested structure. In order to explore more randomly located depressions, some of which could be nested, the laboratory experiment was replicated on natural surfaces, working at approximately the same spatial scale.

### **4.3.1 The Study Area**

#### **Site Selection and Description**

The site for small scale field experimentation was selected on the basis of the following considerations: proximity of location to University of Guelph, representativeness of the area, and availability of a water supply and power. Based on these considerations, runoff plots which had been monitored for 32 years by the Department of Land Resource Science in the Ontario Agricultural College (O.A.C.) of the University of Guelph were selected. The ten plots are situated in the south-west corner of the Guelph campus, and a simple plan of the plots is shown in Figure (4.11). This figure reveals 10 plots, each of which is  $202 \text{ m}^2$  in area, with a length of 44.2 m, a width of 6.4 m and a relatively uniform slope of 7 to 9% along the plot length. These runoff plots have been extensively used by other researchers for various purposes over the years, including the characterization of surface depressions (Rudra et al., 1985; Rudra et al., 1989; Ullah, 1974).

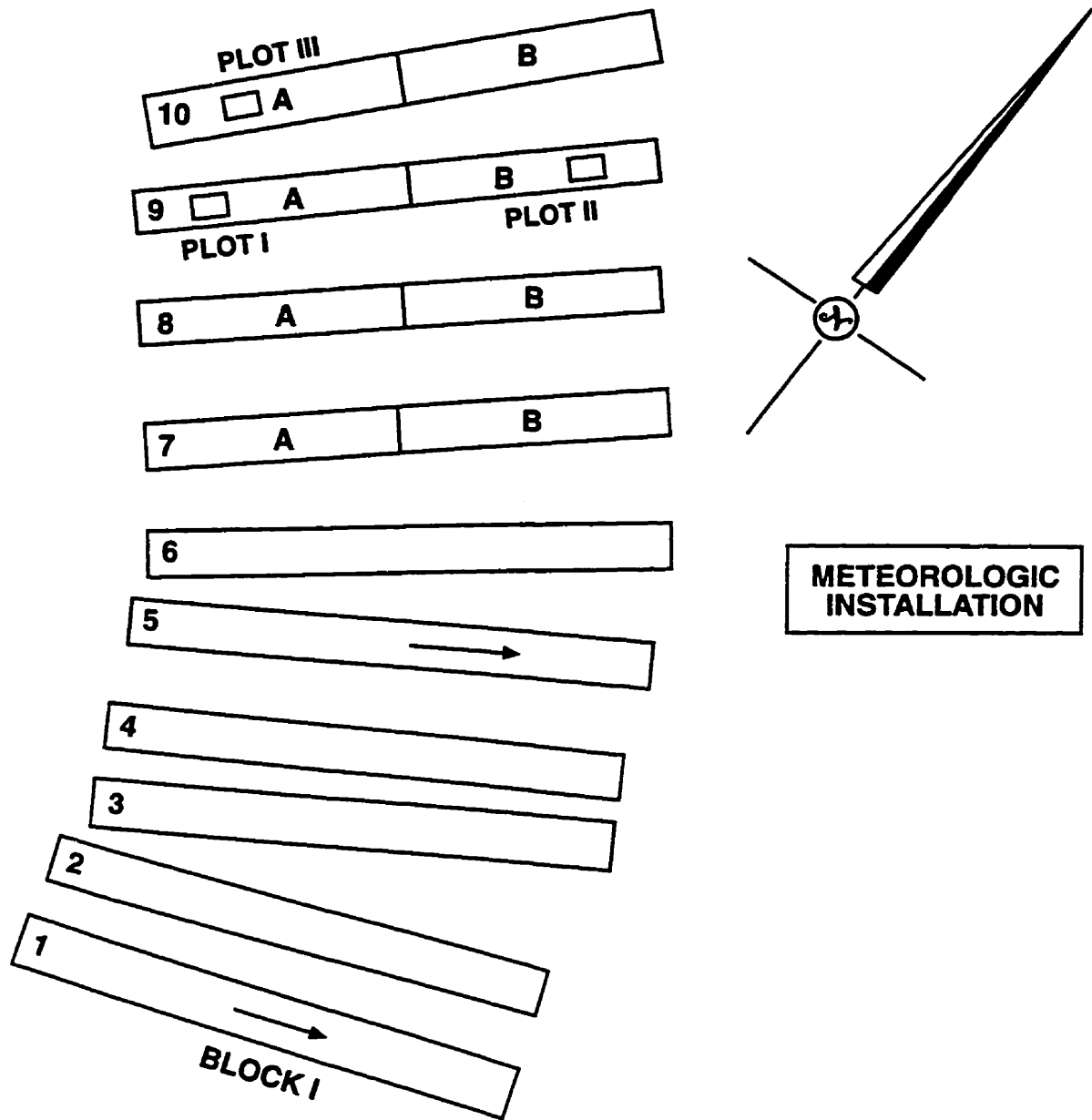


Figure 4.11: Runoff plots, University of Guelph, Ontario, Canada.

The plot site is on the east slope of a drumlin, a characteristic land form of southern Ontario. The calcareous glacial till material has developed over the course of time into a well-drained loam textured soil which has been classified as Guelph loam (Ketcheson and Onderdonk, 1973). During the year of this study, the runoff plots were under a corn crop management system; and the surface treatment consisted of moldboard plowing in the fall, with disc harrowing in the spring followed by smoothing of the surface with a spike tooth harrow. These are reasonably standard tillage operations employed for corn and some other crops in southern Ontario. At the time of conducting field experiments in this area (i.e. summer, 1996), all runoff plots had received the same surface treatment with corn residuals left over the ground.

#### **4.3.2 Sample Micro-catchments**

After visual inspection of the plot surfaces, three micro-catchments (identified as Plots I, II and III in Figure 4.11) having relatively similar slopes were selected to study the impact of surface storage variability on hydrologic response. Since the depth of overland flow increases with slope length due to an increase in the upslope contributing area (Dunne et al., 1991), changes in surface characteristics are likely to be more pronounced in the lower portion of sloping plots. In light of this, two of the micro-catchments were delineated in one runoff plot, one in the center of the upper half and the other in the center of the lower half. The third micro-catchment was delineated in the upper half of another runoff plot. Preparation of each micro-catchment for experimentation followed the following steps.

### **Micro-catchment Size**

The following items were considered in establishing the size of each micro-catchment:

- Areal coverage of the laser scanner ( $1.0 \times 0.5$  m)
- Areal coverage of the rainfall simulator,
- Maximum capacity of the runoff measurement instrument,
- Availability of pre-dimensioned plot separators ( $1.0 \times 1.0$  m), and
- Cost of sealing and painting the surface and also removing vegetation.

On the basis of the above criteria, an area of  $1.0 \times 1.0$  m was selected and established for each micro-catchment.

### **Removal of Vegetation**

The vegetative cover on the plot surfaces had to be removed to permit effective use of the laser scanner. To avoid disturbing the topographic pattern of the surface, removal of vegetative cover was achieved via pouring kerosene over the surface and then burning it. Figure (4.12) shows a picture of one of the micro-catchments after the vegetative cover had been removed.

### Sealing the Surface

It was decided to seal the surface of each micro-catchment to (i) stabilize the micro-topographic pattern against rainfall and runoff effects, and (ii) reduce if not eliminate the effect of infiltration.



Figure 4.12: One of micro-catchment after removing vegetative cover

After some initial experiments on soil samples in the lab, Acetone Methyl ISO-butyl Ketone was applied to the field plots to create a very thin layer of plastic over the natural surface. Application of simulated rainfall on the surface with a medium-size nozzle for 25 min did not generate appreciable runoff, so it was concluded that the surface was not sufficiently sealed. A heavier commercial sealing material, Varathane, was then applied to the surface, resulting in a more completely sealed although not

totally situation. Figure (4.13) shows a picture of one of the micro-catchments after the surface was sealed.



Figure 4.13: One of the micro-catchments after sealing of the surface.

### 4.3.3 Micro-topography Characterization

Due to the success of the triangulation method, instrument availability and its adaptation by the USDA for soil erosion studies, the scanner used in this research for micro-topography quantification of each micro-catchment was based on the design described in Huang et al. (1988) and Huang and Bradford (1990b). The following subsections describe the general configuration and design of the laser profile meter used, including the optical transducer, the traversing frame, the system calibration and elevation data collection procedure.

#### The Optical Transducer

The operational principles of the optical transducer for measuring surface elevation are presented in detail in Huang et al. (1988) and Huang and Bradford (1990b). A brief description of the principle and the electronics are presented here. To determine surface elevation, a low powered HeNe laser projects a parallel beam onto the soil surface. The reflected laser light from the soil surface is focused by a conventional 50 mm camera lens onto a linear photo-diode array mounted at the back of a camera. The high intensity of the reflected laser spot produces a strong output from the diode array. The position of the highest output on the array can be related to the surface elevation by trigonometric relationships.

The elevation ( $z$ ) range which can be detected depends on four parameters: the laser-camera distance and angle ( $L$  and  $\alpha$ ), the focal length of the lens ( $F$ ) and the length of the photo-diode array ( $S$ ). Different measurement ranges can be set by changing any one or a combination of these parameters (Huang and Bradford, 1990b).

The optical transducer used in this particular setup was a monolithic self-scanning linear 512 element photo-diode array (EG & G Reticon, model RL0512GAG). According to Huang and Bradford (1990b), a 512-element array offers a resolution of approximately 0.1% of the measurement range. The diode array is mounted within a modified 35 mm SLR camera. The array is positioned within the camera body such that the sensing elements lie along the centerline of the lens in the perpendicular axis and at the plane at which the film would lie.

The relative position of the laser image along the photo-diode array is detected electronically in three modes: an analog voltage output, transistor-transistor logic (TTL) and visually on an oscilloscope display. The TTL digital output of the photo-diode is sampled by a digital input/output (DI/O) board (Computer Boards Inc., model CI0- DI024) in a personal computer.

The diode array processing electronics has a refresh rate of 500 *Hz* which is much faster than the sampling rate which is defined as the time between successive elevation readings. If the surface elevation is sampled every 1 mm along a transect line and the traversing time for a 1 m pass is 20 s, the sampling rate is 50 *Hz*. In effect, the frequency at which the system can determine elevation is of sufficient speed to be unaffected by the movement of the traversing frame holding the transducer.

Detection of the diode receiving the most light energy is accomplished by circuitry comprised of a voltage comparator with a threshold detector. The signal from the diode array is a train of 512 pulses which the voltage comparator can count and compare to a reference voltage. When the train passes through the comparator at some point the voltage value exceeds a pre-set threshold. The pulse number at which this

occurs is equivalent to a position on the diode array and this number is temporarily stored. As the train of pulses progresses through the circuit the voltage increases, reaching a peak and then declining. At the point when the voltage drops to the threshold, the pulse number is stored. The peak voltage, and hence diode position, is inferred to be halfway between the up-crossing and the down-crossing (Huang et al., 1988). The calculated diode number is automatically stored in a file.

The camera mounting assembly consisted of a tripod mechanism bolted to an aluminum block on the sensor platform. This mechanism provided adjustment of the camera with respect to the angle subtended between the surface and the photo-diode array. The laser source was fixed to a slotted aluminum square tube to facilitate alignment of the beam with the diode array. This arrangement allowed for the positioning of the camera and laser to be set to different angles and vertical positions, which facilitated optimization of signal resolution for surfaces of different elevational variation.

#### **Control of the Laser Scanner**

Software to control the movement of the traversing frame and acquisition of the photo-diode array output was developed by C. Huang (NSERL, Purdue University, West Lafayette Ind.). The software, written in BASIC language, controls the functions of the specialized circuitry through the DI/O board in a PC. The software controls the following tasks:

- i. Optimization of the ramping velocities to ensure proper step counts,
- ii. The grid size and spacing for sampling elevation,

- iii. The sampling rate,
- iv. The file output names, and
- v. Independent carriage control functions outside the scanning program.

The control logic of the scanner is shown in Figure (4.14).

A 33-MHz, 386 PC was used as the control and data storage device of the scanner. The computer has a 85-megabyte hard disk and an expansion slot to house the DI/O board.

The size of the elevation data file depends on the density of sampling and the mode of the data storage. Since surface elevations were measured at regularly spaced grid points,  $x$  and  $y$  coordinates did not need to be stored as long as the total scan area and spacing between grid points was known. The data storage requirement was therefore reduced to one number per recorded position.

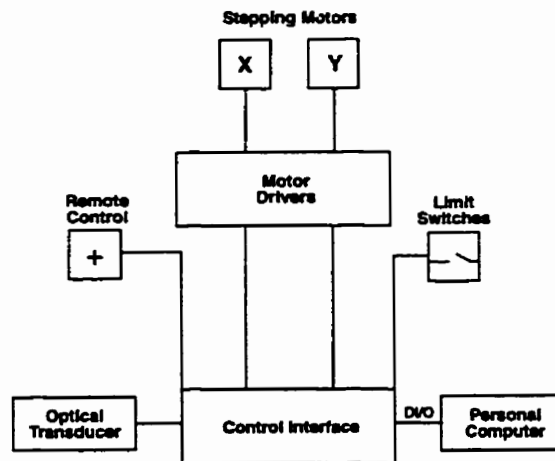


Figure 4.14: The control logic of the laser scanner electronics.

## **System Calibration**

Calibration of the laser scanner to measure surface elevation was accomplished through several steps. The most demanding component of the calibration procedure was the alignment of the laser beam spot and the photo-diode array. To facilitate this, high standards of precision fabrication for the traversing frame, transducer head and diode emplacement in the camera were required.

Ideally, the laser beam projecting normally onto the surface must be in exactly the same vertical plane as the photo-diode array. The laser and diode array can be roughly aligned by looking through the camera eye-piece and seeing if the laser spot appears in the center of the field of view. If this is the case, then the shutter can be tripped, allowing the light to be focused on the diode array. The diode array is positioned inside the camera to be in the plane at which the film would lie so that the lens will properly focus the incoming image. If the laser spot and the diode array are in alignment then the signal should appear on the oscilloscope display as a sharp peak. The aperture of the lens should be fully open and the lens should be focused to make the peak of the signal as sharp as possible. To check for non-normal alignment of the diode array and the incident laser beam, the surface can be raised and/or lowered by moving the traversing frame so that the laser spot moves up and down the calibration block. As the spot moves up and down in elevation it traverses the photo-diode array. If the array is mis-aligned, then the signal will disappear at some point, which suggests that the camera and diode array are not in exactly the same plane and adjustment is required. Once the positioning has been optimized in terms of signal reception, the system can be calibrated for measuring elevation.

Calibration for elevation was achieved via the use of a static calibration block. The block was of machined aluminum with square steps of 2 mm, painted with a flat paint finish (beige or grey). Calibration was accomplished by scanning the calibration block and recording the laser bit number associated with every step change in elevation. A typical calibration curve is shown in Figure (4.15).

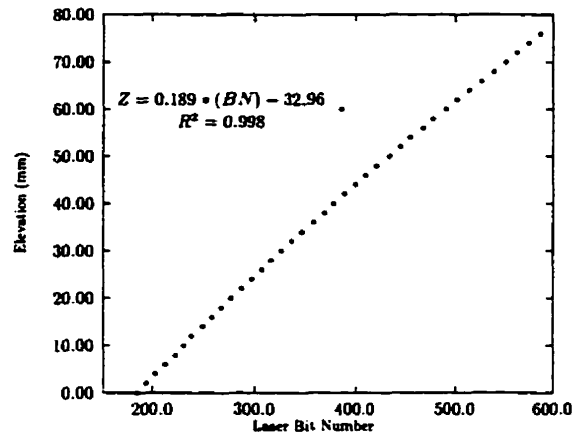


Figure 4.15: The relationship between laser scanner bit number and relative elevation.

It is obvious from Figure (4.15) that there is a minor non-linearity in the system. This calibration curve was utilized to create a look-up table which assigned an elevation value for every one step increment in laser bit number. This look-up table was utilized by a second software program which interchanged laser bit number for elevation from a raw scan file to create a final elevation data file for a given test surface. According to Huang (1996), the calibration remains constant for a given set-up unless the system is disturbed by jarring of the frame or refocusing of the lens. For this research, the scanner was re-calibrated before every set of scans. This was required because the angle between the surface and the diode-array/camera was adjusted to account for different ranges in surface elevations. By adjusting the camera position

with respect to the surface and re-focusing the lens, the system precision could be maximized for a given elevational variation.

The laser scanner recorded elevation difference with respect to a reference plane. The zero reference plane was arbitrarily assigned in the calibration procedure. For some of the test surfaces, it was not possible to put the calibration block at the lowest point of the test surface. As a result, some points within the surface were assigned negative elevation values. Standard practice was to set the camera-laser configuration such that the middle diode on the array (represented by the output bit #512) was associated with approximately the mid-range of the elevation of the surface. Elevation was then determined to be positive or negative with respect to this value. Of course, this procedure utilized the most linear part of the response curve for bit number and elevation.

#### **Collection of Elevation Data**

Collection of elevation data started with mounting the scanner above each micro-catchment one at a time. Since the actual areal coverage of the laser scanner was  $1.0 \times 0.5$  m, each plot was divided into two pieces, and each piece was scanned separately with some overlapping. Two control points with higher elevations were established in each overlapping region for registration and rectification purposes.

To achieve consistency and comparability of DEMs for each piece, the orientation of the laser scanner (both in vertical and horizontal direction) was fixed by rolling it over a fixed railing frame during the course of scanning. Figure (4.16) clearly shows the cited railing frame surrounding one of the micro-catchments as well as the scanner

Table 4.9: Summary of scanning results for the three plots.

Plot No.	Areal coverage, mm	Storage (byte)
Plot I	1025 × 495	228,311
	1025 × 510	235,177
Plot II	1023 × 513	235,867
	1032 × 513	237,931
Plot III	1023 × 513	235,867
	1023 × 513	235,867

mounted on it.

During the initial course of scanning, more than 20% of the data in each scan line were considered suspect, due to an apparent shiny patch on the surface. After the surface was painted with a gray color, the percentage of suspect data was reduced to less than 4%. The grayish nature of the surface can be seen in Figure (4.13). A summary of the scanning results for all three plots is presented in Table (4.9).

#### 4.3.4 Surface Treatment

For each micro-catchment, three different surface treatments were considered for the rainfall:runoff experiment. Two of the surface treatments related to initial conditions (i.e. antecedent soil-water content): one treatment was completely dry, and the other completely wet. For the third surface treatment, the soil surface was covered with very thin plastic. For the wet condition, the outlet side of the plot was blocked and water was applied to the plot at the rate of 140 mL/s. Upon reaching a ponding depth of around 13 cm, the water application was stopped and water depth was recorded versus time elapsed. As soon as there was no sign of ponding over the surface, the rainfall:runoff experimentation was started.

Figure (4.17) illustrates rate of water depletion for all three plots. As is clear from

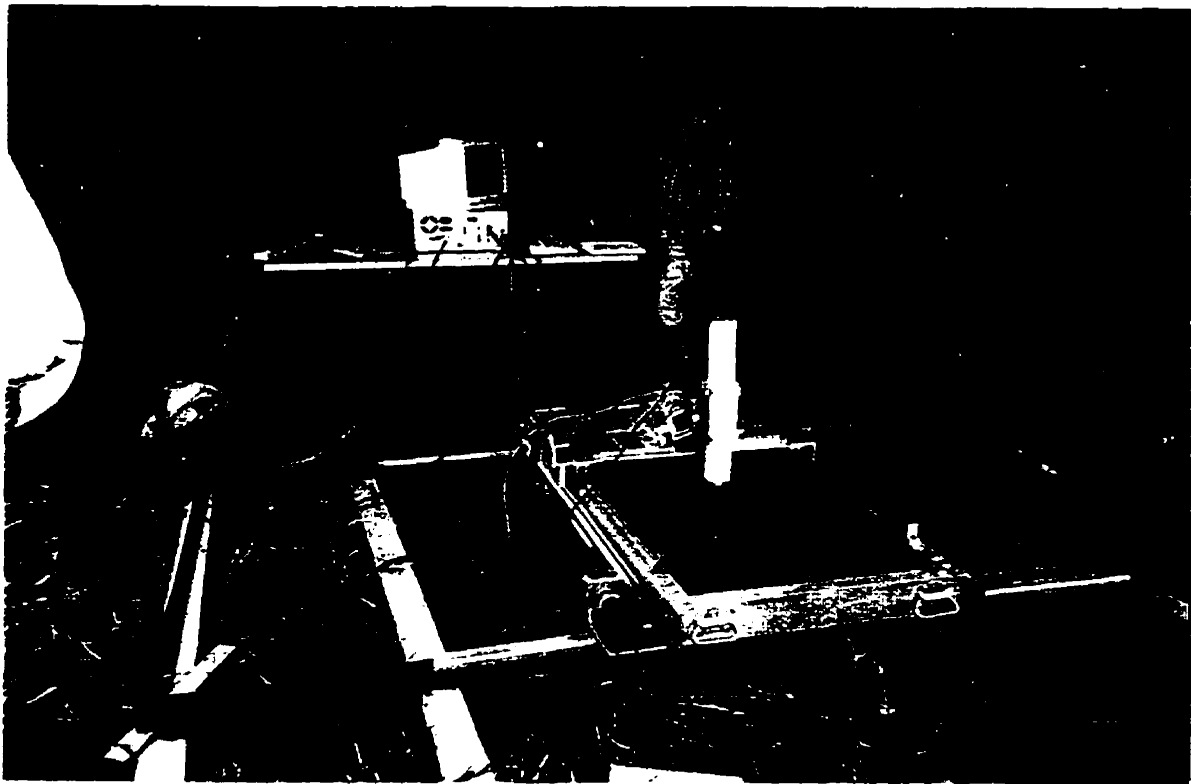


Figure 4.16: One of the micro-catchments during the course of scanning.

this figure. the rate of water depletion is the highest for plot II and the lowest for plot I. lying somewhere in between for Plot III.

#### 4.3.5 Rainfall Treatment

As for the case of the laboratory experiment, three different rainfall patterns were selected for the rainfall treatment (see Table 4.4). To achieve suitable rainfall intensities and areal uniformity on the field plots, and taking into account the maximum capacity of the runoff measurement instrument, the nozzles were installed at a height of 110 cm above the center of the study area for the dry condition and for the wet and plastic cover conditions, the nozzles were set at 130 cm above the plots. Table (4.2) summarizes the range of intensities used for field experiment.

A typical rainfall event consisted of three pulses, each of different intensity and each lasting for five minutes, with a total simulated rainfall duration of fifteen minutes. A typical experimental run consisted of raining on a particular plot with a pre-defined and established initial condition.

# Water Depletion Curve For three plots

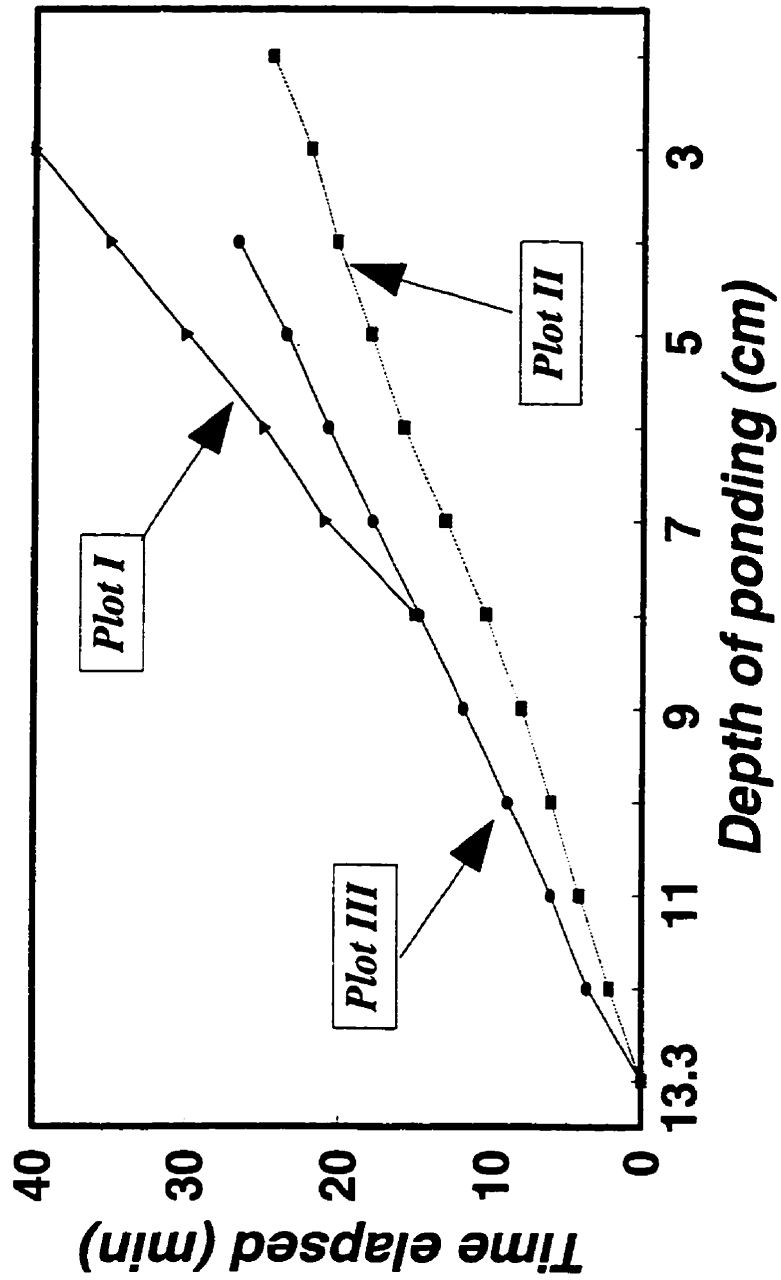


Figure 4.17: Rate of water depletion for different plots.

#### **4.3.6 Runoff Measurement System**

Runoff measurement in the field was slightly different than runoff measurement in the lab. The major components of the runoff measurement system were as follows: a triangular chute below the micro-plot, a peristaltic pump, a water collector and a datalogger. A peristaltic pump was installed between the plot outlet and the water collector, and runoff water was withdrawn from the triangular chute to water collector via the pump. The maximum capacity of the peristaltic pump was a governing factor in selecting the maximum rainfall intensity. The addition of the pump led to one more constraint and source of error in the system, as compared to the counterpart in the lab; and such a system can affect the timing of the resulting hydrograph. However, since the water velocity through the peristaltic pump was high, the lag introduced by the pump was very small.

#### **Experimental Procedure**

For each experimental run, the following variables were measured and/or calculated:

**Total runoff volume:** The total volume of runoff for each experimental run was calculated by subtracting the initial datalogger reading from the final datalogger reading, and multiplying the result by a datalogger conversion factor.

**Runoff hydrograph:** The time-wise variation of runoff rates was determined by passing (measured by means of the digital datalogger) the cumulative runoff data through a derivative filter.

**Time synchronization:** Initiation of rainfall was synchronized with datalogger time by means of a stopwatch.

## **4.4 Large Scale Catchment Experiment**

For the sake of investigating the possibility of using the same model structure at various spatial scales, data from a few highly instrumented experimental watersheds were also used in this study (BEAK Consultants, 1994). For each watershed, the state of surface storage at different times of the year could be expected to be different and to lead to dramatic changes in catchment response. A brief description of the watersheds and the data set are given below.

### **4.4.1 The Study Area**

#### **Site Selection and Description**

Suitable rainfall:runoff data were available for three sub-watersheds within the Lake Erie Watershed: the Essex watershed, the Kettle Creek watershed and the Pittock Creek watershed. Figure (4.18) shows the locations of the three sub-watersheds.

The Essex watershed is located in the Essex-Kent climatic region of Southern Ontario. This watershed was formed on the St. Clair clay plains, where the soils have been derived mainly from glacial till parent materials smoothed by a shallow deposit of lacustrine clays. The most common soil type in this watershed is clay loam overlaying prominently mottled blue-grey, gritty clay and clay loam parent material. In the A, B and C horizons the soil structure is medium/fine, very fine/medium, medium/coarse and subangular blocky respectively.

The Kettle Creek watershed is located within the Mount Elgin-Ridges physiographic region of Southern Ontario. This region contains the Westminster moraine. Within this moraine system, the ridges are composed of calcareous, well to moderately drained, clay loam and clay till. In the low lying poorly drained areas alluvial soils are common.

The Pittock Creek watershed is located in the Oxford till plains physiographic region. The topography of the region is generally level to gently sloping. The dominant soil types are imperfectly drained Tavistock and Embro silt loams. The Tavistock soils have developed on clay and clay loam till parent materials. The Embro soils have developed on loam till materials. Poorly drained Maple-wood and Crombie soils are also present in this watershed.

The conventional practices in this watersheds consisted of moldboard plowing in the fall, with disc harrowing in the spring followed by smoothing of the surface with a spike tooth harrow. These are reasonably standard tillage operations employed for corn and some other crops in Southern Ontario. A paired watershed design had been adopted for the study for which the basins were initially selected. This particular design had been selected to undertake direct comparisons between the defined **test** (i.e. conservation oriented agricultural systems) and **control** (conventional agricultural systems) areas. Since this range of agricultural practices had a direct effect on surface storage elements on the basins, they provided a unique opportunity to investigate the impact of various practices on hydrologic response from a modeling perspective. A summary of selected basin characteristics for the three paired watersheds is given in Table (4.10).

Table 4.10: Selected Sub-watershed Characteristics within the Lake Erie Watershed.

Basin Name	Type of Practice	Drainage Area ha	Seasonal Average Rainfall† mm
Essex	Test	435	434
	Control	281	
Kettle Creek	Test	410	435
	Control	348	
Pittock	Test	359	405
	Control	378	

† Summer and Fall

For each watershed, temperature, precipitation, solar radiation, wind speed, wind direction and discharge had been gathered on an hourly basis while relative humidity had been collected on a daily basis. The sampling system had been designed to collect runoff event samples at each sub-watershed mouth during at least ten representative events per year, distributed over the spring snowmelt, late spring, summer and fall runoff periods. The climatological and streamflow data covered approximately four years from 1988 to 1992. From these data, it was primarily the hourly precipitation and corresponding streamflow which were used in this study for a modeling application.

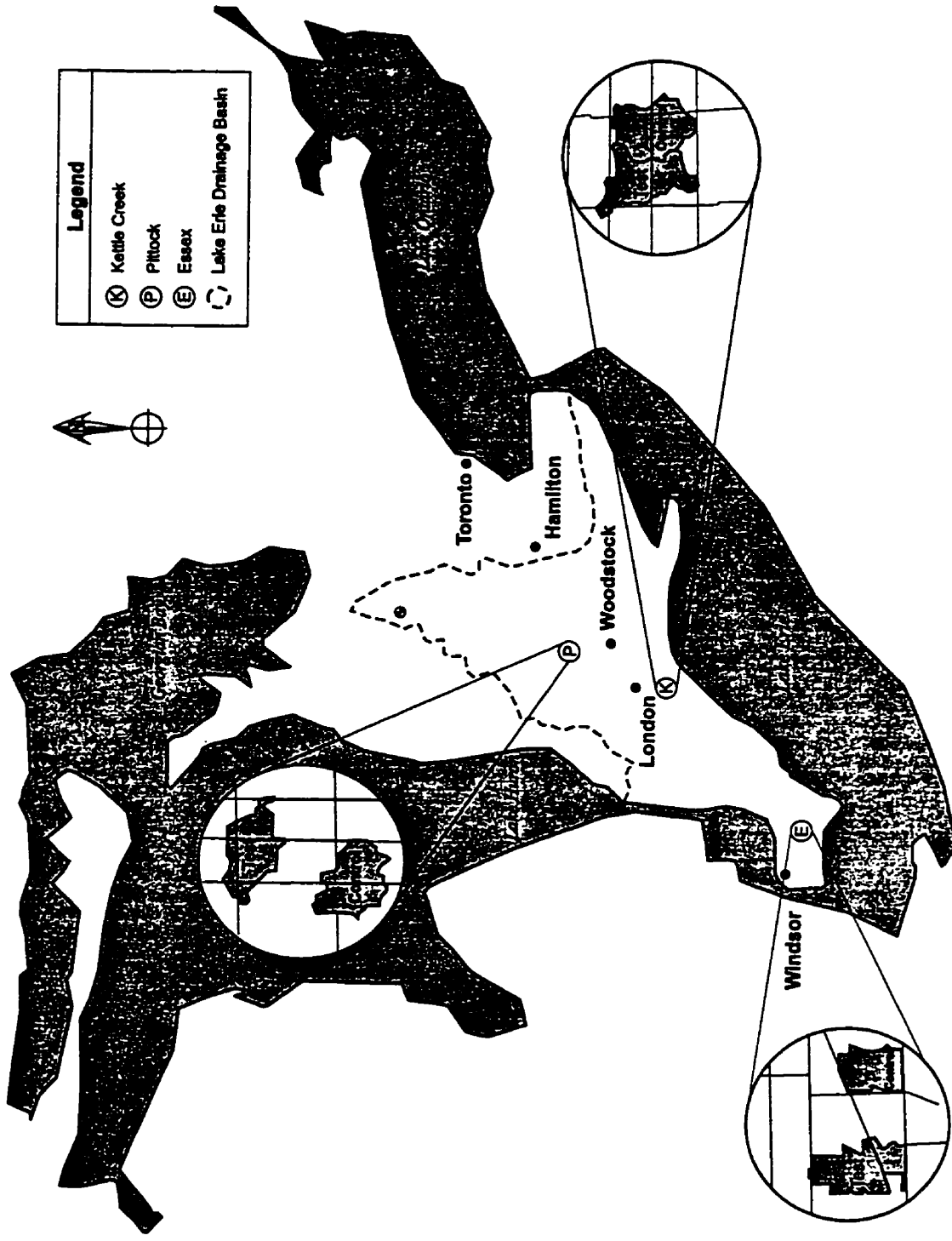


Figure 4.18: Location of pilot watersheds in Southern Ontario.

## Chapter 5

# CHARACTERISTICS OF SURFACE DEPRESSIONS

### 5.1 Introduction

The data set of surface elevations developed with the laser scanner on small field plots (as described in Section 4.3.3) proved very valuable for exploring objective-related questions such as the following: Can one assume that the size of the study area and the maximum size of depressional storage are independent of each other? Can one objectively map depressions over a fiberglass surface in the lab? Are there any meaningful relationships between geometric features of surface depressions and their corresponding contributing areas? Can depressional storages be described with fractal geometry? Are actual spatial patterns of depressional storage necessary for rainfall:runoff modeling or can their statistical patterns suffice? In this chapter, results of analyses of surface elevation data from the small field plots in both the spatial and frequency domains and implications of these results are discussed, paving the way for a discussion of the above questions.

## **5.2 Analysis of Laser-Scanned Digital Elevation Data**

To develop a data set which could be considered to represent the three dimensional distribution of elevation on the small field plots, a number of analyses were conducted on the raw digital data collected with the laser scanner. These analyses included steps to remove unwanted noise in the raw data, merging of partial data sets, frequency and spatial analyses of elevations and consideration of missing values. A description of these analyses is presented below with a discussion of results from the analyses in subsequent sections.

### **5.2.1 Manipulation of Upper and Lower 1% Elevation Data**

The micro-topographic cross profiles prepared for the field micro-catchments revealed that there were elevations amongst the raw data which were very deep compared to the majority of points along a transect. These relatively low elevation values were considered to be a result of very deep penetration of the laser beam through the matrix of macro-pores distributed over the surface. Such artifacts (i.e. uncharacteristic low elevations) are not uncommon in laser-scanned elevation data (Gillies, 1994), being produced whenever the size of the penetration zone is equal to or greater than the diameter of the laser beam. However, the presence of such values in the current data set adversely affected the characterization of micro-topography, increasing the effective elevation range and other elevation statistics. Since these data points had no meaningful influence on the surface roughness or storage characteristics, they were removed from the data set (i.e. replaced with 999) by eliminating the lowest values constituting one percent of the data. Another reason for removing such data from the

file was that the lowest elevation coordinates were also most subject to measurement error, these points having the greatest chance of becoming obscured from the line of view to the photo-array via the projected laser light (Bertuzzi et al., 1990).

Similar arguments were used to justify the removal of data points with very high elevation values (i.e. spikes). These too were found to be artifacts of the surface, and their presence only served to increase the calculated elevation range and other statistics beyond any meaningful surface storage effect. Again the top one percent of the elevation data were removed from the data set (i.e. replaced with 999) before further analysis of the digital elevation data.

### **5.2.2 Manipulation of Ground Control Points**

It was noted earlier that the areal coverage of the laser scanner was approximately  $1 \times 0.5$  m (effective), whereas each micro-catchment selected for scanning was  $1 \times 1$  m. As a result, each surface was scanned in two separate pieces with some overlapping of the images. Some precautions were required to guarantee that the elevations of the two parts were comparable:

- A horizontal frame was built to surround each micro-catchment surface, and the overall laser scanner frame (along with its two horizontal legs) was mounted over this frame. With this mounting arrangement, the orientation of the laser scanner (in both the vertical and horizontal directions) was fixed during the course of scanning. In addition, the scanner was leveled along the scan line prior to each scan.

- Two control points were established near the middle of each surface, and the laser scanner was adjusted such that at least one of these control points was situated along one or two of the scan lines.

Since the markers (i.e. the frames and control points) were not part of the surface elevation data, they were removed (i.e. replaced with 999) from the data set, once their  $z$  coordinates were delineated and recorded (for matching purposes).

### 5.2.3 Merging of the Two Pieces

A number of approaches have been described in the literature for merging multiple scanned images for a single surface. These include the straightforward piecing together of data when the scanner is set level but at different elevations, using the mean elevation of common first and last scan lines (Huang, 1996), and running linear regressions on the mean elevation data for  $X$  and  $Y$  scan lines for each image (Gillies, 1994). None of these approaches was appropriate for merging the elevation data collected in this study as the scanner was level along the scan line but not in the perpendicular direction, the overlapping portion of the two images obtained for each micro-catchment involved more than one scan line, and no specific linear trend was observed along scan lines.

Rather, each raw bit number file was first matched through the elevation of one or two control points and then converted to an elevation file via its respective look-up table file. When the files for the two parts were put together for each micro-catchment, and the ASCII file was converted to a grid file in ARC/INFO, the two parts were found not to match together properly. This mismatch in the merging process was attributed

to problems with data conversion (i.e. from bit number to elevation).

Upon further analysis it was found that the slope of the calibration curve depended upon the hardware setup (four factors mentioned in Section 4.3.3) plus environmental control at the time of preparation of the look-up table. As the hardware parameters were not changed from one scan to another, the slopes for the two look-up tables were not significantly different from one another. The minor difference was basically due to environmental control (e.g. wind). On the other hand, the intercepts on the look-up table depended on the location of the calibration block that was put over the surface. Therefore, the slope was a global parameter while the intercept was a site-specific local parameter. The flexibility involved in locating the calibration block created a non-uniqueness problem and gave rise to the mismatch cited in the merging process.

In a second trial, the raw bit number file was adjusted according to the Bit Number (BN) of the control points, and the BNs were multiplied by the slope of the appropriate calibration curve. The combined file in ARC/INFO revealed that the discrepancies noted earlier between the files being merged had completely disappeared. Further justification for this procedure was that relative, rather than absolute elevation data were quite sufficient for the purpose of this study.

The elevation data so obtained for each field micro-catchment could then be treated as a set of points which had both frequency and spatial distribution. The frequency distribution could be characterized by measures relating to central tendency and dispersion (Koch and Link, 1986), while the spatial distribution could be handled via variogram modeling (Isaaks and Srivastava, 1989; Journel, 1989).

## 5.2.4 Frequency Analysis of Elevation Data

Standard statistical measures, including the mean and standard deviation of elevation, were calculated for the merged data sets using the method of moments (Koch and Link, 1986), and a summary of these results is given in Table (5.1) for the three field plots.

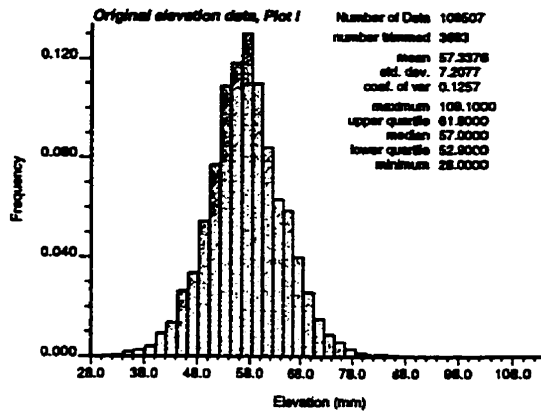
Table 5.1: Elevation statistics for the three field micro-catchments.

Plot No.	Bad data (%)	Mean (mm)	Std. dev. (mm)	Coef. of var.	Max. (mm)	Upper quartile	Median (mm)	Lower quartile	Min. (mm)
I	3.4	57.34	7.2	0.12	109.1	61.8	57.0	52.9	28.0
II	4.2	61.34	15.4	0.25	128.0	71.5	61.4	51.5	24.3
III	4.2	43.4	11.1	0.25	134.6	50.0	42.5	35.5	14.4

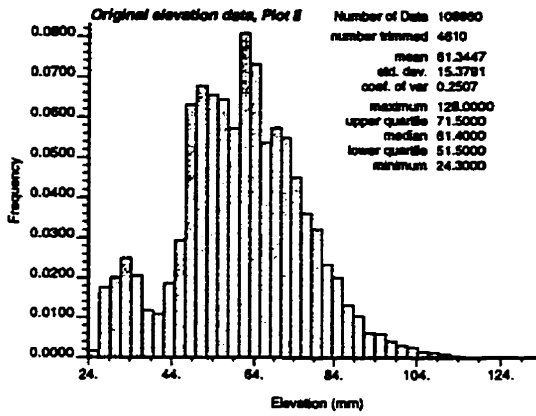
The standard deviation of elevation has been used as an index of surface roughness (Mwendera and Feyen, 1992; Zobeck and Onstad, 1987). This measure of dispersion characterizes to some extent the degree of irregularity of a surface, but supplies no information on how the irregularity is distributed areally. On the basis of the values provided in Table (5.1), Plot II could be considered to have had the roughest surface and Plot I to have been the smoothest. Part of the reason for plot II to be the roughest, could be attributed to the fact that changes in surface characteristics are likely to be more pronounced in the lower portion of sloping plots (Figure 4.11). The higher value for mean and standard deviation of elevation data for plot II compared with plots I and III, clearly explained the locational position of plot II on the hillslope. It should be mentioned that global variance, sometimes referred to as random roughness, can be misleading as surface roughness can appear to be random at one scale and orderly at another scale depending on the size of the study area. Nonetheless, the field micro-

catchments seem to be smoother than those selected by Mwendera and Feyen (1992) (with similar size) with respect to the numerical values of random roughness.

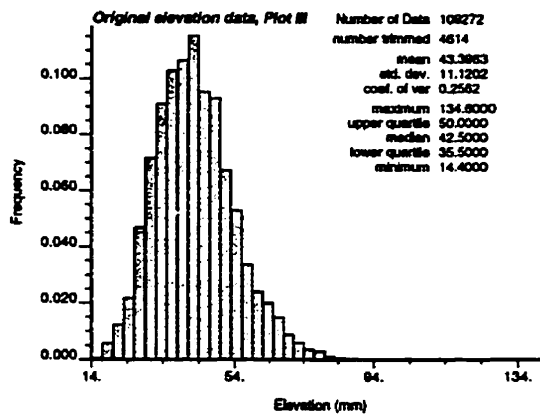
Another common and useful form of data presentation is the frequency table or its corresponding graph, the frequency histogram. This representation reveals the frequency with which observed values fall within selected intervals or classes. Figure (5.1) shows the histograms of elevation data for the three micro-catchments. It is clear from this figure that the data points for Plot I and III are symmetrically distributed, perhaps even normally distributed, while the data points of Plot II are somewhat bimodal. Again, this anomaly in normality behavior for plot II can be attributed and/or explained by the position of plot II on the hillslope (Figure 4.11). Similar patterns in frequency histograms (i.e. normality) for surface elevation data have been reported in the literature (Gillies, 1994, p. 120). These observations are noted here, as estimation tools such as Kriging (used and discussed in Section 5.3) are more appropriate when the frequency distribution of data values approximates the Gaussian or normal distribution (Isaaks and Srivastava, 1989, p. 13).



(a) Micro-catchment I



(b) Micro-catchment II



(c) Micro-catchment III

Figure 5.1: Frequency histogram and some relevant statistics for DEMs for three micro-catchments.

### 5.2.5 Spatial Analysis of Elevation Data

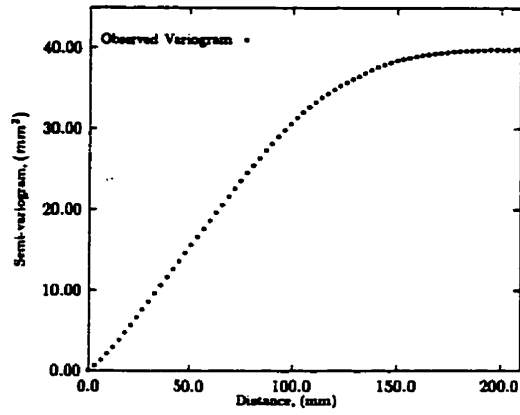
Both the scale and spatial distribution of surface roughness can alter characteristics relating to fluid flow over the ground surface; and improved knowledge of the scale of roughness and the form of its spatial distribution is needed to provide clearer explanations as to how the spatial distribution of elevation can affect micro-catchment response. Huang and Bradford (1992) suggested that the spatial structure of elevation data can be usefully quantified by examining the semi-variance of the data set.

GSLIB (Deutsch and Journel, 1992) was utilized to analyze the spatial structure of the elevation data sets collected for the three field micro-catchments with the laser scanner. Within the framework of GSLIB, it was possible to estimate geometric and zonal anisotropy of the elevation data sets (Zimmerman, 1993), topics which have not received much attention in the past (Gillies, 1994; Huang and Bradford, 1992). The subroutines could handle many different directions, variables and variogram types in a single pass. For example, it was possible to consider four different variables, eight directions, all four direct (auto-)variograms, two cross variograms and the correlogram in one subroutine call.

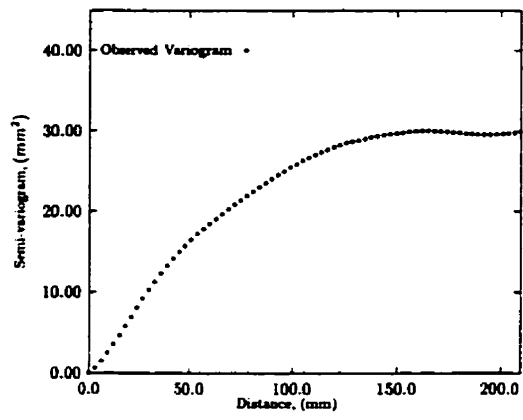
Quantification of semi-variance was achieved via the `gam2m.f` subroutine. This program calculated the square of the elevational difference between points along a pre-defined direction for each specified lag separation ( $h$ , mm). The initial lag separation was defined by the smallest spatial resolution of the laser scanner (3.0 mm), and the lag separation was increased sequentially by this length to a maximum of 210 mm. According to Oliver et al. (1989), semi-variance should be calculated for only one fifth of the total transect length, a criterion that has also been recommended for time

series analysis. In order to investigate the possibility of zonal anisotropy (Isaaks and Srivastava, 1989, p. 385) in the elevation data sets, three different directions were selected: namely,  $x$ ,  $y$  and  $x = y$  directions.

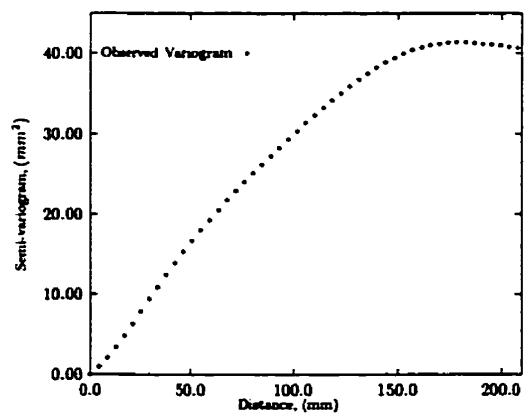
The graphical representations of the semi-variance function, or variogram, which were determined for each of the micro-catchments are shown in Figures (5.2) through (5.4). The plots reveal a general trend of sloping straight lines linked at longer lag separations to a region where the slope decreases gradually toward an asymptote. For micro-catchments I and III, it appears that the variogram remains asymptotic to a semi-variance value or so-called "sill" (Isaaks and Srivastava, 1989). In the case of micro-catchment I, the sill value in the  $x$ -direction was  $40 \text{ mm}^2$ , while its value in the  $y$ -direction was  $30 \text{ mm}^2$ . For micro-catchment III, the sill value along the  $x$ -direction was  $105 \text{ mm}^2$ , while its value in the  $y$ -direction was  $75 \text{ mm}^2$  and exhibited multi-structure behavior (i.e. a combination of basic variogram models) along the  $x = y$  direction. The sill value for both micro-catchments I and III in the  $x = y$  direction lies somewhere in between the sill values in the  $x$  and  $y$ -directions of the corresponding variograms for each micro-catchment. The variogram for plot II increases with increasing separation distance without reaching a plateau, implying an infinite capacity for dispersion (i.e. no global variance), which is a property of power variogram models. A possible explanation regarding the distinct nature of the variogram for plot II, as compared to the ones for plot I and III, might be the locational position of plot II on the hillslope (Figure 4.11).



(a) Along  $x$ -axis

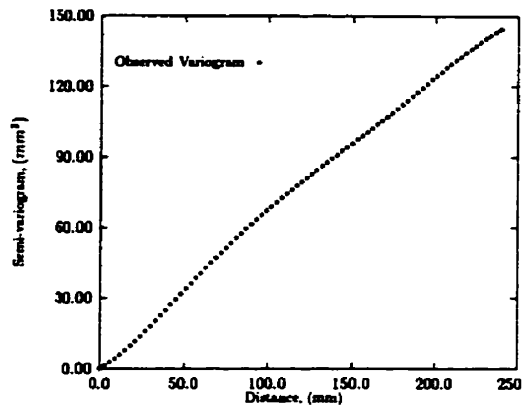


(b) Along  $y$ -axis

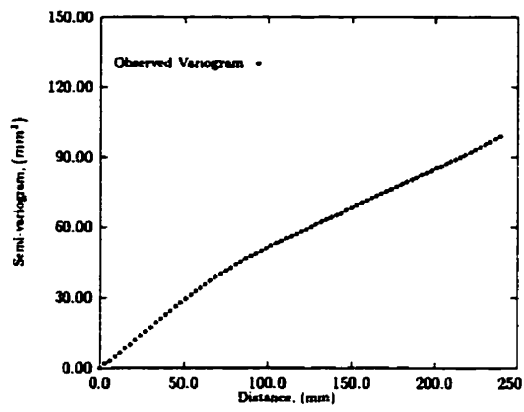


(c) Along  $x = y$

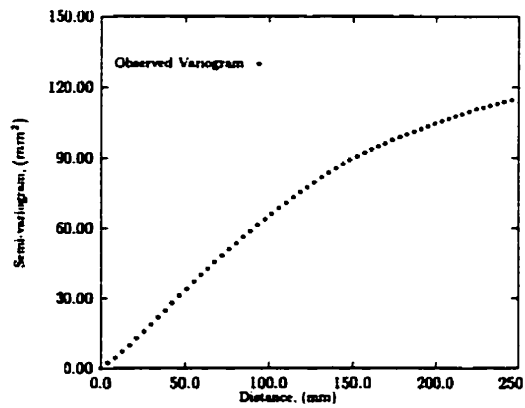
Figure 5.2: Experimental variogram along three different directions, Plot I.



(a) Along  $x$ -axis

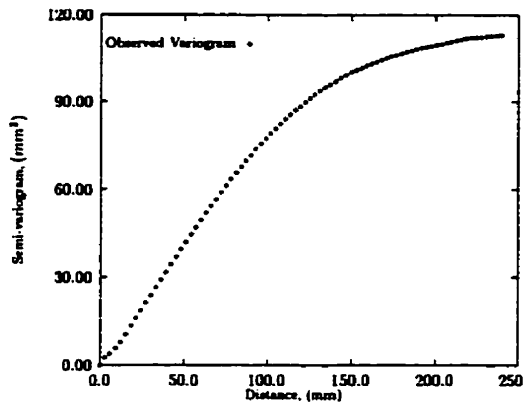


(b) Along  $y$ -axis

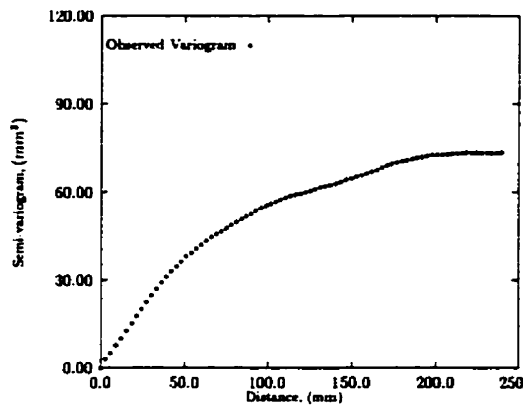


(c) Along  $x = y$

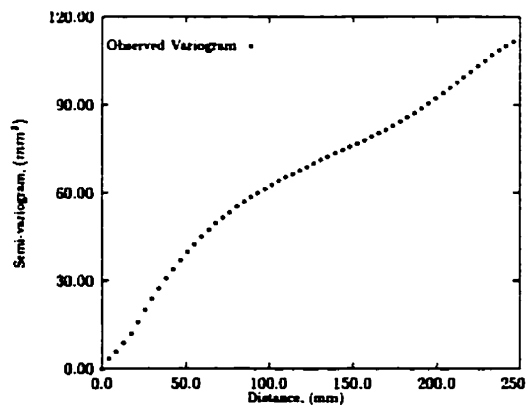
Figure 5.3: Experimental variogram along three different directions, Plot II.



(a) Along  $x$ -axis



(b) Along  $y$ -axis



(c) Along  $x = y$

Figure 5.4: Experimental variogram along three different directions, Plot III.

The overall shape of the variograms for micro-catchments I and III is representative of transition models (Isaaks and Srivastava, 1989, p. 373), indicating that values within each data set are highly correlated. The correlation among elevation data points indicates that they are not randomly distributed, and therefore the form has a distinct spatial structure that can be successfully modeled. The correlation length, the distance above which the data points are independent of each other, is almost the same for both micro-catchments I and III and equal to 150 mm. Furthermore, the change in sill value along the  $x$  and  $y$  axes, as mentioned before, implies that the elevation data are not isotropic regarding spatial continuity. As the sill value along  $x = y$  is somewhere in between the sill value of the variograms along the  $x$  and  $y$  axes, the latter two directions could be considered to be axes of anisotropy, the  $x$  axis being the principal direction and the  $y$  axis being the minor direction. According to Huang and Bradford (1992), this form is indicative of a Markov-Gaussian model with an exponential type of correlation structure for the most part, which can be represented by a combination of the following “basic models” (Kitanidis, 1993, p. 20.4):

1. Gaussian model

$$\gamma(h) = c[1 - \exp(-\frac{h^2}{a^2})] \quad (5.1)$$

2. Exponential model

$$\gamma(h) = c[1 - \exp(-\frac{h}{a})] \quad (5.2)$$

3. Spherical model

$$\gamma(h) = c(\frac{3h}{2a} - \frac{1}{2}\frac{h^3}{a^3}) \quad (5.3)$$

4. Power model defined by a power  $0 < a < 2$  and positive slope  $c$ .

$$\gamma(h) = ch^a \quad (5.4)$$

The shape of the variogram for micro-catchment II resembles a power type variogram model. In cases where the variogram exhibits a distinct upturn in the semi-variance value, one can successfully combine a transition model (depending on the behavior of the variogram near the origin) and a power model to model the experimental variogram.

#### **Variogram modeling**

The set of directional sample variograms provides an excellent descriptive summary of the spatial variability in elevation on the field plots, but most likely does not provide all of the variogram values needed for conventional estimation methods such as Kriging. In order to fit a combination of basic variogram models to a particular directional sample variogram, a decision had to be made as to which of the basic models best describes the overall shape of the variograms. Since the experimental variograms for micro-catchments I and III had a plateau (i.e. global variance), one or more of the transitional models seemed most appropriate.

Among the three transition models, the choice usually depends on the behavior of the sample directional variogram near the origin. In this case, the sample variogram showed a parabolic behavior near the origin, which was indicative of the continuous behavior of the underlying phenomenon (i.e. elevation). The preliminary exploratory data analysis confirmed that a Gaussian structure provided the best goodness of fit

among other competing models. Once the basic models were chosen, modeling the sample variogram became an exercise in nonlinear curve fitting. A discussion of the variogram modeling of elevation data for micro-catchment I is provided below in some detail, and the final results for all three micro-catchments are subsequently summarized in tabular format (Table 5.2).

In light of the zonal anisotropy revealed in the experimental variograms for each micro-catchment, it has been suggested that each nested structure in any particular directional variogram model must appear in all the other directional models with the same coefficient (i.e. similar sill value for each basic model) (Isaaks and Srivastava, 1989, p. 383). That means if the best variogram model along the  $x$  axis is Gaussian with two parameters, then the variogram along the  $y$  axis should be Gaussian with one parameter since the other parameter has already been determined. Subjecting the variogram to such a constraint along the  $y$  axis leads to the curve fitting process with one less degree of freedom, resulting in a dramatic deterioration of goodness of fit criteria along that direction. This decrease in goodness of fit criteria virtually forced the selection of a nested structure instead of a single structure.

The variogram modeling of elevation data for micro-catchment I started with a single structure, selected from the three competing transition models. Each model was fit to the experimental variogram values using nonlinear least squares regression (Gill and Murray, 1978). The subroutine **E04GCF** from the NAG library (Phillips, 1986; NAG, 1991) was utilized to perform the nonlinear regression analysis. The nonlinear regression analysis on the variogram values along the  $x$  axis revealed that the Gaussian structure provided the best fit.

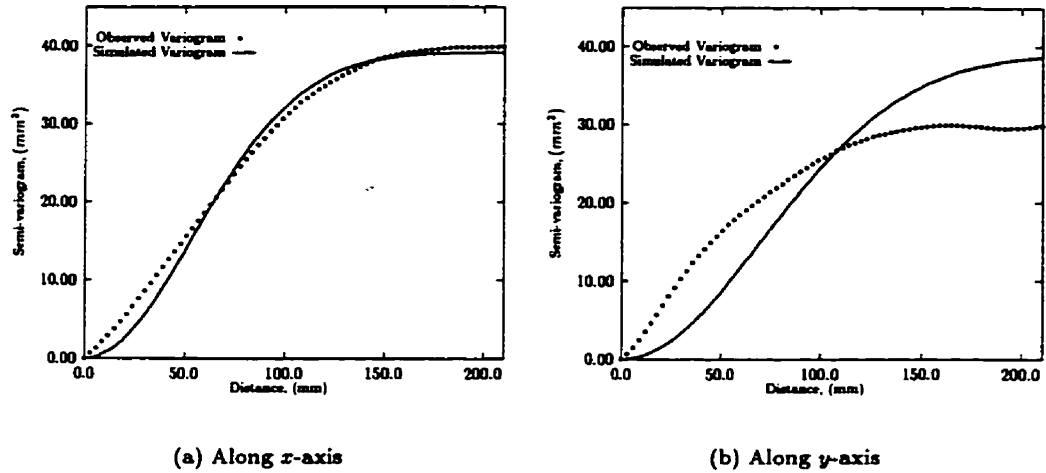


Figure 5.5: Variogram modeling-Single structure.

The simulated variogram along the  $x$  axis became:

$$\gamma(h) = 39.14\left[1 - \exp -\left(\frac{h}{76.44}\right)^2\right]$$

Sticking to this structure along the  $y$  axis, the simulated variogram was:

$$\gamma(h) = 39.14\left[1 - \exp -\left(\frac{h}{100.9}\right)^2\right]$$

Figure (5.5) demonstrates a graphical representation of the above fitting process. As is clear from the graph, the fit mimics very well the experimental variogram along the  $x$  axis, while there are large discrepancies between the experimental and fitted results for the  $y$  axis due to one less degree of freedom.

Non-linear regression analysis of the variogram values along the  $x$  axis for a double structure revealed that a combination of Gaussian and exponential structures provided the best fit among competing alternatives. The simulated variogram along the  $x$  axis

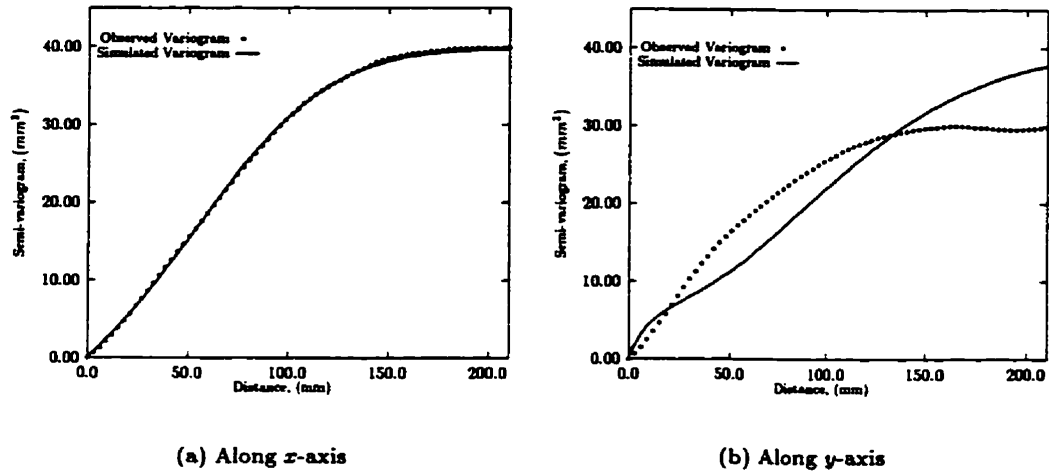


Figure 5.6: Variogram modeling-Double structure.

for this case was:

$$\gamma(h) = 6.36\left[1 - \exp\left(-\frac{h}{23.08}\right)\right] + 33.41\left[1 - \exp\left(-\left(\frac{h}{86.48}\right)^2\right)\right]$$

Using the above nested structure along the  $y$  axis, the simulated variogram was:

$$\gamma(h) = 6.36\left[1 - \exp\left(-\frac{h}{9.07}\right)\right] + 33.41\left[1 - \exp\left(-\left(\frac{h}{125.75}\right)^2\right)\right]$$

Figure (5.6) demonstrates a graphical representation of this fitting process. As is clear from the graph, the fit again mimics the experimental variogram along the  $x$  axis extremely well, while there are still some discrepancies for the fit along the  $y$  axis.

A non-linear regression analysis of the variogram values along the  $x$  axis with the assumption of a triple structure, involving all three transition models, started to contribute to the sill, with a Gaussian structure having the highest contribution. For this case, the simulated variogram along the  $x$  axis was:

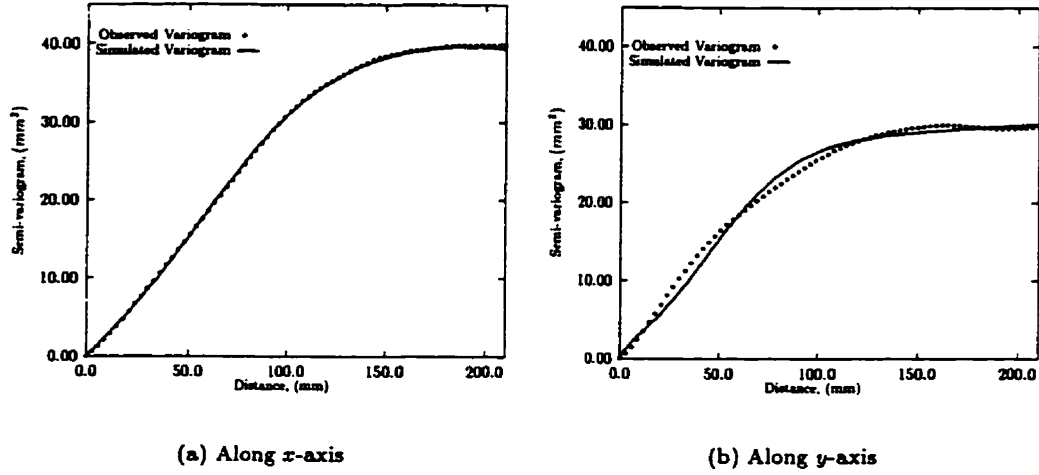


Figure 5.7: Variogram modeling-Triple structure.

$$\begin{aligned} \gamma(h) = & 2.89\left[1 - \exp\left(-\frac{h}{19.25}\right)\right] + 23.55\left[1 - \exp\left(-\left(\frac{h}{82.14}\right)^2\right)\right] \\ & + 13.33\left[\frac{3}{2}\frac{h}{185.97} - \frac{1}{2}\left(\frac{h}{185.97}\right)^3\right] \end{aligned}$$

Again with a nested structure along the  $y$  axis, the simulated variogram became:

$$\begin{aligned} \gamma(h) = & 2.89\left[1 - \exp\left(-\frac{h}{5.94}\right)\right] + 23.55\left[1 - \exp\left(-\left(\frac{h}{61.16}\right)^2\right)\right] \\ & + 13.33\left[\frac{3}{2}\frac{h}{1127.78} - \frac{1}{2}\left(\frac{h}{1127.78}\right)^3\right] \end{aligned}$$

Figure (5.7) demonstrates the graphical representation of this last fitting process. Now, as is clear from the graph, the simulated variogram mimics the experimental variograms along both the  $x$  and  $y$  axes very well.

This modeling process was pursued similarly for all three micro-catchments, and

a summary of the results along with the residual sums of squares is presented in Table (5.2).

The surface roughness length parameters (i.e. sill and range) for the scaled spatial structure models listed in Table (5.2) provide quantitative measures of roughness based on the fitting of structural function models to the semi-variance data. These parameters are qualitative descriptors of surface roughness, and may give some indication of potential hydrodynamic behavior. The micro-catchment surfaces are dominated for the most part by the Markov-Gaussian roughness form, indicating an elevation structure in which points of elevation are highly correlated within the scale range defined by the lag at which the sill value (parameter  $c$ ) or global variance ( $\sigma^2$ ) is attained. Micro-catchments I and III apparently share similar characteristics regarding overall shape as shown by the shape of the experimental variograms, while micro-catchment II has quite a different variogram structure.

Table 5.2: Fractal (fBm) and basic models parameters for various micro-catchments.

Plot No.	Basic models	Sill value ( $mm^2$ )		Range value ( $mm$ )		Fractal Dimension, $D_f$		Crossover length $l_x$ , $mm$		Residual sum of squares	
		$x-x$	$y-y$	$x-x$	$y-y$	$x-x$	$y-y$	$x-x$	$y-y$	$x-x$	$y-y$
Plot I	Gaussian	23.55		82.14	61.16	-		-		1.6044	53.1555
	Exponential	2.89		19.25	5.94	-		-			
	Spherical	13.33		185.97	1127.78	-		-			
Plot II	Gaussian	18.39	13.75	61.96	47.43	-		-		8.39	2.84
	Power	0.40	0.50	1.05	0.93	2.47	2.53	0.66	0.76		
	Nugget	0.28		-		-		-			
Plot III	Gaussian	65.84		105.23	280.14	-		-		46.65	713.64
	Exponential	46.61		56.43	34.46	-		-			

Once surface roughness is expressed by a structural function, the definition of random roughness becomes misleading. Random roughness represents the largest roughness element that can be measured after removal of slope and any other trends in data set. Here, global variances (i.e. random roughness) for both micro-catchments II and III are the same yet their variogram structure are totally different. Differences in surface features are clearly depicted by the variogram.

Huang and Bradford (1992) suggested using a combination of basic transitional and non-transitional models at different spatial scales to fit experimental directional variograms with distinct upturns such as seen in the variogram for micro-catchment II. Specifically, they proposed a combination model of fractional Brownian motion (fBm) and Markov-Gaussian (MG) processes at different scales to quantify the roughness function. In their study, the fractal regime was used to describe the sloping straight-line portions of the variogram, whereas the MG process was used to describe the region where the slope varied gradually toward 0 at higher spatial scale. Further, a Nugget effect (Isaaks and Srivastava, 1989, p. 373) has been incorporated into the overall structure to accommodate small-scale spatial variability near the origin.

The fractal dimension ( $D_f$ ) and the crossover length ( $l_x$ , mm) are related to parameters of the power model in this way:

$$\gamma(h) = ch^a$$

where  $c$  is the constant of proportionality, and  $a$  is the slope. For a fractional Brownian motion model,  $a$  belongs to the interval  $0 < a < 2$  (Huang and Bradford, 1992). From

the fitted model for micro-catchment II, the fractal dimension,  $D_f$  was determined from the slope,  $a$ , via the following relationships:

$$a = 2H$$

and:

$$D_f = 3 - H$$

A second parameter, called the crossover length ( $l_x$ , *mm*), also defined by the structural function  $\gamma(h)$  for the straight line portion of the curve, was calculated using the following equation (Huang and Bradford, 1992):

$$c = l_x^{2-2H}$$

This length parameter, unlike the non-dimensional parameter  $D_f$ , is dependent on the scale of roughness. The values calculated for  $D_f$  and  $l_x$  for both the  $x$  and  $y$  directions for micro-catchment II are listed in Table (5.2). The range of  $D_f$  values from 2 to 3 falls within ranges that theory has predicted for micro-topography (Culling, 1989); and is within the range of values reported by Huang and Bradford (1992) for agricultural soil surfaces.

### 5.3 Manipulation of Missing Values

With a model of spatial variability or spatial continuity having been established, the estimation of missing values (i.e. data not detected by laser scanner) could be

undertaken. It has been argued that inconsistent elevation data are most likely created by a blocking of the laser beam in the direction of the scan-line (Huang, 1996). Huang (1996) suggested the use of linear interpolation along the same direction to fill in missing values. However, since the elevation data points from the micro-catchments were found to be highly correlated, an effort was made in this study to take this spatial continuity into account. The Kriging method (Isaaks and Srivastava, 1989) has proven to be a powerful tool for this purpose.

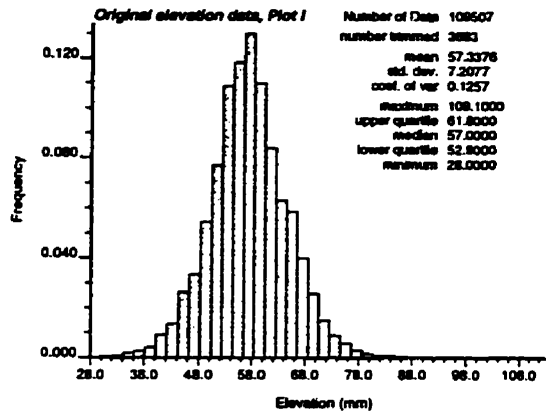
The estimation of missing values was achieved via the `okb2dm.f` subroutine (Deutsch and Journel, 1992, p.91). Contrary to conventional estimation method, Kriging not only provided estimates of the missing values but also assigned a confidence interval for each missing value. This information proved to be very valuable for assessing the reliability of each estimate. As became clear later, estimates with wide confidence intervals had a major impact on the mapping of depressional storage, which was the case around the border of each micro-catchment. In that region, the incidence of inconsistent elevation data was high, and as a result the efficiency of estimations of missing values was low (i.e. wide confidence interval).

Figure (5.8) compares the histograms of original, kriged and adjusted elevation data for micro-catchment I. It is clear from Figure (5.8) that the impact of Kriging was to enlarge and at the same time smooth out the range of elevation data. Similar observations were noticed upon adjusting the digital elevation data for micro-catchments II and III.

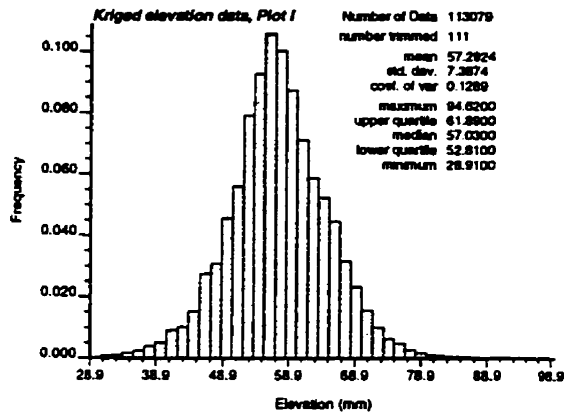
## 5.4 Surface-shaded Relief Display

Surface-shaded relief displays of each micro-catchment provided more insight on how the plots differed from one another in a spatial context. With the availability of adjusted elevation data, an ARC/INFO program was utilized to display the surface-shaded relief for each micro-catchment. Figures (5.9) through (5.11) demonstrate the adjusted histogram along with the surface-shaded relief for each micro-catchment. Visual inspection of the surface-shaded relief for each micro-catchment led to the following conclusions:

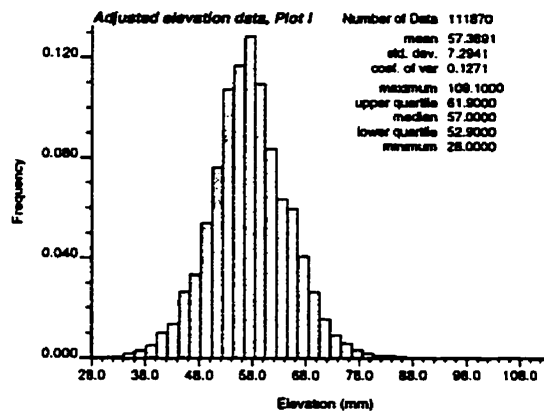
- Continuity of the surface in the middle of each micro-catchment confirms the correctness of the merging process;
- The shadowy nature of surfaces around the border, particularly in micro-catchment III, is a clear indication of poor estimation in that region; and
- Comparison among the three surfaces shows that the surfaces were not uniformly painted and sealed, a result which could have had a major impact on subsequent catchment response experiments.



(a) Original DEM

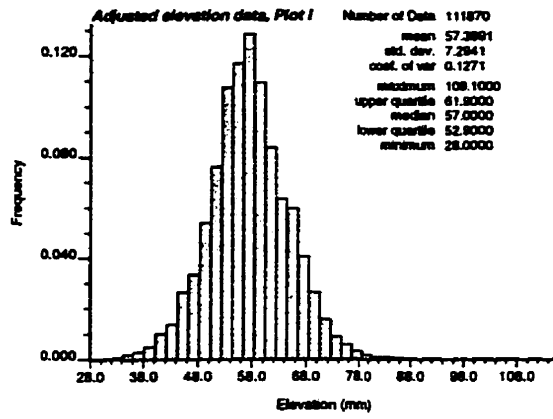


(b) Kriged DEM



(c) Adjusted DEM

Figure 5.8: Histogram and selected statistics of DEM for plot I.

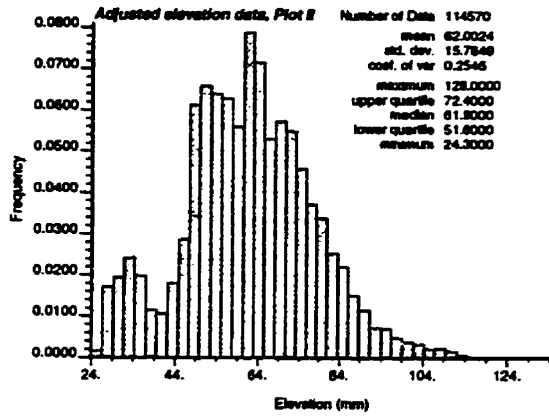


(a) Adjusted DEM



(b) Surface-shaded relief

Figure 5.9: Adjusted histogram and surface-shaded relief display for plot I.

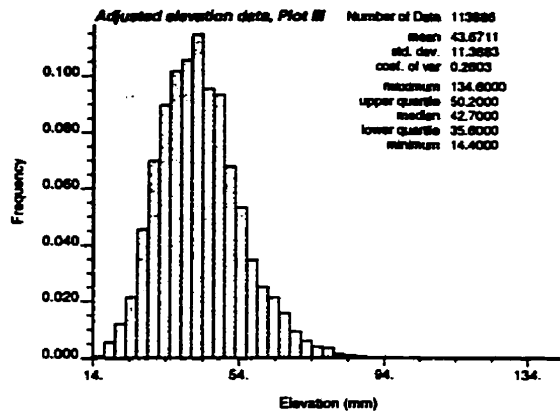


(a) Adjusted DEM

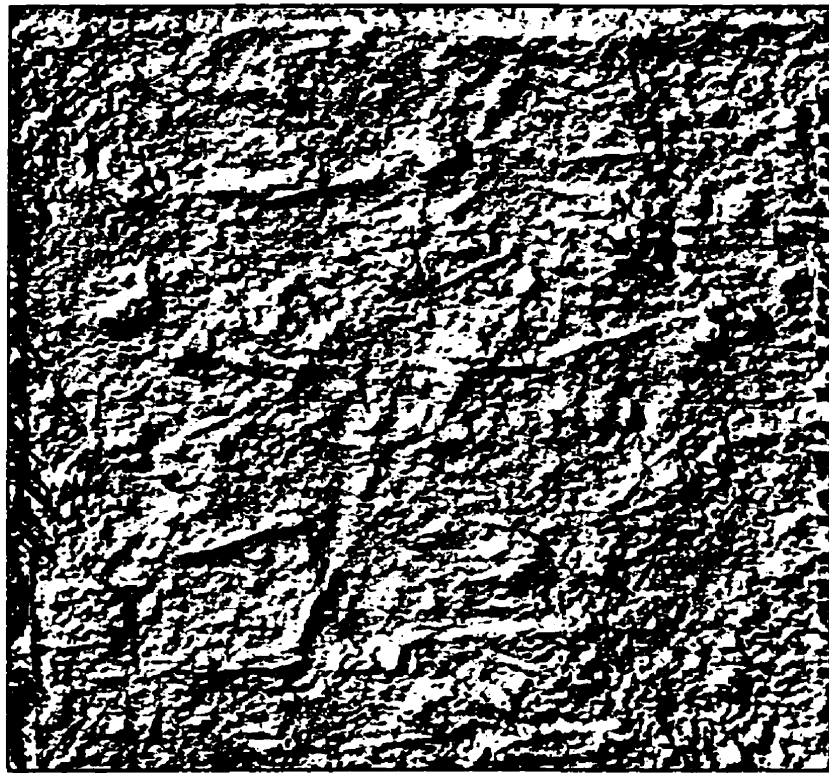


(b) Surface-shaded relief

Figure 5.10: Adjusted histogram and surface-shaded relief display for plot II.



(a) Adjusted DEM



(b) Surface-shaded relief

Figure 5.11: Adjusted histogram and surface-shaded relief display for plot III.

## 5.5 Characterization of Surface Depressions

The availability of corrected digital elevation data made identification and characterization of surface depressions on each experimental micro-catchment relatively easy. The technique used to quantify the depressional storages from each set of elevation data (on square grids) was similar to that originally proposed by Ullah (1974), with one modification. Ullah (1974) used a four-point adjacent neighbor scheme to delineate depressions; in this study, a so-called eight-point adjacent neighbor scheme was used, four orthogonal and four diagonal, as originally proposed by Huang and Bradford (1990a, p. 2237). Before characterization of depressional storages began, the boundary conditions for each micro-catchment (i.e. quadrilateral area) were established to include free drainage for the bottom side, with each of the other three sides having a no-flow boundary condition.

The sequence used to identify a closed basin started by finding a local depression. The scheme then searched for and checked the lowest point from the list of eight neighboring points to see whether it was part of the depression or an overflow (pour) point. An overflow point was identified when one of the neighboring points, except those already included in the depression, had a lower elevation. If the lowest elevation in the list of neighboring points was not an overflow point, that point was then included as part of the depression, and the list of neighboring points was updated to contain neighboring points of the newly added one. The scheme again examined the lowest point from the newly formed list of neighboring points for an overflow point. A closed basin was identified when an overflow point was found. Situations such as

two closed basins sharing a common overflow point causing overflow into each other could be easily handled. For this situation, the two basins were combined, making the common overflow point part of the depression, and the procedure was repeated until a new overflow point was found. The FORTRAN program first developed in CSIRO and then modified by C. H. Huang (to accommodate laser-scanned data) was used for this purpose.

With some modification and the addition of another subroutine, the program provided output in the following three categories:

### **Category I: Summary results**

This category provided the following information:

- Total ponded area for each plot both in  $\text{cm}^2$  and in %;
- Total volume of depressional storages for each plot in  $\text{cm}^3$ ;
- Maximum pond depth for the deepest depression in mm; and
- Average pond depth in mm, which is equal to the total volume of depressions divided by the ponded area.

### **Category II: Individual pond information and their connectivity**

In this category, the following information was provided for each depression.

- Depression number in order of appearance during identification process;
- Pour point location in raster coordinates;
- Pond surface area at pour point in pixel units;

- Contributing area of corresponding pond in pixel units;
- Maximum depth of depression in mm;
- Volume of depression at pour point in cm<sup>3</sup>;
- Average depth of depression in mm;
- Exit point location in raster coordinates;
- Depression number fed by this depression; and
- Depression number(s) feeding this depression.

### **Category III: Pond and watershed location index**

This category provided the following information for each depression.

- Location of pixels (in raster coordinates) which belong to the depression under consideration along with their effective height (i.e. pour point elevation - pixel elevation);
- Location of pixels (in raster coordinates) which contribute (potentially) to the corresponding depression; and
- An external file in ARC/INFO format to be fed to GRID module of that program for the spatial mapping of depressions. This file contains the value of an indicator variable (binary number 0 or 1) differentiating depressional areas from non-depressional ones.

The program was run for six different grid spacings, and the results are summarized in Table (5.3).

Table 5.3: Summary results of pond analysis.

Grid Spacing $\Delta x = \Delta y$ mm	Plot No.	Number of Columns	Number of Rows	Area Ponded cm <sup>2</sup>	Total Area cm <sup>2</sup>	Area Ponded %	Total Pond Volume cm <sup>3</sup>	Maximum Pond depth mm	Average Pond depth mm	Number of Ponds
3	Plot 1	339	330	859.77	10037.79	8.56	52.01	17.9	0.60	3843
	Plot 2	342	335	989.46	10280.52	9.62	62.28	47.3	0.63	4842
	Plot 3	342	333	1014.03	10218.96	9.93	123.38	26.6	1.22	4280
6	Plot 1	170	165	1248.84	10036.8	12.44	229.19	17.4	1.84	759
	Plot 2	171	168	992.52	10280.52	9.65	88.29	5.8	0.89	938
	Plot 3	171	167	1357.56	10218.96	13.28	213.79	15.8	1.57	774
9	Plot 1	113	110	1891.35	9976.77	18.96	356.84	18.1	1.89	275
	Plot 2	114	112	982.53	10249.74	9.59	91.03	8.00	0.93	337
	Plot 3	114	111	1513.08	10157.39	14.90	275.16	21.2	1.82	355
12	Plot 1	85	83	1893.6	10036.8	18.87	389.54	13.40	2.06	126
	Plot 2	86	84	1182.24	10278.72	11.50	160.72	9.40	1.36	193
	Plot 3	86	84	2306.88	10278.72	22.44	677.32	15.60	2.94	154
15	Plot 1	68	66	1941.75	9945	19.52	557.1	25.0	2.87	106
	Plot 2	69	67	1806.75	10246.5	17.63	336.98	9.60	1.86	107
	Plot 3	69	67	1928.25	10246.5	18.82	541.37	20.1	2.81	120
18	Plot 1	57	55	3055.32	9972.72	30.64	965.75	26.8	3.16	54
	Plot 2	57	56	1688.04	10157.40	16.62	281.98	7.50	1.67	65
	Plot 3	57	56	1937.52	10157.40	19.08	486.03	22.2	2.51	70
Coefficient of Variation	Plot 1	-	-	0.41	-	-	0.74	0.26	0.44	1.72
	Plot 2	-	-	0.31	-	-	0.67	1.10	0.40	1.73
	Plot 3	-	-	0.28	-	-	0.56	0.20	0.33	1.72
Pooled				0.36	-	-	0.75	0.54	0.44	1.63

## 5.6 Results and Discussion

Results regarding surface depressions on the field micro-catchments paved the way to investigate the effect of grid spacing and plot treatment on such factors as ponded area, total volume of depressions, number of depressions and also the variation of these variables from one micro-catchment to another.

As seen in Table (5.3), the variation of ponded area and total pond volume of the micro-catchments did not follow a similar trend from one grid spacing to another. For example, for a grid spacing of 3 mm, micro-catchment I had the lowest ponded area and micro-catchment III had the highest value. However, for a grid spacing of 6 mm, the trend was different, with micro-catchment II having the lowest ponded area. This apparent variability from one micro-catchment to another and from one grid spacing to another was also noted for other key variables. Excluding the results for the 3 mm grid spacing, micro-catchment II had the lowest value of ponded area and total pond volume among the three micro-catchments.

Regarding the variability and/or stability of key variables with grid spacing and plot treatments, quantification of coefficient of variation for all key variables both within and among various plot treatments (i.e. pooled coefficient of variation) showed strong fluctuations of coefficients of variation for these key variables both within and among plot treatments. According to data in Table (5.3), the number of depressions exhibited the highest values for coefficient of variation both within and among plot treatments. Furthermore, since the fluctuations in coefficients of variation from one plot to another was minimal for number of depressions, one could conclude that grid

spacing was a major source of variability for the observed values of number of depressions within each plot. Maximum depth of depression exhibited the lowest value of coefficient of variation for plot I, while the fluctuation in the coefficients among the plots was remarkable, implying that plot treatment was a major source of variability for the observed values of maximum depth of depression among the various plots. Key variables such as total pond area, total pond volume and average depth of depressions were not independent of each other, and the nature of variability in the coefficients of variation both within and among plots were almost the same for all these variables. Average depth of depression, the ratio of total pond volume to total pond area, exhibited the lowest amount of variability in coefficient of variation from one plot to another, implying an apparent resistance to grid spacing effects.

In order to further explore the effect of plot to plot and grid spacing variations on each key variable, a nested-design analysis and a one-way analysis of variance were performed on each key variable. Tables (5.4) and (5.5) summarize the results of the analysis for nested design and the analysis of variance for all variables respectively.

Table 5.4: Summary results for analysis of nested design.

Response Variable	Source of Variation (%)	
	Grid Spacing Treatment	Plot Treatment
No. of Depressions	98.44	1.56
Area, $cm^2$	46.48	53.52
Volume, $cm^3$	38.3	61.7
Max. Depth of Depression, $mm$	16.5	83.5
Ave. Depth of Depressions, $mm$	47.1	52.9

According to Table (5.4), the source of variation could be seen to vary dramatically from variable to variable between grid spacing and plot. A grid spacing effect accounts for as much as 98% of the variability in the number of depressions, while the plot

treatment accounts for as much as 83.5% of the variability in the maximum depth of depressions.

Table 5.5: One-way analysis of Variance of data for key variables.

Sources of Variation	Sum of Squares	Degree of Freedom	Mean Square	F-ratio	F <sub>0.95</sub>	Significance Level
<b>a. Total Poned Area</b>						
			Level Code = Plot Treatments			
Between means	949276.9	2	474638.46	1.546	3.68	.2452
Within Samples	4604470.6	15	306964.71			
Total	5553747.5	17				
			Level Code = Grid Spacing Treatments			
Between means	3334244.7	5	666848.94	3.605	3.11	.0319
Within Samples	2219502.8	12	184958.57			
Total	5553747.5	17				
<b>b. Total Pond Volume</b>						
			Level Code = Plot Treatments			
Between means	226210.32	2	113105.16	2.153	3.68	.1507
Within Samples	788175.36	15	52545.02			
Total	1014385.7	17				
			Level Code = Grid Spacing Treatments			
Between means	551772.64	5	110354.53	2.863	3.11	.0629
Within Samples	462613.04	12	38551.09			
Total	1014385.7	17				
<b>c. Average Depth of Depression</b>						
			Level Code = Plot Treatments			
Between means	3.144	2	1.572	3.044	3.68	.078
Within Samples	7.746	15	.516			
Total	10.890361	17				
			Level Code = Grid Spacing Treatments			
Between means	6.582	5	1.316	3.667	3.11	.0303
Within Samples	4.308	12	.359			
Total	10.890	17				
<b>d. Number of Depressions</b>						
			Level Code = Plot Treatments			
Between means	145517	2	72758.4	.026	3.68	.9744
Within Samples	42066550	15	2804436.6			
Total	42212066	17				
			Level Code = Grid Spacing Treatments			
Between means	41684698	5	8336939.6	189.703	3.11	.000
Within Samples	527369	12	43947.4			
Total	42212066	17				
<b>e. Maximum Depth of Depression</b>						
			Level Code = Plot Treatments			
Between means	117.701	2	58.851	.585	3.68	.569
Within Samples	1508.468	15	100.565			
Total	1626.169	17				
			Level Code = Grid Spacing Treatments			
Between means	648.849	5	129.770	1.593	3.11	.235
Within Samples	977.320	12	81.443			
Total	1626.169	17				

Differences from plot to plot and from grid spacing to grid spacing could be significant or non-significant depending on the variable considered. As seen in Table (5.5), for almost all key variables, differences in observed values for each key variable were non-significant among plot treatments while the degree of significance varies among key variables regarding grid spacing. Differences in observed values for the number of depressions were highly significant among the grid spacings, while for other key variables, the differences in observed values were more or less non-significant.

In order to further explore the effect of plot treatment on the observed data for each key variable, it is helpful to refer to Table (5.4) and Table (5.5) simultaneously. From Table (5.4), with the exception of the number of depressions, at least 50% of the variability in the other variables considered (i.e. area of depressions, volume of depressions, maximum and average depth of depressions) was attributable to plot treatment. Yet, the differences in plot means of these variables were non-significant among the plot treatments. In other words, from a nested-design analysis standpoint, the variability in observed values from one plot to another was considerable, while from an analysis of variance standpoint, such variability lacked consistent significant. Since no significant plot effect was delineated for the surface depression variables, it can be argued that the plots were effectively random replications, with the variances reflecting random variability. The effect of grid spacing on the observed data for each key variable is explored in more detail in subsequent sections,.

An effort was also made to compare and contrast numerical results of the pond analysis with those from similar studies reported in the literature. Due to differences in study area sizes and diversity in objectives, such a comparison was found to be

extremely difficult.

### 5.6.1 Effects of Grid Spacing on Poned Area

As Table (5.3) reveals and Figure (5.12) more clearly demonstrates, the ponded area on the micro-catchments was highly grid-spacing dependent: as grid spacing increased, ponded area increased. There is also some evidence in the graph (at least for each separate data set) of the existence of a length scale below which the ponded area is highly grid-spacing dependent, perhaps due to small-scale spatial variability, and above which again the ponded area increases with grid spacing, perhaps due to larger-scale spatial variability in elevation. For plot I, this length scale is in the vicinity of 9 to 15 mm, for plot II, around 6 to 12 mm, and for plot III, between 15 to 18 mm. In addition, total ponded area seems to have more fluctuation with increase in grid spacing among the various plots. In between the dependent portions of each curve (i.e. for each plot), the ponded area appears to be relatively stable and grid spacing independent. Therefore, the grid spacing in this region constitutes what might be termed a "preferred length scale".

The analyses of variance, summarized in Table (5.5) for each variable, confirm the above assertions on a quantitative basis. Taking plot treatment as one source of variability, since the calculated F value of 1.55 is less than the tabular value of  $F_{0.95}(2, 15) = 3.68$ , it can be concluded that all the samples were taken from the same population at a 5% significance level with regard to plot treatment. Taking grid spacing treatment as another source of variability, since the calculated F value of 3.605 is greater than the tabular value of  $F_{0.95}(5, 12) = 3.11$ , it can be concluded that

all the samples were not taken from the same population at a 5% significance level with regard to grid spacing treatment, implying grid spacing to be a major source of variability in total ponded area. In other words, the observed differences in the magnitude of total pond area from one plot to another were not statistically significant, while variations from one grid spacing to another were statistically significant.

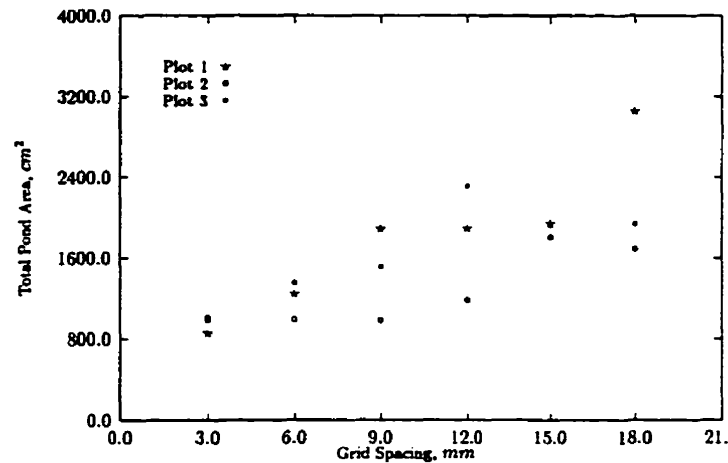


Figure 5.12: Total ponded area as a function of grid spacing for various plots.

### 5.6.2 Effects of Grid Spacing on Total Volume of Depressions

Figure (5.13) demonstrates also that the total volume of depressions determined for the micro-catchments was found to be dependent upon grid spacing. Here, the preferred length scale was less distinct, at least for plots I and III. For plot II, this length scale is in the vicinity of 5 to 9 mm. Further, for plot I, the total pond volume increases upon increase in grid spacing, while for plot II and III, the total pond volume increases up to a certain grid spacing and then decreases upon further increase in grid spacing. The grid spacing corresponding to maximum pond volume was not the same for the two plots.

Comparing the calculated and tabulated values of  $F$  in Table (5.5), it can be concluded that the samples for observed values of total pond volume were taken from the same population at a 5% level of significance, being independent of plot and grid spacing treatments. In other words, the observed difference in the magnitude of total pond volume were not statistically significant.

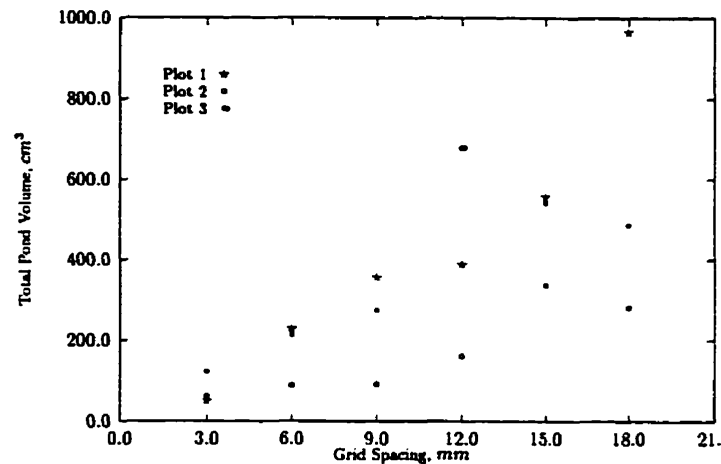


Figure 5.13: Total depressions volume as a function of grid spacing for various plots.

### 5.6.3 Effects of Grid Spacing on Number of Depressions

The total number of depressions on the micro-catchments was found to be strongly inversely related to grid spacing as seen in Figure (5.14), yet the relationship is slightly nonlinear as the slope decreases in a smooth manner implying a pure power law relationship on arithmetic coordinate axes. Visual inspection of Figure (5.14) further reveals that the relative decrease in the number of depressions for increases in grid spacing was much greater than the relative increases noted in Subsection 5.6.1 and 5.6.2 for area and volume respectively. Close similarity of data points for various micro-catchments led to the conclusion that the variation of number of depressions

with grid spacing is plot independent. In other words, the fluctuation in observed values from one plot to another was minimal.

As seen in Table (5.5), the calculated  $F$  value of 0.026 is much less than the tabular value of  $F_{0.95}(2, 15) = 3.68$  for the case of plot treatments, implying that all the samples were taken from the same population at a 5% significance level. Taking grid spacing treatments as another source of variability, since the calculated  $F$  value of 189.7 is much greater than the tabular value of  $F_{0.95}(5, 12) = 3.11$ , it can be concluded that grid spacing was a major source of variability for observed value of number of depressions. In other words, the observed differences in the magnitude of number of depressions from one plot to another were not statistically significant, while variations from one grid spacing to another were strongly statistically significant at a 5% significance level.

Generally speaking, processes such as micro and macro topography manifest themselves at a range of spatial scales. Different elements, ranging from individual grains, aggregates, clods, tillage marks and landscape features contribute to fluctuations in surface topography at their respective scales. Data sets with very fine spatial resolution at the size of a grain or less could resolve changes in elevation at the grain level; while data sets at higher spatial resolutions simply dismiss fluctuations in elevation at the grain size level. This nested structure of surface topography at different spatial scales clearly explains the strong inverse relationship between grid spacing and number of depressions.

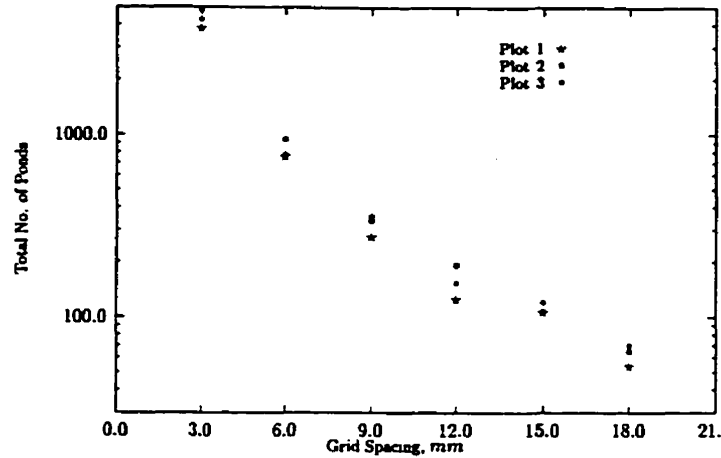
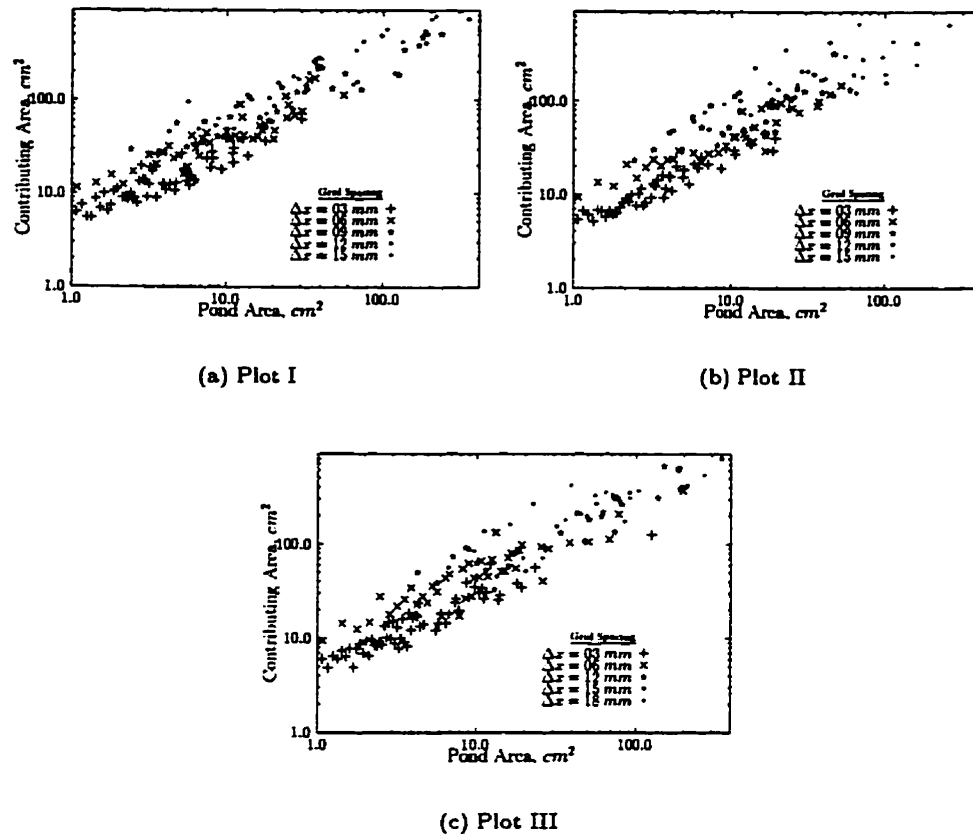


Figure 5.14: Total number of depressions as a function of grid spacing for various plots.

#### 5.6.4 Contributing Area vs. Pond Area

The program also provided the total pond area for individual pour point(s) along with the corresponding potential contributing areas for the various grid spacings. A relationship between pond area and associated contributing area (both in  $\text{cm}^2$ ) was found to exist for each plot following a linear trend on log-log axes (as shown in Figure (5.15)), implying a power law relationship on an arithmetic scale. Inspection of Figure (5.15) showed that:

- The slope of the power-law relationship is constant at a range of grid spacings;
- The power-law relationship is independent of plot number, following the same pattern for each micro-catchment;
- The variance (i.e. band width of variation) is constant, i.e. independent of grid spacing;
- The variance is also independent of plot number, following the same pattern for each micro-catchment; and



ponding contributing area, then the selection of a particular set of grid spacings is immaterial as far as estimation is concerned. In other words, estimation is equally reliable for different grid spacings. The relatively uniform distribution of data points vis-a-vis each logarithmic axis has implications regarding the scale-invariance nature of the frequency distribution of ponded area and its corresponding contributing area.

When contributing area and pond area were graphed in pixel units (Figure (5.16)), the same observations noted above were apparent. Furthermore, the dispersion (i.e. variance) in the scatter-plot was considerably diminished, implying some sort of scaling property (i.e. Hurst phenomenon). For both cases, the graphs in each category could be matched completely on each other implying that the pattern of variation was data set independent. On the basis of the data set established for a 3 mm grid spacing as a population, the constant width of dispersion (i.e. constant variance) implies that estimation again is equally reliable at different grid spacings.

## 5.7 Spatial Mapping of Depressions

Mapping of the surface depressions for the micro-catchments in a spatial context provided results which helped to clarify earlier findings and to explore some hypotheses. For this purpose, an indicator variable was defined to have a zero value for pixels belonging to depressions and a value of one for pixels not belonging to depressions. Those depressions with only one or two pixels were eliminated from the spatial mapping exercise. The output results were then linked to the GRID module of ARC/INFO to derive polygon coverage of depressional versus non-depressional areas. This digital mapping, shown in Figures (5.17) through (5.19), provided results which

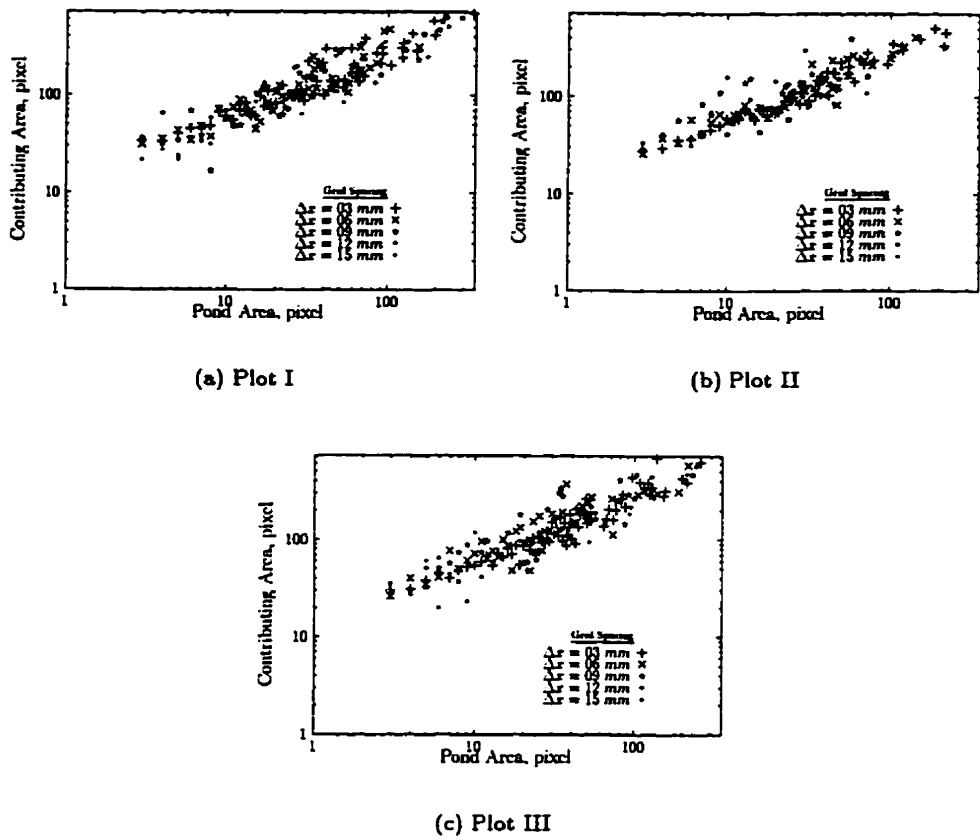


Figure 5.16: Contributing area as a function of pond area in pixel units for various plots.

were very fruitful for the visualization of the locations and topology of potential water surfaces, the consideration of discrepancies observed later in catchment response from each micro-catchment, and further examination of results and discussion relating to pond area, pond volume etc. and grid spacing.

From the mapped figures, it is clear that at very fine grid spacing (i.e.  $\Delta x = 3$  mm), the depression spatial pattern was almost the same for each plot; and as grid spacing increased, some discrepancies in spatial pattern started to develop both within a plot for various grid spacings and also among plots. These discrepancies were mainly concerned with the number of depressions within a plot and the areal coverage of

mapped depressions for various grid spacings. As mentioned previously, the total number of depressions on the micro-catchments was found to be strongly inversely related to grid spacing as seen in Figure (5.14). The mapping of depressions in a spatial context further confirmed this finding regarding discrepancies in mapping for different grid spacings. At small grid spacings, depression storages at the aggregate and clod level, for which the areal extent of coverage was very small, could be distinguished, while at higher spatial resolution, small depression storages became nested in large depressions, giving rise to larger areal extent of coverage. Cushman (1987) rightfully attributed the discrepancies among various grid spacings to the spatial resolution of equipment used to observe the phenomenon of interest referring to it as another source of randomness.

A multiple range test analysis based on Least Significant Difference (LSD) was performed on the observed data to investigate the possibility of “plateaus” in grid spacing. A quick glance at the results summarized in Table 5.6, demonstrated that the cited plateau seems to be different for different variables. The star beside a few numbers in Table 5.6 implies that the variable mean corresponding to a respective grid spacing is significantly different from the adjacent mean. The values for most of the variables corresponding to grid spacing between 9 to 18 mm were not significantly different from one another, implying the possibility of a “plateau” in that range. However, this similarity in values for each variable, particularly for higher values of grid spacing are not so distinct for the same variable in graphical representation, perhaps due to the lack of averaging over plot treatment. For example, according to Figure (5.13), volume started to decrease after a certain value of grid spacing for

plots II and III; while the average value over all plots eliminated this trend, and the plateau became more distinct.

A comparison was made between the hypsometric hill-shading of each micro-catchment surface in a color-map format and between the depression pattern of the same surface at various grid spacings. From these comparisons and field observations, it was found that a grid spacing of 18 *mm* seemed to capture the spatial pattern of depressions (as observed by eye) more accurately than any of the other grid spacings, i.e. 18 *mm* seemed to be an optimum grid spacing for visualizing the spatial pattern of depressions. Of course, as has been mentioned earlier, an optimum grid spacing is objective dependent. Its value for the reproduction of the spatial mapping of depressions is not necessarily the same as its value for the reproduction of some selected geometric features of depressions. For example, one could compare this optimum “visual” grid spacing (i.e. 18 *mm*) for the reproduction of the spatial pattern of depressions with the 11 *mm* “preferred length scale” noticed earlier in Figure (5.12).

The digital spatial mapping of depressions also aided the evaluation of the alternative hypothesis regarding the mismatch observed in the original merging of the two pieces of digital elevation data available for each plot. The continuity and smoothness in depression patterns near the middle of each surface verified the alternative hypothesis regarding the piecing together of elevation data for each plot.

Table 5.6: Results of multiple range analysis<sup>†</sup> for key variables w.r.t. grid spacing.

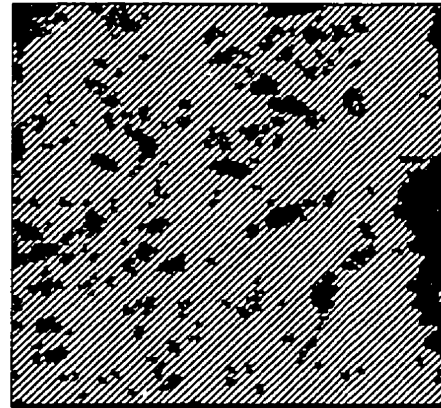
Grid Spacing	Code No.	Average Value	Difference between mean for respective variable				
			Code No.				
			(6)	(5)	(4)	(3)	(2)
<b>a. Area</b>							
3	(1)	954.42	1272.54*	937.83*	837.82	507.90	245.22
6	(2)	1199.64	1027.32*	692.61	594.60	262.68	
9	(3)	1462.32	764.64	429.93	331.92		
12	(4)	1794.24	432.72	98.01			
15	(5)	1892.25	334.71				
18	(6)	2226.96					
			LSD(0.95)=937.12				
<b>b. Volume</b>							
3	(1)	79.22	498.7*	399.26	329.97	161.79	97.87
6	(2)	177.09	400.8	301.39	232.10	63.92	
9	(3)	241.01	336.9	237.47	168.18		
12	(4)	409.19	168.7	69.29			
15	(5)	478.48	99.4				
18	(6)	577.92					
			LSD(0.95)=427.83				
<b>c. Average depth</b>							
3	(1)	.82	1.69*	1.63*	1.30	0.73	0.61
6	(2)	1.43	1.08	1.02	0.69	0.12	
9	(3)	1.55	0.96	0.90	0.57		
12	(4)	2.12	0.39	0.33			
18	(5)	2.45	0.06				
15	(6)	2.51					
			LSD(0.95)=1.30				
<b>d. Maximum depth</b>							
12	(1)	12.80	17.8	6.0	5.4	2.97	0.2
6	(2)	13.00	17.6	5.8	5.2	2.77	
9	(3)	15.77	14.8	3.1	2.5		
15	(4)	18.23	12.4	0.6			
18	(5)	18.83	11.8				
3	(6)	30.60					
			LSD(0.95)=19.66				
<b>e. No. of Depression</b>							
18	(1)	63.00	4321.7*	760.7*	259.33	94.67	48.0
15	(2)	111.00	4373.7*	712.7*	211.33	46.70	
12	(3)	157.67	4227.0*	666.0*	164.67		
9	(4)	322.33	4062.3*	501.3*			
6	(5)	823.67	3561.0				
3	(6)	4321.67					
			LSD(0.95)=456.80				

<sup>†</sup> Method: Least Significant Difference (LSD) Intervals.

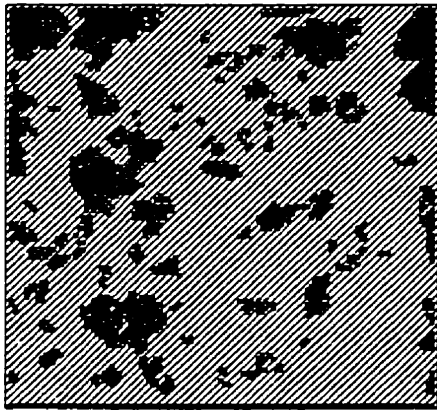
\* Difference in Mean is significant



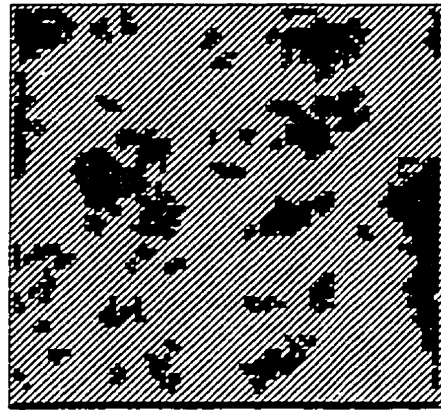
(a)  $\Delta x = \Delta y = 3 \text{ mm}$



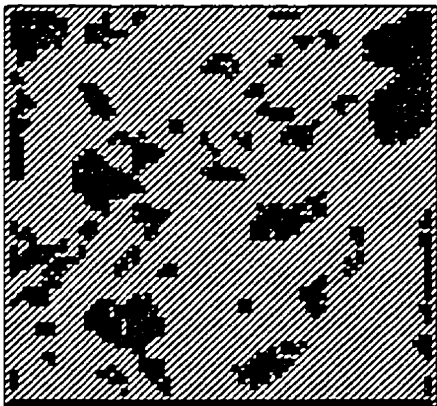
(b)  $\Delta x = \Delta y = 6 \text{ mm}$



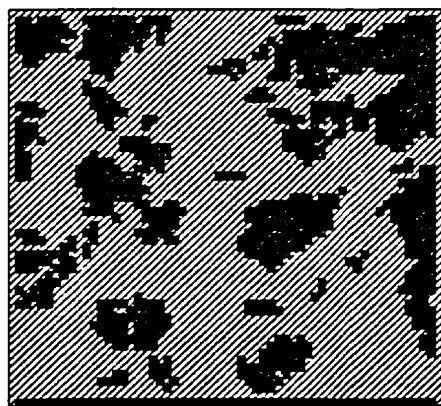
(c)  $\Delta x = \Delta y = 9 \text{ mm}$



(d)  $\Delta x = \Delta y = 12 \text{ mm}$

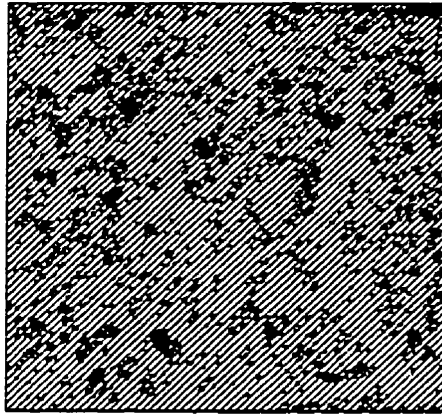


(e)  $\Delta x = \Delta y = 15 \text{ mm}$

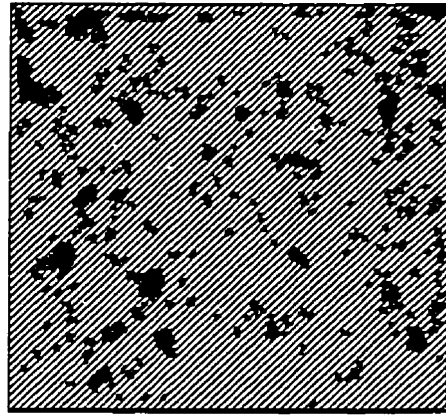


(f)  $\Delta x = \Delta y = 18 \text{ mm}$

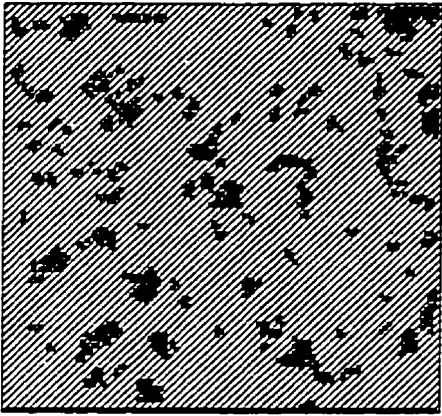
Figure 5.17: Spatial mapping of depression for various grid spacing, plot I



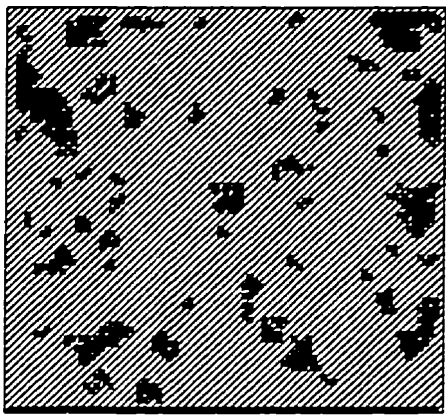
(a)  $\Delta x = \Delta y = 3 \text{ mm}$



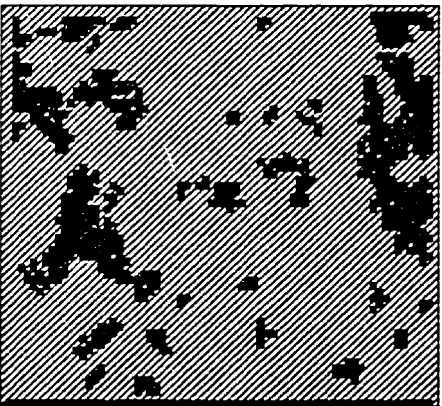
(b)  $\Delta x = \Delta y = 6 \text{ mm}$



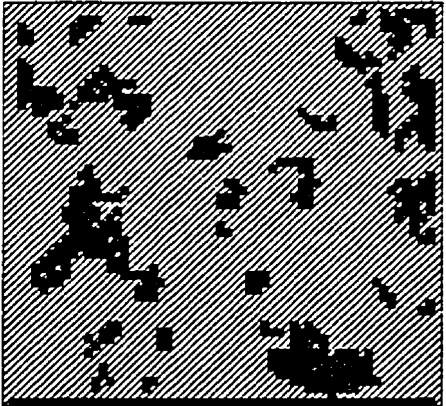
(c)  $\Delta x = \Delta y = 9 \text{ mm}$



(d)  $\Delta x = \Delta y = 12 \text{ mm}$

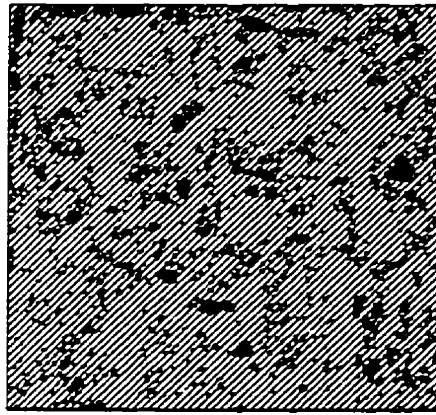


(e)  $\Delta x = \Delta y = 15 \text{ mm}$

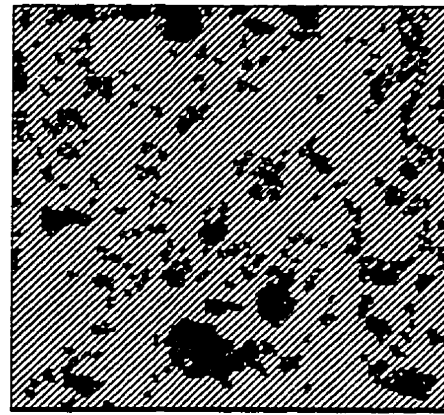


(f)  $\Delta x = \Delta y = 18 \text{ mm}$

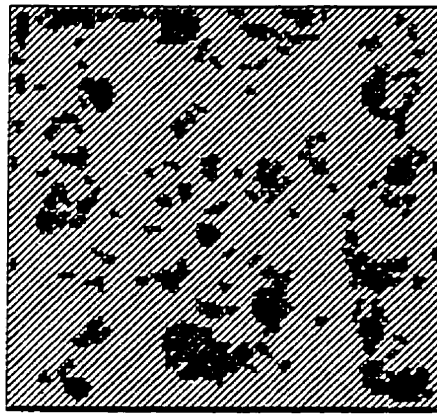
Figure 5.18: Spatial mapping of depression for various grid spacing, plot II



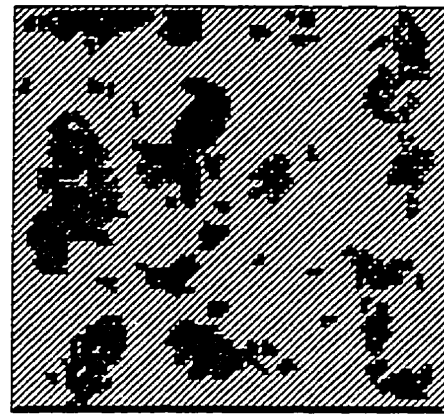
(a)  $\Delta x = \Delta y = 3 \text{ mm}$



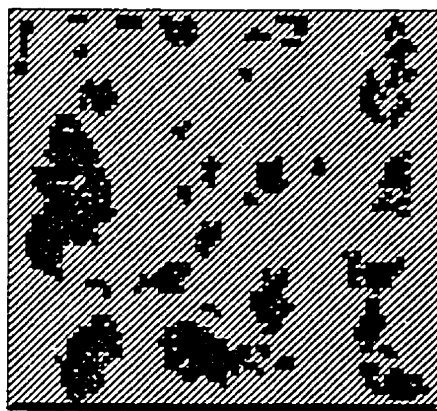
(b)  $\Delta x = \Delta y = 6 \text{ mm}$



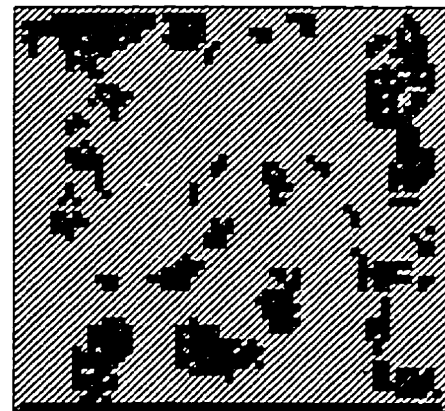
(c)  $\Delta x = \Delta y = 9 \text{ mm}$



(d)  $\Delta x = \Delta y = 12 \text{ mm}$



(e)  $\Delta x = \Delta y = 15 \text{ mm}$



(f)  $\Delta x = \Delta y = 18 \text{ mm}$

Figure 5.19: Spatial mapping of depression for various grid spacing, plot III

### 5.7.1 Effect of Re-sampling on Spatial Mapping

It was important and informative to investigate the impact of re-sampling on the digital spatial mapping of depressions. The need for such an investigation arose from the fact that development of the digital elevation data sets with different grid spacings could have been achieved in two totally different ways: on the one hand, the laser scanner could have been set for each grid spacing, and the surface scanned one spacing at a time; while on the other hand, the surface could have been scanned at a relatively fine grid spacing (such as 3 *mm*), and subsequent data sets re-sampled from this initial data set. In this study, the latter method was adopted. The first row and column of laser-scanned data were included in all data sets, and the next one, two and three row(s) or column(s) were selectively eliminated depending on the prescribed grid spacing. Figures (5.20) through (5.22) illustrate a few spatial mappings of depressions for various re-sampling schemes for plot I.

As can be seen from these figures and their comparison with Figure (5.17), at both very low (i.e.  $\Delta x \leq 6$  *mm*) and very high (i.e.  $\Delta x \geq 15$  *mm*) grid spacings, the mapping becomes comparable to the results of mapping for other re-sampling schemes and also the earlier pattern observed in Section (5.7). For grid spacings in between, the major discrepancies among the various spatial mappings are around the borders. Possible reasons for such discrepancies and the observed patterns from one re-sampling technique to another are explained in the following paragraph.

Visual inspection of the digital mapping of depressions obtained in Section (5.7) for the original sampled data sets and the ones from re-sampling schemes revealed that the major degree of discrepancies, i.e. zones belonging to depressional areas

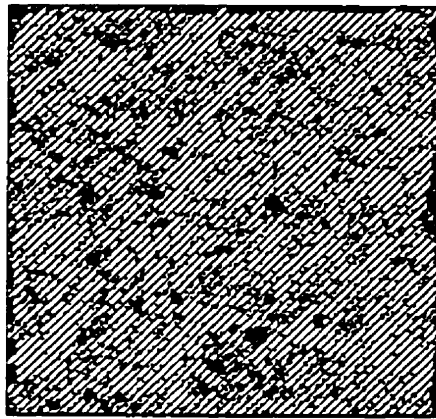
in one figure and non-depressional areas in another figure, were almost all around the edges of each figure where the estimated values had a relatively large confidence interval (i.e. shadowy zones in Figure 5.9). One possible cause of poor estimation and wide confidence intervals around the edges may have been the nature of the Kriging process itself, as the necessary condition for this Geostatistical tool to work properly regarding a uniform distribution of data points in all four quadrants around any point of unknown elevation was lacking.

Another argument here is the continuous nature of the topographic pattern explored in variogram modeling (i.e. highly spatially correlated elevation data). The cited continuity could be viewed from two totally different perspectives. According to one viewpoint, since topography is a continuous process, then digital spatial mapping of depressions should be least affected by re-sampling. In other words, spatial mapping of depressions should not be that sensitive to grid spacing, and the switching of a few spots between depressional versus non-depressional areas should be minimal. Poor results of estimation in a few pixels on the one hand, and the way the algorithm utilized elevation data after elimination of one row or column in those regions on the other hand, might explain the discrepancies observed from one grid spacing to another. Indeed, the algorithm made decisions in light of even a very small change in elevation value giving rise to different spatial mappings even for similar grid spacings, but different re-sampling schemes.

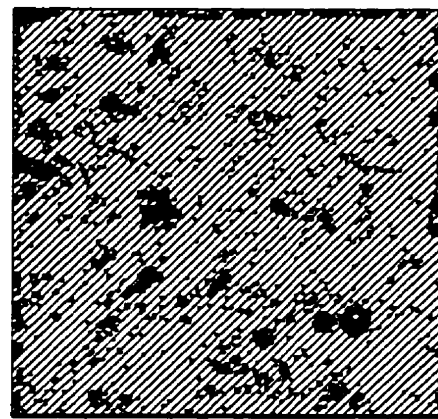
It has been argued that in reality, the spatial mapping of depression storage is unique. In other words, if one were to seal the surface completely and then pour water on the surface up to the potential capacity of depressions over the surface, it

should be verifiable that depressional and non-depressional areas are unique. However, this cited uniqueness, if it can be seen, cannot be replicated. Hence, the difference between observing something in nature and trying to reproduce it. Indeed, science itself is about the difference between knowing something and understanding the same thing. As such, the cited discrepancies were justifiable, and the elimination of one row or one column from the whole data set gave rise to different spatial mappings even for the same grid spacing.

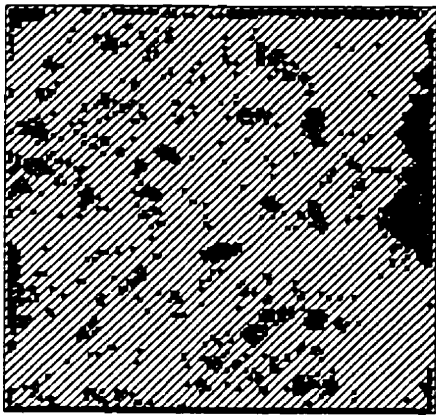
At this stage, it has to be stated that such a lack of uniqueness in spatial mapping of depressions has least or no impact on subsequent analyses as rainfall-runoff model structure will benefit from statistical pattern of depression as opposed to their actual pattern.



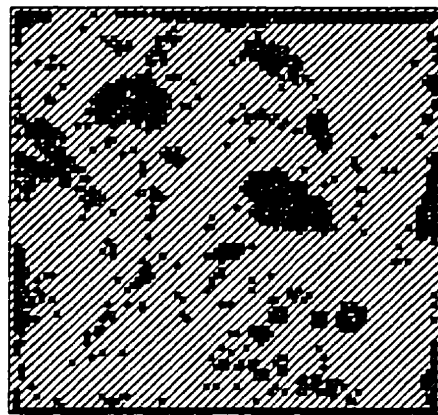
(a)  $\Delta x = \Delta y = 3 \text{ mm}$



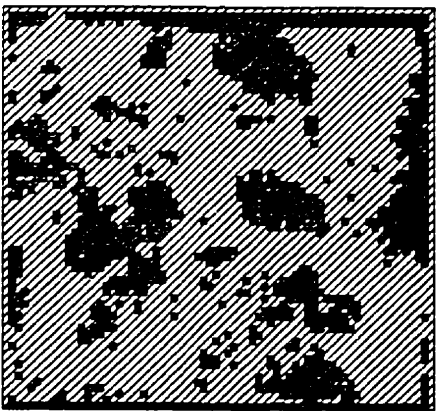
(b)  $\Delta x = \Delta y = 6 \text{ mm}$



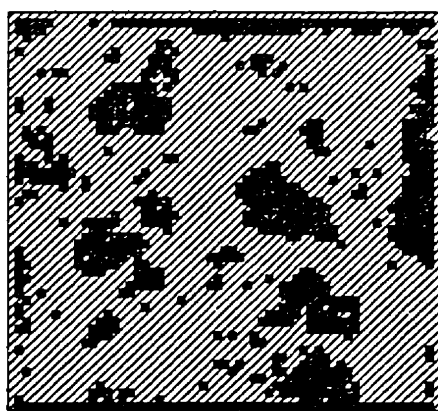
(c)  $\Delta x = \Delta y = 9 \text{ mm}$



(d)  $\Delta x = \Delta y = 12 \text{ mm}$



(e)  $\Delta x = \Delta y = 15 \text{ mm}$



(f)  $\Delta x = \Delta y = 18 \text{ mm}$

Figure 5.20: Spatial mapping of depression for various grid spacing, plot I (Elimination of first column)

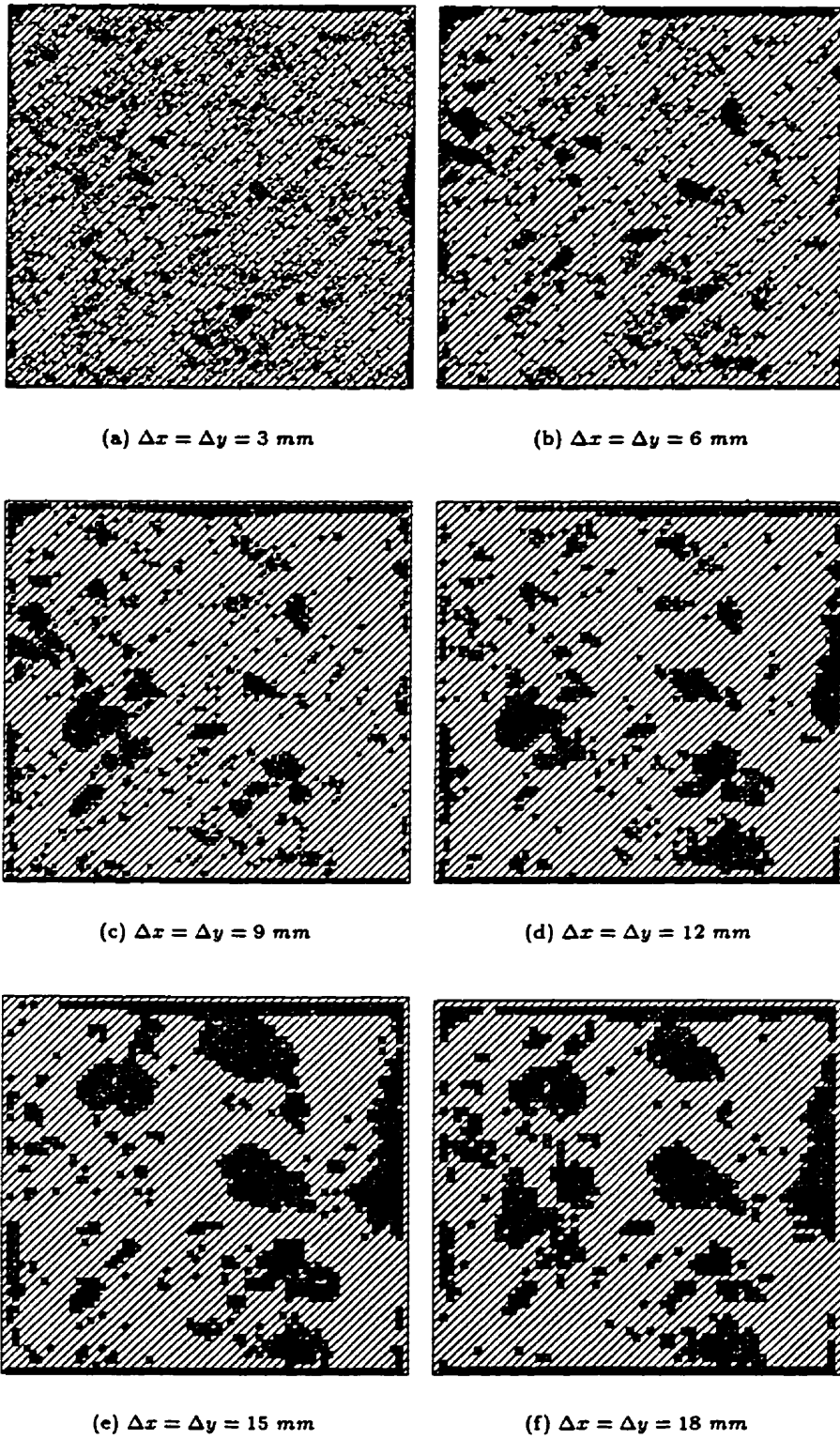
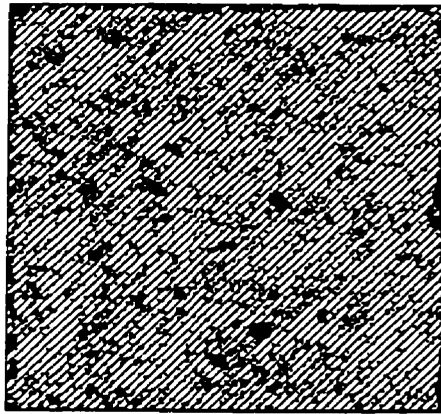


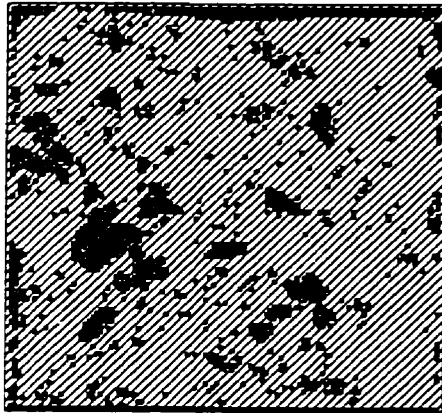
Figure 5.21: Spatial mapping of depression for various grid spacing, plot I (Elimination of first row)



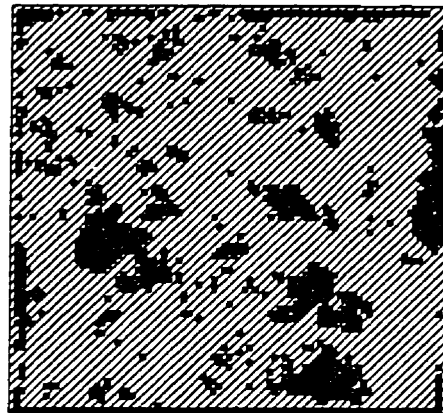
(a)  $\Delta x = \Delta y = 3 \text{ mm}$



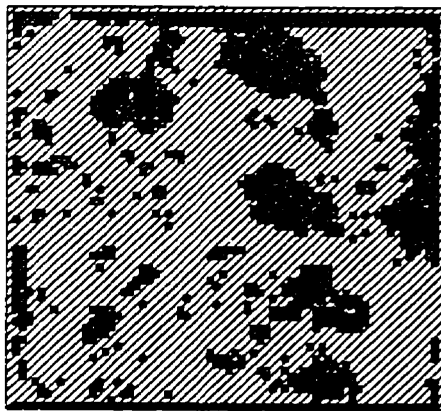
(b)  $\Delta x = \Delta y = 6 \text{ mm}$



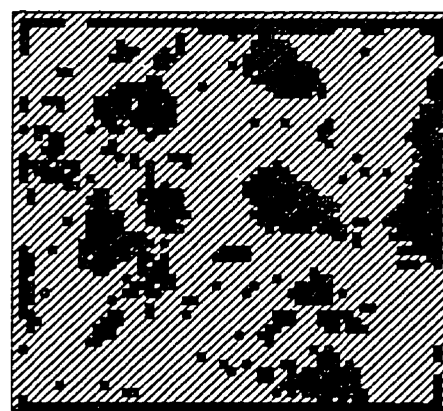
(c)  $\Delta x = \Delta y = 9 \text{ mm}$



(d)  $\Delta x = \Delta y = 12 \text{ mm}$



(e)  $\Delta x = \Delta y = 15 \text{ mm}$



(f)  $\Delta x = \Delta y = 18 \text{ mm}$

Figure 5.22: Spatial mapping of depression for various grid spacing, plot I (Elimination of second row)

## **5.8 Implications of Pond Results**

Results of the analyses of the digital elevation data in both the spatial and frequency domains paved the way to address the implications of such analyses. Issues such as:

1. Dependency of study area size and maximum size of depression storage;
2. Existence of optimum grid spacing;
3. Possibility of describing geometric features of depression storage by fractal geometry;
4. Development of meaningful relationship between contributing area and other geometric features of depressions; and
5. Sufficiency of statistical pattern of depressions for rainfall:runoff modeling rather than their actual patterns.

are discussed in the following sections under the two broad headings of “scale-invariance property” and “power law relationship” building further upon the pioneering work of Ullah (1974). In particular, items 1 and 2 above are discussed exclusively under the first heading, while the other items are discussed under the second heading.

### **5.8.1 Scale-invariance property**

As early as the initiation of the experimental design and performing of the laboratory experiment, one of the main issues was the delineation of depression storages on the laboratory surface. Acknowledging the two pitfalls associated with the delineation of surface depressions over the surface, i.e. the row-wise pattern and the lack of a nested

structure, it became clear after the pond analysis that there was still another pitfall associated with the way the depressions were laid down over the fiberglass surface. The pitfall was somehow concerned with an interaction between the overall size of the study area and geometric features of the depressions such as their maximum size. The pond analysis of the small-scale field plots revealed that in terms of frequency of occurrence, the depression storages appeared to be statistically scale-invariant, i.e. statistically unchanged under magnification or contraction, at least over a fairly wide range of spatial scale resolutions (see Section 5.6.4). This scale-invariance might mean that by increasing the spatial scale (i.e. size of the study area), the probability density function would remain invariant even though its parameters might change. In light of constant parameters, simple scaling is applicable, while for the case of varying parameters across spatial scales, multi-scaling is applicable (DeCoursey, 1996). Such a scale-invariance nature of the probability distribution function and the possible change in parameter values from one spatial scale to another could then be interpreted as dependency of study area size and size of depression storage implying that depression storage could not be located over the fiberglass surface without due consideration to size of study area. This assertion conforms with the salient finding of Huang and Bradford (1990a) who argued that in a field of high-scale dependency such as surface topography, any measure (in this case delineation of surface depression) is controlled by not only the global statistics of elevation data, but also the upper and lower cutoff length scales of the study area. In their study, the upper cutoff length scale was found to be the side length of the test area, and the lower cutoff length scale was the grid spacing. They found that for scaling of depressional storages, both cutoff length scales

were key parameters.

Regarding the constant variance attribute and the stability of the pond area versus contributing area relationship at a range of grid spacings regardless of plot number explored in Section 5.6.4, the results conform with the assertion made by Hastings and Sugihara (1993). They defined a pattern or object to be scale-invariant within the scaling region if the pattern or object contained no natural internal measures of size, and thus appeared the same at all scales within the scaling region. Here, the scaling region is defined as a length scale (time or space) whereby the relationship between two variable of interest stays constant. This relationship could be a linear relationship in log-log coordinate system or a frequency distribution. For example, in Section 5.6.4, the pond area and its corresponding contributing area of a set of depression storages were found to be scale-invariant, despite the fact that the area and/or contributing area of each depression could be measured. In this case, scale-invariance simply means that the small depressions were essentially reduced versions of the large depressions, and the large depressions were enlarged versions of the small ones. Extrapolation of results obtained at one grid spacing to another, could be considered one direct implication of this scale-invariance behavior.

More generally, there may be several scaling regions with unique properties, separated by breakpoints whereby the inherent organization is still distinct but with different parameters, with scale-invariance holding within each region but failing when a break-point is crossed. Delineation of the cited breakpoints is a matter of accessibility to digital elevation data sets at a range of spatial scales.

Generally speaking, changing the scale of observation or averaging has a significant

but poorly understood impact on the apparent variability of hydrological quantities as explored in this chapter for depressional storages. Interaction between spatial variability and spatial scale is also another poorly understood concept and is widely perceived as a substantial obstacle to progress in hydrology. In response to the delineation of the optimum grid spacing, the above insights imply that any rational analysis of depressional storages or runoff from depressional storages areas must specify “a priori” the range of spatial resolution (i.e. scaling region) of the experimental apparatus and the associated window size (Cushman, 1987) for which the relationship between associated variables conform to a well-defined law. What might be a preferred (i.e. optimum) spatial resolution for an experimental apparatus as far as establishing a relationship between say pond area and contributing area is concerned would probably become an irrelevant concern when working and/or moving in a scaling region (i.e. region between breakpoints).

### **5.8.2 Power Law Relationship Among Various Geometric Attributes**

Considering depression storages as irregular, seemingly complex shapes that display similar patterns over the range of scales (as found in this chapter and elsewhere, e.g. Huang and Bradford (1990a)), fractals provide a mathematical framework for their treatment. Many objects in nature possess a property cited as statistical self-similarity. This may be defined as invariance of the probability distributions describing the object’s composition under simple geometric transformations or changes of scale. As such, depression storages on the natural surfaces fall into this class of geometric objects.

On the study of depression storage characterization and inter-relationships, Ullah (1974) found that the relation between depth and area or depth versus volume or volume versus area, ...all exhibit a linear pattern (i.e. power law) in log-log space, implying that depressions are fractal objects and the rule of fractal geometry (Feder, 1988) is exclusively applicable to them. In this study, it was found that the relationship between potential contributing area for each depression versus area of depression at each pour point exhibited a linear pattern (i.e. power law) in log-log space, implying that the process is self-organized.

In response to the question of whether the actual spatial distribution of storages or their statistical distribution should be considered in structuring a rainfall-runoff model, results from the pond analysis and in particular from the analysis of variance for the number of depressions (Section 5.6.3) clearly reveal that the total number of depressions on the micro-catchments is strongly inversely related to grid spacing as seen in Figure(5.14). As a result, one may argue that these storage elements manifest themselves at a range of spatial scales and that their number approaches infinity for very small grid spacing, making consideration of their actual storage patterns nonsense. One possible approach whereby statistical patterns of depressions rather than their actual patterns could be utilized to structure rainfall-runoff model, is provided in Section 7.9.

## Chapter 6

# Rainfall:Runoff Experimental Results and Discussion

### 6.1 Introduction

The sets of rainfall:runoff data collected and assembled from the laboratory experiments, the field micro-catchments and the small watersheds provided much valuable information for consideration of a range of questions such as: What was the impact of overall slope on micro-catchment response? How could the nature of water movement over the surface (i.e. both in the laboratory and field) be explained on the basis of the observations of catchment response? What was the impact of surface storage elements on catchment response over the range of spatial scales explored? What was the role of spatial and temporal variability in rain on catchment response over the range of spatial scales? Could, and how could, results obtained at one scale be effectively used at another scale (at least on a qualitative basis)? Such questions are addressed in this chapter in light of the various catchment response data and their analyses, components of the lumped water balance equation being addressed first, then the time-wise

variation of outlet hydrographs.

## 6.2 Small-scale Laboratory Experiments

Sample results obtained from the laboratory experiments for each surface treatment are presented and discussed in this section. Details regarding the laboratory experimental results have been provided in Appendix A.

### 6.2.1 Sample Results of Laboratory Experiments

In the small-scale laboratory experiments, five surface treatments were considered at different levels of complexity, starting with flat surfaces and moving to surfaces with different patterns of depression storage and conditions of infiltration. Combining these surface treatments with five slope treatments and three rainfall treatments, and with two replications for each experimental run, 150 sets of rainfall-runoff data were collected. The following presentation and discussion deals with the experimental results in both a lumped form (i.e. water balance results) and a distributed form (i.e. hydrograph analysis).

#### Water Balance Results

The water balance equation, lumped in space and time and treating evaporation as negligible, can be expressed as:

$$P - R - F = \Delta S \quad (6.1)$$

where  $P$  = rainfall for the period  $\Delta t$ ,  $R$  = runoff for the same period,  $F$  = cumulative

infiltration in  $\Delta t$ , and  $\Delta S$  = amount of water remaining in storage for the same time period. Not all components of the water balance equation were present for each surface treatment in the laboratory experiment. For surface treatment I, only the first two components (i.e. rainfall and direct runoff) were present (with the exception of water held by surface tension); while for surface treatments II and III, the infiltration component was absent, but there were storage elements placed over the surface. For surface treatments IV and V, all components of the water balance equation were present. In these latter cases, some of the surface depressions ponded water temporarily for subsequent infiltration, while those with no infiltration stored water more permanently.

Rainfall and runoff were measured in all experimental runs, while the total amount of water trapped in depression storages was measured only for surface treatments II and III. For surface treatments IV and V, an effort was made to measure time-wise and cumulative infiltration from those depressions for which drainage was allowed. Infiltration loss from those depressions was directed to a water collector via transparent hoses, and the water collector in turn was connected to the datalogger. During experimentation, it was noticed that the air entrapped inside the hoses hindered continuous flow of water to the water collector. This discontinuous flow of water hampered an objective analysis of infiltrating water, resulting in data related to infiltrating water not being analyzed further.

Table (6.1) summarizes lumped results from the experimental runs for all slopes and rainfall patterns for surface treatment II. The data in the water loss column were determined from the amount of water trapped in depressions as measured directly

after each experimental run.

Table 6.1: Summary of experimental runs (water balance components) for surface treatment II.

Slope Treatment %	Rainfall Pattern	Total Rainfall mm	Surface runoff, mm			Water losses,* mm			Runoff Coefficient %
			Rep. (1)	Rep. (2)	Average Value	Rep. (1)	Rep. (2)	Average Value	
6%	LMH	3.16	2.53	2.56	2.54	0.61	0.63	0.62	80
	MLH	3.28	2.68	2.72	2.70	0.63	0.64	0.64	82
	HML	3.18	2.57	2.58	2.58	0.64	0.65	0.64	81
8%	LMH	3.16	2.64	2.57	2.60	0.63	0.62	0.63	82
	MLH	3.28	2.68	2.62	2.65	0.62	0.63	0.63	81
	HML	3.18	2.55	2.62	2.58	0.64	0.65	0.64	81
10%	LMH	3.16	2.57	2.58	2.58	0.62	0.63	0.62	82
	MLH	3.20	2.61	2.66	2.64	0.63	0.62	0.62	82
	HML	3.23	2.58	2.59	2.58	0.65	0.64	0.64	80
12%	LMH	3.30	2.56	2.58	2.57	0.62	0.62	0.62	78
	MLH	3.27	2.75	2.65	2.70	0.64	0.62	0.63	82
	HML	3.23	2.63	2.58	2.60	0.65	0.65	0.65	81
14%	LMH	3.30	2.63	2.63	2.63	0.62	0.62	0.62	80
	MLH	3.27	2.62	2.68	2.65	0.62	0.61	0.62	81
	HML	3.23	2.59	2.70	2.64	0.65	0.65	0.65	82

\* Equivalent depth of water accumulated in depression storages. The corresponding volume was measured at the end of each experimental run.

In order to investigate the impact of surface treatments on the lumped behavior of the system, components of the water balance equation were extracted from similar tables for the various surface treatments for a slope of 10% and are summarized in Table (6.2).

An extensive analysis of variance was conducted to explore the impact of surface treatment, slope treatment and rainfall pattern on key variables such as cumulative rainfall amount, cumulative runoff amount and cumulative water loss due to depression storage and infiltration. Details of this analysis are provided in Appendix B, with a summary account provided below:

Table 6.2: Summary of experimental runs (water balance components) for various surface treatments ( $S = 10\%$ ).

Surface Treatment	Rainfall Pattern	Total Rainfall <i>mm</i>	surface runoff, <i>mm</i>			Water losses, <sup>*</sup> <i>mm</i>			Runoff Coefficient %
			Rep. (1)	Rep. (2)	Average Value	Rep. (1)	Rep. (2)	Average Value	
I	LMH	3.56	3.37	3.33	3.35	-	-	-	94
	MLH		3.37	3.45	3.41	-	-	-	96
	HML		3.26	3.34	3.30	-	-	-	93
II	LMH	3.16	2.57	2.58	2.58	0.62	0.63	0.62	82
	MLH	3.20	2.61	2.66	2.64	0.63	0.62	0.62	82
	HML	3.23	2.58	2.59	2.58	0.65	0.64	0.64	80
III	LMH	3.12	2.72	2.78	2.75	0.35	0.35	0.35	88
	MLH		2.78	2.79	2.78	0.34	0.35	0.35	89
	HML		2.69	2.74	2.72	0.42	0.39	0.41	87
IV	LMH	3.56	2.48	2.45	2.46	1.07	1.11	1.09	69
	MLH		2.52	2.56	2.54	1.04	1.00	1.02	71
	HML		2.40	2.52	1.16	2.46	1.03	1.10	69
V	LMH	3.56	2.87	2.83	2.85	0.68	0.73	0.70	80
	MLH		2.74	2.71	2.72	0.82	0.85	0.84	76
	HML		2.75	2.73	2.74	0.81	0.83	0.82	77

\* Measured depression storage for surface treatments II and III, calculated storage plus infiltration for treatments IV and V (i.e. rainfall-runoff).

### Highlights of Significant Effects

#### 1. Surface treatment effect-

- The effect of surface treatment on total runoff amount was found to be significant at the 5% level; and correspondingly
- The effect of surface treatment on water losses<sup>1</sup> was found to be significant at the 5%.

#### 2. Rainfall pattern effect-

- Variations in total runoff amount from one rainfall pattern to another were found to be significant at the 5% level, implying importance to quantification

<sup>1</sup> By water losses, it meant total volume of water stored in depressions for surface treatments II and III, storage plus infiltration for surface treatment IV and V.

of the rainfall temporal pattern in a typical event; and correspondingly

- The effect of rainfall pattern on water losses was found to be significant for the same surface treatment.

### 3. Combined effect of surface treatment and slope-

- The combined effect of surface treatment and slope on total runoff amount was found to be significant for different surface and rainfall patterns; and correspondingly
- The combined effect of surface treatment and slope on water losses was found to be significant for various rainfall patterns.

### 4. Slope treatment effect-

- The effect of slope treatment on the potential value of depression storage<sup>2</sup> was found to be significant at the 5% level.

## Highlights of Non-significant Effects

### 1. Slope treatment effect-

At the 5% probability level for the same surface treatment, the effect of slope treatment was found to be non-significant on:

- Cumulative rainfall,
- Total runoff, and
- Water loss.

---

<sup>2</sup>The potential storage defined by the geometry of the depressions.

## 2. Rainfall pattern effect–

- The effect of rainfall pattern on cumulative rainfall amount was found to be non-significant at the 5% level for the same surface treatment.

The lack of significant variations in the cumulative rainfall amounts offered assurance in the reliability of the rainfall simulator and the rainfall data, freeing consideration of impacts of various surface treatments on other key variables.

### **Hydrograph Results**

Response hydrographs and cumulative storage (plus infiltration) versus time graphs were prepared for the experimental runs, and sample graphs are provided in this section. Figures (6.1) and (6.2) summarize the time-wise variation of catchment response and cumulative storage with fixed surface treatment and rainfall pattern but slope changing. Figures (6.3) and (6.4) illustrate sample experimental results of runoff rate and cumulative storage respectively for a fixed slope and rainfall pattern but variable surface treatment.

Discussion regarding effects noted above and regarding other observations made both during experimentation and after analysis is presented in the subsequent section.

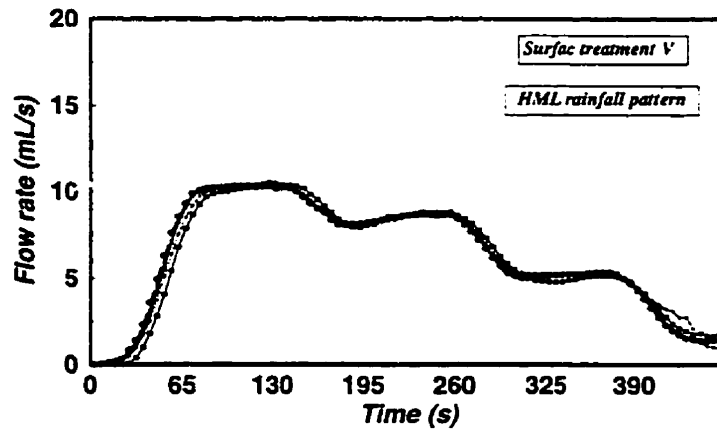
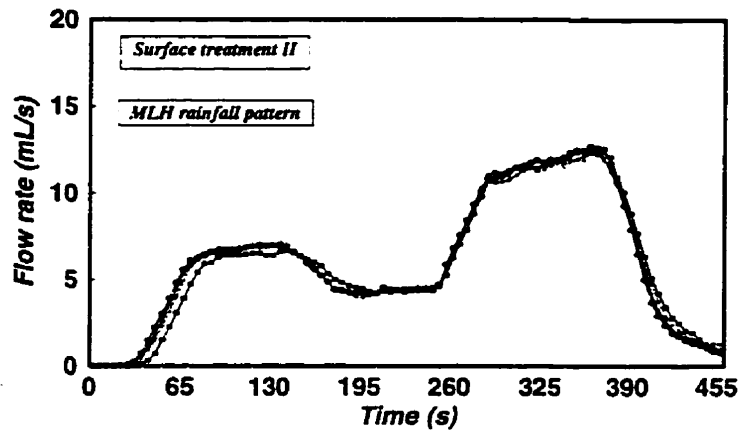
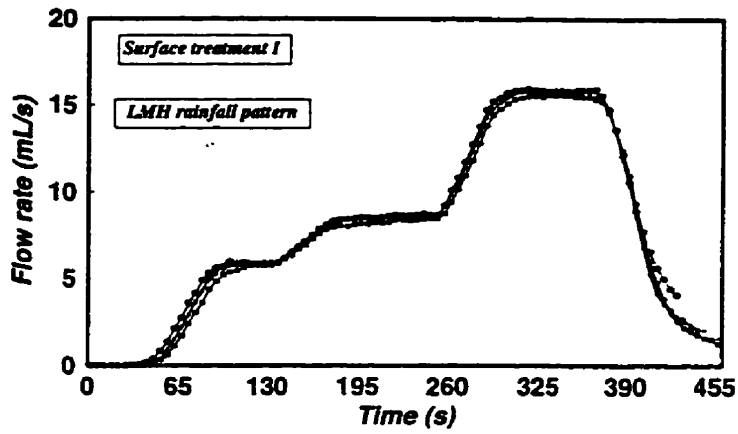
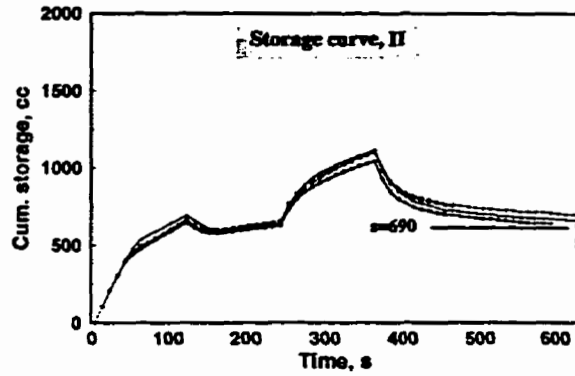
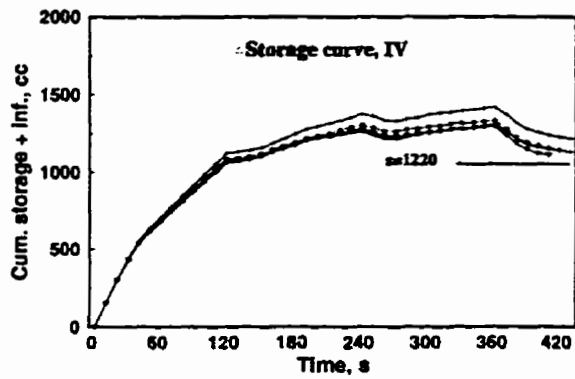


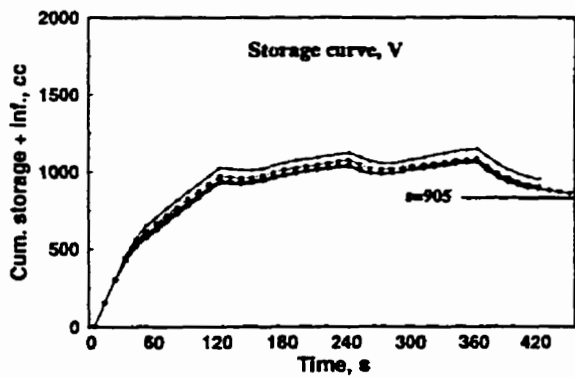
Figure 6.1: Catchment response of various surface treatments for different rainfall patterns and slopes.



(a) MLH rainfall pattern



(b) HML rainfall pattern



(c) HML rainfall pattern

Figure 6.2: Cumulative storage of various surface treatments for different rainfall patterns with different slopes.

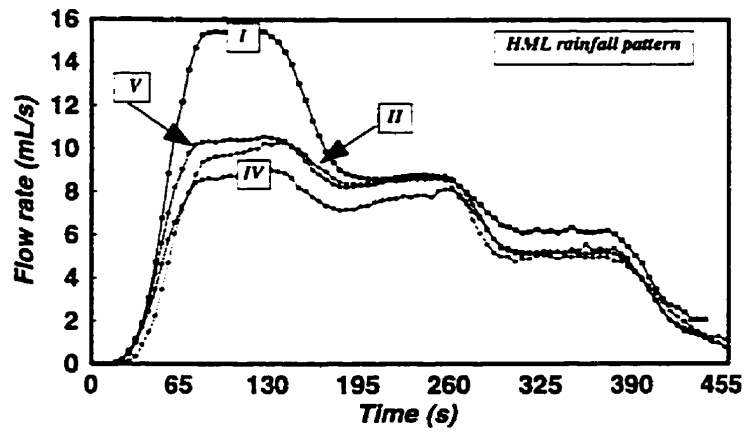
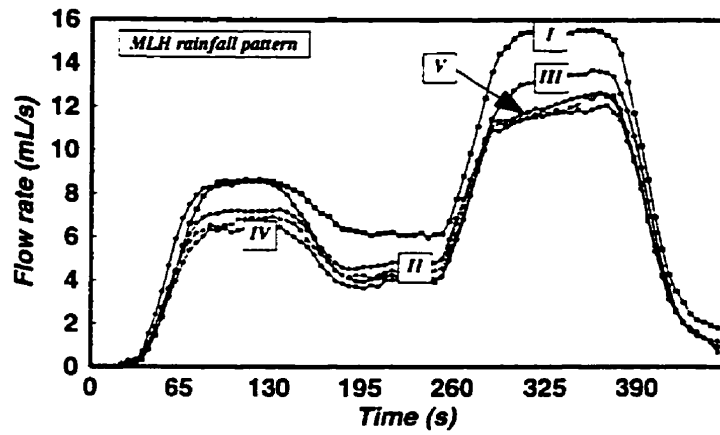
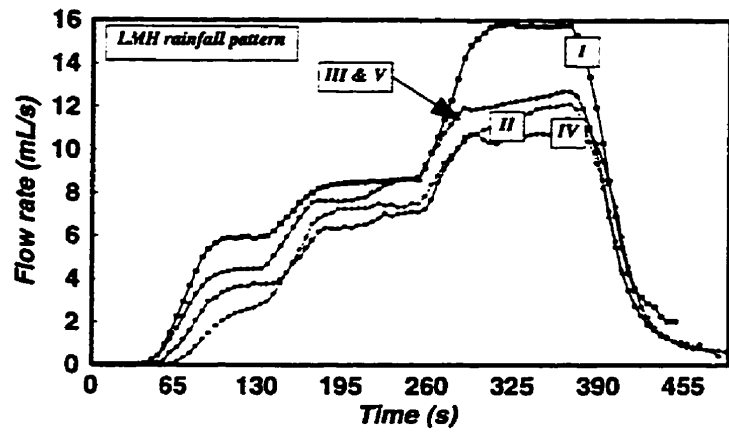


Figure 6.3: Catchment response of various surface treatments for different rainfall patterns,  $S = 10\%$ .

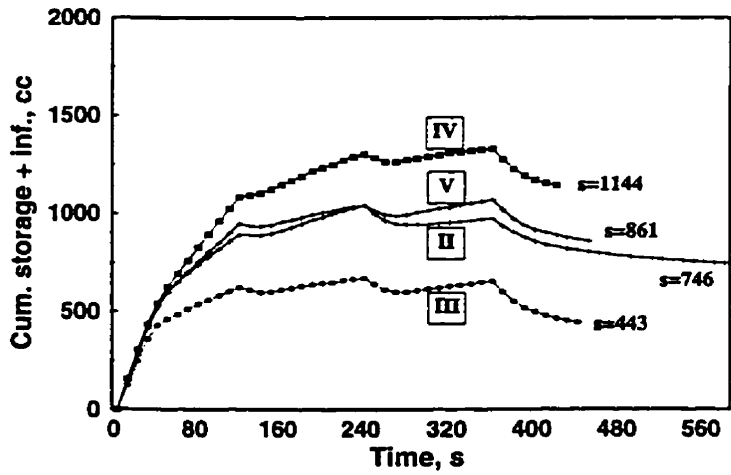
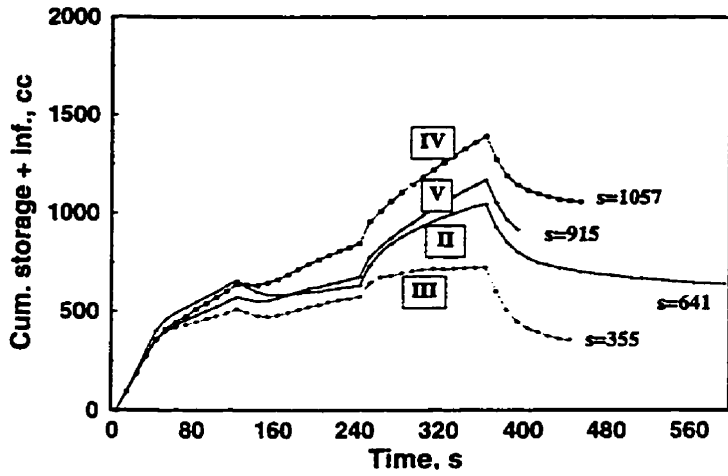
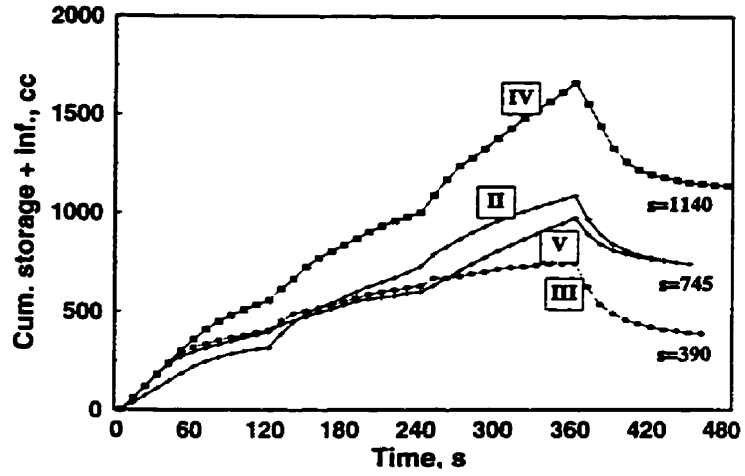


Figure 6.4: Cumulative storage curves for various surface treatments for various rainfall patterns and  $S = 10\%$  (potential storage=911  $cm^3$ ).

## 6.2.2 Discussion of Experimental Results

The mass balance, analysis of variance and time response results for the lab experiments reveal a number of points worthy of discussion. General observations and conclusions relating to all the runs include the following:

1. The slopes used for the experiments yielded essentially the same responses regarding surface runoff and water loss, despite the geometry of the depressions (and therefore the potential volume available for depression storage) decreasing significantly from 974 to 849  $\text{cm}^3$  with increasing slope. Some literature has argued that depressional storages lose their effectiveness in attenuating runoff hydrographs as overall slope increases (Hairsine et al., 1992; Ullah, 1974).
2. Surface tension appears to have played a significant role in influencing the volume of water held on the experimental surfaces. The runoff coefficients of 93 to 96% for surface treatment, I, suggest that on the order of 0.2 mm, or a volume of 210  $\text{cm}^3$ , of water might have been retained on the smooth surface. Visual observations during the experiments confirmed that considerable water was retained on the flume surface due to surface tension effects particularly on small slopes.

### **Surface Treatment Effects (in combination with rainfall effect)**

The laboratory experiments included five different surface treatments. These treatments led to runoff responses that were significantly different in magnitude and time variation, due to the absence or presence of surface detention, surface depressions and infiltration. Key findings regarding surface treatment effects are discussed here.

Results of the laboratory runs for surface treatments II and III reveal a number

of significant effects attributable to depression and detention storage, and spatial differences in depression storage, in combination with various rainfall patterns. There was consistently more water detained on the surface and stored in depressions on surface treatment II, where the largest depressions were near the outlet than on surface treatment III. For surface treatment III, it would appear that the surface depressions, particularly upslope ones, were never completely filled during the experimental runs, the final cumulative storage remaining considerably below the potential depression storage available (particularly allowing for an appropriate amount of detention storage). Again, visual observations confirmed that depressions were not all filled with water, particularly larger ones located upslope with relatively small contributing areas. The rate at which storage accumulated on treatments II and III was also significantly affected by the rainfall rate, the rate being greatest at the highest rainfall rate, and the differences in rates of accumulation of storage (between II and III) being greatest at the highest rainfall rate. Whatever the specific reasons for these differences, it is clear that variations in the spatial pattern of surface depressions (even when the distribution of depression sizes remained the same) can significantly affect the rate of accumulation of stored water and the total accumulation of stored water.

When infiltration was allowed to occur from some of the surface depressions, i.e. surface treatments IV and V, the accumulated storage plus infiltration amounts for these runs surprisingly were not significantly greater than the accumulated storage amounts obtained for treatments II and III. As for II and III, the rate of accumulated storage plus infiltration (and the total accumulation for each run) for treatment IV was significantly greater than the corresponding rate (and total) for treatment V,

once again the difference in rates being a function of the temporal pattern of rainfall. Since depression storage (and possibly detention storage) was observed for surface treatments IV and V to continue to accumulate during the duration of the runs, often not becoming full by the end of a run, it was virtually impossible to separate the infiltration amount from the stored amount. In fact, it became clear that one had to be careful estimating effective infiltration rates from apparent steady state response conditions (with full depression storage). Table (6.3) was prepared on the basis of such an assumption, only to yield infiltration rates which could not be rationalized.

Table 6.3: Summary of infiltration capacity (mm/hr) calculations for surface treatment IV.

Slope %	Rainfall Pattern	Rainfall intensity, mm/hr		
		$I_L = 21$	$I_M = 32.9$	$I_H = 52.9$
6%	LMH	9.61	11.19	21.42
	MLH	9.0	13.9	19.3
	HML	5.86	6.67	23.34
8%	LMH	8.37	9.44	17.02
	MLH	7.03	12.46	17.92
	HML	2.95	6.67	23.34
10%	LMH	8.44	10.03	15.72
	MLH	7.54	10.88	13.28
	HML	3.01	5.98	22.86
12%	LMH	8.23	9.10	15.45
	MLH	7.27	11.36	12.32
	HML	2.09	4.95	21.62
14%	LMH	8.23	9.54	15.1
	MLH	7.27	11.47	11.77
	HML	3.84	4.40	22.52

When an attempt was made to take into account variations in rate of accumulation of depression storage throughout the runs, the estimated infiltration rates became those in Table (6.4). It clearly remains very difficult to separate the storage and infiltration amounts.

Therefore, from the laboratory experiments, it is clear that the spatial pattern of

Table 6.4: Summary of infiltration rate (mm/hr) calculations for surface treatment IV.

Slope %	Rainfall Pattern	Rainfall intensity, mm/hr		
		$I_L = 21$	$I_M = 32.9$	$I_H = 52.9$
6%	LMH	9.00	2.47	9.47
	MLH	6.73	5.59	13.15
	HML	5.08	6.28	12.60
8%	LMH	1.24	1.51	8.14
	MLH	4.39	3.19	9.51
	HML	2.57	2.92	8.86
10%	LMH	0.45	1.17	7.52
	MLH	5.70	1.44	5.04
	HML	0.82	1.34	8.17
12%	LMH	4.60	0.62	3.67
	MLH	4.29	0.62	5.84
	HML	0.48	0.69	7.79
14%	LMH	4.29	0.72	4.94
	MLH	4.80	1.17	4.36
	HML	1.27	0.31	7.79

surface depressions in combination with the temporal pattern of rainfall rate, with and without infiltration, can have a significant effect on the manner and rate at which water is stored and accumulated on the surface. If the specific pattern of depressions is known, a deterministic component might be considered for the prediction of an appropriate effect on response. However, in the absence of details regarding spatial patterns of depressions and temporal patterns of rainfall, and in light of the fact that many characteristics of the spatial pattern are scale dependent (as noted in Chapter 5), it is likely that effects of depressions on response will have to be linked to some average depressional characteristic such as mean depth, with allowance for statistical variability in depressions and possibly in response.

## **6.3 Small-scale Field Experiments**

In the case of the small-scale field experiment, it was hypothesized that providing simulated rainfall on the three micro-catchments would result in different catchment responses. A main question was how much of the variability in catchment response from one micro-catchment to another could be attributed to variability in micro-topography and how much could be assigned to some other factors? Then, in light of the variability observed, a question would still remain regarding how a hydrologic model should be structured to capture this variability and imitate the behavior of the system? With such questions in mind, the experimental results are presented and discussed in the following sections.

### **6.3.1 Sample Results of Field Experiments**

In the small-scale field experiment, three micro-plots were considered with three different antecedent soil-water conditions ranging from dry conditions to wet conditions to covering the surface with very thin plastic. Combining these surface treatments for each plot with three rainfall patterns and three replications for each experimental run, 63 sets of rainfall-runoff data were collected. The following presentation and discussion deals with the experimental results in a lumped way (i.e. water balance results) and as distributed in time (i.e. hydrograph analysis). It should be noted that, in the case of the plastic cover condition, only the MLH rainfall pattern was used.

### **Dry condition**

One set of runs was conducted for a so-called dry condition, with existing pre-experimental wetting of the surface. As was the case with the laboratory experiment, the rainfall simulator nozzles were installed at 170 cm above the surface and experimentation was started on plot I. With the low and medium rate nozzles at the same height over plot II, no runoff was generated. Therefore, the nozzle height was reduced to 110 cm. With the nozzles at this height, the experiment was conducted for all three plots. The first part of Table (6.5) shows the components of the water balance equation [i.e. Equation (6.1)] measured for the various plots and rainfall pattern treatments. It should be noted that neither water trapped in depression storages nor infiltration was measured during field experimentation.

### **Wet Condition**

The second surface treatment used in the course of experimentation involved having the soil surface at saturation. Under these conditions, the peristaltic pump could not keep up with the runoff produced with the rainfall nozzle at a height of 110 cm. The nozzle height was increased to 130 cm and experimentation for wet conditions was initiated. The middle part of Table (6.5) summarizes the results of the water balance analysis.

### **Plastic cover**

Due to difficulties associated with sorting out the variability in catchment response from one plot to another caused by either changes in micro-topography and/or infiltration, the surface was covered with a very thin plastic sheet, similar to those used for

wrapping cold foods. Due to tenting and damming effects introduced by the plastic cover, some sort of averaging effect was introduced into the topographic pattern. Further, with all the provided measures, the leakage of water through seams in the plastic and perhaps at some edges could not be avoided, resulting in the plastic cover runs, not representing a completely impermeable surface. However, as this surface could be dealt with as a distinct topographic pattern in its own right, it was considered as another surface treatment.

Once again the peristaltic pump could not handle the flow generated by the rainfall nozzles installed at 110 cm height. The nozzle height was raised to 130 cm and the results of the experimental runs for the MLH rainfall pattern are summarized in the third part of Table (6.5).

Table 6.5: Summary of experimental runs (water balance components) for small-scale field experiment.

Initial Condition	Plot No.	Rainfall Pattern	Total Rainfall mm	Surface runoff, mm			Water Losses, mm			Runoff Coefficient %		
				Rep. (1)	Rep. (2)	Rep. (3)	Average Value	Rep. (1)	Rep. (2)		Rep. (3)	Average Value
Dry Condition	Plot I	LMH	14.05	3.26	3.33	3.46	3.35	11.00	10.92	10.80	10.9	23
		MLH		3.62	3.55	3.43	3.53	10.62	10.70	10.82	10.7	25
		HML		4.41	4.16	4.06	4.21	9.84	10.10	10.19	10.04	30
	Plot II	LMH	14.05	1.32	1.53	1.60	1.48	12.59	12.38	12.32	12.43	11
		MLH		1.29	1.46	1.13	1.29	12.62	12.44	12.78	12.61	10
		HML		1.00	1.21	-	1.10	12.91	12.70	-	12.80	8
	Plot III	LMH	14.05	2.65	2.48	2.48	2.54	11.34	11.52	11.52	11.46	18
		MLH		2.37	2.25	2.25	2.29	11.63	11.74	11.74	11.70	16
		HML		1.87	1.95	2.00	1.94	12.11	12.04	12.01	12.05	14
Wet Condition	Plot I	LMH	11.92	3.04	3.32	2.93	3.10	9.04	8.76	9.16	8.99	25
		MLH		3.64	3.60	3.20	3.48	8.44	8.48	8.89	8.60	29
		HML		2.43	2.98	2.58	2.68	9.66	9.11	9.50	9.42	22
	Plot II	LMH	11.92	2.98	3.01	3.55	3.18	8.82	8.80	8.25	8.62	27
		MLH		3.68	3.24	2.87	3.26	8.17	8.57	8.93	8.56	27
		HML		1.83	2.53	3.00	2.45	9.97	9.27	8.81	9.35	14
	Plot III	LMH	11.92	4.04	4.53	3.32	3.96	7.83	7.35	8.55	7.91	33
		MLH		4.50	3.84	4.71	4.35	7.37	8.03	7.17	7.52	37
		HML		4.27	4.60	4.23	4.37	7.61	7.27	7.65	7.51	37
Plastic Cover	Plot I	MLH	11.92	8.22	8.12	-	8.17	3.87	3.97	-	3.92	68
	Plot II	MLH	11.92	7.83	7.72	-	7.78	3.97	4.08	-	4.02	66
	Plot III	MLH	11.92	9.36	8.21	-	8.78	2.52	3.67	-	3.10	73

An extensive analysis of variance was conducted to explore the impact of plot treatments, initial conditions and rainfall patterns on key variables such as cumulative runoff amount and cumulative water loss due to depression storage and infiltration. Details of this analysis are provided in Appendix B. A summary of key results is included below, and a full discussion is provided in Section (6.3.2).

#### **Highlights of Significant Effects**

##### **1. Plot treatment effect**

Although physical characteristics relating to surface depressions were found not to be significantly different from plot to plot in the field (as noted in Chapter 5), significant plot treatment effects were observed in the runoff response, and the nature of these effects was related to the surface and antecedent soil-water conditions. So, at the 5% probability level:

- Variations among cumulative observed runoff amounts from one plot to another were found to be significant for both the dry and wet conditions, but not significant for the plastic cover condition; and correspondingly
- Variations among cumulative observed water losses (i.e. combined effect of surface storage, surface detention and infiltration) from one plot to another were found to be significant for both the dry and wet conditions, but not significant for the plastic cover condition.

##### **2. Surface and antecedent soil-water condition effect–**

- Variations among the cumulative observed runoff amounts from dry to wet

conditions were found to be significant at the 5% level, implying the importance of quantification of the initial state of the system; and correspondingly

- Variations among cumulative observed water losses from one initial condition to another were found to be significant at the 5% level.

#### **Highlights of Non-significant Effect**

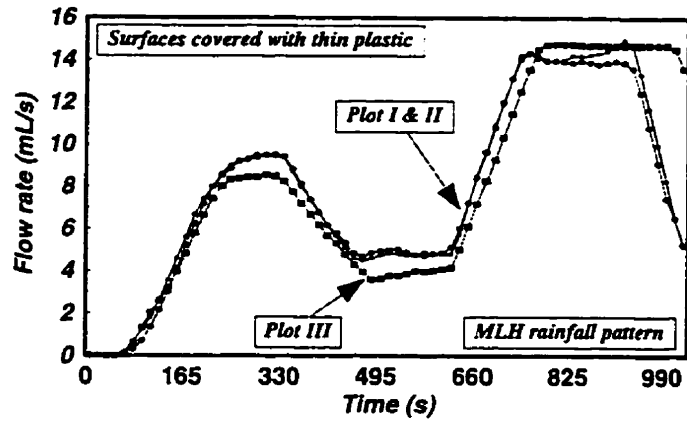
##### 1. Rainfall pattern effect–

- Variations among the cumulative observed runoff amounts from one rainfall pattern to another were found to be non-significant for both the dry and wet conditions; and correspondingly
- Variations among cumulative observed water losses from one rainfall pattern to another were found to be not significantly different for both the dry and wet conditions.

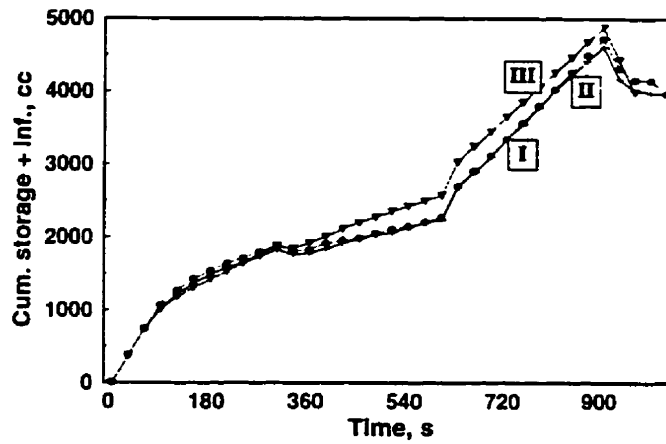
It is worth noting that the rainfall simulator was not calibrated in the field for different rainfall patterns. Rather, results of rainfall simulator calibrations in the laboratory with the rainfall nozzles installed at various heights were used for the field experiments. Indeed, extrapolation of the rainfall simulator calibrations from laboratory to field might have contributed to errors in the field plot results as the environmental conditions in the field were somewhat different from those in the laboratory.

### **Hydrograph Results**

To further pave the way for a discussion of the results, a few sample storage graphs and hydrographs are provided in this section. Figure (6.5) illustrates results of experimental runs when each plot was covered with very thin plastic; Figures (6.6) and (6.7) illustrate sample experimental results of runoff rates and cumulative storage respectively for wet conditions; and Figures (6.8) and (6.9) summarize time-wise variations of catchment response and cumulative storage for the case of dry conditions.

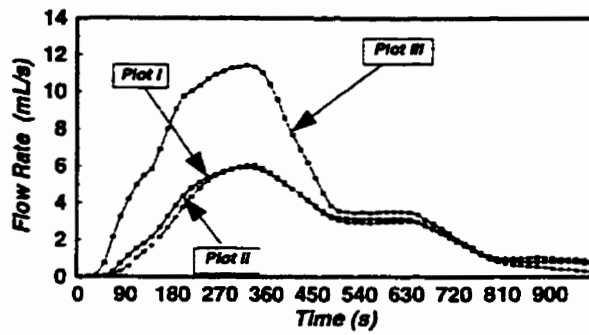


(a) Runoff rate.

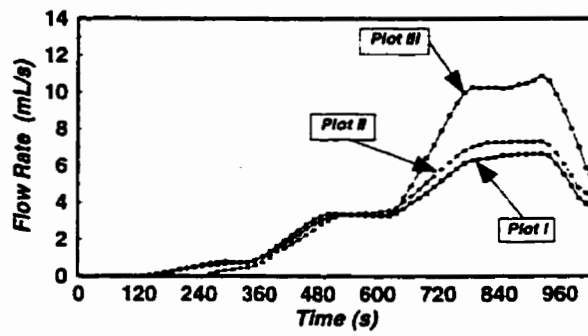


(b) Cumulative storage.

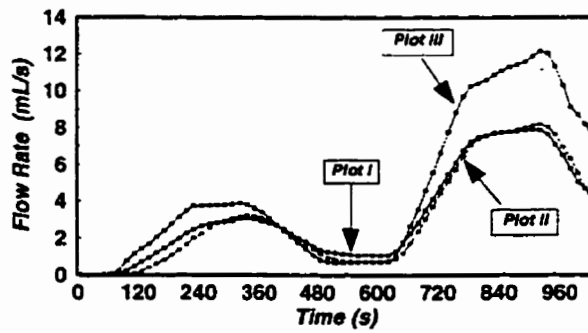
Figure 6.5: Catchment response comparison for various plots for MLH rainfall pattern–plastic cover.



(a) HML rainfall pattern

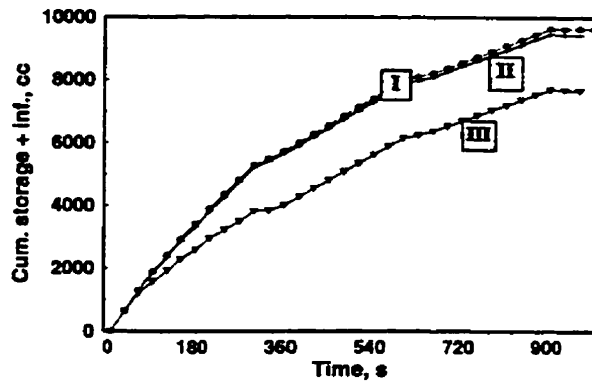


(b) LMH rainfall pattern

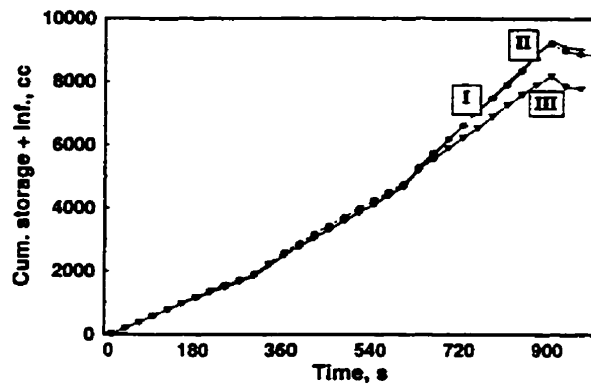


(c) MLH rainfall pattern

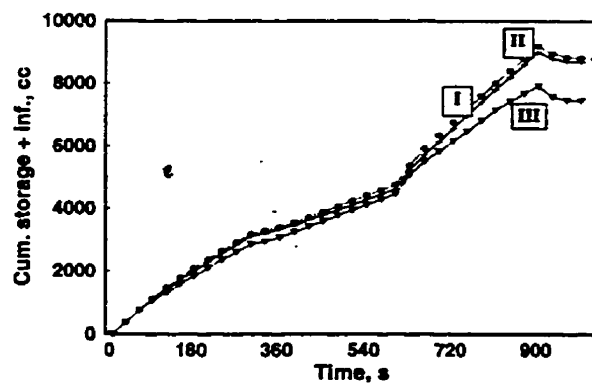
Figure 6.6: Catchment response comparison for various plots for different rainfall patterns—wet condition.



(a) HML rainfall pattern

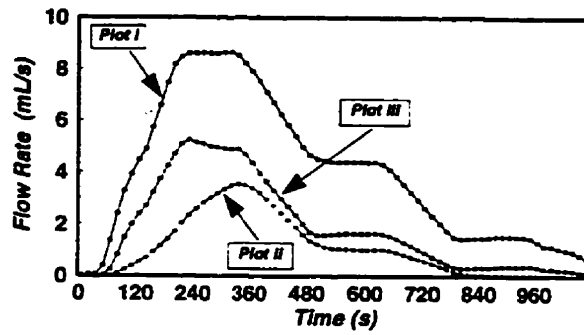


(b) LMH rainfall pattern

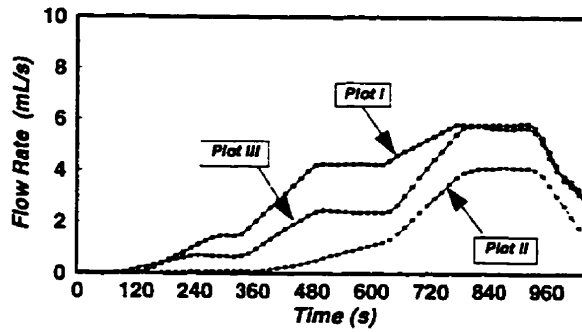


(c) MLH rainfall pattern

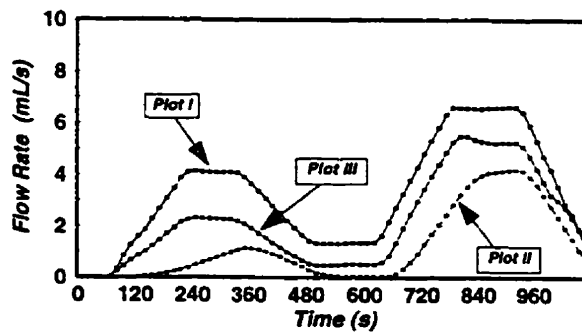
Figure 6.7: Cumulative storage + infiltration curves of various plots for different rainfall patterns—wet condition.



(a) HML rainfall pattern

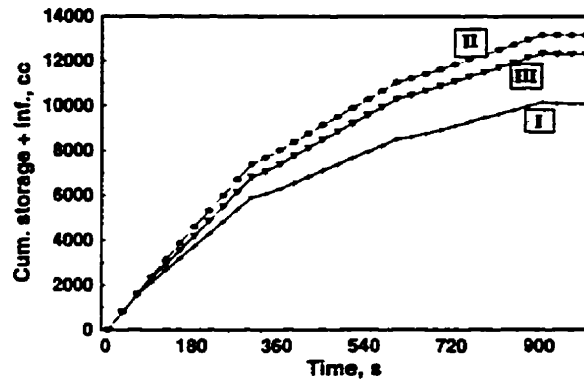


(b) LMH rainfall pattern

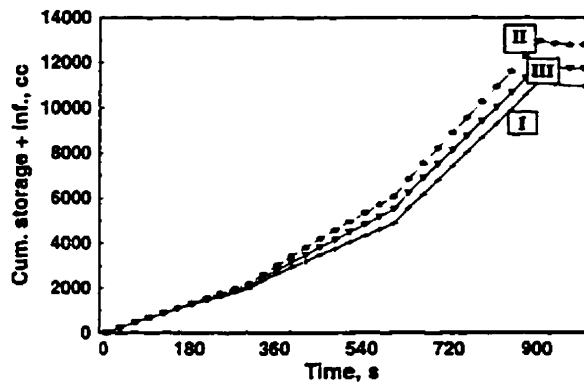


(c) MLH rainfall pattern

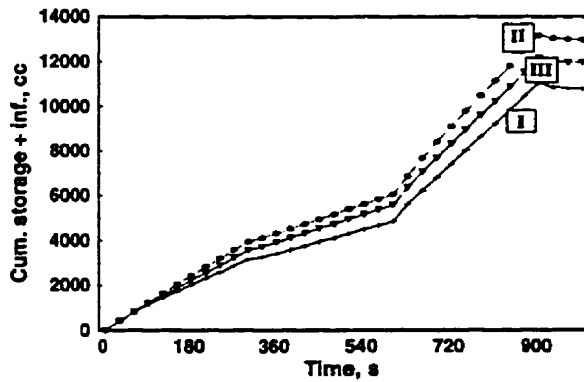
Figure 6.8: Catchment response comparison for various plots for different rainfall patterns—dry condition.



(a) HML rainfall pattern



(b) LMH rainfall pattern



(c) MLH rainfall pattern

Figure 6.9: Cumulative storage + infiltration curves of various plots for different rainfall patterns—dry condition.

### **6.3.2 Discussion of Experimental Results**

A discussion of field plot experimental results, in light of the questions raised in Sections 6.1 and 6.3 along with some explanation regarding the causes of similarities and differences in catchment response and their possible implications are provided in some detail in subsequent sections.

#### **Detention Storage**

From the portions of Figures 6.5(b), 6.7 and 6.9 for the period of times after the simulated rainfall had ceased, it is clear that the amount of water detained on each field plot during the course of each run, and which subsequently drained from the surface by surface runoff, was dependent on the surface and antecedent soil-water conditions. The amounts were greatest (about 650 to 750 cc) when the plots were covered with plastic, somewhat less (30 to 400 cc) under wet conditions, and virtually zero under dry conditions. There was also some evidence that the amount of water detained on the surface was directly related to the rainfall rate. For almost all experimental runs, regardless of initial conditions, the amount of water detained being greatest for the highest rainfall rate. The nature of these results were not unexpected; and it was important to take the magnitude of detained water into consideration when analyzing other effects.

#### **Plot Treatment Effect**

Analysis of Variance results indicated that there were significant plot treatment effects under wet and dry conditions; and the response graphs in Figures 6.5 through 6.9 confirm these results, the largest differences in response occurring under the dry

conditions. Taking into account that plot III may have experienced somewhat different pre-wetting conditions for the wet runs, possibly being inundated twice, it may be that only under dry conditions did the plots behave differently. Certainly for the dry antecedent conditions, runoff response from the three plots varied significantly, probably indicating the different rates that such small plots can wet up and generate runoff, even when the surface depression characteristics are not significantly different. According to Figure (6.8), the catchment response for plot II appeared to be governed totally by the surface; while for plots I and III, the catchment responses were governed partly by the surface and partly by rainfall. Furthermore, as Figure (6.8) clearly reveals, the peak values for the various rainfall patterns on the three plots lag a certain amount, which might be attributed to the nature of the surface storage. The peak for plot II had the largest lag due to the presence of a drainable micro-depression near the outlet. Plot I had the smallest lag compared to the other plots, possibly due to an extensive sealing process.

During removal of the vegetative cover and sealing of the surface, it was noticed that the higher parts of the micro-topography (i.e. residual of vegetation) were occupied by cracks and large holes, and therefore the likelihood of greater hydraulic conductivities as confirmed in an earlier study by Dunne et al. (1991). This apparent non-uniform spatial distribution of hydraulic conductivities over the surface might also be a part of the cause for variability in micro-catchment response from one plot to another. In the field, variability in apparent or effective infiltration rates from one micro-catchment to another was one of the main obstacles to an objective evaluation of effects of variability in surface micro-topography on system response. Sealing of the surface along with

controlling the initial conditions was an attempt to minimize the effects of variability in infiltration. Indeed, for such a small-scale micro-catchment, variability in hydraulic conductivity from one plot to another seems to have been more dominant than any other factors in shaping the timing of outflow hydrographs.

#### **Surface and Antecedent Soil-water Condition Effect**

The water balance and hydrograph results from the small field plots reveal some very significant differences due to surface and antecedent soil-water conditions. For example, about 69% of the input rainfall ran off the plastic surface; about 28% of the input rainfall ran off the plots under wet initial conditions; and about 17% of the input rainfall ran off under dry initial conditions.

Since accumulated depression storage volumes might have been expected to be in the order of several hundred  $cm^3$  (from the results in Chapter 5), the accumulated storage plus infiltration values in the order of 5, 10 and 15000  $cm^3$  are likely to reflect primarily leakage (through the plastic) and infiltration rates for the wet and dry initial conditions. Whatever the exact magnitude of these rates, certainly they were significant and significantly different.

The accumulated storage plus infiltration curves may give some indication of the role of depression storage. According to Figure (6.5), depression storage probably filled rather quickly (during the first 90 s), decreased a bit during low rainfall (due to leakage), and likely filled even further at the start of a higher rate of rainfall. Figure (6.7) suggests that depression storage may have filled in 90 s to 135 s under initial H or M rainfall; may have emptied a small amount under secondary L rainfall

and secondary M rainfall (although the short dips may have been drops in detention storage) and likely increased under tertiary H rainfall. For the case of dry conditions, Figure (6.9) suggests that depression storage may not have filled very much at all. The loss rates are virtually constant for each rainfall rate, suggesting very significant infiltration into the dry soils; and very little runoff occurred, so there was very little ponding.

In conclusion, for the field plot responses, it seems that:

- There is evidence of depression storage;
- The maximum amounts of depression storage realized are likely to have been of the order of magnitude estimated in Chapter 5.
- It remains difficult if not impossible to ascertain amounts of depression storage from runoff response alone; and
- The rate and extent to which surface depressions fill appears to be a function of factors such as degree of impermeability of the surface, infiltration rates under different antecedent soil-water conditions, and the temporal pattern of rainfall rates.

Again, it seems difficult to have a totally deterministic approach to characterizing how and to what extent depression storage affects runoff response.

## 6.4 Large-scale Field Experiments

It was acknowledged at the start of the experiments that separation of depression storage effects would be extremely difficult if not impossible on the basis of run-

off response from selected small watersheds. At this scale the temporal and spatial variability in rain and soil hydraulic properties dampen catchment response to such an extent that direct effects of depression storage and surface storage in general are totally obscured. Yet data from this scale have been included in this study to address the topic of developing and applying a model with a structure appropriate for a variety of scales, from lab flumes to small watersheds. In addition, the pair-wise nature of the selected watersheds, with regard to different remedial measures, provided a unique opportunity to explore the possibility of relating different remedial measures to mean depth of storage over the surface, such measures directly affecting the surface features of each watershed. For each watershed, temperature, rain, solar radiation, wind speed, wind direction and streamflow rate were extracted from tables prepared by BEAK Consultants (1994). Almost all data were collected on an hourly basis, while relative humidity was collected on a daily basis. The climatological as well as streamflow data covered approximately four years, from 1988 to 1992.

#### **6.4.1 Sample Results of Field Experiments and their Discussion**

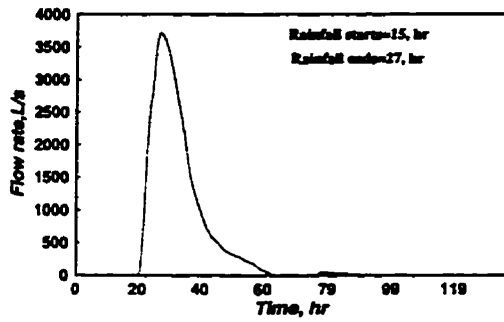
For the purpose of the modeling exercise, discussed fully in Chapter 7, all hydrological and climatological data were carefully analyzed and a few sample events during the period between early June and late September of each year were selected from each watershed for further analysis. Each event was selected in such a way that it was preceded by a prolonged dry period. This initial condition allowed the model storage component to be assumed empty at the beginning of simulation.

In Table (6.6), characteristics of a few typical events, along with drainage area,

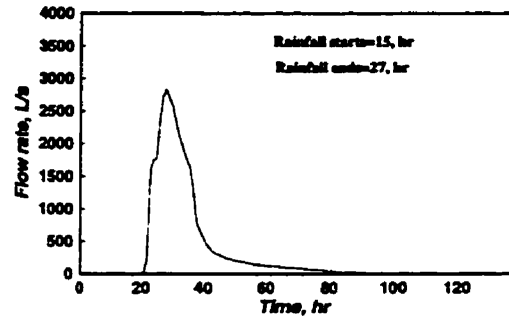
cumulative rainfall and runoff are summarized. Figures (6.10) and (6.11) present sample results of runoff rate and cumulative storage curves of the same events.

Table 6.6: Typical rainfall-runoff events on the selected small watersheds.

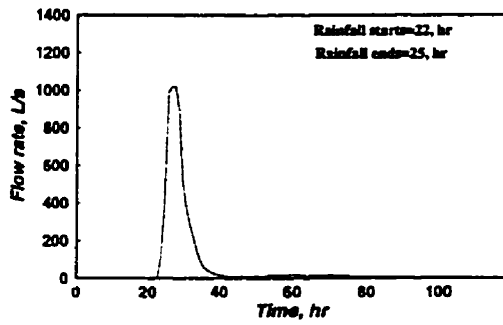
Basin	Basin	Date	Drainage Area (ha)	Rainfall (mm)	Runoff (mm)	Runoff coefficient %
Name	Type					
Essex	test	Sept. 6, 1990	435	86.3	44.76	52
	control	Sept. 6, 1990	281	86.3	51.6	60
Kettle	test	July 13, 1990	410	44.9	6.2	14
	control	July 13, 1990	348	44.9	7.8	17
Pittock	test	July 8, 1990	359	60.5	5.65	9.3
	control	July 8, 1990	378	60.5	3.54	6



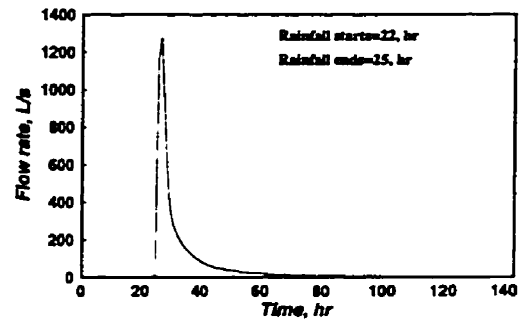
(a) Essex, Test Watershed



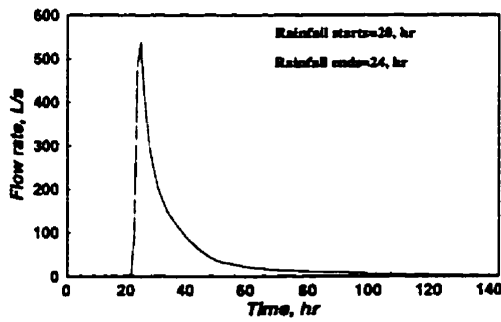
(b) Essex, Control Watershed



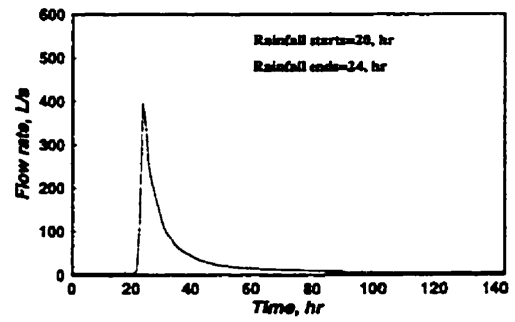
(c) Kettle, Test Watershed



(d) Kettle, Control Watershed

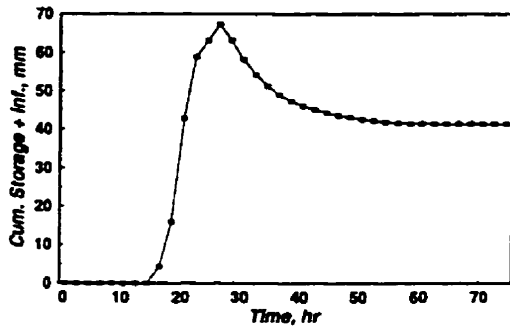


(e) Pittock, Test Watershed

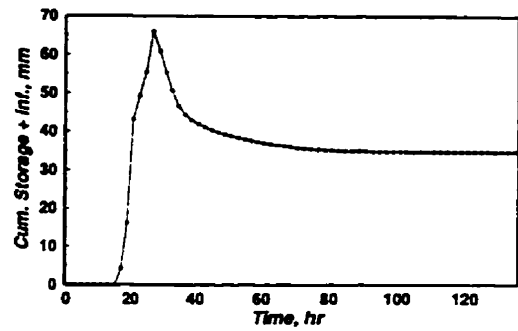


(f) Pittock, Control Watershed

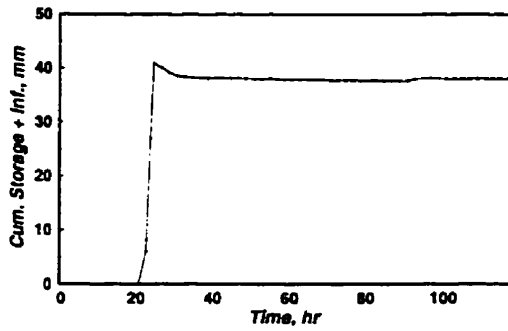
Figure 6.10: Sample observed runoff hydrographs-PWS Watershed in Southern Ontario.



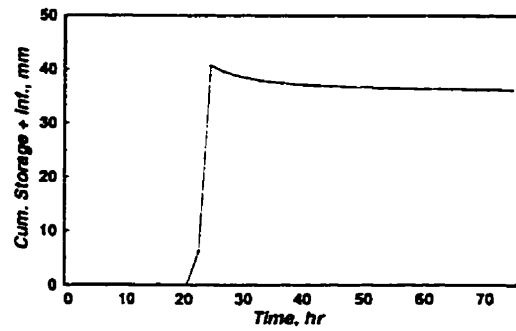
(a) Essex, Test Watershed



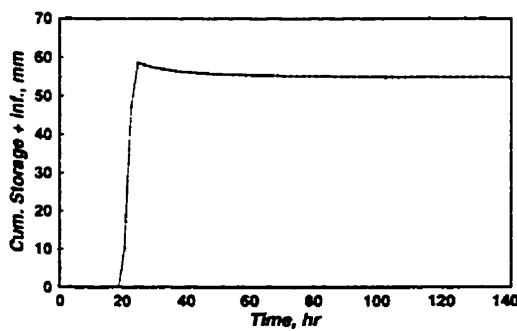
(b) Essex, Control Watershed



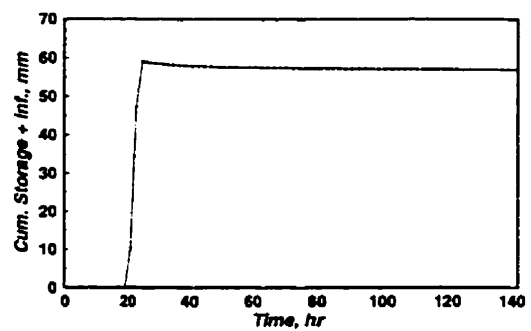
(c) Kettle, Test Watershed



(d) Kettle, Control Watershed



(e) Pittock, Test Watershed



(f) Pittock, Control Watershed

Figure 6.11: Sample observed storage graphs—PWS Watershed in Southern Ontario.

Visual inspection of the collected data and observed hydrographs revealed that:

- The watershed runoff responses resulting from distinct rainfall events were themselves distinct and sharply peaked, rising very abruptly and falling almost as abruptly with some tailing off.
- The volumes of runoff, and the relative runoff volumes, i.e. relative to rainfall amount (revealed in runoff coefficient), varied dramatically from event to event and from watershed to watershed. Variations from event to event on any given watershed could be attributed to variations in antecedent soil-water conditions and stages of vegetative growth. For example, runoff from rainfall during spring months was usually significantly greater (in volume, in peak and as a percentage of rainfall), where the vegetative cover was sparse and antecedent soil-water conditions were relatively wet. Variations in response from watershed to watershed for similar rainfall events were likely due to differences in physiography. For example, runoff volumes and percentages tended to be greatest for the Essex watersheds, where soil contains a significantly higher percentage of clay.
- Differences in the runoff volumes and the runoff hydrographs for the test and control watersheds at each of the three sites revealed effects primarily attributable to remedial measures implemented on the test watersheds for the management of runoff and associated soil erosion and non-point source pollution.
- The sample storage graphs (Figure 6.11) clearly reveal that only the Essex watersheds exhibited a significant and marked depletion from detention storage at the end of most rainfall events. The significant detention storage on these water-

sheds is attributable to the less permeable clay soil, particularly in the extensive surface drainage ditches.

#### **6.4.2 Discussion of Comparative Results**

It is helpful at this stage to discuss salient points brought out in disparate form in various parts of previous sections when viewed together. Analysis of the observed runoff data obtained at the various spatial scales and for various experimental designs revealed the following.

Within the laboratory, moving from a smooth surface to surfaces characterized by various patterns of surface depressions, the system response became less replicable. Moving from the laboratory experiments to the field plot experiments, the system response became even less replicable as more environmental factors such as wind and soil variability were introduced. Indeed, within the lab experiments, the depressions were very organized in a physical sense due to being row-wise and lacking a nested structure. Yet even here there were a few probabilistic components associated with runoff response, one of which was due to the manner in which runoff was generated on the surface through and among the depressions. When infiltration was added, there was an additional source of randomness, relating to the way infiltration and depression storages interacted with each other. Some depressions held water on a permanent basis, while others upon drainage provided more room for further storage. In the field plots, the nested structure of the depressions along with variability in infiltration added more complexity into the system. When it came to the small watersheds, lack of certainty about inputs (i.e. spatial and temporal variability in rainfall) in addition

to the other factors contributed further to the probabilistic behavior of the system. In general, as the size of the study area increased, the lack of knowledge and certainty about each system regarding quantification of input variables and identification of system parameters increased. The apparently hierarchical nature of randomness at the various spatial scales prompted the notion of taking a holistic approach to the structuring of a rainfall-runoff model.

Regarding the flexibility in choosing treatments, treatments relating to overall slope, surface storage spatial pattern, and rainfall temporal pattern could be controlled in the laboratory. In the small-scale field experiment, neither overall slope nor surface storage spatial pattern could be controlled; but by keeping the study area small enough, the temporal pattern of rainfall could be considered controllable. Moving to the large scale field experiment, almost none of the treatments could be controlled, and replicability in a statistical framework made no sense at all.

Variability in runoff coefficients within a particular experimental setup and among the various spatial scales was another common feature of this research. The variability in runoff coefficients in the laboratory experiments could be easily attributed to seemingly known factors; and in the small-scale field experiments, explanation of sources of variability in runoff coefficients was still possible to some extent. However, for the small watersheds, the variability in coefficients could be attributed only to a wide variety of sources, including climatic parameters such as spatial and temporal variability in precipitation and temporal dependent parameters such as percent cover, soil soil-water balance and farm management.

Difficulties involved in partitioning water loss between depression storage and in-

filtration was another common problem in this research for the range of spatial scales. Among other things, it was found that the manner in which storage filled with time was a function of position of depressions, rainfall rate and also infiltration rate; and without detailed knowledge of each component, such partitioning was almost impossible.

On one occasion, the response from lab surface treatment IV and the response from small field plots covered with thin plastic were found to resemble each other for the MLH rainfall pattern. This similarity in catchment response somehow related to the nature of flow on each surface. When the field plots were covered with thin plastic, direct observations noted that droplets of water merged to create droplets of increasing size, similar to what happened in the laboratory experiments. Furthermore, leakage from overlapping parts of the plastic cover resembled drainage from some of the depression storages in the laboratory setup. For both the laboratory and small field plot cases, the contribution to storage during low rainfall intensities was minimal as can be seen in Figure (6.12).

In response to the question: Can, and how can, results obtained at one scale be effectively used at another scale (at least on a qualitative basis)?, the following points are noteworthy:

- For the small-scale laboratory experiments, given the temporal pattern of rainfall in advance, it was found that temporal resolution of the runoff measurement facility could not be selected arbitrarily. A direct implication of this finding is that the temporal scale of runoff and the spatial scale of the study area could not be selected independently, as they are highly interconnected.

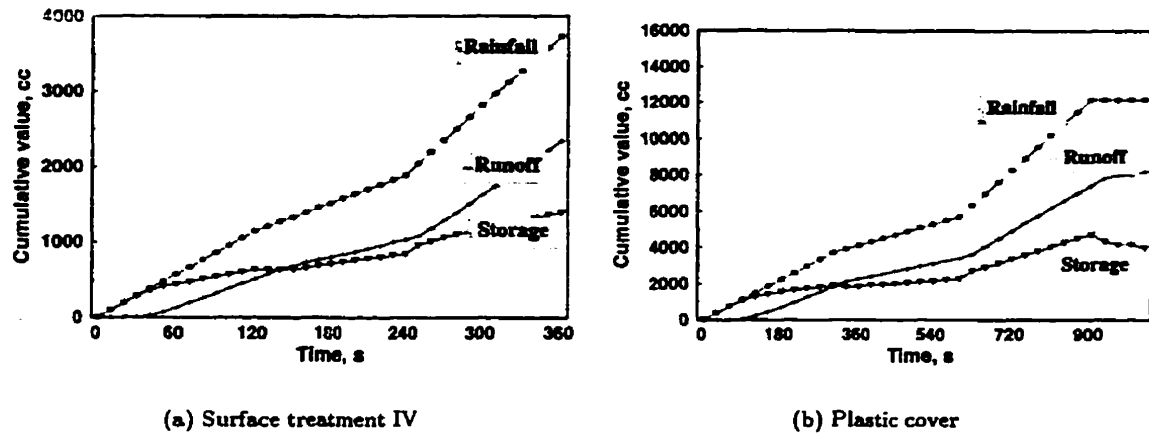


Figure 6.12: Comparison of cumulative storage curves for laboratory and field experiment, MLH rainfall pattern

- At the small scales (both laboratory and microplot), quantification of the temporal pattern of rainfall was found to be quite important, directly affecting the timing of the runoff hydrograph. At the small watershed scale, the effect of the temporal pattern of rainfall is less since the routing of runoff through channel storage smooths out the runoff response. At the watershed scale, the spatial pattern of rainfall may be more important than the temporal pattern.
- Antecedent conditions were very important at all scales. Their description and the manner in which they affected response were much more easily dealt with at the lab and small field plot scales. At the watershed scale, its quantification is a major obstacle in objective evaluation of rainfall:runoff models.
- Surface treatment was also important at all scales. For the lab scale, it was relatively easy to identify the treatments and their effects on runoff response. For the small field plots, it was less easy to quantify the treatments, although the effects were clear. For the small watersheds, the surface treatments could be

named (i.e. remedial measures), but not quantified, and investigation of effects is not a simple task.

## Chapter 7

# MODELING STUDIES

### 7.1 Introduction

The sets of rainfall-runoff data collected and analyzed at a range of spatial scales, including the small-scale laboratory experiment, the small-scale field experiment and the small watersheds, provided much valuable information for a consideration of questions such as the following: How can rainfall-runoff models be structured to take into account deterministic and statistical characteristics of depressions? Can results from model studies conducted at one scale prove to be useful as input to studies at other scales? In other words, can, and how can, model results obtained at one scale be effectively used at another scale (at least on a qualitative basis)? Such questions are addressed in this chapter in light of modeling studies conducted over the range of spatial scales dealt with earlier in the thesis.

It may be informative to summarize the main points of previous two chapters with regard to model building as far as depression storages are concerned. Extensive analysis of pond prompted the idea that many of the characteristics of depression storages

were scale dependent which made deterministic representation of their spatial pattern an impossible task; observation of catchment response from depression areas added more probabilistic components, even for a fully-controlled situation of laboratory experiments. Generation of runoff through and among the depressions in a random way and interaction between infiltration and surface storages add more complexity to the model-building process.

In this chapter, two possible approaches to the structuring of rainfall-runoff models are considered in some detail. The first approach, an electrical analogy, is applicable to a hypothetical example; the second approach, a holistic type analogy, applicable to some of the data sets presented earlier for a range of spatial scales. Advantages and disadvantages of each approach are included in the discussion of results.

## 7.2 Identification of Stores

As was emphasized in Section (2.9.6), for a realistic simulation of watershed response in a distributed manner, a conceptual hydrologic model must account for the rate of accretion to and depletion from each depression storage. Up to now, identification of stores—for the purpose of delaying and routing water flux in each store—has been mainly concerned with conceptual stores. In considering the whole watershed in terms of conceptual store, the modeler has assumed that a linear or non-linear reservoir acts as a routing component, and that a linear or non-linear channel acts as a lagging or delaying component. The modeler has not been concerned about the spatial locations of such conceptual stores or about their interrelationships (Dooge, 1959; Sugawara, 1961). At most, in some of the conceptual models, the effect of catchment

configuration was introduced by incorporating the so-called area time<sup>-1</sup> vs. time curve (Dooge, 1959; Laurenson, 1964), while some “distributed type” models, have assigned conceptual stores to grid squares or other spatial units and thus have dealt with those elements in a spatial context. If the reproduction of runoff at the mouth of a nonvarying-configuration watershed is the main objective in a modeling exercise, then perhaps there is no need to be concerned about internal interrelationships among depression storage components. However, if an objective is to search for source areas or assess the sensitivity of overland flow to the spatial distribution of depression storage under different conditions of rainfall, infiltration, land use changes, depth to water table and so on, then there may be a need to think more specifically in terms of the physical nature of depressional storage.

It is clear that the response of pixels belonging to surface depressions is different from the response of pixels not in depressions. That is, assuming that the surface soil profile is at a saturation state at the beginning of a rainfall event, only those portions of the landscape which do not involve depressions generate runoff. As the rainfall continues, small depressions become filled up, and part of the surface area under depressions starts contributing to runoff. With further passage of time, larger-sized depressions are filled up and begin to contribute to runoff. This process will continue until practically all the area of depressions contributes to runoff, the areal increase occurring in a step-wise manner (Moore and Larson, 1979). As a result, it would seem to be crucial to attempt to physically characterize depression stores. Figure (7.1) shows a schematic arrangement of stores for a typical hill-slope.

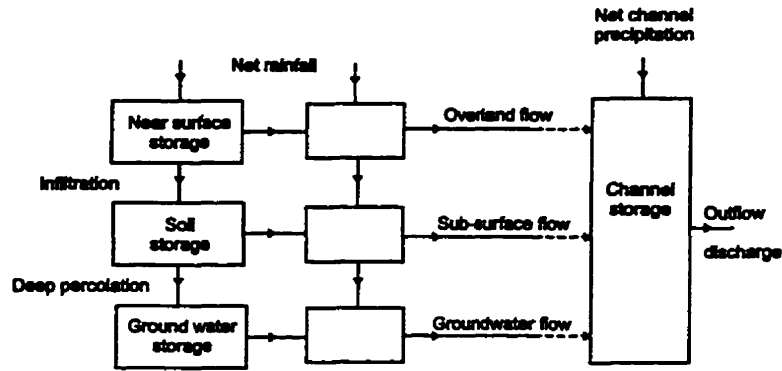


Figure 7.1: Schematic arrangement of stores in a typical hill-slope

### 7.3 Mathematical Formulation—Electrical Analogy

From the point of view of an electrical analog, each depression storage can be represented by a capacitor, and the channel connecting two depression storages in a particular direction can be represented by a resistor. In this way, the whole system can be simulated by an RC circuit network. Each resistor in the RC network represents the resistance to flow in one specific direction across opposite extremities of the area associated with that resistor. The resistors therefore simulate the energy-dissipating or damping characteristics of the original field. The capacitors, on the other hand, represent the energy-storage properties—in this case, potential energy. The mathematical formulation of the problem in terms of electrical terms demands the specification of a number of items, as presented below.

#### System Configuration

When the landscape is conceptualized in terms of a discrete number of reservoirs and conduits, the system can be represented by a number of depression storages and their associated connecting conduits in the x and y-directions, Figure (7.2). Figure (7.3)

illustrates a typical node with its associated resistors and capacitor for the cases of both non-leaky and leaky depression storages.

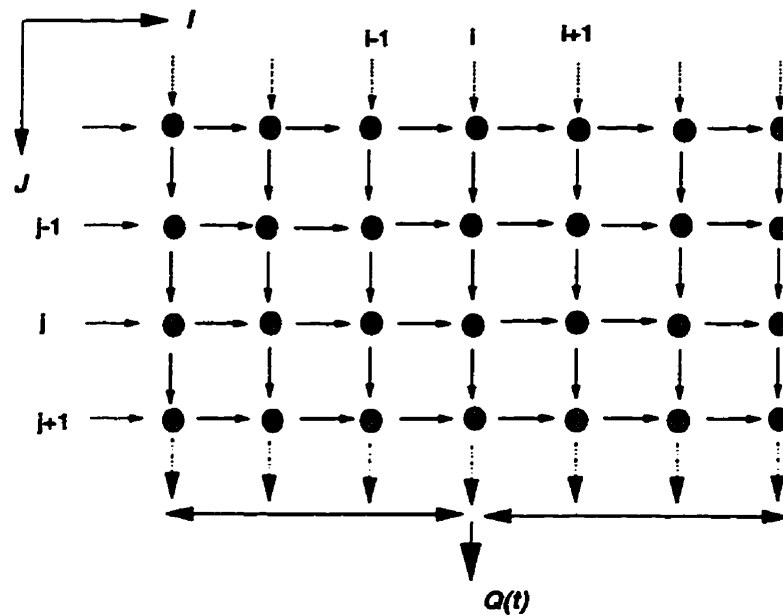


Figure 7.2: Typical network of reservoirs and conduits.

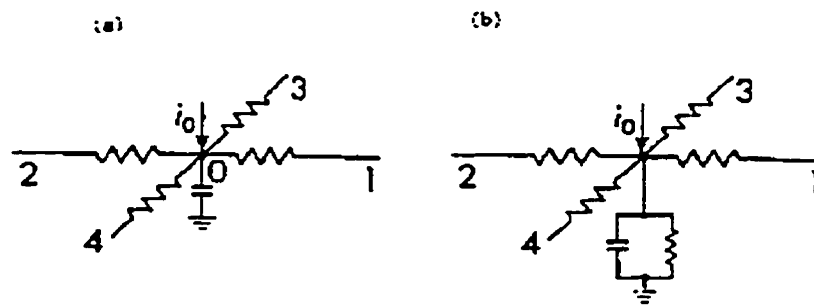


Figure 7.3: A typical node (a). Non-leaky capacitor (b). Leaky capacitor.

### System Field Parameters

The system field parameters consist of channel resistances in the x and y-directions, the capacitance for each node, and the resistance associated with each leaky capacitor.

These parameters can be defined as follows:

1. Channel resistance in the x-direction

Defining  $RX(i, j)$  as the resistance of the channel connecting nodes  $(i, j)$  and  $(i + 1, j)$ , the resistance matrix in the x-direction is:

$$\mathbf{RX} = \begin{bmatrix} RX(1,1) & RX(2,1) & RX(3,1) & \cdots & RX(I-1,1) \\ RX(1,2) & RX(2,2) & RX(3,2) & \cdots & RX(I-1,2) \\ RX(1,3) & RX(2,3) & RX(3,3) & \cdots & RX(I-1,3) \\ \vdots & \vdots & \vdots & \ddots & \vdots \\ RX(1,J) & RX(2,J) & RX(3,J) & \cdots & RX(I-1,J) \end{bmatrix}$$

2. Channel resistance in the y-direction

Defining  $RX(i, j)$  as the resistance of the channel connecting nodes  $(i, j)$  and  $(i, j + 1)$ , the resistance matrix in the y-direction is:

$$\mathbf{RY} = \begin{bmatrix} RY(1,1) & RY(2,1) & RY(3,1) & \cdots & RY(I,1) \\ RY(1,2) & RY(2,2) & RY(3,2) & \cdots & RY(I,2) \\ RY(1,3) & RY(2,3) & RY(3,3) & \cdots & RY(I,3) \\ \vdots & \vdots & \vdots & \ddots & \vdots \\ RY(1,J-1) & RY(2,J-1) & RY(3,J-1) & \cdots & RY(I,J-1) \end{bmatrix}$$

3. Subsurface resistance associated with each depression

Defining  $RG(i, j)$  as the resistance of the leaky capacitor at node  $(i, j)$ , the resistance matrix associated with the whole network is:

$$\mathbf{RG} = \begin{bmatrix} RG(1,1) & RG(2,1) & RG(3,1) & \cdots & RG(I,1) \\ RG(1,2) & RG(2,2) & RG(3,2) & \cdots & RG(I,2) \\ RG(1,3) & RG(2,3) & RG(3,3) & \cdots & RG(I,3) \\ \vdots & \vdots & \vdots & \ddots & \vdots \\ RG(1,J) & RG(2,J) & RG(3,J) & \cdots & RG(I,J) \end{bmatrix}$$

#### 4. Storage coefficient of each capacitor

This coefficient can be considered to be either constant or a function of the voltage level of the capacitor at each node. In the case of variable capacitance, the shape of each depression can be easily simulated. With reference to implications drawn from the pond analysis in Section (5.8.1) and other studies in the literature and for a landscape that has not been disturbed, then the geometric shape of depressions follows a set pattern which can be explained in terms of fractal geometry. On this basis, one can assume that  $c = av^b$ , where  $c$  is capacitor coefficient,  $v$  is voltage level across the capacitor,  $a$  and  $b$  are intercept and slope of power law relationship. Coefficients  $a$  and  $b$  remain the same from one depression (capacitor) to another (Haan and Johnson, 1968; Ullah, 1974).

#### System State Variable

- $v(i, j, n - 1)$  : Voltage of node  $(i, j)$  at the beginning of time step  $n$
- $v(i, j, n)$  : Voltage of node  $(i, j)$  at the end of time step  $n$
- $OX(i, j, n)$  : Outflow from node  $(i, j)$  in the x-direction during time step  $n$
- $OY(i, j, n)$  : Outflow from node  $(i, j)$  in the y-direction during time step  $n$
- $TO(i, j, n)$  : Total outflow from node  $(i, j)$  during time step  $n$
- $TI(i, j, n)$  : Total inflow to node  $(i, j)$  during time step  $n$

### **System Initial Conditions**

Numerical simulation of any field problem requires the specification of initial conditions. Here the voltage level at each node (i.e. the voltage across the capacitor) must be specified at the beginning of each simulation, i.e.  $v(i, j, 0)$  is known everywhere throughout the domain.

### **System Boundary Conditions**

Defining a series of fictitious nodes along  $x = 0$  and  $y = 0$ , the boundary conditions take the following forms:

- Along  $x = 0$  (left side)

$$OX(0, j, n) = 0$$

where  $OX(0, j, n)$  is the outflow from fictitious node  $(0, j)$  to node  $(1, j)$  during time step  $n$ .

- Along  $y = 0$  (top side)

$$OY(i, 0, n) = 0$$

where  $OY(i, 0, n)$  is the outflow from fictitious node  $(i, 0)$  to node  $(i, 1)$  during time step  $n$ .

- Along  $x = L$  (right side)

$$OX(L, j, n) = 0$$

- Along  $y = M$  (bottom side), the condition is determined by simulation.

•

### **Internal Distributed System Excitation**

Internal excitation due to direct rainfall is proportional to rainfall intensity times the contributing area associated with each depression. This excitation is applied at each node  $(i, j)$  during time step  $n$ . Regarding the spatial and temporal variability of rainfall, four different situations can be considered as follows:

1. Constant rainfall with regard to both space and time
2. Constant rainfall w.r.t space, but variable w.r.t. time
3. Constant rainfall w.r.t. time, but variable w.r.t. space
4. Variable rainfall w.r.t. both time and space.

### System Physical Constraints

As was emphasized in previous sections, each depression does not contribute to runoff until such time as the depth of water in that depression exceeds the overflow depth (pour depth). This threshold imposes a physical constraint on the RC network. Defining a breaking voltage for each node, the above constraint simply means that the voltage level at each node is not responsible for induced current, but the net voltage beyond the breaking voltage is responsible for induced current. The breaking voltage is a matrix corresponding to the overflow depth at each depression, i.e.

$$\mathbf{vb} = \begin{bmatrix} vb(1,1) & vb(2,1) & vb(3,1) & \cdots & vb(I,1) \\ vb(1,2) & vb(2,2) & vb(3,2) & \cdots & vb(I,2) \\ vb(1,3) & vb(2,3) & vb(3,3) & \cdots & vb(I,3) \\ \vdots & \vdots & \vdots & \ddots & \vdots \\ vb(1,J) & vb(2,J) & vb(3,J) & \cdots & vb(I,J) \end{bmatrix}$$

As the depth of water in each depression cannot exceed a certain limit dictated by the detention depth, the voltage level at each node will have a maximum value corresponding to the maximum detention depth. Again, the maximum voltage level is a matrix with its elements corresponding to maximum detention depths plus overflow depths. It worths noting that in hydrological system, Manning equation serves to link

continuity and momentum equations, while in electrical system, the maximum voltage level serves to link Kirchoff's current law (KCL) and Kirchoff's voltage law (KVL) to make the corresponding governing equation amenable to solution. In reality, the depth can rise above the pour depth and the amount of rise above pour depth is proportional to runoff rate.

### System Governing Equation

For a typical node such as the one shown in Figure (7.3b), Kirchoff's current law (KCL) can be used for the continuity equation (Johnson et al., 1984), i.e.

$$i_2 + i_3 + i_0 - i_1 - i_4 - i_L - i_c = 0 \quad (7.1)$$

where  $i_0$  is the source or sink;  $i_c$  is the current through the capacitor;  $i_1, i_2, i_3, i_4$  are the currents through surface resistors; and  $i_L$  is the current through a resistor parallel to the capacitor. Due to this last resistor, the capacitor is considered leaky, and the leakage is analogous to infiltration from the depression.

The momentum equation for this system is Ohm's law in each direction, i.e.

$$i = \frac{\Delta v}{R} \quad (7.2)$$

Combining Equations (7.1) and (7.2), and recalling that the current through the capacitor is  $i_c = c \frac{dv}{dt}$ ,

$$\frac{v_2 - v_0}{R_2} + \frac{v_3 - v_0}{R_3} + i_0 - \frac{v_0 - v_1}{R_1} - \frac{v_0 - v_4}{R_4} - \frac{v_0}{RG} - c \frac{dv_0}{dt} = 0 \quad (7.3)$$

where  $v_0$  is the voltage for the node under consideration. Rearranging terms,

$$\frac{v_2 - v_0}{R_2} + \frac{v_1 - v_0}{R_1} + \frac{v_3 - v_0}{R_3} + \frac{v_4 - v_0}{R_4} = c \frac{dv_0}{dt} + \frac{v_0}{RG} - i_0 \quad (7.4)$$

Equation (7.4) is the finite difference form of the diffusion wave equation. With the identification of boundary and initial conditions and also field parameters (resistance and capacitance coefficients) for the whole network, Equation (7.4) can be solved subject to the cited physical constraints. Based on the definition of current through a resistor, one can write the component of outflow from each node as follows:

Outflow from node  $(i, j)$  in the x-direction:

$$OX(i, j, n) = \frac{\bar{v}(i, j, n) - \bar{v}(i + 1, j, n)}{RX(i, j)} \quad (7.5)$$

Outflow from node  $(i, j)$  in the y-direction:

$$OY(i, j, n) = \frac{\bar{v}(i, j, n) - \bar{v}(i, j + 1, n)}{RY(i, j)} \quad (7.6)$$

where, for example,  $\bar{v}(i, j, n)$  is the net average voltage level during time step  $n$ , defined as:

$$\bar{v}(i, j, n) = \frac{v(i, j, n) + v(i, j, n - 1)}{2} \quad (7.7)$$

Total outflow from node  $(i, j)$ , taking into account leakage from the capacitor is:

$$TO(i, j, n) = OX(i, j, n) + OY(i, j, n) + \frac{\bar{v}(i, j, n)}{RG(i, j)} \quad (7.8)$$

Total inflow to node  $(i, j)$ , including direct rainfall, is:

$$TI(i, j, n) = OX(i - 1, j, n) + OY(i, j - 1, n) + Rain(i, j, n) \quad (7.9)$$

After expanding the right hand side of Equation (7.4) in finite difference form:

$$v(i, j, n) = v(i, j, n - 1) + \frac{\Delta t}{c(\bar{v}(i, j, n))} [TI(i, j, n) - TO(i, j, n)] \quad (7.10)$$

It is clear that  $v(i, j, n)$  appears on both sides of Equation (7.10). As a result, an iterative approach must be adopted to determine the voltage level at the end of each time step.

#### 7.4 Analogy Between Electrical and Hydrological System

Generally speaking, each parameter and variable in the electric analog proposed above should correspond to a parameter or variable in the hydrological system (Karplus, 1958). In order to design an electric circuit which reasonably relates such an electrical system to its hydrological counterpart, and also makes available the solution of the problem in a reasonable length of time, it is necessary to select scale factors. These scale factors are conversion constants relating the corresponding parameters and variables in the two systems. A summary of analogous relationships in the electric and hydrologic systems is presented in Table (7.1). These analogous quantities include three dependent variables, two field parameters and the independent time variable. A scale factor must be selected to relate each of these analogous quantities. These scale factors are not independent, but are related by three basic equations. In the case of

the electrical system, these equations include the following:

$$i = \frac{dq}{dt}$$

$$i = \frac{\Delta v}{R}$$

$$i = c \frac{dv}{dt}$$

Similar relationships exist for the hydrologic system. It is apparent, therefore, that only three of the six scale factors relating the hydrologic system to the electrical system can be independent. It is also apparent that the three independent scale factors cannot be chosen arbitrarily. For example, basic scale factors relating current, charge and time in the electrical system to the corresponding variables in the hydrological system would not constitute an independent set, because all three of these quantities appear in the first of the preceding three equations.

To assure complete independence of the basic scale factors, the quantities in Table (7.1) can be divided into two groups: the first including time, resistance and capacitance; and the second including voltage, charge and current. A basic requirement of the scaling process is that two scale factors be selected from the first group and that only one be selected from the second group.

The three basic scale factors are defined as

$$\Delta v = l \Delta z$$

$$C_e = \frac{1}{m} C_h$$

$$t_e = nt_h$$

where the subscripts  $e$  and  $h$  refer to the electrical and hydrological systems. Relationships between the other parameters and variables of the two systems in terms of  $l$ ,  $m$  and  $n$  can be derived by dimensional analysis and are included in Table (7.1).

Table 7.1: Comparison of analogous quantities in electrical and hydrological system

Parameter or variable	Electrical			Hydrological			Scale factor
	Description	Symbol	Unit	Description	Symbol	Unit	
Across variable	Voltage	$\Delta v$	Volt	Elevation diff.	$\Delta z$	meter	$\Delta v = l\Delta z$
Through variable	Current	$i$	Ampere	Discharge	$Q_h$	$\frac{m^3}{s}$	$i = \frac{l}{m\eta} Q_h$
Integral of through variable	Stored charge	$q_e$	Coulomb	Volume	$V$	$m^3$	$q_e = \frac{l}{m} V_h$
Time	Time in ele. circuit	$t_e$	Second	Time	$t_h$	hr	$t_e = nt_h$
Dissipating or damping par.	Resistance	$R_e$	Ohm	Channel resistance	$R_h$	$\frac{m^{-2}}{m^3}$	$R_e = mnR_h$
Potential energy res.	Electrical capacitance	$C_e$	Farad	Depression Storage area	$C_h$	$m^2$	$C_e = \frac{C_h}{m}$

## 7.5 A Hypothetical Example

### System Configuration

In order to check whether the methodology proposed in the preceding section can satisfy expectations relating to the hydrologic system, a simple example is provided in this section. Figure (7.4) illustrates a system configuration along with directions of overland flow from one depression to another.

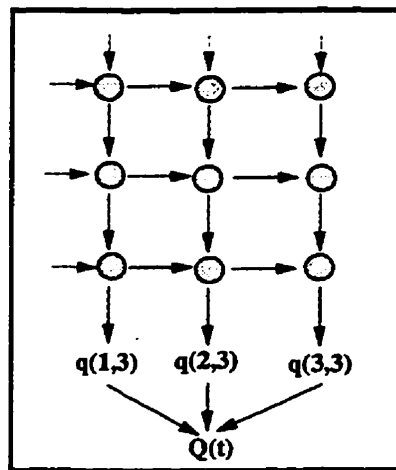


Figure 7.4: System configuration.

### Field Parameters

The field parameters for the above configuration are:

$$\mathbf{RX} = \begin{bmatrix} 2 & 3 \\ 1 & 5 \\ 4 & 2 \end{bmatrix} \quad \mathbf{RY} = \begin{bmatrix} 3 & 1 & 2 \\ 5 & 3 & 1 \end{bmatrix}$$

$$C = \begin{bmatrix} 0.5 & 0.1 & 1.0 \\ 0.2 & 0.1 & 0.25 \\ 0.2 & 0.1 & 0.4 \end{bmatrix}$$

In the following simulation exercises, the three depressions near the outlet are given a generic name according to ranking of their capacitance values. Thus, node (2, 3) is referred to as small depression, while node (3, 3) is called large depression.

### **Breaking Voltage**

The minimum voltage level corresponding to each depression storage is given by the matrix,

$$vb = \begin{bmatrix} 150 & 145 & 140 \\ 135 & 130 & 125 \\ 120 & 115 & 110 \end{bmatrix}$$

### **Maximum Voltage level**

As was mentioned before, the voltage level at each node cannot increase without limit. In this example, it was assumed that the maximum voltage level corresponding to the maximum detention depth had a constant value of 25 units everywhere within the system.

### **Initial condition**

The voltage level in each depression was considered to be zero at the start of simulation.

### Boundary conditions

Flow along the left, right and top boundary of the test area was considered to be zero (i.e. no-flow-at-boundary conditions).

### Rainfall Input

The rainfall input was considered to be constant with respect to both time and space. Its base value for subsequent simulation runs was 175 units and lasted for 0.2 second corresponding to ten time intervals (i.e.  $\Delta t = 0.02$  s).

## 7.6 Simulation Run

With a rainfall intensity of 175 units and the base values selected for other input parameters, the model was run and the results summarized in Figure (7.5). As expected, outflow from depressions with high storage capacity is not only delayed, but also attenuated to a certain extent, while outflow from depressions with low storage capacity is peaked without any delay.

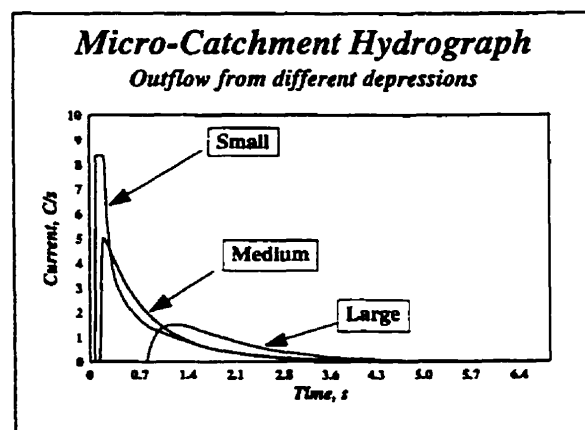


Figure 7.5: Micro-catchment outflow hydrograph for nodes (1,3), (2,3), (3,3).

### 7.6.1 Scale Issue in the Proposed Methodology

The outflow hydrograph from the whole surface is shown in Figure (7.6). Based on the model structure proposed in this methodology, there is a strong justification for minor peaks such as those occurring in the micro-catchment hydrograph. In essence, runoff from upslope contributing areas are utilized to fill the depressions near the outlet. As soon as depth of water in those depressions exceeds overflow depth for the corresponding depressions, they will start to contribute to runoff while at early period of runoff generation, there are no contributions from those depressions. Conventional rainfall-runoff models do not often yield such minor bumps in outflow hydrographs for small scale catchments like the one considered in this example, mainly because the model does not accommodate such phenomenon in its structure.

One important aspect of the proposed methodology is its scale independence. That is, the model works at a range of scales provided the data resolution is consistent with that scale. Therefore, such a model opens up the possibility of addressing the issue of dominant processes at a range of scales. It may happen that for a small scale micro-catchment, surface resistance has a dominant effect on shaping the runoff hydrograph; while at a larger scale, surface resistance may have a minor effect and surface storage components may shape the runoff hydrograph. Furthermore, questions such as what happens if a large depression is located near the outlet can be addressed by this methodology very easily.

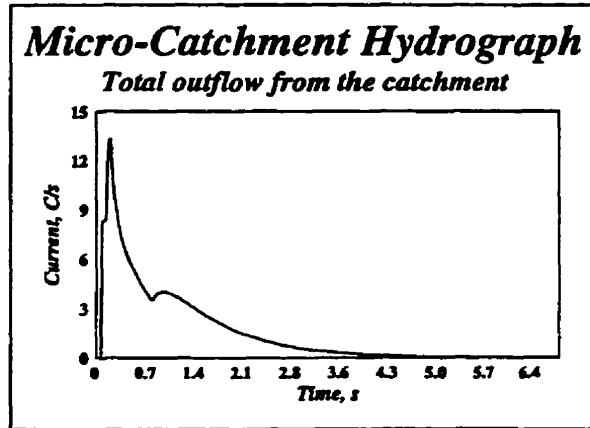


Figure 7.6: Total outflow from the micro-catchment.

### 7.6.2 Effects of Storage Capacity of Each Depression

When the storage capacity of a depression near the outlet was increased significantly (i.e.  $2.5 \times$  larger), outflow from that depression was greatly altered, as shown in Figure (7.7). Moreover, the shapes of hydrographs from other depressions can also be affected, the nature of the effects being related somewhat to the relative positioning of the large depression. To further explore the relative positioning of the large depression on outflow response, the storage capacity of a depression distant from the outlet was increased. Outflow from the individual depression near the outlet was changed and the minor bump in lumped response of the catchment disappeared completely. Figure (7.8) clearly demonstrates the lumped and individual responses for this scenario. The dramatic change in the shape of catchment response caused by changing the relative positioning of large depression implies the importance of consideration of actual pattern of depressions for this hypothetical scenario.

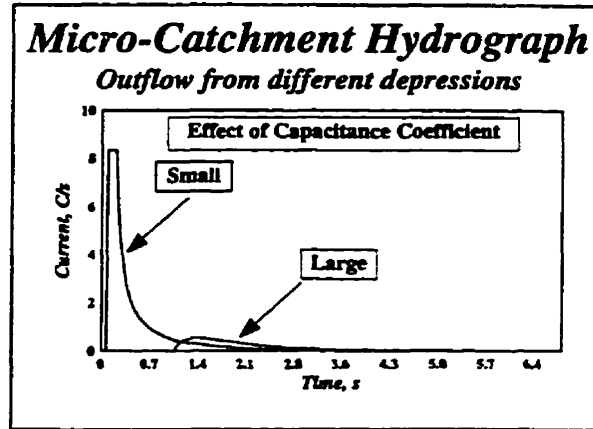


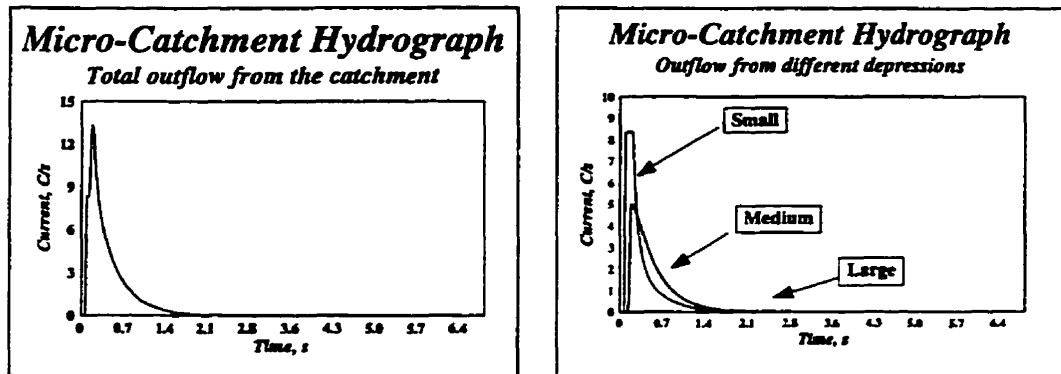
Figure 7.7: Effects of surface storage components on outflow hydrograph.

### 7.6.3 Effects of Channel Resistance

When the resistance of channel connecting node (2, 2) to (2, 3) was increased, it was found that the outflow from node (2, 3) was diminished. Figure (7.9) summarizes the results of this simulation run. Moreover, the shapes of hydrographs from other depressions were also affected due to a change in resistance coefficient of a particular channel. To further explore the impacts of channel resistance in different positions, channel resistance of a channel distant from the outlet was altered. Figure (7.10) clearly illustrates the impact of such a change implying that the effect somehow related to the relative positioning of the changed channel resistance.

### 7.6.4 Effects of Initial Condition

As mentioned before, the rainfall intensity for all previous simulation runs was 175 units for a specified period and the voltage level in each depression was considered to be zero at the start of simulation. When the rainfall intensity was decreased to  $r = 75$  units, it was found that the outflow from nodes (1,3) and (3,3) were



(a) Lumped response

(b) Component response

Figure 7.8: Outflow hydrograph for changed position of one large depressions.

diminished to zero, as can be seen in Figure (7.11). In essence, the rainfall amount was not enough to satisfy depression storage demand for their contribution to runoff. When the voltage level in each depression was increased to 100 units (i.e. change of initial condition), then the outflow hydrograph for those depressions did appear even for rainfall intensity as low as  $i = 25$  units (for the same time period) as could be seen in Figure (7.12).

### 7.6.5 Capability of the Model

At first, it has to be said explicitly that this electrical model was not meant to actually be applied to a watershed but rather be used to explore the relative roles of resistance, capacitance and perhaps leakage along with their relative spatial positions on catchment response. Further, results of simulation runs given in previous sections clearly demonstrate that investigating the relative roles of resistance, capacitance and perhaps leakage along with their relative spatial positions on catchment response should be done in ways that are consistent with data resolution and also the way the model

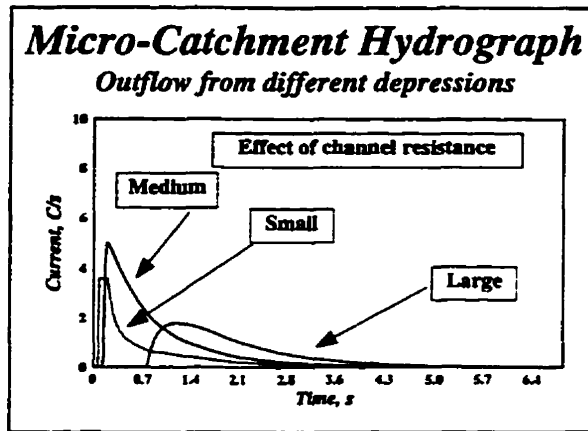


Figure 7.9: Effects of channel resistance on outflow hydrograph.

was structured to utilize those data. In other words, the model structure should have room for incorporation of change in channel resistance, depression storage capacitance and its subsequent effect on catchment response. In a majority of cases, either the data needed to support the model structure are not available or the model structure could not accommodate the data available. In either case the data resolution and model structure should interact and be consistent with one another. For example, the electrical analog could accommodate actual spatial locations of depression storages. As a result, it is feasible to investigate the impact of the relative spatial positions of depressions on catchment response. However, if a model structure is based on statistical pattern of depressions, then explicit investigation of the impact of relative spatial location of depressions is not considered feasible.

Another major capability of the model is that it is not only possible to determine the runoff hydrograph at the outlet of the micro-catchment, but also to output the runoff hydrograph at any point within the catchment or the water level at any depression within the micro-catchment. It is also possible to map contributing areas at any

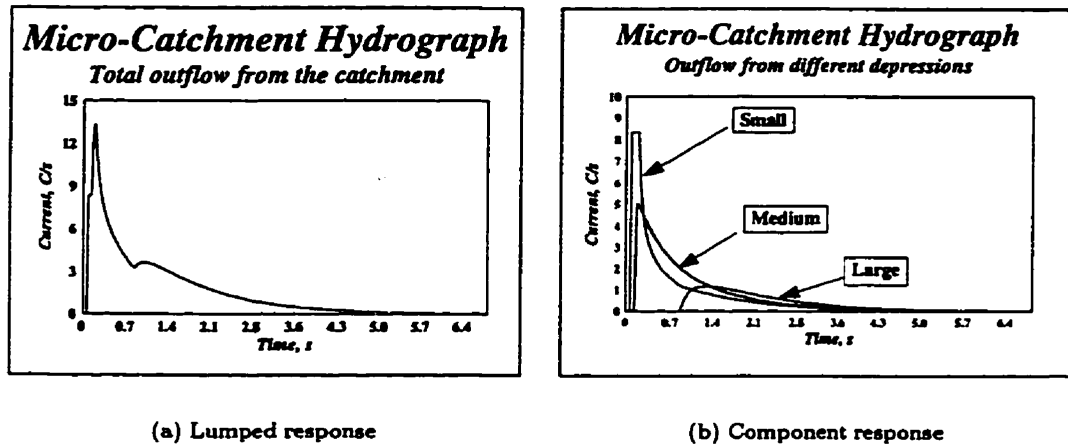


Figure 7.10: Outflow hydrograph for different position of resistive elements.

instant during the course of a rainfall event. Figure (7.13) illustrates the time variation of voltage level at node (2, 3). The curve consists of three segments. The rising part of the curve corresponds to rising limb of actual hydrograph, while the flat part corresponds to a steady state situation implying that the response is governed by rainfall for that segment. Finally, the recession part corresponds to depletion of detention storage over the surface.

### 7.6.6 Discussion of Model

Application of electrical analog on a hypothetical example and the obtained results provided an opportunity to touch on some of the salient features of both small-scale laboratory and field experiments. The following points must be noted in this regard:

- Comparison of both lumped and time-wise variations of response for surface treatments II and III (see Section 6.2.2) clearly revealed that due to different spatial pattern of depressions for these two surfaces, the response was signi-

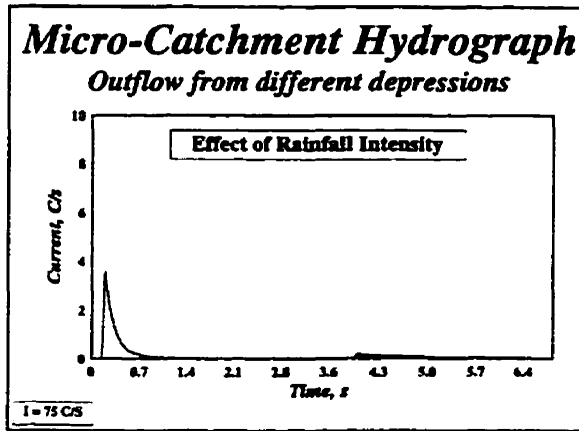


Figure 7.11: Effects of rainfall intensity on outflow hydrograph.

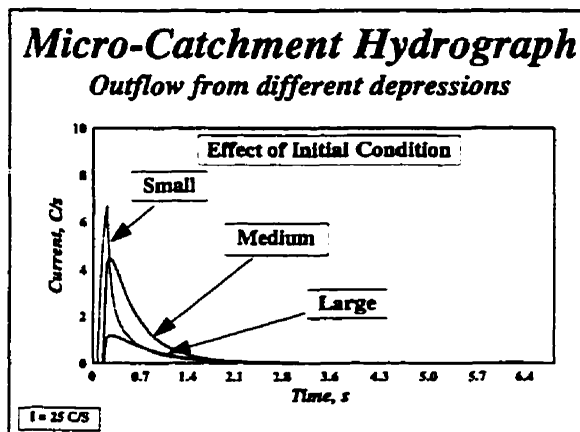


Figure 7.12: Effects of initial condition on outflow hydrograph.

ificantly different. Application of electrical analog on different spatial pattern of depressions and subsequent results clearly confirmed the laboratory experimental observation.

- While delineation of depression storages over the fiberglass surface suffers from a few pitfalls including lack of nested structure, being row-wise and independent from the size of the study area, its electrical counterpart also have a few similar pitfalls including the need for previous designation of direction from one depres-

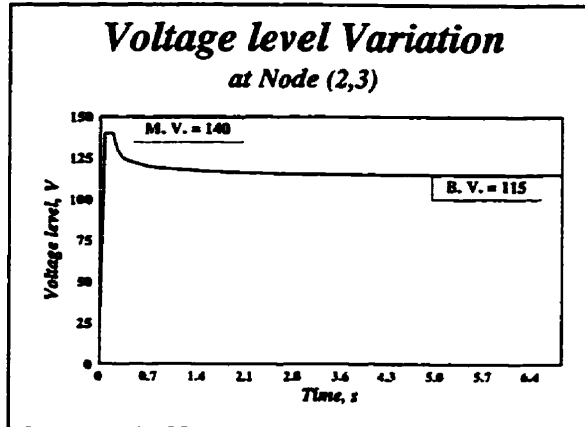


Figure 7.13: Variation of voltage level at node (2,3) with time.

sion to another and also assignment of maximum voltage level at each node which are not consistent with its physical counterpart.

- For both laboratory and field experiments, separation of infiltration from depression storages was found to be extremely difficult if not impossible. Modeling of infiltration (i.e. leakage from capacitance) in electrical analog shares similar concerns. While in hydrological system, upon passage of time, infiltration approached steady state condition, leakage from capacitance is directly proportional to voltage level across the capacitance, i.e. the higher the voltage value, the higher the leakage rate implying that the two systems are not consistent in this respect.
- In small-scale field experiments, initial conditions were found to have a significant effect on catchment response. Application of electrical analog with different initial conditions clearly confirmed the above finding.

While, the use of an electrical analogy to simulate hydrologic response is quite attractive and also very easy to understand, it suffers from shortcomings associated with assumptions of linearity. That is, the relationship between cause and effect in an electrical system is linear (Ohm's law), while this relationship is not necessarily linear in the case of a hydrological system (Shen, 1965). The governing equations of an electrical system could be nonlinear with regard to field parameters, but they are linear with respect to state variables. The governing equations of a hydrologic system are not only nonlinear with respect to field parameters but also nonlinear with respect to state variables. In deriving the governing equations for the electrical system, there is no need to link Ohm's law to Kirchoff's current law by an empirical equation, but to assign the maximum voltage at each node. However, in the case of a hydrologic system, one has to introduce a weak link (e.g., Manning equation) in order to create a combination of the continuity and momentum equations which is amenable to solution.

Another shortcoming is the issue of time lag. For the case of the electrical system, application of even a localized excitation causes sudden effects to appear everywhere within the system; while for the case of a hydrological system, it can take considerable time to establish flow everywhere within the system.

In addition to the linearity and time lag issues, a number of other assumptions have been made in constructing the model. One of the more obvious is that rainfall is applied only onto the surface area of each depression and infiltration occurs only under the depression. These assumptions imply that the time of travel of water from the time it enters a depression until it appears at the catchment outlet is much longer than the time of travel from the instant rainfall strikes the ground until it reaches a

depression.

Due to the above cited shortcomings, in the next section, a more holistic type approach is developed to be applied to the hydrological system directly at a range of spatial scales.

## 7.7 Decision on Model Structure

To further address the question of how to structure a hydrologic model, having a place for depression storage, including even some treatment of the spatial pattern of such storage, three alternative approaches were considered:

- A method of analytical mechanics, i.e. a physically-based distributed parameter approach (i.e. deterministic approach);
- A method of statistical mechanics, i.e. a stochastic approach; and
- A holistic approach, i.e. a method somewhere in between a totally deterministic and a totally stochastic approach.

Unfortunately, in many fields of enquiry including hydrology, the key problems do not fall within the scope of either analytical mechanics or statistical mechanics (Dooge, 1985). In the case of catchment hydrology, the watershed can be treated neither as a large number of objects which are independent of each other (i.e. unorganized complexity) nor as a well-defined system in which the relationships between various components are fully established (i.e. organized simplicity), but rather somewhere in between with a relatively high degree of complexity along with some degree of organization.

The availability of a body of knowledge in hydrological science on one hand, and the inherent self-organization in some hydrological processes such as depression storage on the other hand, favored the rejection of a totally stochastic approach in structuring a rainfall-runoff model for this project. As for a totally deterministic approach, the Control Volume-based Finite Element Method (CVFEM) was considered seriously.

Four major advantages of this numerical method can be summarized as follow (Baliga, 1996):

- Its formulation is amenable to easy physical interpretation;
- Its solution satisfies both local and global conservation requirements even on coarse grids;
- It provides the geometric flexibility that is traditionally associated with Finite Element Methods (FEMs); and
- Each depression could be treated as a control volume.

**LANDFLOW** (Gottardi and Venutelli, 1997), a Fortran program with coding based on CVFEM, was tried and made operational. However, in the end, adopting a totally deterministic approach was rejected due to the existence of many unresolved problems such as the uniqueness issue, the parameterization issue, the numerical diffusion and dispersion issue and hypothesis testing issue, all mentioned in the literature review. As a result, an intermediate so-called holistic approach was tried, incorporating much of what has been learned from both analytical and statistical mechanics in such a way that hypotheses incorporated into the model structure could possibly be verified independently (Dooge, 1985). In Chapter 2, Section (2.9.1), the phrase “grey box approach” was assigned to this method to indicate an approach somewhere between a black box and a white box approach. In what follows, some background is provided to pave the way for the chosen approach.

## 7.8 Two Main Processes in Rainfall-Runoff Modeling

In the past 100 years, many efforts to model the way that rainfall is converted to runoff have been reported on. A common form of model is a network of nodes representing conceptual storages within the catchment, with the directed links between the nodes representing pathways by which water is transmitted from one storage to another, indicating flux to the catchment outlet as 'measured' streamflow, to the atmosphere as evaporation (including transpiration), or to losses from the catchment by deep percolation. The processes of storage and transmission have been dealt with by "lagging and routing", "convection and diffusion", and use of continuity and momentum equations. There is now evidence that storage and transmission, and the response discharge at various spatial scales are self-organized and can be considered to be fractal objects. Some background regarding the self-organization of storage, transmission and discharge processes is provided in what follows.

### 7.8.1 Storage Processes

For the sake of the present research, some physical stores as opposed to conceptual stores were considered. One basic candidate for a physical store is depression storage over the ground surface. These geometric configurations are a direct result surface topography structure (i.e. point elevation) and are, in turn causes of self-organization for other key hydrological variables in a typical watershed (Huang and Bradford, 1990a; Huang and Bradford, 1992; Tarboton et al., 1988). Quite interestingly, for characterization of depression storage, each depression storage was envisioned as a container with the following geometric features:

- Measure of length, such as the maximum depth of depression;
- Measure of area, such as the surface area of the depression at the pour point and the potential contributing area for each depression;
- Measure of volume, such as the volume of depression at the pour point; and
- Frequency of occurrence of the above features.

Referring back to the results of the pond analysis and its implications cited in Section (5.8.1), and also the pioneering work of Ullah (1974), it was found that the inter-relationships among the above measures can be explained by power law relationships, and hence they can be considered to be fractal objects.

### 7.8.2 Translation processes

Extensive research was conducted in Australia and elsewhere during the 1960s and 1970s to delineate isochrones of travel times and the distribution of flood storage. Pioneering work to address this issue was conducted by Pilgrim (1966a; 1966b; 1976; 1977). Pilgrim (1977), in his concluding paper, introduced six parameters to explore relationships with time of travel:

Parameter 1

$$\sum l_i$$

Parameter 2

$$\sum \left( \frac{l_i}{s_i^{\frac{1}{2}}} \right)$$

Parameter 3

$$\sum \left[ \frac{l_i}{s_i^{\frac{1}{2}} r_h^{\frac{2}{3}}} \right]$$

Parameter 4

$$\sum \left[ \frac{l_i n}{s_i^{\frac{1}{2}} r_h^{\frac{2}{3}}} \right]$$

Parameter 5a

$$\sum \left( \frac{l_i}{L_s^{1.17m}} \right)$$

Parameter 5b

$$(L_{so}^{1-1.17m} - L_{sp}^{1-17m})$$

where  $l_i$  = length of reach;  $s_i$  = slope;  $r_h$  = hydraulic radius;  $n$  = Manning's roughness coefficient;  $L_s$  = distance to the point along the stream from the source of the stream on which the point lies;  $o, p$  = subscripts referring to the watershed outlet and the point considered; and  $m$  = exponent in parameter 5a or 5b.

All except parameter 5b is expressed as the summation over all reaches of the streams from the point considered to the watershed outlet.

Parameter 1 implies a constant velocity throughout the watershed for any given runoff event. Research conducted by Pilgrim (1977) has indicated that despite decreasing slopes, average velocities tend to remain constant or to increase slightly in a downstream direction in a given river system. The combined effects of hydraulic radius and roughness are assumed to be the same for all reaches in parameter 2. Some measure of stream length divided by slope to a power in the order of 0.5 has been used successfully in many correlations of time parameters (such as lag time) between

watersheds. Parameters 3 and 4 are based on the Manning equation. As hydraulic roughness is difficult to estimate,  $n$  was omitted from parameter 3, while it was retained in parameter 4 for the sake of completeness and comparison. Parameter 5 is based on hydraulic geometry relationships and takes account of increases in velocity in the downstream direction.

In summary, based on extensive collected data sets, Pilgrim (1977) demonstrated that the variation of travel time with various cited parameters exhibit linear relationships in log-log space, indicating relationships of the form:

$$\text{travel time} = a(\text{parameter})^b$$

Relationships of this type are an indication of the fact that translation time exhibits fractal behavior and the laws of fractal geometry are applicable. Although the spatial scale of the above findings was limited to in-channel processes, one can safely argue that the same idea is applicable to hill-slope processes as well.

### 7.8.3 Power-law Distributions of Discharge

One of the main obstacles to understanding surficial hydrologic processes has been the high spatial variability of surface features in river basins to which those processes are intimately linked. River runoff is a key flux in climate systems. It occurs over a wide range of spatial scales, from a micro-scale of  $1 \times 1$  m to the hill-slope through to the mesoscale of drainage basins, to the macro-scale of continents. In the early 1990s, a group of well-honored hydrologists met to outline research topics for future consideration in hydrological science (*Opportunities in the Hydrologic Sciences*, 1991).

An excerpt of their agreed document deserves to be mentioned here:

The search for an invariance property across scales as a basic hidden order in hydrologic phenomena, to guide development of specific models and new efforts in measurements, is one of the main themes of hydrologic science (*Opportunities in the Hydrologic Sciences*, 1991)[p. 197].

Based on extensive field work on overland flow at a hillslope scale, Emmett (1978) found that for either turbulent or laminar flow, the relationship between discharge per unit width and depth could be expressed as:

$$q = KD^M$$

where  $q$  = discharge per unit length;  $D$  = flow depth;  $K$  = roughness factor and  $M$  is the exponent for depth and reflects, in part, the degree of turbulence. The value of  $M$  is 1.67 for fully turbulent flow and 3 for fully-laminar flow. Thus, with increases in discharge, depth increases more rapidly in turbulent flow than laminar flow. For mixed flow, which Horton postulated to occur in nature, values of  $M$  would range between these two extremes. Recently, Rodriguez et al. (1992) explored the same type of relationship for mass discharge and energy in river systems. The above power type relationship implies that discharge is also a fractal process, and actual cumulative river discharges are aggregations of smaller discharges.

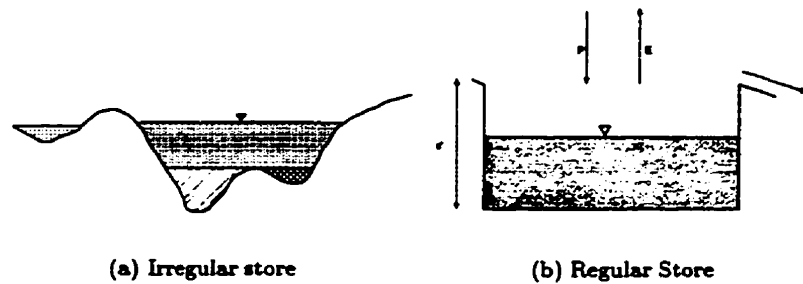


Figure 7.14: Point representation of runoff production

## 7.9 Mathematical Formulation–Hydrological Analogy

In response to the question of whether the actual spatial distribution of storages or their statistical distribution should be considered in structuring a rainfall-runoff model, one may argue that these storages manifest themselves at a range of spatial scales, and since the number of depression storages approaches infinity, consideration of actual storage units seems nonsensical. Since the average depth of depressions for a specified study area is the most stable parameter with regard to grid spacing (as shown in Section 5.6), the process of runoff generation at any point within a typical hillslope can be represented by a simple storage or reservoir characterized by its depth or capacity,  $c'$ . The depth of water in each storage can be increased by rainfall,  $P$ , depleted by evaporation,  $E$ , and depleted by infiltration. As soon as the depth of water exceeds the overflow depth, the surface storage will start to generate runoff, Figure (7.14).

A typical hill-slope may be considered to be made up of many such storage elements, each characterized by its store depth,  $c$ , and acting either dependently or independently of its neighboring element. As a consequence, the spatial variability

in depression storage depth,  $c$ , may be viewed as a random variable with probability density function,  $f(c, \theta)$ , where  $0 \leq c < \infty$ , and  $\theta$  being a vector of parameters. If the hillslope area is  $A$ , then an area  $Af(c, \theta)dc$  of the hillslope has surface storage depth lying between  $(c, c + dc)$ . A mathematical form must be specified for  $f(c, \theta)$  and the quantities  $\theta$  must be either specified or estimated from input/output data.

If depression storages of all possible different depths are conceptually arranged in ascending order of depth as in Figure (7.15), with their open tops positioned at the same horizontal level, then a wedge-shaped diagram results if lines AB and AA' are drawn through the store tops and bottoms. The diagram does not represent the statistical population of stores, but stores of different depth; and the wedge-shaped diagram can be used to establish the water level profile across stores of different depth resulting from a sequence of wet and dry periods. The probability of occurrence of stores of a particular depth is specified through the density,  $f(c)$ , and exemplified alongside the wedge-shaped diagram in Figure (7.15).

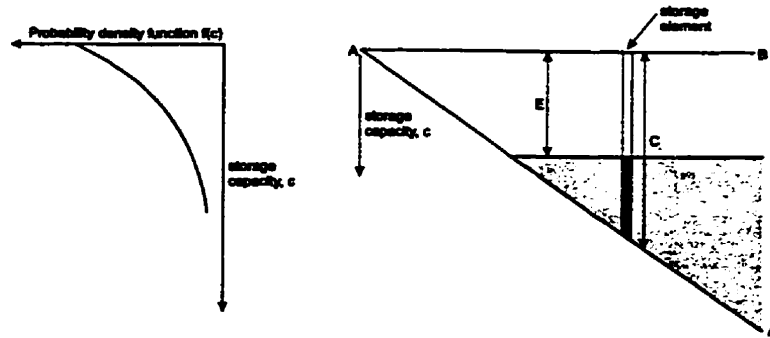


Figure 7.15: Basin representation by storage elements of different depths and their associated density function.

At this stage, it is important to draw a clear distinction between two totally different types of runoff regime: infiltration-excess overland flow (i.e. Hortonian mechanism) and saturation-excess overland flow (i.e. Dunne mechanism), each explained in some detail in Chapter 2. Concentration on infiltration capacity emphasizes the influence of rainfall intensity and soil hydraulic properties, which somehow does not fit easily into the concept of soil water storage. As a result, it becomes difficult to assess changes in infiltration capacity during a complex storm. The infiltration capacity approach differs from most hydrological storage models by emphasizing the rate of *inflow* (or, strictly, maximum rate of inflow) rather than the rate of *outflow* (Kirkby, 1976). It also emphasizes Hortonian, or 'infiltration-excess' overland flow, at the expense of Dunne or 'saturation-excess' overland flow which arises when the soil can accommodate no more water, at which point overland flow occurs even at low rainfall intensities. Giving more emphasis to surface storage is an alternative approach which overcomes some of the difficulties noted above by concentrating on the storage capacity of the near surface soil including depression storage.

In the following section, the structure of the model is explained for each of the

above mechanisms in some detail. Further attention is given to clarifying whether or not there is a redistribution of runoff. In some models, it is explicitly or implicitly mentioned that, if a point generates runoff on a typical hillslope, runoff will reach the outlet without being lost along the route (i.e. with no redistribution in between). In other models, allowance is made to have some form of redistribution of runoff along the route. The model structure presented below takes into account both non-interacting (i.e. independent) and interacting storage (i.e. dependent) elements.

## 7.10 Theory of Non-interacting Storage Elements

For non-interacting storage elements, if a depression generates runoff, that runoff will reach the outlet (without the possibility of being lost between the depression and the outlet). Consider the case when the basin is saturated following a prolonged wet period, with all surface depressions full and evaporation occurring at the potential rate. At the end of a unit time interval, the water level profile can be represented as shown in Figure (7.15). If a rainfall amount,  $P$ , occurs in the next unit time interval, then the water level at the end of this interval can be illustrated by line AWW' in Figure (7.16). The hatched triangular area on the figure indicates the volume of direct runoff produced in the interval as a result of depression storages of increasing depth being progressively replenished and starting to spill. The actual volume generated can be obtained by weighting the runoff generated from a depression of a given size by its probability of occurrence as specified through the density function,  $f(c)$ , as described below.

At the end of the unit time interval, all depression storages of capacity less than  $P$  will be contributing direct runoff, the critical capacity below which all depression storages are full at some time,  $t$ , being denoted by  $C^* \equiv C^*(t)$ . Obviously enough, in this example  $C^*(t) = P$ . The proportion of the basin occupied by depression storages with depths less than or equal to  $C^*(t)$  will be:

$$\text{prob}(c \leq C^*(t)) = F(C^*(t)) = \int_0^{C^*(t)} f(c)dc \quad (7.11)$$

in which the function  $F(\cdot)$  is the cumulative distribution function of depression stor-

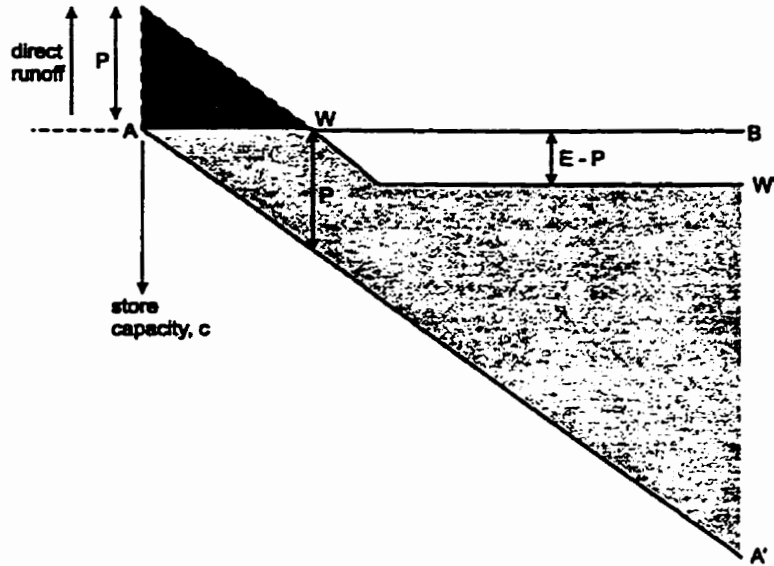


Figure 7.16: Direct runoff production from a population of stores

age depths, related to the probability density function through the relation  $f(c) = dF(c)/dc$ . Since  $F(C^*(t))$  defines the saturated proportion of the basin, it follows that the contributing area of direct runoff generation from a basin of area  $A$  is:

$$A_c(t) = F(C^*(t))A \quad (7.12)$$

The instantaneous rate of runoff generation per unit area from the entire basin,  $q(t)$ , is obtained by multiplying the net rainfall rate, denoted by  $\pi(t)$ , by the proportion of the basin which is saturated, so that:

$$q(t) = \pi(t)F(C^*(t)) = \pi(t) \int_0^{C^*(t)} f(c)dc \quad (7.13)$$

where  $q(t)$  is the time-wise variation of runoff at the point where it was originally generated. Later on, a kernel will be introduced to translate the generated runoff

to the basin outlet. The expanding and contracting nature of the area of storm runoff generation is an attractive feature of this model that accords well with the contributing area concept (i.e. partial area concept) in hydrology (Van de Griend and Engman, 1985).

For the  $i$ -th wet interval,  $(t, t + \Delta t)$ , for which the net rainfall rate is constant and equal to  $\pi_i = P_i - E'_i$ , the critical capacity will increase according to:

$$C^*(\tau) = C^*(t) + \pi_i(\tau - t) \quad \forall \quad t \leq \tau < t + \Delta t \quad (7.14)$$

In the case of  $\tau = t + \Delta t$ , Equation (7.14) becomes:

$$C^*(t + \Delta t) = C^*(t) + \pi_i \Delta t$$

and the volume of basin-direct runoff per unit area generated in this interval is:

$$\begin{aligned} V(t + \Delta t) &= \int_t^{t+\Delta t} q(\tau) d\tau = \int_t^{t+\Delta t} \pi_i F(C^*(\tau)) d\tau \\ &= \pi_i \int_t^{t+\Delta t} \int_0^{C^*(\tau)} f(c) dc d\tau \\ &= \int_{C^*(t)}^{C^*(t+\Delta t)} F(c) dc \end{aligned} \quad (7.15)$$

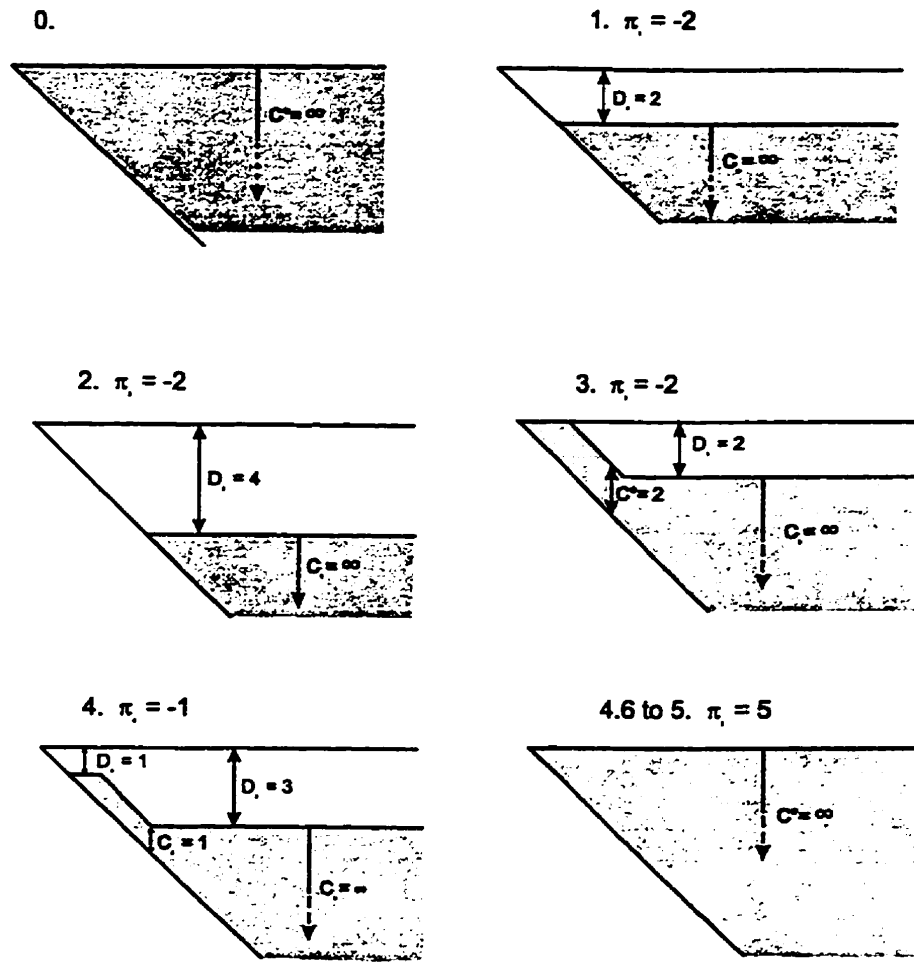


Figure 7.17: Evolution of the water profile across non-interacting stores of different depth in response to net rainfall,  $\pi_i = (-2, -2, 2, -1, 5)$ , falling in successive time intervals with storage full at  $t = 0$ .

The evolution of the water profile across depression storages of different depths as a consequence of a series of net rainfalls,  $\pi_i = P_i - E'_i$ , in successive unit time intervals,  $i = 1, 2, 3, \dots$ , falling on an initially saturated basin, is illustrated in Figure (7.17). A number of horizontal (or deficit) segments,  $D_k \equiv D_k(t)$ , and sloping (or content) segments,  $C_k \equiv C_k(t)$ , are formed across the assemblage of depression storages as a result. This particular water surface profile (i.e. combination of content and deficit) is due to the embedding of a non-interacting nature of depression storages into the

model structure.

Instantaneous direct runoff,  $q(t)$ , resulting from this series of net rainfalls is controlled solely by the temporal evolution of  $C^*(t)$  over this period, and may be calculated using Equations (7.13) and (7.14) for an appropriate distribution of depression storage depths.

The critical capacity,  $C^*(t)$ , will vary according to (7.14) during a wet interval. The interval  $\Delta t$  is equal to the sampling interval  $T$ , except when more than one content segment controls surface runoff generation within the interval  $T$ . In this case, the net rainfall  $\pi_i$  in the interval  $t < \tau \leq t + \Delta t$  exceeds the deficit of the shallowest deficit segment  $D_k^*$ , and so the interval  $\Delta t$  must be chosen such that:

$$\Delta t = \frac{D_k^* T}{\pi_i} \quad (7.16)$$

For example, in the interval (4, 5) in Figure (7.17), at time 4.6 the critical capacity  $C^*(t)$  jumps abruptly from 3 to  $\infty$  as the deficit segment is fully replenished, so two intervals, (4, 4.6) and (4.6, 5), must be used. Then:

$$\Delta t = \frac{D_k^* T}{\pi_i} = \frac{3 \times 1}{5} = 0.6$$

Also, if the density,  $f(c)$ , is bounded to the right by  $c_{\max}$ , the maximum depression storage depth (as would be the case for triangular or power distributions), and  $C^*(t + \Delta t)$  would exceed  $c_{\max}$  according to (7.14), then  $\Delta t$  must be chosen when  $C^*(\tau)$  first equals  $c_{\max}$ , and  $C^*(\tau) = c_{\max}$  used over the remainder of the rainfall sampling interval. It is to be understood that integrals developed later involving an infinite

upper limit on  $c$  should be replaced by  $c_{\max}$  in the case of right-bounded density functions.

### 7.10.1 Calculation of basin soil-water deficit

At this stage, a distinction has to be made with regard to whether the surface is impermeable or not. In light of having an impermeable surface, the deficit is solely related to depression storage, while in the case of permeable surface, the deficit calculation cover depression storage plus storage in top soil. Now consider a basin to be in the state depicted in Figure (7.18), with  $k_c$  content (sloping) segments and  $k_d$  deficit (horizontal) segments, and  $C_1 = \infty$ . Then the area between the ground surface level AB and the water surface level WW', when weighted in accordance with the weighting distribution of depression storage depths,  $dF(c) = f(c)dc$ , will give the instantaneous basin soil-water deficit. By considering the area partitioned as indicated by the vertical dashed lines in Figure (7.18), the soil-water deficit at time  $t$  is:

$$\text{SMD}(t) = \sum_{i=1}^k \int_{C_i+D_{i+1}}^{C_i+D_i} \underbrace{(c - C_i)f(c)dc}_{\text{sloping}} + \sum_{i=2}^k \int_{C_i+D_i}^{C_{i-1}+D_i} \underbrace{D_i f(c)dc}_{\text{horizontal}} + \int_{C_1+D_1}^{\infty} \underbrace{D_1 f(c)dc}_{\text{last horizontal}} \quad (7.17)$$

Here  $D_{k+1} = C_k = 0$ ,  $k_d = k + 1$ , and  $k_c = k$ .

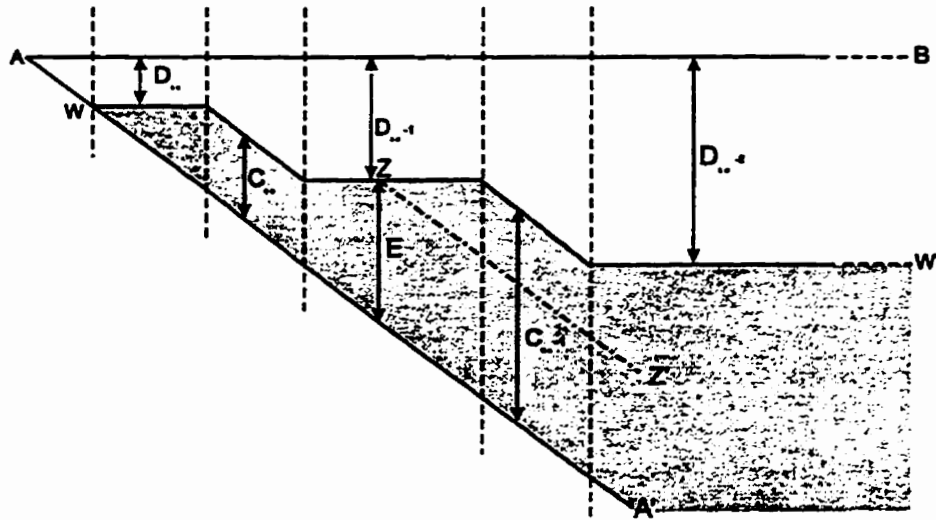


Figure 7.18: Calculation of basin soil-water deficit and actual evaporation at time  $t$ .

An expression describing the potential (i.e. maximum) volume of distributed soil-water over the basin as a whole can now be developed. The total storage available in the basin is given by:

$$S_{\max} = \int_0^{\infty} cf(c)dc = \int_0^{\infty} (1 - F(c))dc = \bar{c} \quad (7.18)$$

Combining Equations (7.17) and (7.18), the available soil-water at any instant  $t$  can be calculated to be:

$$S(t) = S_{\max} - \text{SMD}(t) \quad (7.19)$$

### 7.10.2 Relation of Actual to Potential Evaporation

Since evaporation occurs only from depressions which contain water, the actual evaporation loss from the basin is usually less than the potential rate. A continuity equation gives the actual evaporation over the  $i$ -th interval,  $(t, t + \Delta t)$ , to be:

$$E'_i = \begin{cases} S(t) - S(t + \Delta t) & \text{if } P_i = 0 \\ E_i \Delta t & \text{if } P_i \geq E_i \\ P_i \Delta t + S(t) - S(t + \Delta t) & \text{if } 0 \leq P_i \leq E_i \end{cases}$$

For the no net rainfall condition, actual evaporation is governed by the available soil moisture condition. In the case of a rainfall rate greater than the potential evaporation rate, actual evaporation will be governed by potential evaporation while for the case of  $P_i \leq E_i$ , the actual evaporation rate will be governed partly by soil moisture availability and partly by precipitation. One basic shortcoming of the above formulation is that the role of soil hydraulic properties as another controlling agent has not been taken into account. Using  $D^* \equiv D^*(t)$  to denote the depth of the minimum deficit segment, the instantaneous rate of actual evaporation at time  $t$  will be:

$$E'(t) = \begin{cases} E_i \int_{D^*(t)}^{\infty} f(c) dc & \text{if } P_i = 0 \\ E_i & \text{if } P_i \geq E_i \\ P_i + (E_i - P_i) \int_{D^*(t)}^{\infty} f(c) dc & \text{if } 0 \leq P_i \leq E_i \end{cases}$$

### 7.10.3 Incorporation of Drainage into Model Structure

To this point in the model development, it has been assumed that each depression can potentially lose water from only evaporation. An extension of the approach is possible to account for drainage of water from each depression. When a depression storage allows drainage to occur at a constant rate,  $\gamma$ , until the store empties, then the instantaneous drainage rate,  $b(t)$ , from the population of storage elements at time  $t$  can be calculated for three different conditions.

### Dry Condition (no Rainfall)

At some time  $t$  during a dry period, consider the water level surface across a population of depression stores to be as illustrated by the line  $AWW'$  in Figure (7.18). Further, consider drainage to occur at the instantaneous rate  $\gamma$  from all depressions containing water, i.e. from all depressions of depth greater than  $D_{k_d} = D^*(t)$ . Then the instantaneous drainage rate from the basin at time  $t$  is:

$$b(t) = \int_{D^*(t)}^{\infty} \gamma f(c) dc = \gamma(1 - F(D^*(t))) \quad (7.20)$$

Over the dry interval,  $(t, t + \Delta t)$ , the critical deficit,  $D^*(\tau)$ , will vary according to:

$$D^*(\tau) = D^*(t) - (\pi_i - \gamma)(\tau - t) \quad (7.21)$$

If  $\tau = t + \Delta t$ , Equation (7.21) becomes:

$$D^*(t + \Delta t) = D^*(t) - (\pi_i - \gamma)\Delta t$$

where the interval,  $\Delta t$ , is usually the sampling interval, but may be a shorter time interval if a content segment is fully depleted during a full-length sampling interval. Note that the emptying of a content segment will result in an abrupt instantaneous increase in  $D^*(\tau)$ , in a manner analogous to the replenishment of a deficit segment during a wet period, causing  $C^*(\tau)$  to change its value abruptly.

The volume of water drained in the  $i$ -th interval,  $(t, t + \Delta t)$ , can be calculated to be:

$$B(t + \Delta t) = \int_t^{t+\Delta t} b(\tau) d\tau = \gamma \Delta t - \int_{D^*(t)}^{D^*(t+\Delta t)} F(z) dz \quad (7.22)$$

**Wet Condition ( $P_i \leq E_i$ )**

For rainfall conditions involving rainfall rates less than potential evaporation, Equations (7.20) and (7.22) clearly still hold, as the state of deficit segments and  $D^*(t)$  do not change.

**Wet Condition ( $P_i \geq E_i$ )**

When rainfall rates exceed the potential evaporation rate, then drainage from depressions with depth less than  $D^*(\tau)$  must also be considered, even though some or all may remain empty due to drainage losses. Two cases must be considered:

**Case 1:  $\pi_i \geq \gamma$**

When the net rainfall,  $\pi_i = P_i - E'_i$ , exceeds the drainage rate, then there is no limit to the availability of water and all depression storages will drain at the instantaneous rate,  $\gamma$ . As a result, the instantaneous drainage rate from the basin over the wet interval,  $(t, t + \Delta t)$ , is:

$$b(\tau) = \int_0^\infty \gamma f(c) dc = \gamma \quad (7.23)$$

That is, the drainage rate remains constant and equal to the maximum rate,  $\gamma$ . In addition, the volume of drainage over the interval,  $(t, t + \Delta t)$  will be:

$$B(t, t + \Delta t) = \gamma \Delta t \quad (7.24)$$

**Case 2:  $\pi_i \leq \gamma$**

When the net rainfall rate (i.e.  $\pi_i = P_i - E'_i$ ) is less than the drainage rate, then depressions with depths less than  $D^*(\tau)$  will lose water by drainage at a rate  $\pi_i$ , while depressions with depths greater than  $D^*(\tau)$  will drain at the maximum instantaneous rate,  $\gamma$ . Consequently the instantaneous basin drainage rate is given by the sum of two integrals:

$$\begin{aligned} b(\tau) &= \int_{D^*(t)}^{\infty} \gamma f(c) dc + \int_0^{D^*(\tau)} \pi_i f(c) dc \\ &= \gamma + (\pi_i - \gamma)F(D^*(\tau)) \end{aligned} \quad (7.25)$$

Integrating  $b(\tau)$  over the interval,  $(t, t + \Delta t)$ , to obtain the volume of basin drainage,  $B(t + \Delta t)$ , results in the same expression derived for the no-rain case, given by Equation (7.22). It is worth noting that, since  $\pi_i \leq \gamma$ , the minimum depth of depressions containing water,  $D^*(\tau)$ , will increase over the interval  $(t, t + \Delta t)$ , and  $\Delta t$  must be chosen such that Equation (7.21) is satisfied. Thus the time  $t + \Delta t$  may coincide with the time at which a content segment is fully depleted and not the end of the sampling interval.

The above discussion completes the development of the probability-distributed theory for the case of non-interacting depression storage elements, providing expressions for basin direct runoff, drainage, and actual evaporation, both in terms of instantaneous rates and volumes (expressed as depths over the basin) over any interval of time. Expressions for basin soil-water storage and soil-water deficit at any instant in time have also been derived.

## 7.11 Theory of Interacting Storage Elements

If the assumption that depression storages act independently of each other is relaxed, and water is allowed to redistribute itself between adjacent depressions, then the probability-distributed based approach becomes both simpler and more flexible. Indeed, relaxation of the cited assumption is more consistent with reality as part of the generated runoff at a point is likely to be lost along the way to the outlet. Two modes of redistribution are considered initially. The first mode allows water to redistribute in such a way as to cause all depression storages to have an equal depth of water,  $C^*(t)$ , with the exception of those with depths less than  $C^*(t)$  which are full. This mode is called "equal storage redistribution". A second possibility is to imagine that water redistributes itself such that a constant deficit,  $D^*(t)$ , is maintained across the population of stores, except for stores with depths less than  $D^*(t)$  which remain empty. This second mode is called "equal deficit redistribution".

The effect of allowing redistribution according to these two modes of behavior is to replace the water level profile of deficit and content segments shown in Figure (7.18) by either a single content segment or a single deficit segment depending on the mode assumed. The equal deficit redistribution mode was quickly rejected as a realistic candidate, since immediate redistribution according to this mode would result in an abrupt switch from no areas contributing direct runoff to the total basin contributing as the deficit  $D^*(t)$  is completely replenished by rainfall. Such a result is contradictory to physical reality. On the other hand, the equal content redistribution mode seems attractive, since the temporal evolution of  $C^*(t)$  will reflect the overall wetness state

of the basin, and it is  $C^*(t)$  which is used to determine the contributing area of direct runoff generation. The equal storage redistribution mode was therefore adopted for subsequent developments.

### 7.11.1 Calculation of Basin Water Storage

Consider the water level across the assemblage of depression storages of different depths to be as illustrated in Figure(7.19), so that all depressions contain water to a depth  $C^*(t)$ , except those that are smaller than  $C^*(t)$  which will be full. Then the total water in storage over the basin is:

$$S(t) = \int_0^{C^*(t)} cf(c)dc + C^*(t) \int_{C^*(t)}^{\infty} f(c)dc \quad (7.26)$$

Making use of the general result:

$$\int_0^x cf(c)dc = xF(x) - \int_0^x F(c)dc, \quad (7.27)$$

$$S(t) = \int_0^{C^*(t)} (1 - F(c))dc \quad (7.28)$$

Equation (7.28) takes on great importance, since it allows the basin water storage (i.e.  $S(t)$ ) to be calculated for a given critical content,  $C^*(t)$ , and vice versa. Given a cumulative distribution function for depression storage with respect to critical content,  $S(t)$  represents the area above that function between zero and  $C^*(t)$ . Figure (7.20) presents a clear graphical illustration of this statement.

Over a wet interval,  $(t, t + \Delta t)$ , the critical capacity,  $C^*(\tau)$ , will vary according

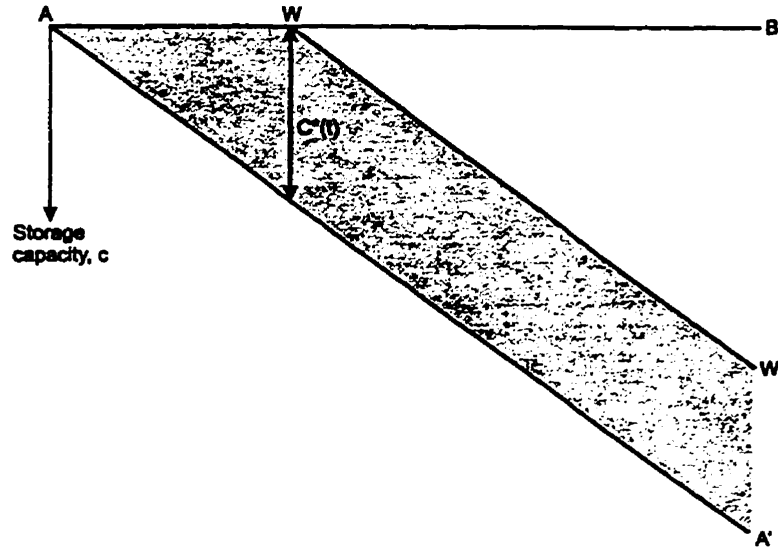


Figure 7.19: Water level across stores of different depth according to the equal storage mode of water distribution.

to Equation (7.14), the instantaneous direct runoff given by Equation (7.13), and the volume of basin runoff generated in the interval given by Equation (7.15). When the net rainfall  $\pi_i \leq 0$  in the interval  $(t, t + \Delta t)$ , then no direct runoff is generated. In that case, the basin water storage can be determined by continuity to be:

$$S(\tau) = S(t) + \pi_i(\tau - t) \quad (7.29)$$

and Equation (7.28) can be solved for  $C^*(\tau)$ , given  $S(\tau)$  when required at the beginning of a subsequent wet interval in order to calculate basin direct runoff.

### 7.11.2 Relation of Actual to Potential Evaporation

The allowance for redistribution of runoff between depression storages has a major weakness. As each depression contains either the same depth of water or not, the occurrence of evaporation at the potential rate is ensured throughout the basin until it

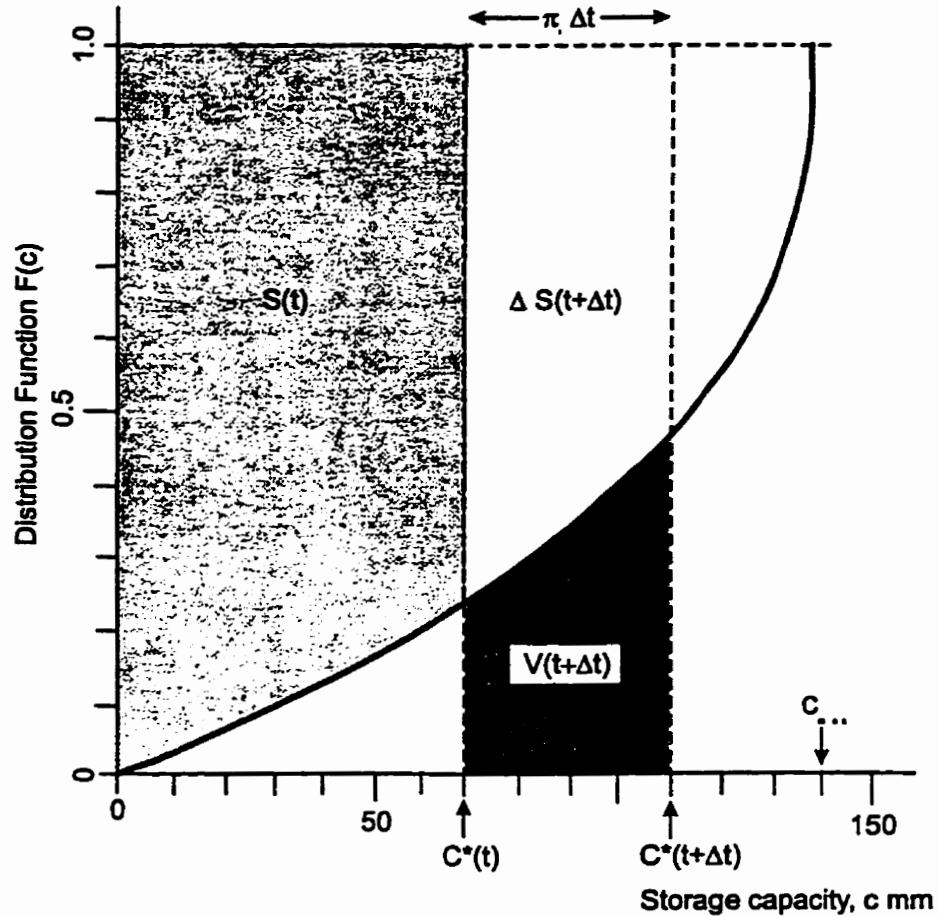


Figure 7.20: Graphical representation of storage capacity distribution and its relationship to  $S(t)$  and other variables.

dries up completely. This pitfall is readily overcome by allowing the actual evaporation rate to depend upon the basin soil moisture deficit,  $S_{\max} - S(t)$ . One possible relationship in this regard could be the linear one proposed by Moore and Clarke (1982):

$$\frac{E'_i}{E_i} = 1 - \frac{S_{\max} - S(t)}{S_{\max}} = \frac{S(t)}{S_{\max}} \quad (7.30)$$

where dependence on storage  $S(t)$  at the beginning of the  $i$ -th interval,  $(t, t + \Delta t)$  is assumed for simplicity so that actual evaporation,  $E'_i$ , is also constant over the

interval. The continuity equation for basin storage (i.e. Equation (7.29)) then requires modification, substituting  $\pi'_i = P_i - E'_i$  for  $\pi_i$  and changing the boundary condition to  $\pi'_i \leq 0$ .

### 7.11.3 Incorporation of Drainage into Model Structure

Generalization of the model to accommodate drainage to base-flow from depression storages,  $\gamma_i$ , can also be accomplished by substituting  $(P_i - E'_i - \gamma_i)$  for  $\pi_i$  in the continuity Equation (7.29) and in the expressions used to compute direct runoff generation in a wet interval (Equations (7.13), (7.14) and (7.15)). It is also possible to take into account temporal variability of drainage rate,  $\gamma$ , by correlating it with water storage level. To take account of the dependency of drainage on the amount of water storage,  $S(t)$ , a simple linear relation may be invoked:

$$\gamma_i = k_b S(t) \quad (7.31)$$

where  $k_b$  is the percolation rate (i.e., ground water recession rate) with units of inverse time. The continuity equation in this general case becomes:

$$S(\tau) = S(t) + (P_i - \frac{E_i S(t)}{S_{\max}} - k_b S(t))(\tau - t) \quad (7.32)$$

during a period,  $(t, t + \Delta t)$ , when no runoff generation occurs.

The general development of the probability of the probability distributed theory of interacting storage elements is now complete. Again, it should be emphasized that, for interacting storage elements, no distribution of water is necessary during periods

of direct runoff generation since all stores will contain the same depth of water, except of course those of smaller depth which will be full. Redistribution of water to equalize the depth of water in each depression storage only occurs during periods when stored water is being depleted. Equalization of storage levels during inter-storm periods does not seem too unreasonable, and the unique relationship between soil-water storage,  $S(t)$ , and critical capacity,  $C^*(t)$ , which results leads to considerable simplification.

#### 7.11.4 Transmission of Runoff

Up to this point, only the characteristics of basin storage have been considered. A second important function of the basin is to translate the direct runoff and drainage, generated at points within the basin, to the basin outlet. The translation function or time of travel function has been incorporated in some models by the area time<sup>-1</sup> vs. time method to take the catchment properties (e.g. shape, hydraulic length, surface roughness) into account. One could consider time of travel at each point to be a random variable with probability density function  $p(t, \phi)$ , where  $0 \leq t < \infty$ . Thus an area of size  $A p(t, \phi) dt$  would consist of points for which the translation time to the basin outfall would lie in the range  $(t, t + dt)$ .

By assigning randomness to time of travel, it means that it will take a variable amount of time,  $t$ , for a droplet of water to cover a fixed distance,  $x$ , based on the physical characteristics of the pathway. It is worth noting that the function  $p(t, \phi)$  conveys physiographic features of the study area, and will not in general be of the same form as  $p(c, \theta)$  used to describe depression storage distribution. These two functions may be dependent or independent of each other.

The translation function is essentially equivalent to the instantaneous unit hydrograph for the basin, representing the response to an instantaneous unit depth of rain falling when all depression storages have been filled. Assuming that the random variables  $c$  and  $t$  are independent and their bivariate distribution is  $dF = p(c, \theta)p(t, \phi)dc dt$ , then the rate of translated runoff at the catchment outfall at time  $t$  is given by:

$$Q(t) = \int_0^t q(\tau)p(t - \tau, \phi)d\tau \quad (7.33)$$

where  $q(\tau)$  is given by Equation (7.13).

In light of the random variables  $c$  and  $t$  being considered to be dependent, the translated runoff at the catchment outfall at time  $t$  is given by:

$$Q(t) = A \int_0^t \pi(\tau) \int_0^{C^*(\tau)} p(c, t - \tau)dc d\tau \quad (7.34)$$

## 7.12 Selection of Probability Density Function for Depression Storage

From the extensive work conducted by Ullah (1974), the three geometric properties of depression storage (i.e. depth, surface area, and volume) can be expected to have similar types of frequency distribution. This warranted an investigation into the applicability of theoretical probability distributions to describe the cited properties. The exponential and Weibull distributions were among those selected for that study. Since in that and the present study, the average depth of depressions was found to be the most consistent parameter with increasing grid spacing, the following explanation

is limited to depth of depression.

### 7.12.1 The Exponential Distribution

For a specific grid spacing, Ullah and Dickinson (1979b) asserted that when the depth of depression storage decreases, the number of depressions  $N$  increases. In the limit, when  $D \rightarrow 0$ , then  $N \rightarrow \infty$ . Also, it was observed that the number of depressions decreases with increasing depth of depression; that is, when  $D \rightarrow \infty$ , then  $N \rightarrow 0$ . One probability distribution model which suits a variable with the above description is the exponential distribution. The exponential density function  $f(x)$  is given by the relationship:

$$f(x) = \lambda \exp(-\lambda x), \quad \forall \quad x \geq 0 \quad \text{and} \quad \lambda > 0 \quad (7.35)$$

The unbiased estimator of the parameter  $\lambda$  is obtained as follows:

$$\hat{\lambda} = \frac{1}{\bar{x}}$$

The discussion provided by Ullah and Dickinson (1979b, p. 86) noted that histograms of observed depths of depression and the corresponding values estimated by means of an exponential distribution indicated varying degrees of discrepancies. It was therefore decided that a distribution with a greater degree of flexibility would be more appropriate to describe the geometric features of depressions including depth. The Weibull distribution, known for its extreme flexibility in fitting exponentially distributed and also skewed data, is considered below.

### 7.12.2 The Weibull Distribution

The Weibull distribution function, though lacking a sound theoretical basis, has successfully been applied not only to life expectancy problems for which it was originally intended but also to other fields such as breaking strength, and reliability studies. An early application of this distribution in the field of hydrology was undertaken by Haan and Johnson (1968) to describe geometric properties of potholes to synthesize a watershed model. The frequency density function is given by the relationship:

$$f(x) = \frac{\gamma}{\beta} \left(\frac{x - \alpha}{\beta}\right)^{\gamma-1} \exp\left[-\left(\frac{x - \alpha}{\beta}\right)^\gamma\right] \quad (7.36)$$

where  $\alpha$ ,  $\beta$ , and  $\gamma$  are the location, scale and shape parameters and  $x$  is a random variable. The quantity  $\alpha$  corresponds to the position of the mode, the quantity  $\beta$  is the scale parameter analogous to standard deviation, and the term  $\gamma$  represents the skewness.

The frequency distribution function for the Weibull distribution has the simpler form:

$$F(x) = 1 - \exp\left[-\left(\frac{x - \alpha}{\beta}\right)^\gamma\right] \quad (7.37)$$

### 7.13 Selection of Probability Density Function for Time of Travel

Based on the work of Pilgrim (1977), it was clear that time of travel falls into fractal geometry (i.e. power law). However, the choice of an appropriate travel time distri-

bution is not immediately obvious as extensive data are still required for verification. Moore and Clarke (1981) selected the exponential distribution for translation times for a simple one-parameter translation model for a preliminary analysis. One shortcoming of the cited model when applied to rainfall-runoff data from a number of small upland basins was its inability to represent recessions which decayed rapidly initially and then at a much slower rate. Gamma and Weibull distributions of travel times were also considered as more suitable candidates due to their positively skewed and unimodal shapes, but little improvement was obtained, the tails of these two distributions not being too different from the exponential. They were also unable to represent the “heavy-tailed” nature of observed recessions. In order to overcome some of the shortcomings of the above cited distributions, Moore and Clarke (1983) proposed to look at hydrodynamics and the associated convection-diffusion equation of transport processes for the development of a possible translation model.

### 7.13.1 The Convection-Diffusion Equation

Wide use of the convection-diffusion equation in transport theory suggests that it warrants serious consideration in the development of a suitable kernel function for flow over the landscape. The convection-diffusion equation of discharge can be expressed as the parabolic partial differential equation, neglecting the inertia terms in the linearized St. Venant equations, (Ponce, 1989) as follows:

$$\frac{\partial Q}{\partial t} + \frac{\partial Q}{\partial A} \frac{\partial Q}{\partial x} = \frac{Q_0}{2TS_0} \frac{\partial^2 Q}{\partial t^2} \quad (7.38)$$

The left side of Equation (7.38) is the kinematic wave equation, with  $\partial Q/\partial A = \beta$

as the kinematic wave celerity. The right side is a second-order (partial differential) term that accounts for the physical diffusion effect. The coefficient of the second-order term has the units of  $[L^2T^{-1}]$ , being referred to as the hydraulic diffusivity, or channel diffusivity. The Manning equation is the resistance formula used in the development of Equation (7.38).

The hydraulic diffusivity is a characteristic of the flow and channel, defined as:

$$\nu_h = \frac{Q_o}{2TS_o} = \frac{q_o}{2S_o}$$

in which  $q_o = Q_o/T$  is the reference flow per unit of channel width. Here  $Q_o$ ,  $S_o$ , and  $T$  are the reference flow rate, channel bottom slope and top width. When the Chezy formula is considered as the friction formula, then Equation (7.38) becomes:

$$\frac{\partial Q}{\partial t} + \nu \frac{\partial Q}{\partial x} = \frac{1}{2}\sigma^2 \frac{\partial^2 Q}{\partial t^2} \quad (7.39)$$

here the wave celerity parameter is  $\nu = 3Q_o/2A_o$ , and  $D = \sigma^2/2$  is the hydraulic diffusivity.

The solution of Equation (7.39) for a Dirac delta function at  $x = 0$  and  $t = 0$  gives the impulse response function, equivalent to a probability density function:

$$f(t, x; \nu, \sigma) = \frac{x}{\sigma(2\pi t^3)^{\frac{1}{2}}} \exp\left[-\frac{(x - \nu t)^2}{2\sigma^2 t}\right], \quad \forall \quad t > 0, \quad \text{and} \quad \nu > 0 \quad (7.40)$$

where  $x/\nu$  is the mean translation time, and  $\sigma^2$  is a diffusion constant. By invoking randomness on time of travel, direct runoff is assumed to be generated only from

those points in the basin at a distance  $x$  from the basin outlet, traveling at a constant velocity  $\nu$  along paths of different length. The time taken to reach the basin outlet depends upon the particular path taken; hence, it is a random variable.

Re-parameterization of the density function (i.e. Equation (7.40)), such that  $\mu = x/\nu$  and  $\lambda = x^2/\sigma^2$ , leads to the following density function:

$$f(t; \mu, \lambda) = \left(\frac{\lambda}{2\pi t^3}\right)^{1/2} \exp\left[-\frac{\lambda(t - \mu)^2}{2\mu^2 t}\right] \quad (7.41)$$

where the parameters  $\mu$  and  $\lambda$  are positive, and of dimension  $[T]$ . The above transformation has essentially led from a Lagrangian description of the transport phenomenon, in which both space and time coordinates are considered, to an Eulerian description in which  $x$  is a specified distance. The density function in this form is more appropriate for incorporation into a probability-distributed based rainfall-runoff model when the fixed distance  $x$  is considered to be a characteristic length of the basin. Tweedie (1957) termed the density (i.e. Equation (7.41)) an inverse Gaussian pdf; Folks and Chhikara (1978) provided a review of its development; and Johnston and Kotz (1970) summarized its properties. The mean and the variance of this distribution are  $\mu$ , and  $\mu^3/\lambda$  respectively, so the parameter  $\mu$  may be interpreted physically as the mean translation time. The distribution is positively skewed and unimodal, with the mode (or time-to-peak) given by:

$$t_m = \frac{2\lambda}{3 + [9 + 4(\frac{\lambda}{\mu})^2]^{1/2}} \quad (7.42)$$

An important special case is obtained for zero wave celerity ( $\nu = 0$ ) or no convec-

tion when  $\mu \rightarrow \infty$  and:

$$f(t; \lambda) = \left(\frac{\lambda}{2\pi t^3}\right)^{1/2} \exp\left(\frac{-\lambda}{2t}\right) \quad (7.43)$$

which is the impulse response function corresponding to the diffusion equation:

$$\frac{\partial Q}{\partial t} = \frac{1}{2} \sigma^2 \frac{\partial^2 Q}{\partial t^2} \quad (7.44)$$

This is a density function having a single parameter,  $\lambda$ , which is unimodal ( $t_m = \lambda/3$ ) and positively skewed.

Both density functions offer promise as suitable functions for representing the transport of water to the basin outlet. The cumulative distribution functions corresponding to functions are given by:

$$F(t; \mu, \lambda) = \Phi\left[\left(\frac{\lambda}{t}\right)^{1/2}\left(-1 + \frac{t}{\mu}\right)\right] + \exp\left(\frac{2\lambda}{\mu}\right) \Phi\left[-\left(\frac{\lambda}{t}\right)^{1/2}\left(1 + \frac{t}{\mu}\right)\right] \quad (7.45)$$

$$F(t; \lambda) = 2\Phi\left[-\left(\frac{\lambda}{t}\right)^{1/2}\right] \quad (7.46)$$

where  $\Phi(\cdot)$  is the normal distribution function:

$$\Phi(z) = (2\pi)^{-1/2} \int_{-\infty}^z \exp(-u^2/2) du$$

## 7.14 A Bivariate Exponential Storage-Translation Model

Up to now it has been assumed that the depression storage depth  $c$  and the translation time  $t$  are independent, so that the weighting  $dF = p(c, t)dc dt$  can be expressed as  $dF = p(c)p(t)dc dt$ . However, the random variables  $c$  and  $t$  in general will not be independent. It was found by Ullah (1974) that upon increasing the overall slope, the size of depression storage will decrease. Since points far from the channel network are likely to be located on higher slopes, their storage capacities can be expected to be lower than points near the channel network. Furthermore, points far from the channel network have higher times of travel than compared to points near the channel network. In conclusion, one may argue that these two random variables are negatively correlated. Although there are a number of different bivariate exponential distributions (Johnston and Kotz, 1972), only two are known to give the desired negative correlation. These two distributions give a correlation  $\rho$  in the range  $-0.40365 \leq \rho \leq 0$ , and  $-0.25 \leq \rho \leq 0.25$ . Gumbel's bivariate exponential distribution giving the largest negative correlation can be considered as one candidate for incorporation into a bivariate exponential storage-transport model. Its joint density function is:

$$p(c, t) = (\theta\phi)^{-1}[(1 + \delta c/\theta)(1 + \delta t/\phi) - \delta] \exp(-c/\theta - t/\phi - \delta ct/\theta\phi) \quad (7.47)$$

In light of the probability distribution function suggested for both storage and time of travel, Table (7.2) summarizes possible combinations for the univariate case.

Table 7.2: Possible combinations of pdf for storage and time of travel.

Code No.	Frequency distribution	
	Storage	Time of travel
Model 1	Exponential distribution	Exponential distribution
Model 2	Exponential distribution	Inverse Gaussian
Model 3	Weibull distribution	Exponential distribution
Model 4	Weibull distribution	Inverse Gaussian

## 7.15 Probability Distributed Model of Infiltration-excess Overland Flow

So far, the modeling approach was revolving around a central theme, i.e. the soil can accommodate no more water, at which overland flow can occur even at low rainfall intensity. The emphasis was on the rate of outflow rather than rate of inflow (or, strictly, maximum rate of inflow). Other research on the application of the probability-based approach to derive models of direct runoff generation has not been based on the variability of surface storage over the surface but rather on the spatial variation in the rate at which water can enter the soil. This runoff mechanism invariably called infiltration-excess overland flow or Hortonian mechanism is generally more common on those upslope areas where surface hydraulic conductivities are relatively low and during periods when rainfall intensities are high. For the sake of completeness, a very brief account of this approach is provided in this section.

Generally speaking, for a given watershed and at a given rainfall intensity ( $P$ ) only those small areas with  $i \leq P$  generate runoff. Other areas of the soil surface absorb rainfall only at the rate  $P$ , which is less than their respective values of  $i$ . As the rainfall intensity increases it exceeds the  $i$  values of an increasing proportion of the surface which is brought to saturation and started to generate runoff. The spatially

averaged infiltration rate increases with rainfall intensity until all part of the plot are saturated.

Again, as mentioned before, accumulation of runoff at the mouth of the catchment could be achieved in two steps. At first, runoff has to be generated at a point and then via a proper translation mechanism and convolution integral, is transferred to the outlet. Considering  $f(i)$  as the probability density function for infiltration capacity, the runoff rate per unit area for a plot or small watershed generated at a point then becomes:

$$q = \int_0^P (P - i)f(i)di \quad (7.48)$$

where  $P$  is the rainfall intensity, and  $f(i)$  is the pdf of  $i$  which weighs the rainfall excess in the integral.

Perhaps one of the best known example of the probability-based infiltration capacity approach to rainfall-runoff modeling is contained in the Stanford Watershed Model which uses a rectangular density function to describe the spatial variation of infiltration capacity over the basin, allowing the maximum infiltration capacity parameter to vary as a function of soil-water storage (Crawford and Linsley, 1966).

As a simple illustration of the type of runoff calculation made in the Stanford Watershed Model, consider a rectangular pdf for  $f(i)$ , then the cumulative distribution function of infiltration capacity becomes:

$$F(i) = \frac{i}{i_{max}} \quad 0 \leq i \leq i_{max} \quad (7.49)$$

Graphical representation of Equation 7.49 was presented in Figure (7.21). Rain falling at a rate  $P$  in a unit interval generates runoff at all points in the basin with infiltration capacity less than  $P$ . The direct runoff rate per unit area in the basin indicated by the hatched area in Figure (7.21), becomes:

$$q = \int_0^P (P - i)f(i)di \quad \forall \quad 0 \leq P \leq i_{max} \quad (7.50)$$

$$q = P - i_{max} + \int_0^{i_{max}} i f(i)di \quad \forall \quad P \geq i_{max} \quad (7.51)$$

Again, the runoff rate represented by either Equation (7.50) or (7.51) is the generated runoff at a point which has to be transferred to the outlet through proper translation mechanism.

Different probability density function of infiltration capacity have been developed and used by other workers. While rectangular probability density function was used in Stanford Watershed Model for infiltration capacity, Freeze (1980) used lognormal probability density function for infiltration capacity at a hillslope scale to model rainfall-runoff process.

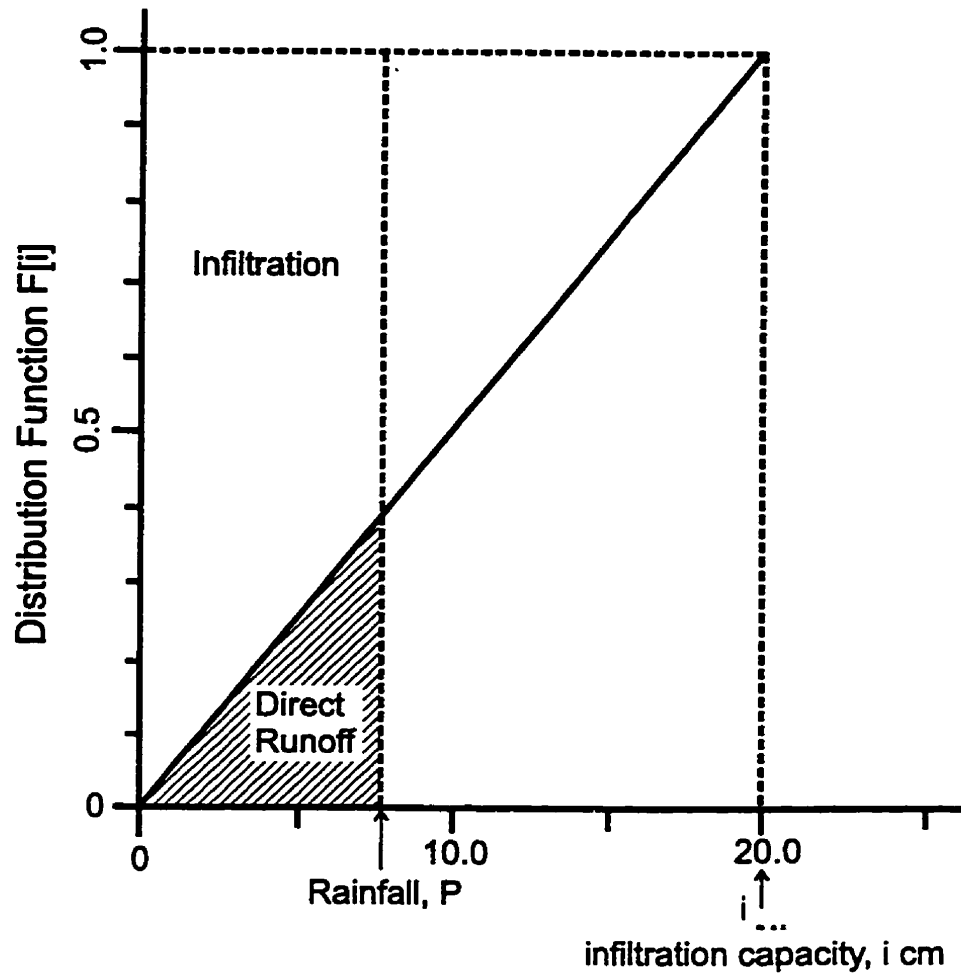


Figure 7.21: Basin direct runoff production for probability-based infiltration capacity model.

## 7.16 Development of Probability-distributed Approach for Particular Distribution

Further development of the general theory for a particular distribution of depression storage and time of travel will serve to clarify the approach outlined in previous sections. Development of the probability-distributed approach for some of the combinations noted above are provided in what follows.

### Model 1

For the so-called Model 1 combination, the probability density functions for both depression storage and time of travel are exponential and independent of each other, so that  $dF = p(c, \theta)p(t, \phi)dc dt$ , and:

$$dF = \theta^{-1} \exp\left(-\frac{c}{\theta}\right) \phi^{-1} \exp\left(-\frac{t}{\phi}\right)$$

where  $\theta$  is the mean storage depth, and  $\phi$  is the mean translation time. Substituting the distribution functions in Equation (7.33) results in:

$$Q(t) = A \int_0^t \pi(\tau) \phi^{-1} \exp\left(-\frac{t-\tau}{\phi}\right) \left[1 - \exp\left(-\frac{C^*(\tau)}{\theta}\right)\right] d\tau \quad (7.52)$$

During periods of rain, when  $\pi(\tau) \geq 0$ , an exact solution to the integral in (7.52) may be obtained as follows:

$$Q(t + \Delta t) = \exp\left(\frac{-\Delta t}{\phi}\right) Q(t) + A \pi_i \left[1 - \exp\left(\frac{-\Delta t}{\phi}\right) - \phi^{-1} \exp\left(\frac{-C^*(t + \Delta t)}{\theta}\right) Y\right] \quad (7.53)$$

where  $Y = (1 - \exp(-\omega\Delta t))/\omega$  and  $\omega = (\theta - \pi_i\phi)/\phi\theta$ .

The usefulness of the above closed form solution is assessed later for testing a number of hypotheses.

A special case of the above formulation is the case when the surface lacks any depressions (i.e. flat surface). In that case, the exponential population of depressions tends to a spike at the origin  $c = 0$ . Consequently, this store represents the translation phase of runoff generation only. The surface behaves as a simple linear reservoir, such that:

$$\begin{aligned} Q(t + \Delta t) &= A \int_0^{t+\Delta t} \pi(\tau)\phi^{-1} \exp\left(\frac{-(t + \Delta t - \tau)}{\phi}\right) d\tau \\ &= \exp\left(\frac{-\Delta t}{\phi}\right)Q(t) + A\pi_i(1 - \exp\left(\frac{-\Delta t}{\phi}\right)) \end{aligned} \quad (7.54)$$

Again, the usefulness of this single parameter model is utilized later for testing some hypotheses relating to a flat surface.

## Model 2

For this combination, the probability density function for depression storage is exponential while that for time of travel is inverse Gaussian, and the two functions are independent of each other, so that  $dF = p(c, \theta)p(t; \mu, \lambda)dc dt$ . It was shown earlier that the translation of runoff to the basin outlet led to the following convolution integral expression:

$$Q(t) = \int_0^t q(\tau)p(t - \tau)d\tau$$

where  $q(\tau)$  is given by:

$$q(\tau) = \pi(\tau)A[1 - \exp(\frac{-C^*(\tau)}{\theta})]$$

Here  $\theta$  is the mean storage depth. Upon replacing  $p(t - \tau)$  with its equivalent Inverse Gaussian distribution (i.e. Equation (7.41)) in the above equation:

$$Q(t) = A \int_0^t \pi(\tau)[1 - \exp(\frac{-C^*(\tau)}{\theta})](\frac{\lambda}{2\pi(t - \tau)^3})^{\frac{1}{2}} \exp[\frac{-\lambda(t - \tau - \mu)^2}{2\mu^2(t - \tau)}]d\tau \quad (7.55)$$

Evaluation of the above convolution to give volumetric flow rate  $Q(t)$  is not straightforward, as there is no closed form solution available, except for the case of the exponential density function. Therefore, the integral is evaluated as the sum of all the  $M_t$  past  $\Delta t$  increments during which net rainfall is  $\pi(\tau) > 0$ . Thus:

$$Q(t) = \sum_{i=0}^{M_t} I_{t,t_i^*} \quad (7.56)$$

where

$$I_{t,t_i^*} = \int_{t_i^* - \Delta t}^{t_i^*} q(\tau)p(t - \tau)d\tau \quad (7.57)$$

and  $t_i^*$  is the time at the end of the  $i$ th wet interval of duration  $\Delta t$  when  $\pi(\tau) > 0$ . A simple and computationally efficient approximation to the integral in Equation (7.57) is the mid-point approximation:

$$I_{t,t_i^*} = q(t_{i,m})p(t - t_{i,m})\Delta t \quad (7.58)$$

where  $t_{i,m} = t_i^* - \frac{1}{2}\Delta t$

### Model Structure Formulation in Light of Drainage Component

In preceding sections, the model structure without a drainage component was formulated in some detail for a few specific distributions. In this section, the model structure with a particular distribution is formulated in light of allowing drainage from each depression storage. At this stage, it might be helpful to compare and contrast non-interacting versus interacting storage elements in the context of having or not having a drainage component. Indeed, interacting storage elements have a distinct advantage for the accommodation of drainage. Usage of the non-interacting storage assumption is greatly hampered because of the difficulty associated with linking storage to drainage. For non-interacting storage elements, storage is related to soil-water deficit via Equation (7.19), for which quantification is not a simple task. However, for an interacting storage approach, storage can be related to the cumulative distribution function via Equation (7.28), for which quantification requires only the choosing of a form for  $F(c)$ .

In light of the above discussion, accommodation of a drainage component into the model formulation was undertaken with the interacting storage assumption in mind. With the provision of exponential distributions for both depression storage and time of travel, and on the basis of Equation (7.28), the storage at time  $t$  becomes:

$$S(t) = \theta(1 - \exp(\frac{-C^*(t)}{\theta})) \quad (7.59)$$

After the introduction of Equation (7.59), critical depth can be expressed in terms of

storage as:

$$C^*(t) = \theta \ln\left(\frac{\theta}{\theta - S(t)}\right) \quad (7.60)$$

Once critical depth has been determined, the calculation of runoff becomes similar to the non-interacting case considered above. In short, the procedure for runoff calculation in light of having drainage can be summarized as follows:

1. Assuming an initial value for  $S(t = 0)$ , the following equation can be used to update storage at time  $(t + \Delta t)$ ;

$$S(\tau) = S(t) + \left(P_i - \frac{E_i S(t)}{S_{\max}} - k_b S(t)\right)(\tau - t)$$

2. Then Equation (7.60) can be used to update critical depth;
3. Having updated critical depth, then Equation (7.53) can be used to update flow rate at  $(t + \Delta t)$ .

For other pdf combinations, similar formulations could also be established.

## 7.17 Model Application

With the provision of a few model structures for different combinations of frequency distributions, the effectiveness of such modeling structures can now be evaluated with regard to the sets of data collected at different spatial scales.

## 7.18 Model Structure Identification and Verification

Model structure identification includes the selection of an efficient algorithm along with a set of input/output data (i.e. rainfall and its corresponding runoff). For the purpose of this research, the so called Shuffled Complex Evolution (SCE) algorithm (Duan et al., 1992; Duan and Sorooshian, 1993; Duan et al., 1994) was used for parameter estimation purposes. Some of the features which the SCE algorithm was designed to address can be summarized as follows (Duan and Sorooshian, 1993).

- There may be several major regions of attraction into which a search strategy may be trapped delineating local as opposed to global optimum.
- Each major region of attraction may contain numerous (possibly uncountable) local minima (stationary points where the first derivatives are zero and the Hessian matrices are positive definite or positive semidefinite). These local optima may occur both close to and at various distances from the best solution.
- The objective function surface in the multi-parameter space may not be smooth and may not even be continuous. The derivatives may be discontinuous and may vary in an unpredictable manner through the parameter space.
- The parameters may exhibit varying degrees of sensitivity and a great deal of interaction and compensation. Much of the interaction can be highly nonlinear.
- The response surface near the true solution is often non-convex.

The Shuffled Complex Evolution (SCE) method is based on a synthesis of four concepts that have proven successful for global optimization:

1. Combination of random and deterministic approaches.
2. The concept of clustering.
3. The concept of a systematic evolution of a complex of points spanning the space in the direction of global optimization.
4. The concept of competitive evolution.

In brief, the first concept is very important. The use of deterministic strategies allows the SCE algorithm to make effective use of response surface information to guide the search, while the inclusion of random elements helps to make the algorithm flexible and robust. The search begins with a randomly selected complex of points spanning the entire feasible space  $\Omega$ . A large enough number of points helps to ensure that the complex contains information regarding the number, location and size of the major regions of attraction. The implementation of an implicit clustering strategy helps to concentrate the search in the most promising regions identified by the initial complex. The use of a systematic complex evolution strategy helps to ensure that the search is relatively robust and is guided by the structure of the objective function. The robustness is a result of the fact that the complex structure is able to cope very well with rough, insensitive and highly non-convex objective function surfaces, and is relatively unaffected by small local minima encountered enroute to the global solution. Furthermore, no derivative information is required.

The algorithm was structured in a modular way so that one could attach his or her own rainfall-runoff model to it for model identification purposes; and the algorithm benefits from two objective functions: Simple Least Squares (SLS) and the Heteros-

cedastic Maximum Likelihood Estimator (HMLE) (Sorooshian and Dracup, 1980; Sorooshian, 1981).

The above global optimization method has been applied in this study for the cases of one, two and three parameter models proposed earlier.

The application of the models is discussed with regard to their suitability to represent in particular surface storage effects in the small-scale laboratory experiments, small-scale field experiments, and large-scale field experiments described earlier.

## 7.19 Model Sensitivity Analysis

The analysis of model sensitivity is a very powerful and important component of a model development and application process. It can assist in keeping the model relatively simple when it reveals model parameters appearing to have insignificant effects. It can also be a tool to identify interactions among model components and parameters. When conducted prior to a model being applied in a predictive mode, a sensitivity analysis can help to identify the possible stability of results in relation to uncertainties associated with assumptions.

The simple form of sensitivity analysis adopted in this study involved the visual comparison of graphs of model outputs produced on the basis of various assumptions, including initial conditions, different model structures and systematic adjustments to input data. This particular approach was found to be quite straightforward, surprisingly powerful and easily understood.

## **7.20 Model Application for Small-Scale Lab Experiment**

Model application for the small-scale laboratory experiments consisted of running some of the developed models on data sets collected at a range of conditions including various rainfall patterns applied on different surface treatments set at different slopes. The surface treatments involved surfaces with no depressions, and a random mix of unnested depressions with and without leakage. This variety of conditions provided much valuable information for consideration of a range of questions such as: Can, and how can, information contained in such data be utilized to enhance model performance? Could such models be used to link surface characteristics to outflow response? Can a hierarchy of complexity in surface treatments be incorporated into model structure in a modular manner? Can some of the key observations in previous chapters be confirmed via modeling exercises? Such questions are addressed in this section in light of modeling applications to rainfall-runoff data collected and analyzed in previous chapters. For each surface treatment, after running the relevant model on associated data, results have been summarized either in tabular or graphical format, and then key observations have been highlighted and discussed.

### **7.20.1 Smooth Surface Treatment**

For the case of the smooth surface treatment (i.e. no depressions), five slopes along with three rainfall patterns were available. Some of the specific issues that were addressed by this modeling exercise can be summarized as follows:

- Sensitivity of model structure to various data sets;

- Effect of slope on optimum model parameters;
- Effect of data smoothing on goodness of fit criteria;
- Effect of model structure on goodness of fit criteria;
- Delineation of instrument imperfection; and
- Effect of goodness of fit criteria on model results.

### One Parameter Model

The one parameter model is a special case of the so-called “Model 1” (see Section 7.16) involving no depressions. The apparent physical meaning of the parameter incorporated into this model structure is the mean travel time of runoff over the surface. Results from running the model for various slope treatments and rainfall patterns are summarized in Table (7.3). Inspection of Table (7.3) has led to the following key observations:

- Mean time of travel ( $\phi$ ) fluctuates minimally for a particular slope among various rainfall patterns, but decreases with increasing slope.
- Among the various rainfall patterns on a particular slope, the sum of squares (SS) has the highest value and the coefficient of determination ( $R^2$ ) the lowest value for the HML rainfall pattern. Eliminating this pattern, the coefficients of determination were always greater than 92%.
- For a selected rainfall pattern, the optimized parameter has virtually the same value for both the SLS and HMLE objective functions.

Table 7.3: Model output for combination of slope and rainfall treatments—One parameter model, flat surface (without data smoothing).

Slope %	Rainfall Pattern	SLS <sup>a</sup>			HMLE <sup>b</sup>		
		$\phi$	SS <sup>c</sup>	$R^{2d}$	$\phi$	NWSS <sup>e</sup>	$R^{2d}$
6%	HML	42.4	344	0.82	35.2	3.46	0.80
	LMH	36.3	178	0.96	34.0	1.66	0.96
	MLH	36.1	225	0.93	31.5	1.91	0.91
8%	HML	35.9	265	0.86	29.2	2.71	0.84
	LMH	33.7	164	0.96	31.2	1.56	0.96
	MLH	35.5	237	0.93	29.3	2.09	0.90
10%	HML	36.4	277	0.84	29.9	3.06	0.82
	LMH	33.1	169	0.96	29.9	1.65	0.96
	MLH	32.6	227	0.93	29.0	2.13	0.91
12%	HML	31.2	252	0.86	24.8	2.64	0.83
	LMH	30.9	166	0.96	28.8	1.73	0.96
	MLH	33.6	226	0.92	28.6	1.94	0.91
14%	HML	31.3	232	0.88	25.8	2.36	0.86
	LMH	34.1	162	0.96	31.3	1.87	0.96
	MLH	31.6	244	0.92	26.5	2.31	0.90

<sup>a</sup> Simple Least Square

<sup>b</sup> Heteroscedastic Maximum Likelihood Estimator

<sup>c</sup> Sum of Squares

<sup>d</sup> Coefficient of determination

<sup>e</sup> Normalized Weighted Sum of Squares

An extensive analysis of variance was conducted on the  $\phi$  parameter values obtained with both objective functions. It was found that while its variation was significantly different at the 5% level among the various slopes, it was not significantly different among rainfall patterns within a particular slope.

It has been argued in the literature that system identification is often highly data set dependent, creating a non-uniqueness problem. An inability to clearly identify the initial state of the system has been cited as a major cause of this non-uniqueness. The very careful control of initial conditions for the relatively simple smooth surface laboratory experiments for various rainfall patterns allowed the determination of essentially unique values of  $\phi$ . The lack of variability of  $\phi$  along with the high  $R^2$  values

also imply to some extent the soundness of the model structure.

The decreasing trend in  $\phi$  with increasing slope can be attributed to the fact that time of travel is velocity dependent (Laurenson, 1964; Pilgrim, 1977). As slope increases, gravity potential becomes dominant, giving rise to an increase in velocity. The increase in velocity in turn causes a decrease in time of travel.

During the course of conducting the laboratory experiments, it was found that the HML rainfall pattern was the least replicable of the various rainfall patterns (as mentioned in Section (4.2.4)). This lack of replicability may be reflected in the relatively high values of sums of squares (and low values of coefficients of determination) for the HML results. It may also be the case that this particular model structure could not capture the dynamics of flow when high rainfall intensity started first.

One might argue that the lack of sensitivity of the optimized parameter ( $\phi$ ) to the different objective functions implies that the model structure selected was able to capture the information content of the data. However, the overall soundness of the model structure or reliability of the data set cannot be assessed until a unified, universally accepted goodness of fit criterion has been adopted. Here, the criterion was to minimize the sum of squares for point-wise runoff data. If the objective were to match time to peak or volume of runoff, then the above interpretation might take a different route.

As the graphical presentation of observed versus simulated runoff results can often be instructive of a modeling exercise, such example graphs are given in Figure (7.22) for the various rainfall patterns on a slope of 10%. Examination of Figure (7.22) has led to the following key observations:

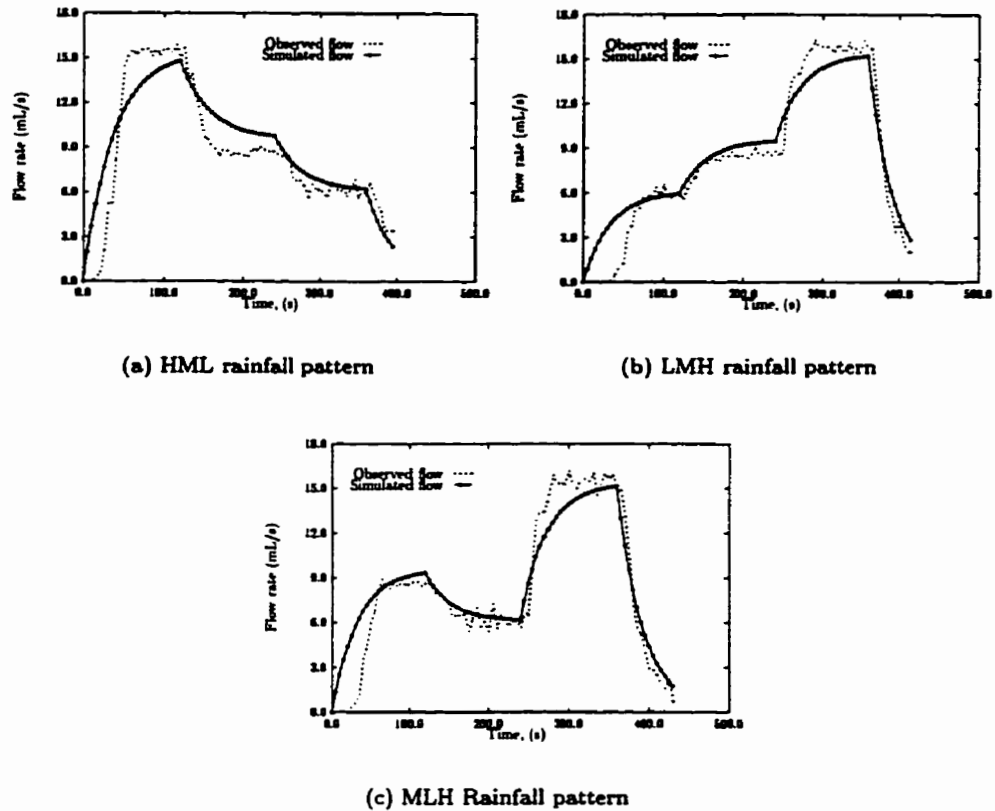


Figure 7.22: Graphical representation of observed vs. simulated runoff for various rainfall patterns before data smoothing, flat surface at  $S = 10\%$ .

- The rainfall intensity for the high intensity nozzle appears to have been a little bit underestimated.
- The model structure has not captured data information content at the very beginning of the simulation runs.
- Some sort of smoothing of the highly fluctuating runoff data would seem to be advantageous.

The experimental runoff time series data was passed through a third order moving average filter, and the model results for these data are summarized in Table (7.4).

These results reveal that no remarkable improvement in  $R^2$  was achieved after such smoothing of the runoff data; however, the cited smoothing caused the optimized parameter value to become more stable for the various rainfall and slope treatments.

Table 7.4: Model output for combination of slope and rainfall treatments—One parameter model, flat surface (With data smoothing).

Slope %	Rainfall Pattern	SLS <sup>a</sup>			HMLE <sup>b</sup>		
		$\phi$	SS <sup>c</sup>	$R^{2d}$	$\phi$	NWSS <sup>e</sup>	$R^{2d}$
6%	HML	48.5	367	0.80	40.4	3.80	0.78
	LMH	42.6	190	0.96	40.8	1.88	0.96
	MLH	42.5	237	0.93	38.5	2.21	0.92
8%	HML	41.5	292	0.84	35.0	3.05	0.83
	LMH	40.3	179	0.96	38.2	1.84	0.96
	MLH	43.1	250	0.93	36.5	2.46	0.91
10%	HML	42.1	306	0.82	34.2	3.34	0.80
	LMH	40.5	179	0.96	37.8	1.91	0.96
	MLH	39.1	237	0.94	35.4	2.35	0.92
12%	HML	36.5	288	0.84	29.9	3.15	0.81
	LMH	37.5	180	0.96	35.9	1.99	0.96
	MLH	40.1	229	0.94	35.1	2.06	0.92
14%	HML	36.7	266	0.86	31.2	2.78	0.84
	LMH	42.6	167	0.96	40.4	2.03	0.96
	MLH	39.0	250	0.93	34.0	2.57	0.92

<sup>a</sup> Simple Least Square

<sup>b</sup> Heteroscedastic Maximum Likelihood Estimator

<sup>c</sup> Sum of Squares

<sup>d</sup> Coefficient of determination

<sup>e</sup> Normalized Weighted Sum of Squares

The graphical display of results also reveals that there is a discrepancy between observed and the simulated runoff at the early stage of simulation. Some possible causes of this discrepancy are as follows:

- The laboratory flume detained water on the surface due to surface tension;
- Flow velocities of initial shallow depths were likely slow.

Since the model used for this surface treatment did not explicitly take these processes into account, a modification was introduced to the fitting procedure to enhance

model performance. Forcing the simulated runoff to be zero during the early stage of simulation (until runoff was observed) led to a remarkable improvement in goodness of fit. Table (7.5) summarizes model simulation results with this modification. The comparable graphical presentation of observed vs. simulated runoff is given in Figure (7.23).

Table 7.5: Model output for combination of slope and rainfall treatments—One parameter Model, flat surface (After zero correction).

Slope %	Rainfall Pattern	SLS <sup>a</sup>			HMLE <sup>b</sup>		
		$\phi$	SS <sup>c</sup>	R <sup>2d</sup>	$\phi$	NWSS <sup>e</sup>	R <sup>2d</sup>
6%	HML	20.94	119	0.93	21.34	1.53	0.93
	LMH	31.1	75.0	0.97	30.92	0.82	0.97
	MLH	34.5	182.0	0.94	30.93	1.63	0.92
8%	HML	31.58	212.0	0.88	26.38	2.24	0.87
	LMH	29.86	77.0	0.97	29.63	0.93	0.97
	MLH	32.0	153.0	0.94	28.3	1.45	0.93
10%	HML	23.6	128.0	0.91	21.45	1.59	0.91
	LMH	27.03	69.3	0.97	27.19	0.82	0.97
	MLH	25.55	69.1	0.97	26.27	0.80	0.97
12%	HML	27.1	196	0.88	22.34	2.14	0.87
	LMH	27.1	85.3	0.97	27.25	1.04	0.97
	MLH	28.9	107.0	0.96	27.38	1.11	0.95
14%	HML	27.3	179.0	0.90	23.34	1.92	0.89
	LMH	28.3	88.3	0.96	29.05	1.16	0.96
	MLH	23.9	63.5	0.97	24.34	0.80	0.97

<sup>a</sup> Simple Least Square

<sup>b</sup> Heteroscedastic Maximum Likelihood Estimator

<sup>c</sup> Sum of Squares

<sup>d</sup> Coefficient of determination

<sup>e</sup> Normalized Weighted Sum of Squares

The results reveal that the simple one parameter model was quite flexible with regard to imitating the behavior of the smooth surface system. This success may be attributable to the recursive nature of the model formulation. The first term in Equation (7.54) conveys the background conditions (i.e. persistent behavior of the system), while the second term acts as a correction factor incorporating the impact

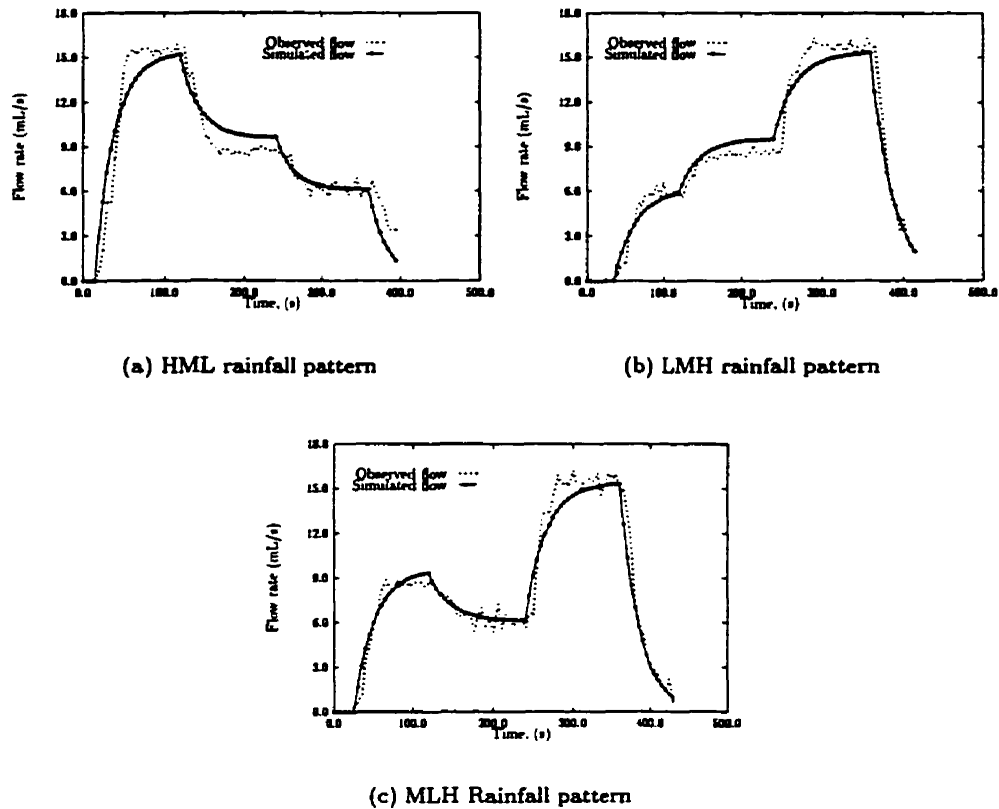


Figure 7.23: Graphical representation of observed vs. simulated runoff for various rainfall patterns after zero correction, flat surface at  $S = 10\%$ .

of the temporal pattern of rainfall and drainage area.

### Two Parameter Model

The two parameter model basically involves an exponential density function for both time of travel and depression storage. The first parameter has something to do with mean time of travel ( $\phi$ ), and the second parameter relates somehow to the mean storage depth over the surface ( $\theta$ ). For application of the two-parameter model to the smooth surface laboratory conditions, it was speculated that the mean storage depth would be near zero and that the mean time of travel ( $\phi$ ) would remain about the same as for the one-parameter model runs. Preliminary sensitivity analysis with

the two-parameter model revealed that a small change in mean depth of storage ( $\theta$ ) gave rise to a dramatic fluctuation in the magnitude of mean time of travel ( $\phi$ ), implying a sensitivity of the response surface to covariation of the model parameters. One direct implication of model parameter covariation and their interaction with one another is the possibility of mislocating the global optimum parameters associated with minimum sum of squares. As a result, two scenarios were used in running the two-parameter model on data sets for surface treatment I: in one set, the two parameters were optimized; for the other set of runs, the mean time of travel was optimized for various fixed values of mean depth of storage. After confirming that the optimization algorithm located global values by providing essentially the same values for both scenarios, the results of calibration runs for the two-parameter model for various rainfall and slope treatments were summarized in Table (7.6). Results of simulation runs with the one-parameter model are also included in that table for the sake of comparison. These results prompted the following key observations:

- When both  $\phi$  and  $\theta$  were optimized via the two-parameter model,  $\theta$  was found to be very small.
- The mean time of travel compared well for both the one and two-parameter models.
- The goodness of fit was excellent for virtually all runs, being slightly and consistently better for the two-parameter model, and being consistently poorer for the HML rainfall pattern.

Table 7.6: Model output for combination of slope and rainfall treatments— One and two-parameter models, flat surface (after correction for zero-runoff period).

Slope %	Rainfall Pattern	One-parameter model				Two-parameter model			
		$\phi$	$\theta$	SS <sup>a</sup>	R <sup>2b</sup>	$\phi$	$\theta$	SS	R <sup>2</sup>
6%	HML	20.94	-	119	0.93	19.64	0.003	117	0.93
	LMH	31.1	-	75.0	0.97	30.74	0.002	74.2	0.97
	MLH	34.5	-	182	0.94	28.29	0.020	88.1	0.96
8%	HML	31.58	-	212.0	0.88	22.28	0.016	147	0.92
	LMH	29.86	-	77.0	0.97	28.5	0.005	67.3	0.97
	MLH	32.0	-	153.0	0.94	26.20	0.018	74.7	0.97
10%	HML	23.6	-	128.0	0.91	18.79	0.004	105	0.93
	LMH	27.03	-	69.3	0.97	25.58	0.004	75.1	0.97
	MLH	25.55	-	69.1	0.97	24.80	0.003	66.1	0.97
12%	HML	27.1	-	196	0.88	19.10	0.015	135	0.92
	LMH	27.1	-	85.3	0.97	26.10	0.004	80.1	0.97
	MLH	28.9	-	107.0	0.96	25.37	0.012	65.1	0.97
14%	HML	27.3	-	179.0	0.90	19.98	0.013	129	0.93
	LMH	28.3	-	88.3	0.96	27.26	0.003	84.2	0.95
	MLH	23.9	-	63.5	0.97	22.64	0.005	56.1	0.97

<sup>a</sup> Sum of Squares

<sup>b</sup> Coefficient of Determination

Small  $\theta$  values obtained from simulation runs with the two-parameter model imply that surface storage (or permanent surface detention) was small, i.e. consistent with the physical situation. The best fits, the lowest  $\theta$  values and virtually identical values of mean time of travel for both one and two-parameter models are encouraging, suggesting the best  $\phi$  values are somewhat unique and the model structure is sound regarding imitating the behavior of the system.

The HML rainfall pattern again created responses that were difficult to fit well. This is likely due to the relatively poor spatial uniformity of the high rainfall intensity and the model structure itself which may not have been able to keep pace with the rapid rate of runoff generation during the early stage of the experimental runs when high intensity rainfall started first.

The table clearly shows that the mean storage depth was near zero. The model structure selected in fact allowed detection of the smooth surface condition when fitted to the runoff response. Rinaldo et al. (1995) also addressed the question : “Can we gauge the shape of the basin from the runoff response?” in the same context with partial success.

### **7.20.2 Other Surface Treatments**

The optimum parameter values obtained from the set of input/output data for the smooth surface provided an excellent background for discussing application of the models to response data for the surface treatments characterized by depressions with and without drainage. Modeling applications are pursued in this section with inclusion of “zero correction” results unless otherwise stated. A main objective here was to test whether the model structure could capture the additional storage elements and infiltration in the other surface treatments.

#### **Surface Treatment II**

For this surface treatment, relatively large depressions were located near the outlet; and the effect of these on the response hydrograph was expected to be reflected in  $\theta$ , the mean depth of storage parameter. Table (7.7) summarizes the results of model applications for surface treatment II, leading to the following key observations:

- The fits remain excellent, but are still not quite so good for the HML rainfall pattern.

- $\phi$  values remained essentially the same as those obtained for the smooth surface condition. The mean  $\phi$  value for the smooth surface conditions was 24.35 s including the HML rainfall pattern and 26.55 s without HML, while the mean  $\phi$  value for surface treatment II was 22.96 s including HML rainfall pattern and 27.46 s without HML, the values comparing quite well to one another.
- $\theta$  values are almost an order of magnitude greater than those for surface treatment I. The mean  $\theta$  value for the smooth surface condition was 0.011 cm; while for surface treatment II, it was 0.067 cm.
- Neither  $\phi$  nor  $\theta$  values are correlated with slope. Results of analysis of variance showed that no statistically significant correlation exists between either  $\phi$  or  $\theta$  and slope at a 5% probability level.
- The “Zero correction” runs provided slightly better fits than the “no correction” runs: the optimum  $\phi$  values were not significantly different, but the optimum  $\theta$  values were significantly less for the “zero correction” runs, implying (quite correctly) that less storage was required when a significant part of the initial storage available was accommodated by means of “zero correction”.

In response to the question: Can some of the key observations in previous chapters be confirmed via the modeling exercises?, one could argue that assuming the calibrating parameters represent system response for each event, some of the key observations in Chapter 6 were captured in the modeling exercises. The finding that calibrated parameter values were statistically insignificant with regard to slope treatment confirmed the non-significant effect of slope on runoff response. In Chapter 6, the effect

Table 7.7: Model output for combination of slope and rainfall treatments—Two parameter model, surface treatment II.

Slope %	Rainfall Pattern	No zero correction				Zero correction			
		$\phi$	$\theta$	SS <sup>a</sup>	R <sup>2b</sup>	$\phi$	$\theta$	SS	R <sup>2</sup>
6%	HML	23.64	0.083	259.03	0.88	15.42	0.053	150	0.94
	LMH	28.29	0.088	198.65	0.92	27.86	0.065	176	0.94
	MLH	31.91	0.046	221.70	0.87	33.54	0.005	90.8	0.97
8%	HML	20.81	0.081	292.97	0.85	12.91	0.053	194.0	0.92
	LMH	26.37	0.081	130.1	0.95	26.15	0.071	125.0	0.95
	MLH	26.87	0.048	198.84	0.89	28.46	0.014	141.0	0.96
10%	HML	19.36	0.053	191.39	0.90	18.85	0.028	141.0	0.96
	LMH	28.38	0.061	119.65	0.95	28.31	0.043	99.9	0.95
	MLH	27.39	0.051	188.66	0.89	28.91	0.017	136.0	0.95
12%	HML	17.30	0.077	254.31	0.88	11.29	0.053	179.0	0.93
	LMH	23.85	0.084	180.35	0.94	23.32	0.064	161.0	0.95
	MLH	25.50	0.045	134.74	0.87	25.79	0.029	120.0	0.95
14%	HML	18.51	0.083	285.66	0.87	11.29	0.053	178	0.93
	LMH	24.60	0.077	151.58	0.96	24.31	0.059	134.0	0.96
	MLH	26.13	0.049	299.24	0.87	28.0	0.006	157.0	0.96
Mean	HML	19.92	0.075	-	-	13.95	0.048	-	-
	LMH	26.30	0.078	-	-	25.99	0.060	-	-
	MLH	27.56	0.048	-	-	28.94	0.014	-	-
Pooled mean		24.59	0.067	-	-	22.96	0.041	-	-

<sup>a</sup> Sum of Squares

<sup>b</sup> Coefficient of Determination

of surface treatment on total runoff amount and water loss was found to be significant at the 5% probability level. Assuming that the main difference between surface treatments I and II was reflected in incorporation of depression storage, the finding that mean depth of storage for surface treatments I and II differed by an order of magnitude confirmed the significant effect of surface treatment on runoff response from a modeling point of view.

The actual mean depth of storage governed by the geometric shape of depressions over the surfaces (from Chapter 6) ranged from 0.081 to 0.093 cm, depending on the overall slope of the surface. Variations in mean depth of storage obtained via the modeling exercise on surface treatment II closely matched these values. A possible

reason for the  $\theta$  values being consistently lower than the “geometric values” is that the full volume of depression storage was not utilized effectively in any of the experimental runs. As for the lower values of mean depth of storage for the zero correction scenario, the zero correction essentially eliminated the initial abstractions leading to lower  $\theta$  values. At this stage, it has to be acknowledged that mathematical optimality is not necessarily in total agreement with physical optimality. While zero correction has led to a better goodness of fit, the physical meaning of mean depth of storage is somewhat lost in this process, implying that some sort of compromise has to be made between mathematical and physical optimality.

Again, the best fits, the consistent variation of  $\theta$  values and virtually identical values of the mean time of travel for both surface treatments I and II are encouraging, suggesting the best  $\phi$  values are somewhat unique and the model structure is sound regarding imitating the behavior of the system in presence of depression storages.

### **Surface Treatment III**

For this surface treatment, relatively large depressions were located remotely from the outlet; and the effect of these on the response hydrograph was expected to be reflected in  $\theta$ , the mean depth of storage parameter. Table (7.8) summarizes the results of model applications for surface treatment III, leading to the following key observations:

- The fits remain excellent, and consistently better than for surface treatment II.
- $\phi$  values remained essentially the same as those obtained for surface treatment I and II.

- $\theta$  values are consistently in between their corresponding values for surface treatments I and II, the mean  $\theta$  values being 0.011, 0.017 and 0.067 cm for surface treatments I, II and III respectively.
- An analysis of variance revealed that neither  $\phi$  nor  $\theta$  values are significantly correlated with slope at a 5% probability level.
- As before, the “zero correction” runs provided slightly better fits than the “no correction” runs. The optimum  $\phi$  values were not significantly different, but the optimum  $\theta$  values were significantly less for the “zero correction” runs, implying (quite correctly) that less storage was required when a significant part of the initial storage available was accommodated by means of “zero correction”.

Differences in observed catchment response between surface treatments II and III due to differences in the spatial patterns of depressions were explored in Chapter 6. If differences in response attributable to differences in spatial patterns of depressions could be captured by the numerical values obtained for mean depth of storage for the respective surfaces, results of the modeling applications did reveal that simulated response for these two surface treatments differed. The  $\theta$  value for surface treatment II was 0.067 cm, while that for surface treatment III was 0.017 cm. It is worth noting that the potential volumes of depressions (governed by the geometry of the surface) were the same for both surface treatments, while the actual volumes of depressions for the two treatments were different due to the fact that when the relatively large depressions were located far from the outlet, they had smaller upslope contributing areas and were never completely filled with runoff water.

Table 7.8: Model output for combination of slope and rainfall treatments—Two parameter model, surface treatment III.

Slope %	Rainfall Pattern	No zero correction				Zero correction			
		$\phi$	$\theta$	SS <sup>a</sup>	R <sup>2b</sup>	$\phi$	$\theta$	SS	R <sup>2</sup>
6%	HML <sup>c</sup>								
	LMH	27.79	0.023	83.7	0.97	27.98	0.017	79.3	0.97
	MLH	26.55	0.017	104	0.94	26.19	0.10	91.5	0.95
8%	HML								
	LMH	27.47	0.012	78.6	0.97	27.55	0.007	75.1	0.97
	MLH	26.78	0.017	110.0	0.94	26.17	0.006	91.7	0.95
10%	HML								
	LMH	26.10	0.012	77.1	0.87	26.11	0.008	74.4	0.98
	MLH	21.32	0.019	93.2	0.95	19.54	0.001	84.4	0.96
12%	HML								
	LMH	24.53	0.013	60.0	0.98	23.19	0.011	81.6	0.97
	MLH	19.28	0.020	71.1	0.96	19.20	0.015	65.1	0.96
14%	HML								
	LMH	23.63	0.017	58.1	0.98	24.09	0.006	58.5	0.98
	MLH	24.46	0.016	125.0	0.93	24.50	0.008	113.0	0.94
Mean	HML								
	LMH	25.91	0.015	-	-	25.78	0.010	-	-
	MLH	23.68	0.018	-	-	23.12	0.008	-	-
Pooled mean		24.79	0.017	-	-	24.45	0.008	-	-

<sup>a</sup> Sum of Squares

<sup>b</sup> Coefficient of Determination

<sup>c</sup> Data not collected

#### Surface Treatment IV

For this surface treatment, relatively large depressions were located near the outlet and drainage from some of them was allowed. Two versions of the model structure seemed applicable for this surface treatment. A three-parameter model with a drainage module was calibrated in addition to the previous two-parameter model structure. Table (7.9) summarizes the results of these model applications.

With a prime focus on the three-parameter model, Table (7.9) prompted the following key observations:

- The fits are still quite good, but not as good as for the earlier treatments con-

Table 7.9: Model output for combination of slope and rainfall treatments–Two and three parameter model, surface treatment IV.

Slope %	Rainfall Pattern	Two parameter model				Three parameter model				
		$\phi$	$\theta$	SS <sup>a</sup>	R <sup>2b</sup>	$\phi$	$\theta$	k <sub>b</sub>	SS	R <sup>2</sup>
6%	HML	13.45	0.144	171	0.78	20.52	0.173	0.007	122	0.86
	LMH	24.69	0.160	344	0.82	27.18	0.054	0.034	228	0.84
	MLH	24.87	0.164	327	0.80	24.04	0.106	0.014	174	0.87
8%	HML	12.57	0.105	237	0.74	16.86	0.169	0.006	179	0.80
	LMH	22.28	0.125	330	0.86	21.07	0.106	0.014	305	0.85
	MLH	23.46	0.134	386	0.79	21.62	0.100	0.014	270	0.83
10%	HML	12.31	0.103	194	0.78	17.59	0.117	0.010	207	0.81
	LMH	42.2	0.100	262	0.87	37.70	0.096	0.014	281	0.85
	MLH	22.03	0.098	285	0.86	24.15	0.018	0.089	236	0.89
12%	HML	12.58	0.097	196	0.77	14.54	0.164	0.005	181	0.78
	LMH	20.15	0.116	277	0.90	19.73	0.041	0.040	264	0.89
	MLH	22.56	0.101	238	0.87	22.43	0.030	0.052	248	0.87
14%	HML	10.39	0.101	205	0.79	13.25	0.158	0.006	175	0.82
	LMH	20.15	0.116	260	0.90	18.45	0.037	0.045	276	0.87
	MLH	21.63	0.089	280	0.86	18.55	0.061	0.024	247	0.89
Mean	HML	12.26	0.110	-	-	16.55	0.156	0.007	-	-
	LMH	25.89	0.123	-	-	24.83	0.067	0.029	-	-
	MLH	22.91	0.117	-	-	22.16	0.063	0.039	-	-
Pooled mean		20.35	0.117	-	-	21.18	0.095	0.025	-	-

<sup>a</sup> Sum of Squares

<sup>b</sup> Coefficient of determination

sidered.

- The parameters once again are not sensitive to slope changes, but are somewhat sensitive to the rainfall patterns, particularly the HML pattern.
- The  $\phi$  values are consistently lower than their corresponding values for the earlier surface treatments considered (excluding HML rainfall pattern). The overall mean for surface treatment IV is 21.18 s, while the means for the earlier surface treatments were 24.35, 22.96 and 24.45 s, corresponding to surface treatments I, II and III respectively.
- The  $\theta$  values are consistently higher than their corresponding values for surface treatment II. The overall mean  $\theta$  value for surface treatment IV is 0.095 cm, while

the mean value for surface treatment II was 0.041 cm. This trend in variation is also evident in the mean  $\theta$  values for each rainfall pattern for the two surface treatments.

- The three parameters reveal some codependence, particularly  $\theta$  and  $k_b$ . To minimize sum of squares,  $\theta$  is high when  $k_b$  is low and vice versa.
- The two-parameter model fit the data almost as well as the three-parameter model, with an increase in  $\theta$  accommodating the drainage component effect. The overall mean  $\theta$  value for the two-parameter model is 0.117 cm, while that for the three-parameter model is 0.095 cm.

In Chapter 6, catchment response data were less replicable for the surfaces characterized by various patterns of depressions with and without drainage than for the smooth surface. This lack of replicability was also reflected in the goodness of fit achieved in the model applications. Coefficients of determination for surface treatment IV were somewhat less than 0.90, while those for the earlier surface treatments with few exceptions were greater than 0.90 for similar condition.

The overall mean  $\theta$  value for surface treatment IV is significantly greater than that for surface treatment II, reflecting to some extent the effect of drainage occurring for surface treatment IV.

#### **Surface Treatment V**

For this surface treatment, relatively large depressions were located far from the outlet and drainage from some of them was allowed. Again, two model structures were applied, in light of the nature of this surface treatment. In addition to the previous

two-parameter model structure, a model with a drainage module (i.e. three parameter model) was also tried. Table (7.9) summarizes the results of model applications for these two structures. Inspection of Table (7.10) has led to the following key observations:

- The fits are still quite good, but not as good as for the earlier surface treatments without infiltration.
- The parameters are very consistent for all slopes and rainfall treatments.
- The  $\phi$  values are consistently lower than their corresponding values for surface treatment IV. The overall mean for surface treatment V is 16.45 s, while that for surface treatment IV was 21.18 s. Further, the  $\phi$  values had the least variability among the various surface treatments.
- The three parameters are somehow codependent, particularly  $\theta$  and  $k_b$ . When  $\theta$  is high, then  $k_b$  must be low to minimize the sum of squares, and vice versa.
- The  $\theta$  values had the least variability among the various surface treatments. Covariation of  $\theta$  with  $k_b$  made parameter comparison a bit misleading. Taking the covariation of  $\theta$  and  $k_b$  into account, while the overall mean  $\theta$  value for V is higher than the corresponding value for IV, the overall mean  $k_b$  for V is lower than that for surface treatment IV.
- The two-parameter model fits almost as well and the goodness of fit criteria are consistently better than those for the three-parameter model. Further, the  $\theta$  values for the two-parameter model are very variable with rainfall pattern.

Table 7.10: Model output for combination of slope and rainfall treatments—Two and three-parameter models, surface treatment V.

Slope %	Rainfall Pattern	Two parameter model				Three parameter model				
		$\phi$	$\theta$	SS <sup>a</sup>	$R^{2b}$	$\phi$	$\theta$	$k_b$	SS	$R^2$
6%	HML	12.59	0.058	241	0.82	18.78	0.126	0.008	164	0.86
	LMH	36.21	0.002	200	0.96	21.22	0.096	0.015	429	0.87
	MLH	34.12	0.002	210	0.94	21.29	0.095	0.014	343	0.88
8%	HML	15.49	0.081	124	0.88	14.27	0.129	0.007	167	0.85
	LMH	34.17	0.013	212	0.96	18.25	0.145	0.009	527	0.85
	MLH	30.90	0.003	221	0.95	17.47	0.095	0.014	390	0.88
10%	HML	10.96	0.066	204	0.87	13.43	0.125	0.008	197	0.88
	LMH	21.23	0.002	247	0.97	9.80	0.058	0.025	453	0.88
	MLH	37.44	0.009	212	0.96	15.71	0.095	0.014	380	0.86
12%	HML	11.65	0.082	129	0.82	11.04	0.129	0.007	171	0.79
	LMH	19.91	0.116	275	0.90	19.70	0.079	0.018	449	0.86
	MLH	27.13	0.002	266	0.94	15.21	0.095	0.014	441	0.85
14%	HML	12.36	0.08	155	0.85	19.98	0.033	0.050	588	0.70
	LMH	28.02	0.023	171	0.97	15.95	0.098	0.014	457	0.87
	MLH	28.64	0.015	295	0.90	14.62	0.174	0.006	602	0.78
Mean	HML	12.61	0.073	-	-	15.55	0.108	0.016	-	-
	LMH	27.91	0.031	-	-	16.98	0.095	0.016	-	-
	MLH	31.65	0.006	-	-	16.86	0.111	0.012	-	-
Pooled mean		24.06	0.037	-	-	16.45	0.105	0.015	-	-

<sup>a</sup> Sum of Squares

<sup>b</sup> Coefficient of determination

The  $\phi$  and  $\theta$  values are significantly different for the two and three-parameter models, implying a codependence on model structure. It seems the three-parameter model structure triggers another aspect of the information content of the data to optimize the calibration parameters. It should be emphasized that in reality for a typical surface, the mean time of travel for a specific event is unique but inaccessible and doesn't depend on different ways of conceptualizing it. Other researchers have reached the same conclusion but in different contexts. A numerical experiment conducted on TOPMODEL by Franchini et al. (1996) raised several serious questions concerning process representation and physical credibility of the model. TOPMODEL's success in predicting catchment response derives from its ability to model contributing areas

(using the topographic index curve), something at which ARNO model is equally successful (Todini, 1996). However, both models predict *different* contributing areas, which must therefore be regarded as model dependent and not necessarily representative of real contributing areas in a catchment.

The noisy nature of the original observed data created a major problem for the optimization algorithm to function properly. A direct consequence of such noise was to cause the objective function to be highly non-linear and non-convex. Sensitivity of the response surface to covariation of model parameters in a certain region, and inherent interactions among the model parameters, may have been a result of the apparent flatness of the response surface in the general region, a series of alternating localized peaks in the response surface, the noisy nature of the data sets themselves, characteristics of the optimization routine, or all of the above. Whatever the causes, interactions among the parameter values and sensitivity of the response surface in light of model parameter covariation suggest a non-uniqueness of parameter values, and that the values are somehow dependent on the nature of the optimization algorithm rather than being related closely to and indicative of physical processes. In addition, the results of modeling applications with the two-parameter model proved to be as good as those with the three-parameter model even though there was no drainage component incorporated into its model structure. This is truly an example of achieving a right solution for a wrong reason. In light of such circumstances, the physical meaning of input parameter will be totally lost.

## 7.21 Modeling Application for Small-Scale Field Experiments

In the case of the small-scale field experiment, neither the overall slope nor the spatial pattern of surface storage was controlled. However, as was mentioned before, keeping the size of the study area small, rainfall treatment and antecedent soil-water content could be controlled. The surface treatments involved three micro-plots with three levels of antecedent soil-water conditions with nested depression storage and allowance for infiltration. This variety of field conditions provided much valuable information to evaluate the soundness of model structures at a range of semi-natural field conditions in addition to those questions raised in Section (7.20). Modeling exercises were conducted on all surface treatments for various rainfall patterns and antecedent soil-water conditions. The main objective in this part was to test whether the developed model structure could capture the variability in surface storage from one micro-catchment to another.

In this part, the suitability of the three-parameter model was explored. In addition to the “zero correction” option, the original data were passed through a moving average filter of order five for possible model performance enhancement. Two scenarios were used in running the model on data sets for all combinations of plot, rainfall and initial condition treatments: in one set, the three-parameter model was calibrated using the original data sets; while for the other sets of runs, the three-parameter model was calibrated using smoothed data sets. Results of simulation runs for various initial conditions, plot treatments and rainfall patterns are summarized in Table (7.11). Inspection of Table (7.11) has led to the following key observations:

- Mean time of travel ( $\phi$ ) values varied essentially in the same range as the ones obtained from simulation runs on the laboratory data sets. Further, while  $\phi$  values were very similar for the wet and plastic cover conditions, the values vary from plot to plot for the dry conditions.
- The mean depth of storage ( $\theta$ ) values decrease with increase in level of antecedent soil-water conditions. Thus, on the average, the upper and lower limits of mean depth of storage correspond to dry and plastic cover conditions respectively.  $\theta$  has its lowest value for the plastic cover condition, which is a result similar to the  $\theta$  values for lab runs with depressions (i.e. surface treatment IV). The  $\theta$  values ranged from 0.097 to 0.924 cm for dry conditions, from 0.140 to 0.767 cm for wet conditions, and from 0.090 to 0.100 for plastic cover conditions; while the  $\theta$  values for surface treatment IV (which behaved hydrologically in the same way) ranged from 0.018 to 0.173 cm, with an overall mean value of 0.095 cm.
- The mean depth of storage ( $\theta$ ) values reveal no consistent variation among the various plot, rainfall and initial condition treatments for the small-scale field experiments; while they did vary consistently among the various surface treatments, slope orientations and to some extent rainfall patterns.
- The recession coefficient values varied significantly among the antecedent soil-water conditions, plot and rainfall conditions. They were definitely highest for the plastic cover condition; but showed no consistent variation among the wet and dry conditions. They were inversely related to mean depth of storage,  $\theta$ . The  $k_b$  values ranged from 0.001 to 0.290 s<sup>-1</sup> for the dry conditions, from 0.007

to  $0.028 \text{ s}^{-1}$  for the wet conditions, and from  $0.029$  to  $0.030 \text{ s}^{-1}$  for the plastic cover conditions; while the  $k_b$  values for surface treatment IV ranged from  $0.006$  to  $0.089 \text{ s}^{-1}$ , with an overall mean value of  $0.025 \text{ s}^{-1}$ .

- Fits were all pretty good, being poorest for the plastic cover conditions and somewhat poorer for dry than for wet conditions.
- The three parameters are somehow codependent, particularly  $\theta$  and  $k_b$ . When  $\theta$  is high, then  $k_b$  must be low to minimize the sum of squares, and vice versa.

Table 7.11: Summary of simulation runs for small-scale field experiment.

Initial condition	Plot No.	Rainfall Pattern	Three parameter model					Runoff Coefficient %
			$\phi$ (s)	$\theta$ (cm)	$k_b^a$ ( $\text{s}^{-1}$ )	Sum of Squares	$R^{2b}$ %	
Dry Condition	Plot I	HML	20.5	0.370	0.012	88.7	93	23
		LMH	29.31	0.169	0.034	115	79	25
		MLH	19.97	0.190	0.290	107	85	30
	Plot II	HML	48.55	0.924	0.013	7.9	94	11
		LMH	36.86	4.740	0.001	11.9	94	10
		MLH	48.31	0.193	0.058	47.9	89	8
	Plot III	HML	20.5	0.097	0.064	16.9	93	18
		LMH	19.8	0.098	0.059	29.8	92	16
		MLH	21.8	0.150	0.044	31.9	90	14
Wet Condition	Plot I	HML	23.312	0.767	0.008	12.3	96	25
		LMH	34.76	0.240	0.025	38.1	94	29
		MLH	36.92	0.180	0.028	25.9	97	22
	Plot II	HML	36.33	0.670	0.010	14.5	96	27
		LMH	37.76	0.340	0.016	36.2	95	27
		MLH	36.76	0.640	0.007	47.8	93	14
	Plot III	HML	13.62	0.360	0.010	100	91	33
		LMH	34.05	0.140	0.028	60.0	96	37
		MLH	32.33	0.230	0.015	91.7	93	37
Plastic Cover	Plot I		30.28	0.100	0.029	705	82	68
	Plot II	MLH	31.98	0.090	0.030	667	81	66
	Plot III		38.27	0.090	0.029	526	85	73

<sup>a</sup> Recession constant

<sup>b</sup> Coefficient of Determination

In earlier sections, it was mentioned that the mean time of travel has something to do with the physiography of the catchment such as drainage area. As the drainage area of both small-scale laboratory and field experiments were about the same, the finding of a similar range of values for  $\phi$  seems reasonable. Further, even though the true value of mean time of travel was not accessible for either scale, yet in terms of order of magnitude, the optimized values seem appropriate for a spatial scale of  $1 \times 1$  m.

The mean depth of storage parameter conceptually reflects the geometric characteristics of the surface and to some extent characteristics of the upper horizon soil-water storage condition. The substantial variability in  $\theta$  values, particularly for dry conditions, closely reflected the variability in micro-catchment response from one surface treatment to another. Further, eliminating a few exceptions, the optimized values of  $\theta$  found in this part were likely to be in the order of magnitude estimated in Chapter 5. The  $\theta$  values had the least variability for the plastic cover conditions, and the variability increased from plastic to wet and from wet to dry conditions.

Covariation of  $\theta$  with  $k_b$  made parameter comparison a bit misleading. Taking the covariation of  $\theta$  and  $k_b$  into account, it can be seen from Table (7.11) that relatively high values of  $\theta$  correspond to low values of  $k_b$  and vice versa. This trend of variation in parameter values hindered exploring the impact of surface conditions (i.e. micro-topography) on runoff response.

A few simulation runs with the two-parameter model confirmed the fact that the optimum values of the calibrated parameters were model structure dependence. One model structure was triggered by one aspect of information contained in the data;

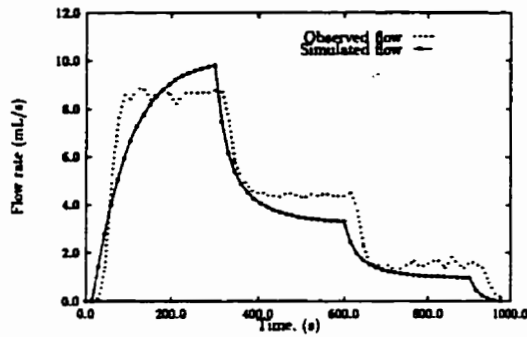
while another model structure was triggered by another aspect, leading to significantly different values for the parameters of each model. Yet all model structures led to plausible values of the goodness of fit criterion. The three-parameter model with three degrees of freedom was found to be more flexible in capturing the behavior of the system, as reflected in relatively high values of  $R^2$  and low values of sums of squares (SS) compared to the two-parameter model. The high values of the sum of squares for the plastic cover conditions may reflect the fact that this criterion depends on the numerical value of flow itself: the higher the relative flow volume, the higher the sum of squares and vice versa. Malfunctioning of the runoff measurement facility during experimentation with the plastic cover conditions might be another cause for high values of sum of squares.

Physically speaking, one would expect  $k_b$  to be negatively correlated to runoff coefficient. Among other factors, interaction between the calibrated parameters and hence possible violation of a fundamental assumption behind the model formulation might have been the cause of inconsistent parameter variation in the modeling application to the field data set. One direct implication regarding the interaction between parameters is that more than one combination of model parameters gave rise to plausible fits causing them to be not physically realistic. One basic assumption behind model formulation is that the model is solely applicable to those scenarios whereby saturation-excess overland flow is dominant. While the overland flow mechanism in the laboratory was runoff dominated, in the small-scale field experiment the runoff mechanism was more infiltration dominated. Lack of consistent variation in parameter values might also be due to improper incorporation of the infiltration process

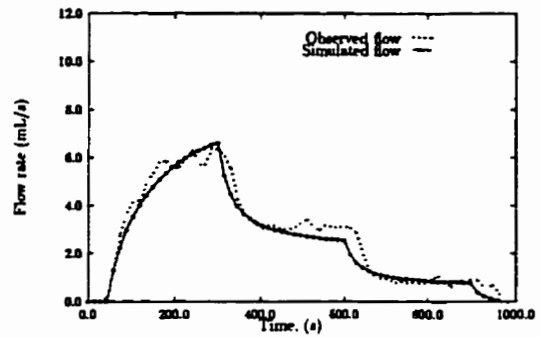
into the model structure, implying that the current model structure may not be suitable for field conditions for which infiltration is dominant.

As the graphical presentation of observed versus simulated runoff results can often be instructive of a modeling exercise, such example graphs are given in Figure (7.24) for the various rainfall patterns, plot treatments and antecedent soil-water conditions. Examination of Figure (7.24) has led to the following key observations:

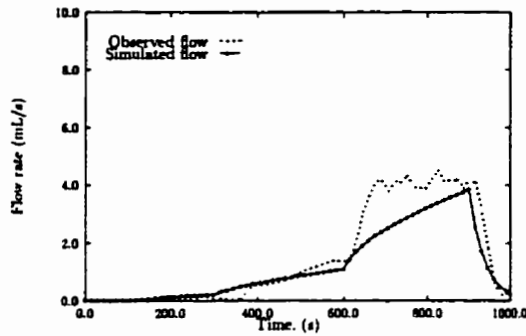
- The degree of match is excellent, particularly during the rising and falling limbs of each hydrograph.
- The recession constant contributed to the plateau portion of each hydrograph, e.g. higher values of  $k_b$  had more effect in leveling off the hydrograph. As an example, the recession constant for Figure (7.24c) was  $0.001 \text{ s}^{-1}$ , while that for Figure (7.24d) was 0.016. The distinct contribution to a leveling off of the runoff rate can be easily seen in Figure (7.24d).
- In all presented hydrographs, the observed flows are those of the original data set, suggesting that passing the data through a moving average filter was not necessary to improve model performance.



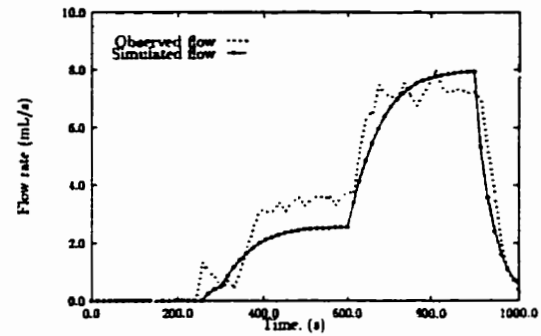
(a) Plot I, dry condition



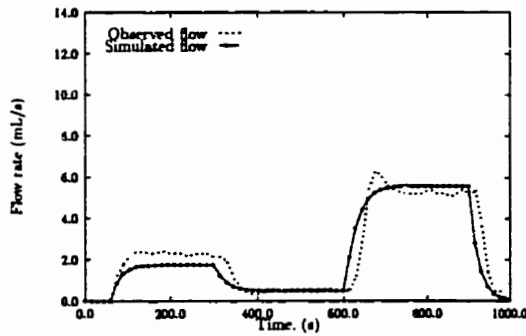
(b) Plot I, wet condition



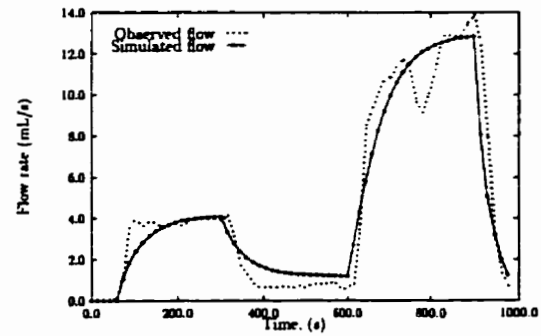
(c) Plot II, dry condition



(d) Plot II, wet condition



(e) Plot III, dry condition



(f) Plot III, wet condition

Figure 7.24: Graphical presentation of observed vs. simulated runoff for various rainfall, plot treatments and antecedent moisture conditions

## 7.22 Modeling Application for Large-Scale Field Experiment

Data from the Pilot Watershed Study (PWS) research basins were employed to evaluate the usefulness of the proposed model structure at a large scale. For the purpose of this modeling exercise, a few sample events during the period between early June to late September of each year for all research basins were selected for analysis. Each event was selected in such a way that it was preceded by a severe dry period. This initial condition allowed the model storage component to be assumed empty at the very beginning of simulation.

The two and three-parameter exponential models were calibrated for all events collected for the various sub-watersheds. It was anticipated that differences in the model parameter values for the paired sub-watersheds would provide a unique opportunity to compare the paired sub-watersheds on the basis of the degree to which each sub-watershed was subjected to conservational and conventional remedial measures.

The numerical results obtained from fitting the two and three-parameter exponential models are summarized in Table (7.12), with two typical example graphs given in Figure (7.25). With a prime focus on the three-parameter model, inspection of the tabulated results and graphical display has led to the following key observations:

- Most notable is the high degree of model fit achieved by the simple model structure, with  $R^2$  values in some cases above 0.90 being obtained for test sub-watersheds of Essex and Pittock.
- Mean time of travel ( $\phi$ ) values exhibit the least amount of variability from one sub-watershed to another.

- The mean depth of storage ( $\theta$ ) values are more variable among the various sub-watersheds, and are negatively correlated with the coefficient of runoff, i.e. the higher the mean depth of storage, the lower the coefficient of runoff.
- The three parameters are somehow codependent, particularly  $\theta$  and  $k_b$ . When  $\theta$  is high, then  $k_b$  must be low to minimize the sum of squares, and vice versa.
- The graphical display of results reveals that the peak of simulated responses were consistently underestimated, which can be attributed to either an underestimation of rainfall amount and intensity or to the model structure itself being unable to keep pace with the rapid rate of increase in the observed response.
- The irregularity in the simulated runoff of Figure (7.25a) on the rising limb may be attributed to an erratic rainfall temporal pattern. While effects of variable rainfall were detected in the simulated response, they appeared to be totally damped in the observed response.
- The two-parameter model fit the data as well as the three-parameter model, with an increase in  $\theta$  accommodating the drainage component effect, particularly for the Essex sub-watersheds.

The most striking thing in these results is that the  $k_b$  parameter played virtually no role. With the exception of the Kettle test sub-watershed, the  $k_b$  values are essentially insignificant (like some of the laboratory runs). Therefore, not surprisingly, the two and three-parameter models have almost identical parameter values and  $R^2$  values. These results may be explained in two ways. First,  $\theta$  and  $k_b$  were found to be codependent, as found in earlier model applications with the data obtained at small-

Table 7.12: Model output for two Exponential Distribution Function Models.

Basin Name	Basin Type	Two parameter model			Three parameter model				Runoff Coefficient %
		$\phi$ (hr)	$\theta$ (mm)	$R^2$ <sup>a</sup> %	$\phi$ (hr)	$\theta$ (mm)	$k_b$ <sup>b</sup> ( $hr^{-1}$ )	$R^2$ %	
Essex	test	11.75	43.56	94	11.01	85.82	0.001	93	52
	control	11.90	35.55	91	11.56	80.18	0.012	90	60
Kettle	test	6.57	134.61	82	6.67	136.84	0.196	81	14
	control	7.86	111.282	28	7.86	134.026	0.010	50	17
Pittock	test	10.0	333.11	94	9.96	361.77	0.001	93	9.3
	control	7.52	606.08	93	7.51	667.53	0.001	93	6

<sup>a</sup> Coefficient of Determination

<sup>b</sup> Recession constant

scale laboratory and field experiments. To explore the impact of this codependence, a few simulation runs were conducted on the Essex test sub-watershed data by fixing  $k_b$  at different values and optimizing the other two parameters. Results of the simulation runs, given in Table (7.13), show that while  $\phi$  values remained essentially the same,  $\theta$  increased when  $k_b$  was decreased and vice versa to minimize sum of squares. Secondly, as the formulation for both the two and three-parameter model structures was based on saturation-excess overland flow, the similarity in results might simply be due to the fact that both model structures simulated the near-channel contributing areas in which the soil mantle had no further room to drain water, hence the low values of the recession constant.

The coefficients of determination for the Kettle sub-watersheds in general and the control sub-watershed in particular were considerably lower than for the other sub-watersheds in the same region. Inspection of the observed rainfall and runoff showed that a remarkable lag, on the order of 2-3 hours, existed between rainfall and its

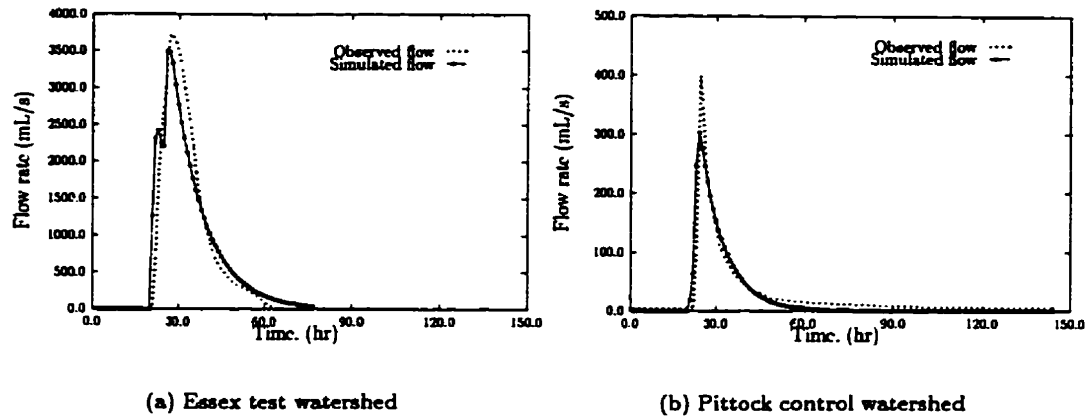


Figure 7.25: Graphical presentation of observed vs. simulated runoff for two typical events

Table 7.13: Results of simulation runs with various fixed values of  $k_b$ , Essex test sub-watershed.

Simulation run	parameter values			$R^2$ %
	$\phi$ (hr)	$\theta$ (mm)	$k_b$ ( $\text{hr}^{-1}$ )	
1	12.04	67.27	0.08	91
2	12.21	64.01	0.10	90
3	12.39	61.04	0.12	90
4	12.58	58.28	0.14	89
5	12.76	55.84	0.16	89
6	13.11	51.41	0.20	88
7	13.50	46.92	0.25	86

corresponding runoff. Further, the observed runoff increased dramatically from 12 to over 1000 L/s in less than perhaps half an hour. The low values for  $R^2$  might be due to the fact that the model structure was not able to keep pace with this rapid increase in observed runoff, and also could not represent the initial lag between observed rainfall and runoff quite well. This situation was also noted in model fitting for the HML rainfall pattern in the laboratory experiments.

## 7.23 Discussion of Results

It is appropriate at this stage to discuss and evaluate salient points brought out in disparate form in various parts of previous sections regarding the modeling applications performed at various spatial scales for various experimental settings. Although some comparisons have already been made among the modeling results, a broad comparison of model applications over the range of scales investigated has proven to be quite enlightening. Key observations from this comparison include the following:

1. Regarding goodness of fit between simulated and observed response hydrographs:

- Various versions of the model structure proposed (1, 2 and 3 parameter), provided very good to excellent estimated response hydrographs over the wide variety of slopes, surface treatments, rainfall patterns and antecedent soil-water conditions, and for the range of scales. In the case of the small-scale laboratory experiments, modeling applications with data sets collected for smooth surface provided an excellent fit, while the goodness of fit indices consistently decreased in passing from surface treatment I to surface treatment V. Indeed, the lack of replicability in observed runoff response mentioned in Chapter 6, moving from the smooth surface to surfaces with depressions and drainage, was also observed in the simulated response. In the case of the small-scale field experiments, the modeling applications with data sets collected for wet conditions provided an excellent fit, and the degree of match consistently decreased from wet to dry and then from dry to plastic cover conditions. As for the large-scale field experiments,  $R^2$  was

above 90% for some events and below 50% for others.

2. Regarding  $\phi$  (conceptually the mean time of travel)-

- Across all scales and conditions considered,  $\phi$  was a very stable, and the most stable, model parameter.
- Conceptually (i.e. in the model structure)  $\phi$  represented the mean travel time. For the scales investigated,  $\phi$  took optimized values that seemed quite indicative of the physical conditions and scales.

3. Regarding  $\theta$  (conceptually the mean depth of surface storage)-

- For the experimental conditions in which infiltration/drainage was not a factor,  $\theta$  proved to be a stable parameter; and took on optimum values indicative of the volume of surface depressions and of the relative location of significant depressions.
- For conditions involving infiltration/drainage,  $\theta$  could take on a wide range of values, at times apparently indicative of the extent of surface depressional storage and/or soil moisture storage, and at times perhaps merely exhibiting a codependence with the infiltration parameter,  $k_b$ . Therefore, under infiltration conditions, the  $\theta$  values could not be counted on to be representative of the nature or extent of depression storage.

4. Regarding  $k_b$  (conceptually drainage recession constant)-

- This parameter proved to be the least stable parameter in the three-parameter version of the model, probably largely because of the strong codependence

between  $\theta$  and  $k_b$ . Therefore, the  $k_b$  values could not be counted on to be representative of the extent of infiltration/drainage.

5. Regarding the codependence of  $\theta$  and  $k_b$ –

- For all experimental situations involving infiltration/drainage,  $\theta$  and  $k_b$  were found to be highly codependent. Although somewhat inconvenient from a modeling standpoint (one would prefer the parameters to be quite independent), this result should perhaps not be unexpected. Conceptually and mathematically,  $\theta$  introduces a storage effect and a water loss effect i.e. it can dampen response and can remove water from the runoff response (i.e. reduce the runoff coefficient).  $k_b$  can also remove water from rapid runoff response. Physically, depression storage and infiltration might be expected to be directly related i.e. the more and larger the depressions, the more water would be stored to infiltrate. However, in the model results,  $\theta$  and  $k_b$  were found to be inversely related i.e. when the optimum  $\theta$  value was relatively high, the optimum  $k_b$  value was relatively low, and vice versa. In other words, the optimization routine found these two parameters very convenient, moving the values up and down to achieve an optimum.

## Chapter 8

# CONCLUSIONS AND RECOMMENDATIONS

### 8.1 Introduction

This thesis was undertaken to investigate the effects of surface storage elements on catchment response at a range of spatial scales and experimental settings. The spatial scales included small-scale laboratory experiments, small-scale field experiments and large-scale field experiments. Interaction of surface treatments, slope orientations, rainfall patterns and initial soil-water conditions on one hand and surface storage elements, and resulting effects on runoff response including the timing of outflow hydrographs on the other hand, were considered at these spatial scales. Direct characterization of surface storage elements was pursued in Chapter 5, indirect characterization of surface storage elements via observation of rainfall and its corresponding runoff at different spatial scales was continued in Chapter 6, and modeling exercises were undertaken in Chapter 7 to quantify these features. With reference to these results chapters, conclusions and recommendations for further studies are provided in

the following sections.

## 8.2 Conclusions

The study reported in this thesis has led to the following conclusions:

1. From the analysis of pond, it became clear that most estimates and/or geometric characteristics relating to size and spatial location of depression storage, including area, volume and depth, are scale dependent. We should perhaps abandon the notion of trying to measure/estimate deterministic quantities related physically to surface depressions. These geometric objects may best be described by resorting to fractal geometry, a popular tool for quantifying variability across scales. We should possibly dismiss the notion of optimum grid spacing or for that matter representative elementary area or volume as these concepts are very much objective and scale dependent; and instead try to delineate scale-invariance relationships between variables of interest at a range of spatial scales, with break-points separating scaling regions.
2. From the analysis of runoff response data, it was found that:
  - When there is no infiltration, depression effects can be detected in response, i.e. effects due to size of depressions and spatial location of different sizes. So, if such spatial information is available, one could delineate and attribute such spatial effects to response. Unfortunately, in general, such detailed information is lacking in practical situations.

- In the presence of infiltration, it is extremely difficult if not impossible to distinguish depression effects from infiltration effects on catchment response.
- Regarding the interaction between infiltration and surface storage, it became clear that one has to be very careful estimating effective infiltrability from apparent steady state response conditions (with full depression storage).

Therefore, since there are effects, but we can't distinguish the sources from the response even for simple systems, perhaps we should look into probabilistic or other ways of describing/modeling the system.

3. From modeling applications, it was found that:

- For simple depressional cases with no infiltration, differences in response due to various spatial patterns of depressions can be delineated well with a simple holistic model. In such situations, the parameters can take on values which appear to have physical meaning in terms of physical characteristics such as mean time of travel and mean depth of depressional storage.
- For simple and more complex situations involving infiltration at a range of scales (from small plots to small watersheds), response can be estimated well with a simple holistic model. However, the parameters can take on values which may or may not have any physical meaning at all.

In short, we should be very cautious assuming parameters of conceptual models actually represent physical processes and take on values indicative of physical processes. Further, we should be very cautious using model parameter values obtained at one spatial scale to be legitimate and/or appropriate values for other spatial

scales of application, even though the mean time of travel parameter appeared to preserve a physical meaning at a range of spatial scales in this study. There are still many ambiguities associated with the routing and partitioning of water between surface and subsurface flows, and estimating associated parameters. We should perhaps try to develop concepts and theories directly at the scale of interest (Rodriguez and Valdes, 1979), and possibly dismiss the notion of transferring information across scales in a quantitative way if not in a qualitative manner.

### 8.3 Recommendations for Further Research

Based on the results of the study, the following are recommended for further investigation.

1. The pond analysis and associated cited implications involved small spatial scale. There is a need to collect digital elevation data with fine resolution at larger spatial scales, and address the following questions:
  - Can one describe depressional storages via fractal geometry at larger spatial scales?
  - Fixing the size of the study area, does the frequency distribution remain similar at different grid resolutions and various spatial scales?
  - Fixing the size of the study area, do the frequency distribution parameters (i.e. characteristics of surface depressions) remain similar at different grid resolutions and various spatial scales?

- What do measurements show about the interaction of spatial scale and spatial variability?
2. There is a need to investigate the effects of nested structure of depressional storages on catchment response in situations where there is no infiltration.
  3. There is a need to refine model structures to eliminate parameter interaction and better accommodate the infiltration process. One possible suggestion might be to introduce storage as a second state variable, and try to have a close match between observed and simulated storage as well. Structuring a model by considering cumulative values of response variables might be another possibility.

# Bibliography

- Abbott, M. B., Bathurst, J. C., Cunge, J. A., O'Connell, P. E. and Rasmussen, J. (1986a). An introduction to the European Hydrological System—Systeme Hydrologique Europeen, 'SHE', 1: History and philosophy of a physically-based, distributed modeling system, *J. Hydrol.* **87**: 45–59.
- Abbott, M. B., Bathurst, J. C., Cunge, J. A., O'Connell, P. E. and Rasmussen, J. (1986b). An introduction to the European Hydrological System—Systeme Hydrologique Europeen, 'SHE', 2: Structure of a physically-based, distributed modeling system, *J. Hydrol.* **87**: 61–77.
- Amerman, C. R. and McGuinness, J. L. (1967). Plot and small watershed runoff: Its relation to larger areas, *Trans. Amer. Soc. Agr. Engrs.* **10**(4): 464–466.
- Andersson, L. (1992). Improvements of runoff models: What way to go?, *Nord. Hydrol.* **23**: 315–332.
- Baliga, B. R. (1996). Control-Volume Finite Element Methods for Fluid Flow and Heat Transfer, in W. J. Minkowycz and E. M. Sparrow (eds), *Advances in Numerical Heat Transfer*, Vol. 1, Hemisphere Publishing Corp., Washington, D. C., chapter Three, pp. 1–39.
- Band, L. E. (1993). Extraction of channel network and topographic parameters from digital elevation data, in K. J. Beven and M. J. Kirkby (eds), *Channel network hydrology*, Wiley Interscience Publications, London, pp. 13–42.
- Band, L. E. (1995). Personal Communication, *Department of Geography*, University of Toronto, Toronto, Ontario.
- Bathurst, J. C. (1986a). Physically-based, distributed modeling of an upland catchment using Systeme Hydrologique Europeen, *J. Hydrol.* **87**: 79–102.

- Bathurst, J. C. (1986b). Sensitivity analysis of the Systeme Hydrologique Europeen for an upland catchment, *J. Hydrol.* **87**: 103–123.
- Bathurst, J. C. and O'Connell, P. E. (1993). Future of distributed modeling: Systeme Hydrologique Europeen, in K. J. Beven and I. D. Moore (eds), *Terrain analysis and distributed modeling in hydrology*, Wiley Interscience Publications, London, pp. 213–226.
- BEAK Consultants, L. (1994). Pilot Water Study, Soil and Water Environment Enhancement Program, *Final Report to Agriculture and Agri-Food Canada*, Guelph, Ontario.
- Beck, M. B. (1987). Water quality modeling: A review of the analysis of uncertainty, *Water Resour. Res.* **23**(8): 1393–1442.
- Bernier, P. Y. (1982). *VSAS2: A revised source area simulator for small forested basins*, PhD thesis, University of Georgia, Athens, Georgia.
- Bertuzzi, P., Caussignac, J. M., Stengel, P., Morel, G., Lorendeau, J. Y. and Pelloux, G. (1990). An automated non-contact laser profile-meter for measuring soil in situ, *Soil Science* **149**(3): 169–178.
- Betson, R. P. (1964). What is watershed runoff?, *J. Geophys. Res.* **69**(8): 1541–1552.
- Betson, R. P. and Marius, J. B. (1969). Source areas of storm runoff, *Water Resour. Res.* **5**(3): 574–582.
- Betson, R. P., Marius, J. B. and Joyce, R. T. (1968). Detection of saturated interflow in soils with piezometers, *Soil Sci. Soc. Amer. Proc.* **32**(4): 602–604.
- Beven, K. (1995). Linking parameters across scales: Subgrid parameterizations and scale dependent hydrological models, *Hydrol. Process.* **9**: 507–525.
- Beven, K. J. (1977). TOPMODEL—A physically-based variable contributing area hydrologic modeling program, *Technical Report 183*, University of Leeds, School of Geography.
- Beven, K. J. (1989). Changing ideas in hydrology—The case of physically based models, *J. Hydrol.* **105**: 157–172.

- Beven, K. J. and Kirkby, M. J. (1979). A physically-based, variable contributing area model of basin hydrology, *Hydrol. Sci. Jour.* **24**(1): 43–69.
- Beven, K. J. and Moore, I. D. (1993). Introduction, in K. J. Beven and I. D. Moore (eds), *Terrain analysis and distributed modeling in hydrology*, Wiley Interscience Publications, London.
- Beven, K. J. and Wood, E. F. (1983). Catchment geomorphology and the dynamics of runoff contributing areas, *J. Hydrol.* **65**: 139–158.
- Bloschl, G. and Sivapalan, M. (1995). Scale issues in hydrological modeling: A review, *Hydrol. Process.* **9**(3): 251–290.
- Boughton, W. C. (1987). Evaluating partial areas of watershed runoff, *J. Irrig. Drain. Engrg., Div.* **113**(3): 356–367.
- Boyd, M. J., Bates, B. C., Pilgrim, D. H. and Cordery, I. (1987). WBNM: A General Runoff Routing Model–Program and User Manual, *Report 170*, University of New South Wales, Water Res. Lab., Kensington, Australia.
- Boyd, M. J., Pilgrim, D. H. and Cordery, I. (1972). A storage routing model based on catchment geomorphology, *J. Hydrol.* **42**: 229–236.
- Caussignac, J. M., Morel, G. and Charrier, J. (1990). A new laser, non-contact method for measuring vehicle-to-pavement distance, *Surface characteristics of roadways: International Research and Technologies*, ASTM STP 1031, American Society for Testing and Materials, Philadelphia, pp. 77–86.
- Chorley, R. J. (1978). The hillslope hydrological cycle, in M. J. Kirkby (ed.), *Hillslope hydrology*, Wiley Interscience Publications, London, pp. 1–42.
- Christiansen, J. E. (1942). Irrigation by sprinkling, *Bulletin 670*, University of California, Agric. Exp. Sta.
- Clark, C. O. (1945). Storage and the unit hydrograph, *Transaction, ASCE* **110**: 1416–1446.
- Clark, I. (1979). *Practical Geostatistics*, Applied Science Publishers LTD., London. 129p.

- Crawford, N. H. and Linsley, R. K. (1966). Digital simulation in hydrology: Stanford Watershed Model Mark IV, *Tech. Report 39*, Dept. of Civil Engineering, Stanford University.
- Culling, W. E. H. (1989). The characterization of regular/irregular surfaces in the soil-covered landscape by Gaussian random fields, *Computers and Geosciences* **15**(2): 219–226.
- Cushman, J. H. (1987). Development of stochastic partial differential equations for subsurface hydrology, *Stochastic Hydrol. Hydraul.* **1**: 241–262.
- DeCoursey, D. G. (1996). Hydrological, climatological and ecological systems scaling: A review of selected literature and comments, *Interim Progress Report*, USDA-ARS-NPA, Fort Collins, CO 80522.
- Deutsch, C. V. and Journel, A. G. (1992). **GSLIB: Geostatistical Software Library and User's Guide**, Oxford University Press, New York. 340p.
- Dickinson, W. T., Rudra, R. P. and Wall, G. J. (1990). Targeting remedial measures to control non-point source pollution, *Water Resour. Bull.* **26**(3): 499–507.
- Dooge, J. C. I. (1959). A general theory of the unit hydrograph, *J. Geophys. Res.* **64**(2): 241–256.
- Dooge, J. C. I. (1973). Linear theory of hydrologic systems, *Technical Bulletin No. 1468*, Agricultural Research Service, Washington, D. C. United States Department of Agriculture.
- Dooge, J. C. I. (1985). Looking for hydrologic laws, *Water Resour. Res.* **22**(9): 46S–58S.
- Dooge, J. C. I. (1988). Hydrology past and present, *J. Hydraul. Res.* **26**(1): 5–26.
- Dozier, J. (1992). Opportunities to improve hydrologic data, *Rev. Geophys.* **30**(4): 315–331.
- Duan, Q. and Sorooshian, S. (1993). A shuffled complex evolution approach for effective and efficient global minimization, *Journal of Optimization Theory and Its Applications* **76**(3): 501–521.

- Duan, Q., Sorooshian, S. and Gupta, V. K. (1992). Effective and efficient global optimization for conceptual rainfall-runoff models, *Water Resour. Res.* **28**(4): 1015–1031.
- Duan, Q., Sorooshian, S. and Gupta, V. K. (1994). Optimal use of SCE-UA global optimization method for calibrating watershed models, *J. Hydrol.* **158**: 265–284.
- Dunne, T. (1978). Field studies of hillslope flow processes, in M. J. Kirkby (ed.), *Hillslope hydrology*, Wiley Interscience Publications, London, pp. 227–293.
- Dunne, T. (1983). Relation of field studies and modeling in the prediction of storm runoff, *J. Hydrol.* **65**: 25–48.
- Dunne, T. (1995). Personal Communication, *Department of Geological Sciences*, University of Washington, Seattle.
- Dunne, T. and Black, R. D. (1970). An experimental investigation of runoff production in permeable soils, *Water Resour. Res.* **6**(2): 478–490.
- Dunne, T., Zhang, W. and Aubry, B. F. (1991). Effects of rainfall, vegetation, and micro-topography on infiltration and runoff, *Water Resour. Res.* **27**(9): 2271–2285.
- Emmett, W. W. (1978). Overland flow, in M. J. Kirkby (ed.), *Hillslope hydrology*, Wiley Interscience Publications, London, pp. 145–176.
- Engman, E. T. (1974). Partial area hydrology and its application to water resources, *Water Resour. Bull.* **10**(3): 512–521.
- Engman, E. T. and Gurney, R. J. (1991). *Remote sensing in hydrology*, Chapman and Hall, New York. 225p.
- Engman, E. T. and Rogowski, A. S. (1974). A partial area model for storm flow synthesis, *Water Resour. Res.* **10**(3): 464–472.
- Faurés, J. M., Goodrich, D. C., Woolhiser, D. A. and Sorooshian, S. (1995). Impact of small-scale spatial rainfall variability on runoff modeling, *J. Hydrol.* **173**: 309–326.
- Feder, J. (1988). *Fractals*, Plenum Press, New York. 283p.

- Folks, J. L. and Chhikara, R. S. (1978). The inverse Gaussian distribution and its statistical application—A review, *J. R. Stat. Soc. Ser. B.* 40(3): 263–289.
- Forsyth, P. A. (1990). A control-volume, finite-element method for local mesh refinement in thermal reservoir simulation, *Soc. Pet. Eng. Res. Eng.* 5: 561–566.
- Franchini, M., Wending, J., Obled, C. and Todini, E. (1996). Physical interpretation and sensitivity analysis of the TOPMODEL, *J. Hydrol.* 175: 293–338.
- Freeze, R. A. (1969). The mechanism of natural ground-water recharge and discharge 1. One dimensional, vertical, unsteady, unsaturated flow above a recharging or discharging ground-water flow system, *Water Resour. Res.* 5(1): 153–171.
- Freeze, R. A. (1971a). Three dimensional, transient, saturated–unsaturated flow in a ground-water basin, *Water Resour. Res.* 7(2): 347–366.
- Freeze, R. A. (1971b). Influence of the unsaturated flow domain on seepage through earth dams, *Water Resour. Res.* 7(4): 929–941.
- Freeze, R. A. (1972a). Role of subsurface flow in generating surface runoff 1. Base flow contributions to channel flow, *Water Resour. Res.* 8(3): 609–623.
- Freeze, R. A. (1972b). Role of subsurface flow in generating surface runoff 2. Upstream source areas, *Water Resour. Res.* 8(5): 1272–1283.
- Freeze, R. A. (1978). Mathematical models of hillslope hydrology, in M. J. Kirkby (ed.), *Hillslope hydrology*, Wiley Interscience Publications, London, pp. 177–225.
- Freeze, R. A. (1980). A stochastic–conceptual analysis of rainfall–runoff process on a hillslope, *Water Resour. Res.* 16(2): 391–408.
- Freeze, R. A. and Harlan, R. L. (1969). Blueprint for a physically–based, digitally–simulated hydrologic response model, *J. Hydrol.* 9: 237–258.
- Fung, L. S.-K., Hlebert, A. D. and Nghlem, L. X. (1992). Reservoir simulation with a control-volume finite-element method, *Soc. Pet. Eng. Res. Eng.* 7: 349–357.
- Garg, N. K. and Sen, D. L. (1994). Determination of watershed features for surface runoff models, *J. Hydr. Div., ASCE* 9: 237–447.

- Gill, P. E. and Murray, W. (1978). Algorithms for the solution of the nonlinear least-squares problem, *SIAM J. Numer. Anal.* **15**: 977-992.
- Gillies, J. A. (1994). *A wind tunnel study of the relationships between complex surface roughness form, flow geometry and shearing stress*, 231p., University of Guelph, Guelph, Ont. Dept. of Geography.
- Goodrich, D. C., Schmutge, T. J., Jackson, T. J., Unkrich, C. L., Keefer, T. O., Parry, R., Bach, L. B. and Amer, S. A. (1994). Runoff simulation sensitivity to remotely sensed initial soil water content, *Water Resour. Res.* **30**(5): 1393-1405.
- Goodrich, D. C., Woolhiser, D. A. and Keefer, T. O. (1991). Kinematic routing using finite elements on a triangular irregular network, *Water Resour. Res.* **27**(6): 995-1003.
- Gottardi, G. and Dall'Olio, D. (1992). A control-volume finite-element model for simulating oil-water reservoirs, *J. Pet. Sci. Engng.* **8**: 29-41.
- Gottardi, G. and Venutelli, M. (1993). A control-volume finite-element model for two-dimensional overland flow, *Adv. water Resour.* **16**: 277-284.
- Gottardi, G. and Venutelli, M. (1997). LANDFLOW: Computer program for the numerical simulation of two dimensional overland flow, *Computers and Geosciences* **23**(1): 77-89.
- Grayson, R. B., Moore, I. D. and McMahon, T. A. (1992a). Physically based hydrologic modeling: 1. A terrain-based model for investigative purposes, *Water Resour. Res.* **28**(10): 2639-2658.
- Grayson, R. B., Moore, I. D. and McMahon, T. A. (1992b). Physically based hydrologic modeling: 2. Is the concept realistic, *Water Resour. Res.* **28**(10): 2659-2666.
- Guy, B. T. (1990). *Sediment transport capacity of shallow overland flow*, 332 p., University of Guelph, Guelph, Ontario.
- Haan, C. T. and Johnson, H. P. (1968). Hydraulic model of runoff from depressional areas Part II: Development of model, *Trans. Amer. Soc. Agr. Engrs.* **11**(3): 368-373.

- Hairsine, P. B., Moran, C. J. and Rose, C. W. (1992). Recent developments regarding the influence of soil surface characteristics on overland flow and erosion, *Aust. J. Soil Res.* **30**: 249–264.
- Hastings, H. M. and Sugihara, G. (1993). *Fractals: A user's guide for the natural sciences*, Oxford University Press, New York. 235p.
- Hewlett, J. D. and Hibbert, A. R. (1967). Factors affecting the response of small watersheds to precipitation in humid areas, *International Symposium on forest hydrology*, Pennsylvania State University, Pergamon, New York, pp. 275–290.
- Hewlett, J. D. and Troendle, C. A. (1975). Non-point and diffused water sources: A variable source area problem, *Proc. Symp. Interdisciplinary aspects of watershed management*, Am. Soc. Civ. Eng., New York, pp. 21–46.
- Hirschi, M. C., Barfield, B. J., Moore, I. D. and Colliver, D. G. (1987). Profile meter for detailed measurements of soil surface heights, *Applied Engineering in Agriculture* **3**(1): 47–51.
- Horton, R. E. (1933). The role of infiltration in the hydrologic cycle, *Trans. Amer. Geophys. Union* **14**: 446–460.
- Hromadka, T. V., Berenbrock, C. E., Freckleton, J. R. and Guymon, G. L. (1985). A two-dimensional dam-break flood plain model, *Adv. water Resour.* **8**: 7–14.
- Huang, C. (1996). Personal Communication, *NSEERL*, Purdue University, West Lafayette Ind.
- Huang, C. and Bradford, J. M. (1990a). Depressional storage for Markov–Gaussian surface, *Water Resour. Res.* **26**(9): 2235–2242.
- Huang, C. and Bradford, J. M. (1990b). Portable laser scanner for measuring soil surface roughness, *Soil Sci. Soc. Amer. Proc.* **54**: 1402–1406.
- Huang, C. and Bradford, J. M. (1992). Application of a laser scanner to quantify soil micro-topography, *Soil Sci. Soc. Amer. Proc.* **56**: 14–21.
- Huang, C., White, I., Thwaite, E. G. and Bendeli, A. (1988). A non-contact laser system for measuring soil surface topography, *Soil Sci. Soc. Amer. Proc.* **52**: 350–355.

- Isaaks, E. H. and Srivastava, R. M. (1989). *An Introduction to Applied Geostatistics*, Oxford University Press, New York. 561p.
- Johnson, D. E., Hilburn, J. L. and Johnson, J. R. (1984). *Basic electric circuit analysis*, Prentice-Hall, Inc., Englewood Cliffs, New Jersey. 629p.
- Johnston, N. L. and Kotz, S. (1970). *Distributions in statistics: Continuous univariate distributions 1.*, Vol. 2, Houghton-Mifflin, Boston, Mass.
- Johnston, N. L. and Kotz, S. (1972). *Distributions in statistics: Continuous multivariate distributions*, Vol. 4, John Wiley, New York. 333p.
- Journel, A. G. (1989). Fundamentals of geostatistics in five lessons, *Short course in Geology: Volume 8*, American Geophysical Union, Washington, D. C.
- Julien, P. Y., Saghafian, B. and Ogden, F. L. (1995). Raster-based hydrologic modeling of spatially varied surface runoff, *Water Resour. Bull.* **31**(3): 523-536.
- Karplus, W. J. (1958). *Analog simulation: Solution of field problems*, McGraw-Hill Book Co., New York. 434p.
- Ketcheson, J. W. and Onderdonk, J. J. (1973). Effect of corn stover on phosphorous in runoff from non-tilled soil, *Agron. J.* **65**: 69-71.
- Kibler, D. F. and Woolhiser, D. A. (1970). The kinematic cascade as a hydrologic model, *Hydrology Paper 39*, Colorado State University, Fort Collins, Colorado.
- Kirkby, M. J. (1976). Hydrograph modeling strategies, in R. Peel, M. Chisholm and P. Haggett (eds), *Processes in Physical and Human Geography*, Heinemann, London, chapter 3, pp. 69-90.
- Kitanidis, P. K. (1993). Geostatistics, in D. R. Maidment (ed.), *Handbook of Hydrology*, McGraw Hill book Com., New York, chapter 20, pp. 20.1-20.39.
- Klemeš, V. (1983). Conceptualization and scale in hydrology, *J. Hydrol.* **65**: 1-23.
- Klemeš, V. (1986a). Dilettantism in hydrology: Transition or Destiny, *Water Resour. Res.* **22**(9): 177S-188S.
- Klemeš, V. (1986b). Operational testing of hydrological simulation models, *Hydrol. Sci. Jour.* **31**(1): 13-23.

- Koch, G. and Link, R. (1986). *Statistical analysis of geological data*, second edn, John Wiley & Sons, Inc., New York.
- Kolstad, O. C. and Schuler, R. T. (1980). An ultrasonic reliefmeter for soil surface measurement, *ASAE Paper No. NCR 80-303*, St. Joseph, MI.
- Kouwen, N. and Soulis, E. D. (1994). Weather radar and flood forecasting, in W. James (ed.), *Current practice in modeling the management of storm-water impacts*, Lewis Publishers, pp. 257–270.
- Kumar, A., Kanwar, R. S. and Hallberg, G. R. (1994). Modeling spatial variability of saturated hydraulic conductivity using fourier series analysis, *Hydrol. Sci. Jour.* **39**(2): 143–156.
- Larsen, J. E., Sivapalan, M., Coles, N. A. and Linnet, P. E. (1994). Similarity analysis of runoff generation processes in real-world catchments, *Water Resour. Res.* **30**(6): 1641–1652.
- Laurenson, E. M. (1964). A catchment storage model for runoff routing, *J. Hydrol.* **2**: 141–163.
- Laurenson, E. M. and Mein, R. G. (1988). RORB–Version 4, Runoff Routing Program, *User Manual*, Department of Civil Engineering, Monash University, Clayton, Victoria, Australia.
- Lefkoff, L. J. (1981). *Application of the variable source area simulator to a forested piedmont watershed*, Master's thesis, University of Georgia, Athens, Georgia.
- Linsley, R. K. (1967). The relation between rainfall and runoff, *J. Hydrol.* **5**: 297–311.
- Linsley, R. K., Kohler, M. A. and Paulhus, J. L. H. (1949). *Applied hydrology*, McGraw-Hill Book Co., New York. 689p.
- Loganathan, G. V., Shrestha, S. P., Dillaha, T. A. and Ross, B. B. (1989). Variable source area concept for identifying critical runoff-generating areas in a watershed, *Bulletin no. 164*, Water Resour. Res. Cen., Polytechnic Institute and State University.
- Mackenzie, K. M. (1995). *Investigation of the effects of temporally distributed rainfall on inter-rill detachment processes*, 270p., University of Guelph, Guelph, Ontario.

- Maidment, D. R. (1995). Personal Communication, *Dept. of Civil Eng.*, The University of Texas at Austin, Texas.
- Mandelbrot, B. B. (1982). *The Fractal Geometry of Nature*, Freeman, San Francisco. 460p.
- Mitchell, J. K. and Jones, B. A. J. (1976). Micro-relief surface depression storage: Analysis of models to describe the depth-storage functions, *Water Resour. Bull.* **12**(6): 1205–1222.
- Mitchell, J. K. and Jones, B. A. J. (1978). Micro-relief surface depression storage: Changes during rainfall events and their application to rainfall -runoff modeling, *Water Resour. Bull.* **14**(4): 777–802.
- Moore, I. D. and Grayson, R. B. (1991). Terrain-based catchment partitioning and runoff prediction using vector elevation data, *Water Resour. Res.* **27**(6): 1177–1191.
- Moore, I. D., Grayson, R. B. and Ladson, A. R. (1993). Digital terrain modeling: A review of hydrological, geomorphological, and biological applications, in K. J. Beven and I. D. Moore (eds), *Terrain analysis and distributed modeling in hydrology*, Wiley Interscience Publications, London, pp. 1–34.
- Moore, I. D. and Larson, C. L. (1979). Estimating micro-relief surface storage from point data, *Trans. Amer. Soc. Agr. Engrs.* **22**: 1073–1077.
- Moore, R. J. (1985). The probability-distributed principle and runoff production at point and basin scales, *Hydrol. Sci. Jour.* **30**(2): 273–297.
- Moore, R. J. (1993). Real-time flood forecasting systems: Perspectives and prospects, *UK-Hungarian Workshop on Flood Defence*, Budapest, 6-10 September. 51 p.
- Moore, R. J. and Clarke, R. T. (1981). A distribution function approach to rainfall runoff modeling, *Water Resour. Res.* **17**(5): 1367–1382.
- Moore, R. J. and Clarke, R. T. (1982). A distribution function approach to modeling basin soil moisture deficit and streamflow, in V. P. Singh (ed.), *Statistical analysis of rainfall and runoff*, Water Resources Publications, Colorado, pp. 173–190.

- Moore, R. J. and Clarke, R. T. (1983). A distribution function approach to modeling basin sediment yield, *J. Hydrol.* **65**: 239–257.
- Mwendera, E. J. and Feyen, J. (1992). Estimation of depression storage and manning's resistance coefficient from random roughness measurements, *Geoderma* **52**: 235–250.
- NAG (1991). *NAG Fortran Library Manual*, first edn. MARK 15A, The Numerical Algorithms Group Ltd.
- Narasimhan, T. N. and Witherspoon, P. A. (1976). An integrated finite difference method for analyzing fluid flow in porous media, *Water Resour. Res.* **12**(1): 57–64.
- Nash, J. E. (1957). The form of the instantaneous unit hydrograph, *Int'l. Assoc. Sci. Hydrol. Pub.* **45** **3**: 114–121.
- O'Connell, P. E. and Todini, E. (1996). Modeling of rainfall, flow and mass transport in hydrological systems: An overview, *J. Hydrol.* **175**: 3–16.
- Oliver, M., Webster, R. and Gerrard, J. (1989). Geostatistics in physical geography. Part I: Theory, *Transactions of the Institute of British Geographers* **14**: 259–269.
- O'Loughlin, E. M. (1981). Saturation regions in catchment and their relations to soil and topographic properties, *J. Hydrol.* **53**: 229–246.
- O'Loughlin, E. M. (1986). Prediction of surface saturation zones in natural catchment by topographic analysis, *Water Resour. Res.* **22**(5): 794–804.
- O'Loughlin, E. M. (1990). Modeling soil water status in complex terrain, *Agric. For. Meteorol.* **50**: 23–38.
- Onstad, C. A. (1984). Depressional storage on tilled soil surfaces, *Trans. Amer. Soc. Agr. Engrs.* **27**: 729–732.
- Onstad, C. A. and Brakensiek, D. L. (1968). Watershed simulation by the stream path analogy, *Water Resour. Res.* **4**(5): 965–971.
- Opportunities in the Hydrologic Sciences* (1991). *National Research Council, Committee on Opportunities in the Hydrologic Sciences*, National Academy Press, Washington, D. C.

- Oreskes, N., Shrader-Frechette, K. and Belitz, K. (1994). Verification, validation and confirmation of numerical models in the earth sciences, *Science* **263**: 641–646.
- Parlange, J.-Y., Rose, C. W. and Sander, G. (1981). Kinematic flow approximation of runoff on a plane: An exact analytical solution, *J. Hydrol.* **52**: 171–176.
- Phillips, E. M. and Pugh, D. S. (1994). *How to get a PhD: A handbook for students and their supervisors*, 2nd edn, Open University Press, Buckingham, Philadelphia. 203p.
- Phillips, J. (1986). *The NAG Library: A Beginner's Guide*, Clarendon Press, Oxford. 245p.
- Pilgrim, D. H. (1966a). Radioactive tracing of storm runoff on a small catchment, 1. Experimental technique, *J. Hydrol.* **4**: 289–305.
- Pilgrim, D. H. (1966b). Radioactive tracing of storm runoff on a small catchment, 2. Discussion of results, *J. Hydrol.* **4**: 306–326.
- Pilgrim, D. H. (1976). Travel times and nonlinearity of flood runoff from tracer measurements on a small watershed, *Water Resour. Res.* **12**: 487–496.
- Pilgrim, D. H. (1977). Isochrones of travel time and distribution of flood storage from a tracer study on a small watershed, *Water Resour. Res.* **13**(3): 587–595.
- Platt, J. R. (1964). Strong inference, *Science* **146**(3642): 347–353.
- Ponce, V. M. (1989). *Engineering hydrology: Principles and practices*, Prentice Hall, Englewood Cliffs, New Jersey. 640p.
- Popper, K. (1972). *The logic of scientific discovery*, 3rd edn, Hutchinson, London.
- Rinaldo, A., Vogel, G. K., Rigon, R. and Rodriguez-Iturbe, I. (1995). Can one gauge the shape of a basin?, *Water Resour. Res.* **30**: 1119–1127.
- Robichaud, P. R. and Molnau, M. (1990). Measuring soil roughness changes with an ultrasonic profiler, *Trans. Amer. Soc. Agr. Engrs.* **33**(6): 1851–1857.
- Rodriguez, I., Ijjasz-Vasquez, E. J., Bras, R. L. and Tarboton, D. G. (1992). Power law distribution of discharge mass and energy in river basins, *Water Resour. Res.* **28**(4): 1089–1093.

- Rodriguez, I. and Valdes, J. B. (1979). The geomorphologic structure of hydrologic response, *Water Resour. Res.* **15**(6): 1409–1420.
- Rudra, R. P., Dickinson, W. T. and Wall, G. J. (1985). Application of the CREAMS model in Southern Ontario conditions, *Trans. Amer. Soc. Agr. Engrs.* **28**(4): 1233–1240.
- Rudra, R. P., Dickinson, W. T. and Wall, G. J. (1989). Evaluation of land use effects on surface soil hydraulics properties using CREAMS, *Trans. Amer. Soc. Agr. Engrs.* **32**(4): 1295–1302.
- Rudra, R. P., Dickinson, W. T., Wall, G. J. and Tan, K. A. (1986). Runoff response to frost layering, *Trans. Amer. Soc. Agr. Engrs.* **29**(3): 735–740.
- Schultz, G. A. (1987). Parameter determination and input estimation in rainfall-runoff modeling based on remote sensing techniques, in J. C. Rodda and N. C. Matalas (eds), *Water for the future: Hydrology in perspective*, IAHS Publication No. 164, pp. 425–438.
- Schultz, G. A. (1994). Meso-scale modeling of runoff and water balances using remote sensing and other gis data, *Hydrol. Sci. Jour.* **39**(2): 121–141.
- Shen, J. (1965). Use of analog models in the analysis of flood runoff, *Geological Survey professional paper*, Geological Survey. 506–A.
- Singh, V. P. and Agiralioglu, N. (1981a). Diverging overland flow, 1. Analytical solutions, *Nord. Hydrol.* **12**(2): 81–98.
- Singh, V. P. and Agiralioglu, N. (1981b). Diverging overland flow, 2. Application to natural watersheds, *Nord. Hydrol.* **12**(2): 99–110.
- Singh, V. P. and Woolhiser, D. A. (1976). A nonlinear kinematic wave model for watershed surface runoff, *J. Hydrol.* **31**: 221–243.
- Sivapalan, M., Beven, K. J. and Wood, E. F. (1987). On hydrologic similarity 2. A scaled model of storm runoff production, *Water Resour. Res.* **23**(12): 2266–2278.
- Smith, R. E. and Woolhiser, D. A. (1971a). Mathematical simulation of infiltrating watersheds, *Hydrology Paper 47*, Colorado State University.

- Smith, R. E. and Woolhiser, D. A. (1971b). Overland flow on an infiltrating surface, *Water Resour. Res.* **7**(4): 899–913.
- Sorooshian, S. (1981). Parameter estimation of rainfall-runoff models with heteroscedastic streamflow errors—the non-informative data case, *J. Hydrol.* **52**: 127–138.
- Sorooshian, S. and Dracup, J. A. (1980). Stochastic parameter estimation procedures for hydrologic rainfall-runoff models: Correlated and heteroscedastic error cases, *Water Resour. Res.* **16**(2): 430–442.
- Stephenson, G. R. and Freeze, R. A. (1974). Mathematical simulation of subsurface flow contributions to snowmelt runoff, reynolds creek watershed, idaho, *Water Resour. Res.* **10**(2): 284–294.
- Sugawara, M. (1961). On the analysis of runoff structure about several Japanese rivers, *Jap. J. Geophys* **2**(4): 1–76.
- Tarboton, D. G., Bras, R. L. and Rodriguez-Iturbe, I. (1988). The fractal nature of river networks, *Water Resour. Res.* **24**(8): 1317–1322.
- Thwaite, E. G. and Bendelli, A. (1980). A non-contact profile recording instrument, *Proc. Int. Conf. on Manufacturing Engineering*, Institute of Engineers in Canberra, ACT, Australia, pp. 393–386. 25-27 Aug.
- Todini, E. (1996). The ARNO rainfall-runoff model, *J. Hydrol.* **175**: 339–382.
- Tossell, R. W. (1987). *A comparison of three methods used to characterize simulated rainfall properties*, 245p., University of Guelph, Guelph, Ontario.
- Tossell, R. W., Wall, G. J., Dickinson, W. T., Rudra, R. P. and Groenevelt, P. H. (1990). The Guelph rainfall simulator II: Part 1 - Simulated rainfall characteristics, *Can. Agric. Eng.* **29**: 205–213.
- Tossell, R. W., Wall, G. J., Rudra, R. P., Dickinson, W. T. and Groenevelt, P. H. (1990). The Guelph rainfall simulator II: Part 2 - A comparison of natural and simulated rainfall characteristics, *Can. Agric. Eng.* **29**: 215–224.
- Troendle, C. A. (1985). Variable source area models, in M. G. Anderson and T. P. Burt (eds), *Hydrological forecasting*, John Wiley & Sons, Inc., New York, pp. 347–403.

- Tweedie, M. C. K. (1957). Statistical properties of inverse Gaussian distributions, *I. Ann. Math. Stat.* **28**: 362–377.
- Ullah, W. (1974). *Quantitative description of depression storage and roughness properties using a digital surface model*, 287p., University of Guelph, Guelph, Ont.
- Ullah, W. and Dickinson, W. T. (1979a). Quantitative description of depression storage using a digital surface model, I. Determination of depression storage, *J. Hydrol.* **42**: 63–75.
- Ullah, W. and Dickinson, W. T. (1979b). Quantitative description of depression storage using a digital surface model, II. Characteristics of surface depressions, *J. Hydrol.* **42**: 77–90.
- Van de Griend, A. A. and Engman, E. T. (1985). Partial area hydrology and remote sensing, *J. Hydrol.* **81**: 211–251.
- Vertessy, R. A. (1995). Personal Communication, *Catchment Hydrology Group*, CSIRO, Canberra, Australia.
- Vertessy, R. A., Hatton, T. J., O'Shaughnessy, P. J. and Jayasuriya, M. D. A. (1993). Predicting water yield from a mountain ash forest catchment using a terrain analysis based catchment model, *J. Hydrol.* **150**: 665–700.
- Ward, R. C. (1984). Hypothesis-testing by modeling catchment response, *J. Hydrol.* **67**: 281–305.
- Whitelaw, R. Z. (1988). *Hydrological modeling using variable source areas*, PhD thesis, University of Bristol, United Kingdom.
- Wooding, R. A. (1965a). A hydraulic model for the catchment-stream problem, I. Kinematic wave theory, *J. Hydrol.* **3**: 254–267.
- Wooding, R. A. (1965b). A hydraulic model for the catchment-stream problem, II. Numerical solutions, *J. Hydrol.* **3**: 268–282.
- Wooding, R. A. (1965c). A hydraulic model for the catchment-stream problem, III. Comparison with runoff observations, *J. Hydrol.* **4**: 21–37.
- Woolhiser, D. A. (1971). Deterministic approach to watershed modeling, *Nord. Hydrol.* **2**: 146–166.

- Woolhiser, D. A., Smith, R. E. and Giraldez, J. V. (1996). Effects of spatial variability of saturated hydraulic conductivity on Hortonian overland flow, *Water Resour. Res.* **32**(3): 671-678.
- Young, P. C. (1978). General theory of modeling for badly defined systems, in G. C. Vansteenkiste (ed.), *Modeling, Identification and control in environmental systems*, North-Holland, Amsterdam, pp. 103-135.
- Zimmerman, D. L. (1993). Another look at anisotropy in geostatistics, *Math. Geol.* **25**(4): 453-470.
- Zobeck, T. M. and Onstad, C. A. (1987). Tillage and rainfall effects on random roughness: A review, *Soil Tillage Res.* **9**: 1-20.

## **Appendix A**

# **Laboratory Experimental Results**

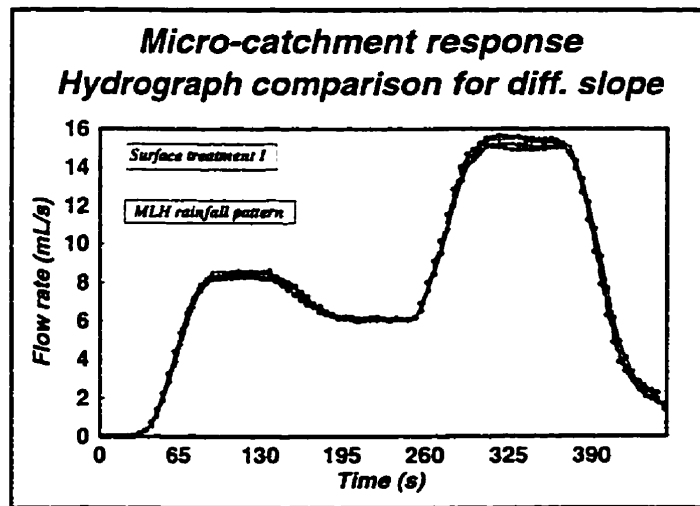
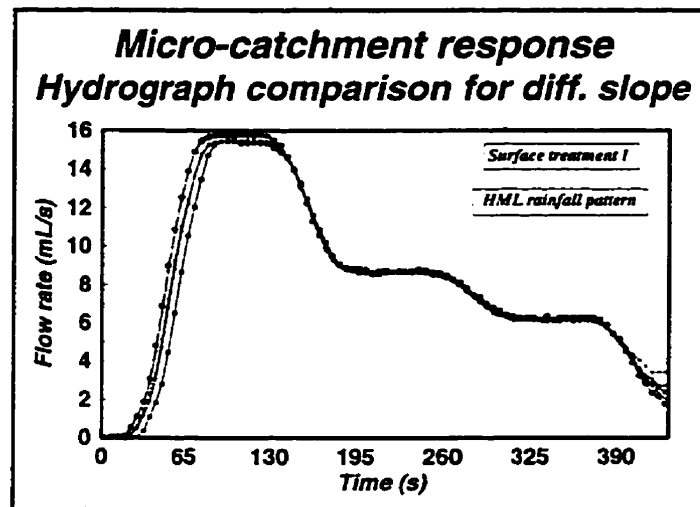
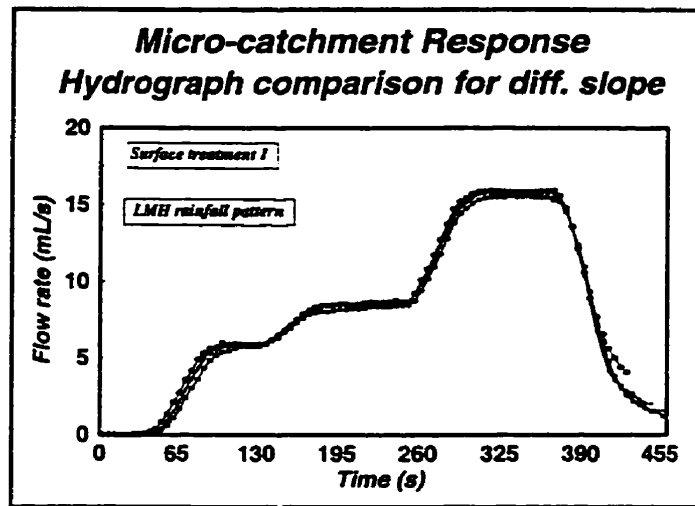


Figure A.1: Catchment response of surface treatment I for different rainfall patterns and slopes.

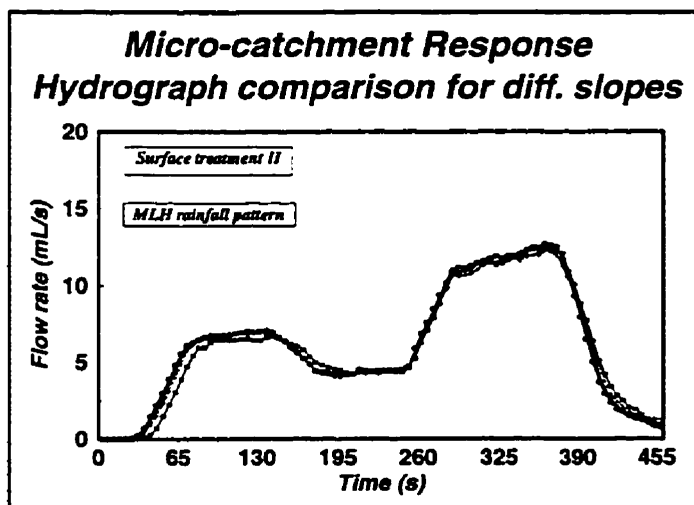
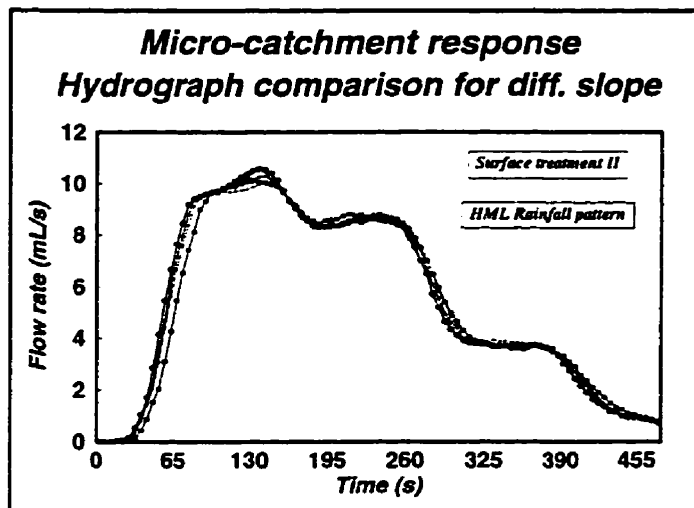
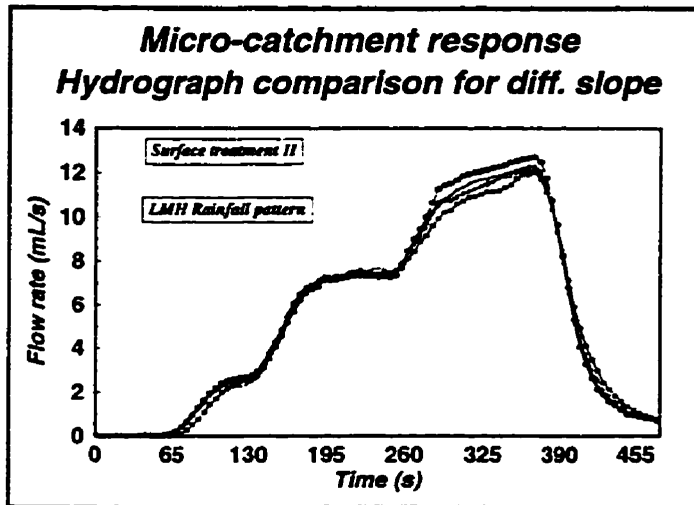
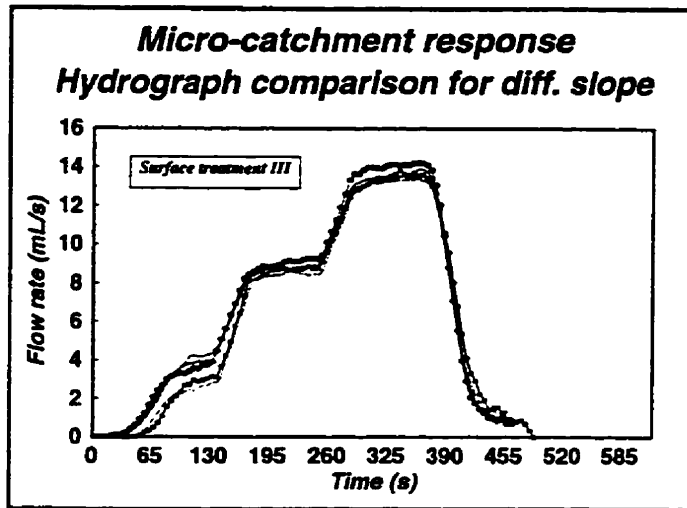


Figure A.2: Catchment response of surface treatment II for different rainfall patterns and slopes.



./appendix/fig/rhml3.eps

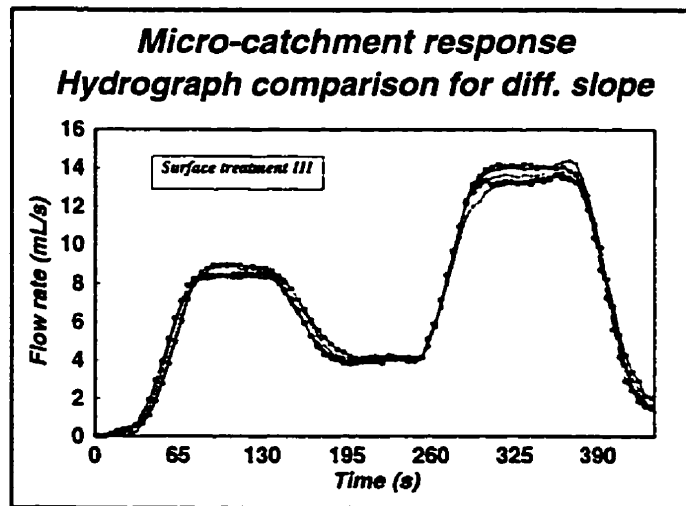


Figure A.3: Catchment response of surface treatment III for different rainfall patterns and slopes.

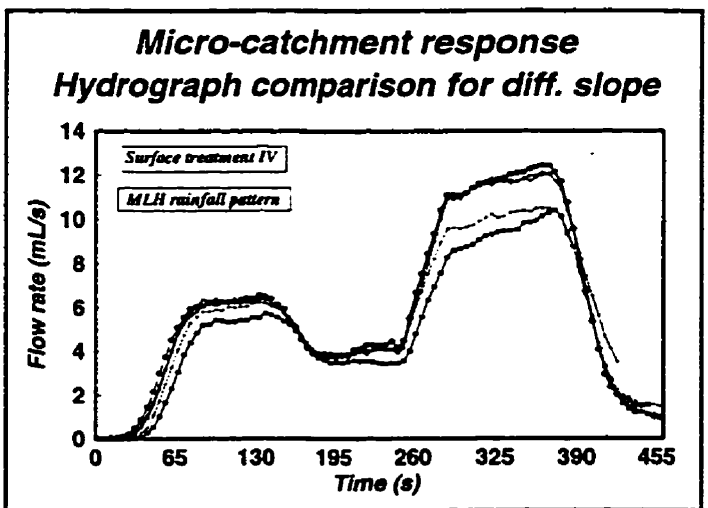
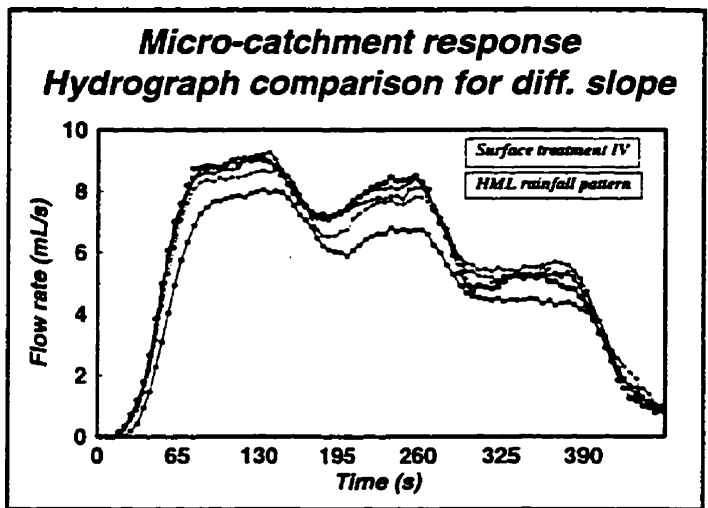
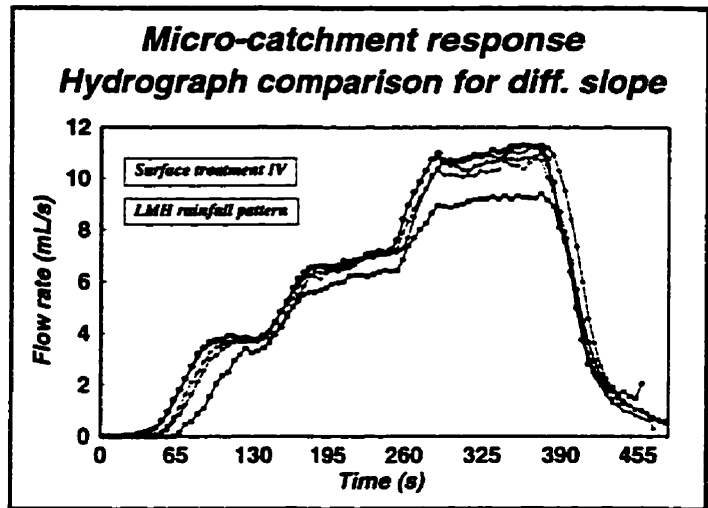


Figure A.4: Catchment response of surface treatment IV for different rainfall patterns and slopes.

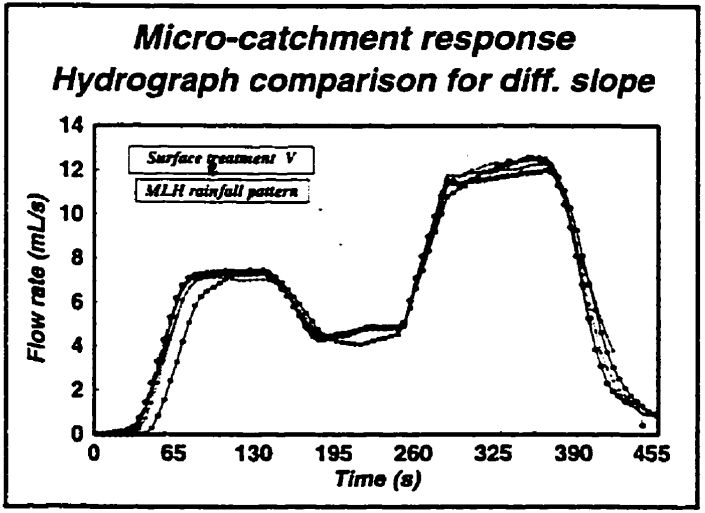
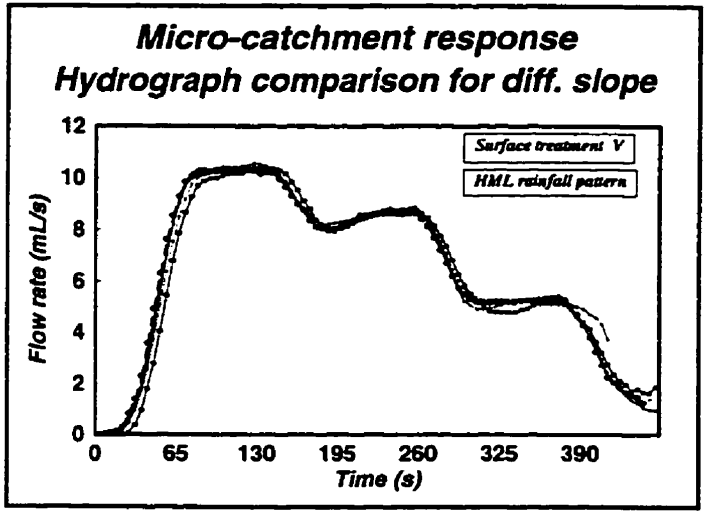
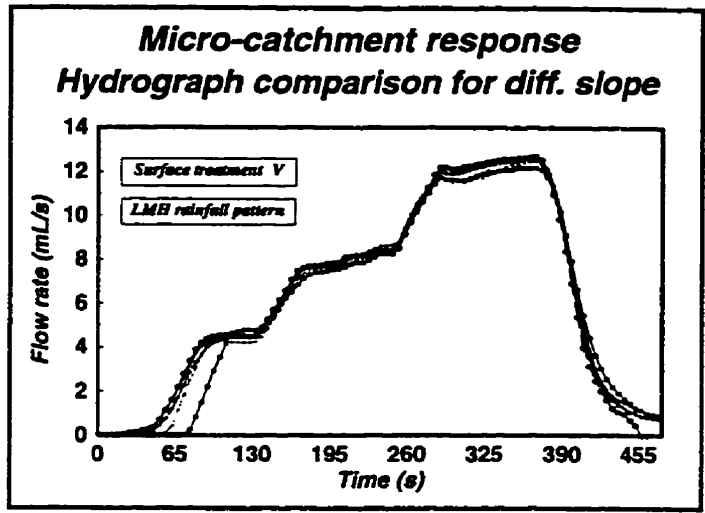


Figure A.5: Catchment response of surface treatment V for different rainfall patterns and slopes.

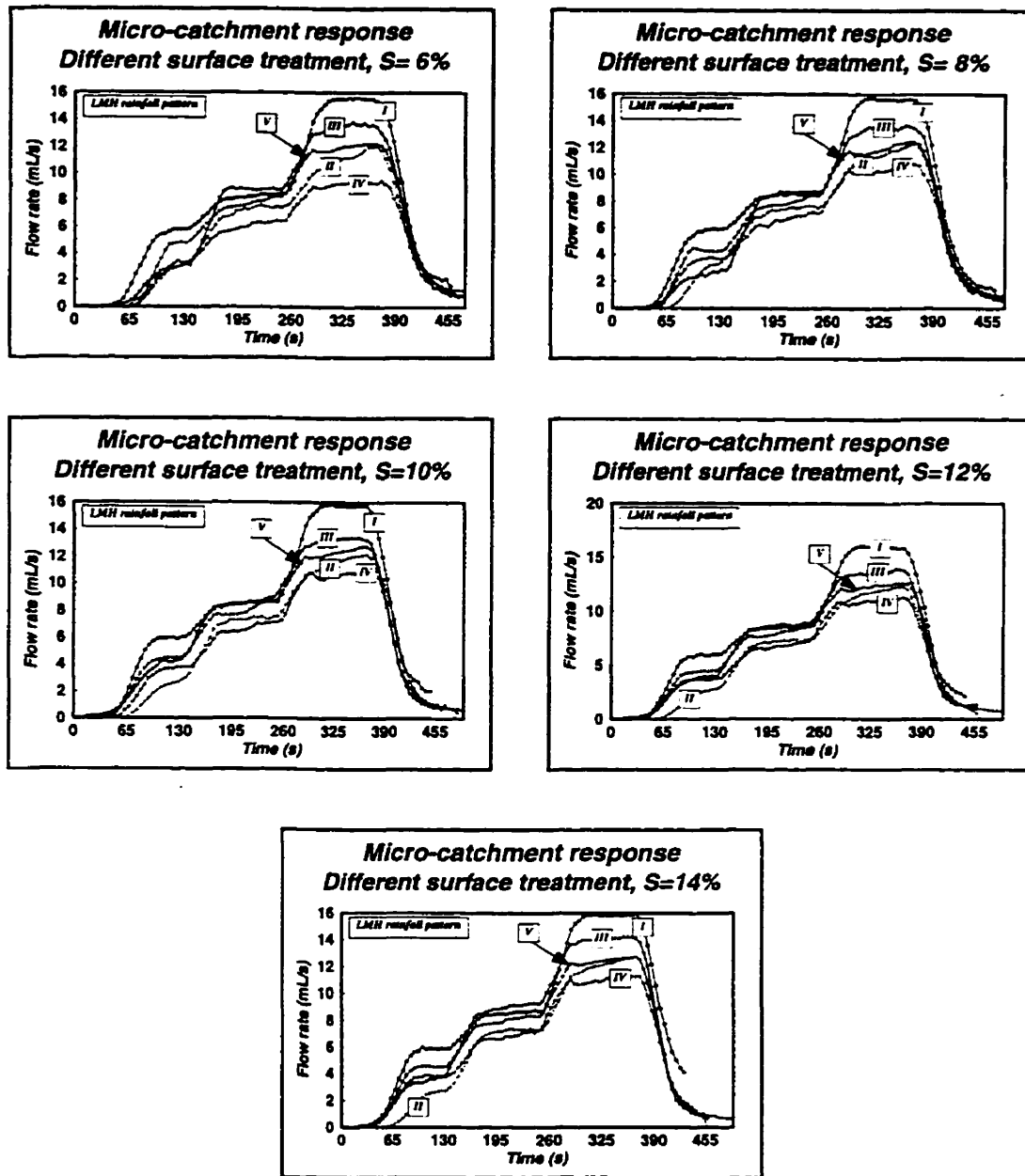


Figure A.6: Catchment response of various surface treatments for different slopes, LMH rainfall pattern.

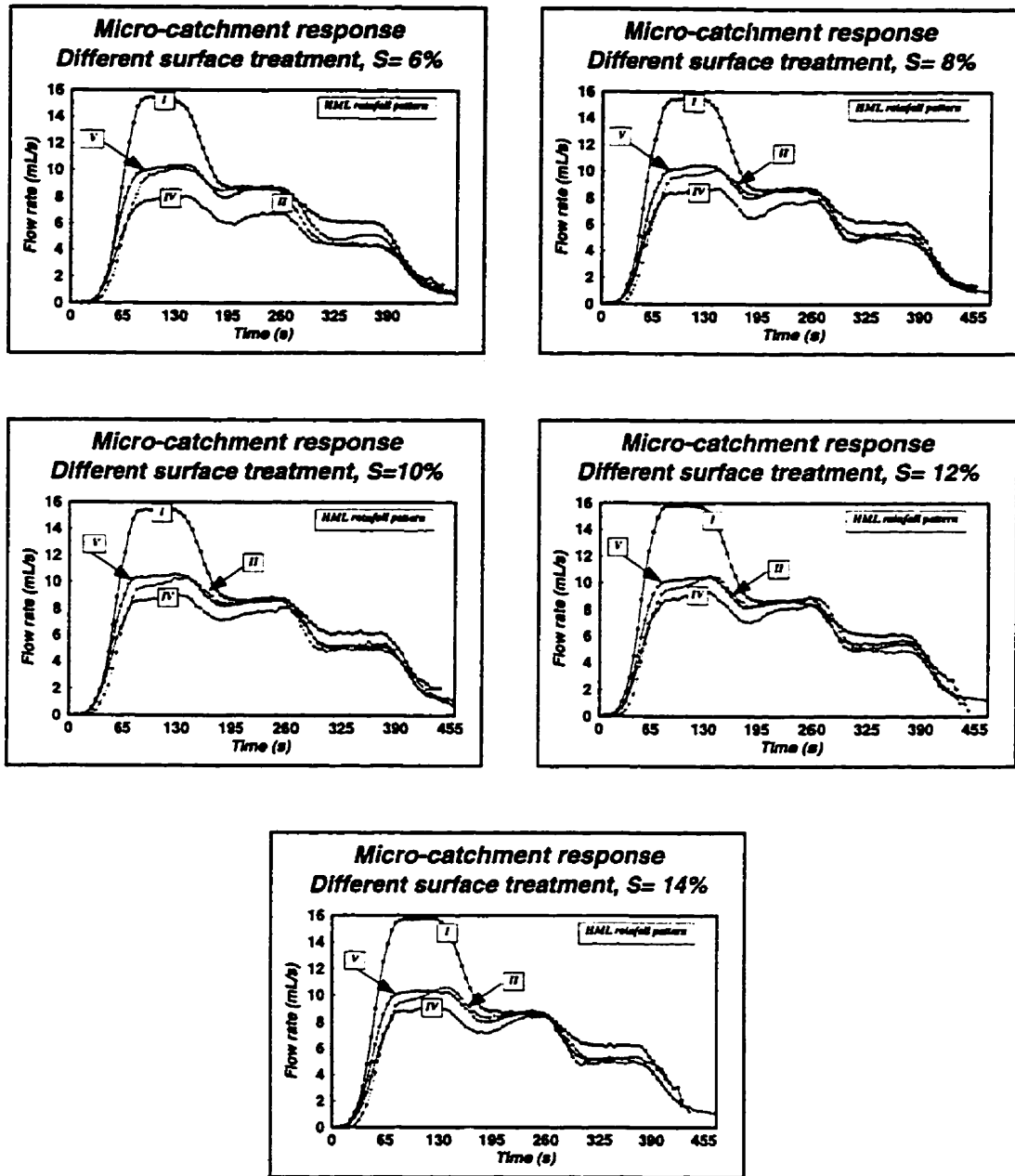


Figure A.7: Catchment response of various surface treatments for different slopes, HML rainfall pattern.

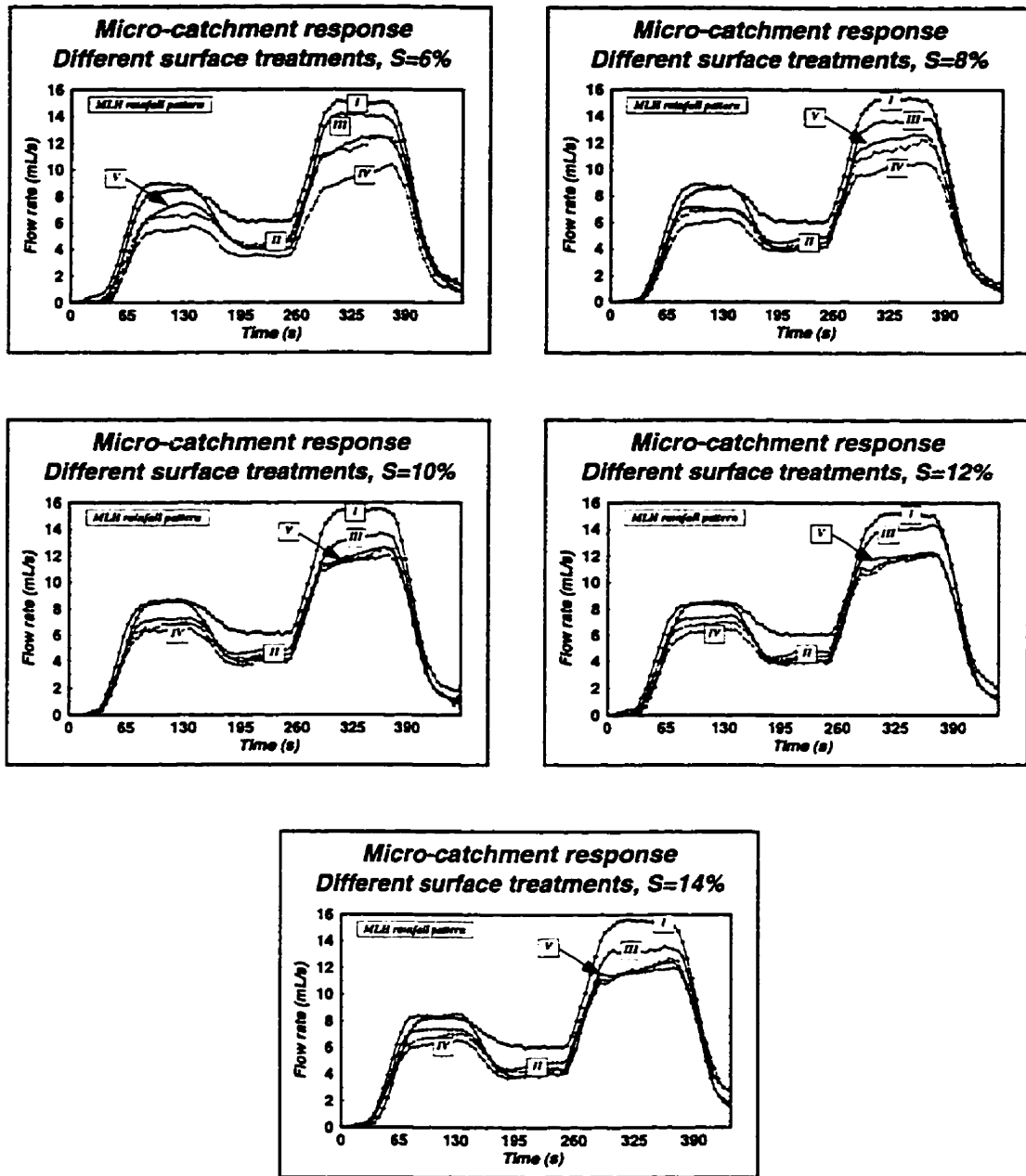


Figure A.8: Catchment response of various surface treatments for different slopes, MLH rainfall pattern.

## **Appendix B**

# **Results of Analysis of Variance**

Table B.1: One-way analysis of Variance of data for key variables.

Sources of Variation	Sum of Squares	Degree of Freedom	Mean Square	F-ratio	$F_{0.95}$	Significant Level
<b>a. Total Runoff Amount (same surface treatment)</b>						
Level Code = Slope Treatments						
Between means	.003	4	.001	.267	3.48	.893
Within Samples	.028	10	.003			
Total	.031	14				
Level Code = Rainfall Patterns						
Between means	.021	2	.010	11.552	3.89	.002
Within Samples	.011	12	.001			
Total	.031	14				
<b>b. Total Runoff Amount (different surface treatment)</b>						
Level Code = Surface Treatments						
Between means	1.241	4	.310	85.392	3.48	.000
Within Samples	.036	10	.004			
Total	1.277	14				
Level Code = Rainfall Patterns						
Between means	.015	2	.008	.072	3.89	.931
Within Samples	1.262	12	.105			
Total	1.277	14				
Level Code = Surface Treatments and Slopes						
Mean	312.93	1	312.93	154152.7	4.35	
Slope tr.	0.061	4	0.015	7.56	2.87	
Surface tr.	4.598	3	1.533	755.2	3.10	
Combined effect	0.262	12	0.022	10.76	2.28	
Error	0.041	20	2.03E-3			
<b>a. Total Rainfall Amount</b>						
Level Code = Slope Treatments						
Between means	.015	4	.005	1.529	3.48	.267
Within Samples	.024	10	.002			
Total	.039	14				
Level Code = Rainfall Patterns						
Between means	.007	2	.004	1.437	3.89	0.276
Within Samples	.031	12	.003			
Total	.039	14				

Table B.2: One-way analysis of Variance of data for key variables.

Sources of Variation	Sum of Squares	Degree of Freedom	Mean Square	F-ratio	$F_{0.95}$	Significant Level
<b>a. Potential Volume of Depressions</b>						
Level Code = Slope Treatments						
Between means	.027	4	.007	999.999	3.48	.000
Within Samples	.000	10	.000			
Total	.027	14				
<b>b. Actual Volume of Depressions</b>						
Level Code = Slope Treatments						
Between means	.0001	4	2.67E-005	.160	3.48	.954
Within Samples	.002	10	1.67E-004			
Total	.0018	14				
Level Code = Rainfall Patterns						
Between means	.001	2	6.47E-004	16.167	3.89	.0004
Within Samples	.00048	12	4.00E-005			
Total	.0018	14				
Level Code = Surface Treatments						
Between means	1.995	4	.499	287.763	3.48	.000
Within Samples	.017	10	.002			
Total	2.012	14				
Level Code = Surface Treatments and Slopes						
Mean	16.47	1	16.47	26252.9	4.35	
Slope tr.	0.08	4	0.02	33.47	2.87	
Surface tr.	6.78	3	2.26	3604.14	3.10	
Combined effect	0.22	12	0.02	29.32	2.28	
Error	0.01	20	6.28E-4			

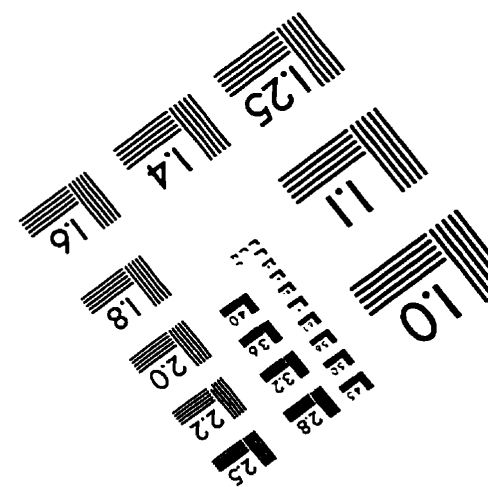
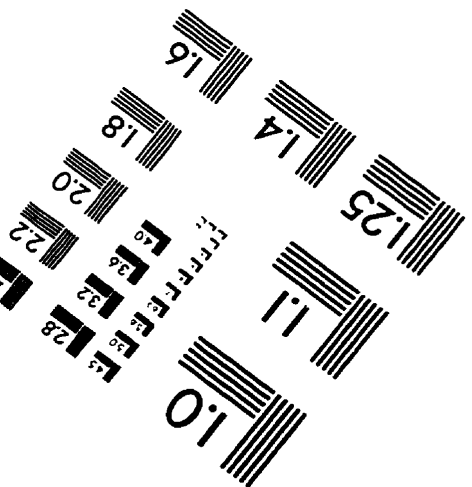
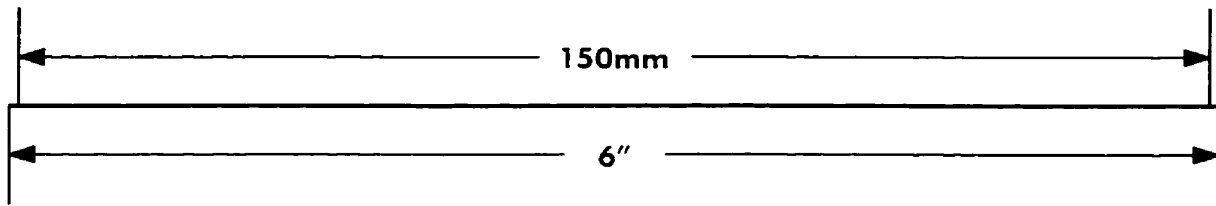
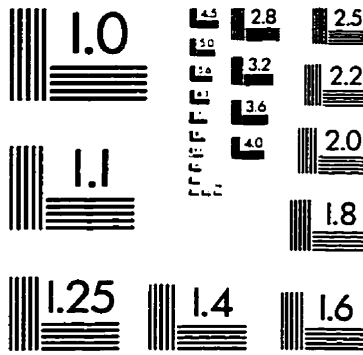
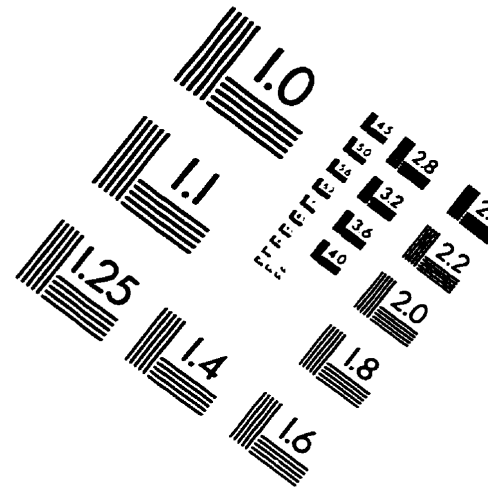
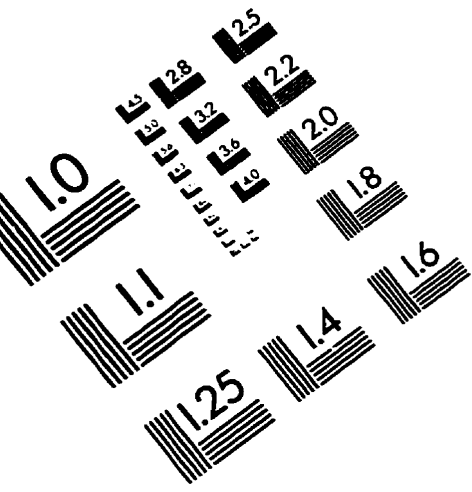
Table B.3: One-way analysis of Variance of data for key variables.

Sources of Variation	Sum of Squares	Degree of Freedom	Mean Square	F-ratio	$F_{0.95}$	Significant Level
<b>a. Total Runoff Amount (dry conditions)</b>						
Level Code = Plot Treatments						
Between means	8.800	2	4.400	39.680	5.14	0.0003
Within Samples	.665	6	.111			
Total	9.465	8				
Level Code = Rainfall Patterns						
Between means	.011	2	.006	.004	5.14	.996
Within Samples	9.454	6	1.576			
Total	9.465	8				
<b>b. Total Runoff Amount (wet conditions)</b>						
Level Code = Plot Treatments						
Between means	2.911	2	1.455	10.577	5.14	.011
Within Samples	.826	6	.138			
Total	3.736	8				
Level Code = Rainfall Patterns						
Between means	.422	2	.211	.382	5.14	.698
Within Samples	3.314	6	.552			
Total	3.736	8				
<b>c. Total Runoff Amount (plastic cover conditions)</b>						
Level Code = Plot Treatments						
Between means	1.036	2	.518	2.312	9.55	.247
Within Samples	.672	3	.224			
Total	1.709	5				
<b>d. Total Runoff Amount</b>						
Level Code = Plot Treatments						
Between means	77.014	2	38.507	50.523	3.55	.000
Within Samples	13.719	18	.762			
Total	90.733	20				

Table B.4: One-way analysis of Variance of data for key variables.

Sources of Variation	Sum of Squares	Degree of Freedom	Mean Square	F-ratio	$F_{0.95}$	Significant Level
<b>a. Total Water Loss (dry conditions)</b>						
Level Code = Plot Treatments						
Between means	6.434	2	3.217	29.571	5.14	.001
Within Samples	.653	6	.109			
Total	7.087	8				
Level Code = Rainfall Patterns						
Between means	.009	2	.004	.004	5.14	.996
Within Samples	7.078	6	1.180			
Total	7.087	8				
<b>b. Total Water Loss (wet conditions)</b>						
Level Code = Plot Treatments						
Between means	2.653	2	1.326	9.650	5.14	.013
Within Samples	.825	6	.137			
Total	3.478	8				
Level Code = Rainfall Patterns						
Between means	.672	2	.336	.719	5.14	.525
Within Samples	2.805	6	.468			
Total	3.478	8				
<b>c. Total Water Loss (plastic cover conditions)</b>						
Level Code = Plot Treatments						
Between means	1.038	2	.519	2.315	9.55	.246
Within Samples	.672	3	.224			
Total	1.710	5				
<b>d. Total Water Loss</b>						
Level Code = Plot Treatments						
Between means	148.579	2	74.290	120.753	3.55	.000
Within Samples	11.074	18	.615			
Total	159.653	20				

# IMAGE EVALUATION TEST TARGET (QA-3)



APPLIED IMAGE, Inc  
1653 East Main Street  
Rochester, NY 14609 USA  
Phone: 716/482-0300  
Fax: 716/288-5989

© 1993, Applied Image, Inc., All Rights Reserved